Ph.D. Thesis

Experimental studies on organic-inorganic interactions between fulvic acid and goethite in the aquatic environment

(溶存有機物と鉄鉱物の有機無機相互作用の実験的研究)

By

Takahiro OTSUKA

February, 2008

Osaka University
Department of Earth and Space Science, Graduate School of Science
Toyonaka, Osaka, JAPAN

ABSTRACT

Humic substances (HS) have abundant hydrophilic functional groups such as –COOH and –OH that give their aqueous solubility, binding sites for metals, buffer capacities and other reactive characteristics (Stevenson, 1994). Because of their high abundance and reactivities, humic substances contribute primarily to the material cycling at the earth's surface. Therefore, long-term behaviors of HS in aquatic environments should be evaluated.

In this thesis, for studying reaction kinetics of organics by accelerating them at higher temperatures, new spectroscopic methods under hydrothermal conditions have been first developed. The reaction gas cell FT-IR system was constructed by combining a gas cell FT-IR with a reaction vessel to observe the formation of CO_2 by the interactions of a fulvic acid and an iron oxide. Two in-situ hydrothermal spectroscopic methods were developed here for monitoring hydrothermal organic reactions: UV-VIS spectroscopy for the determination of organic contents and aromatic natures; and ATR-IR spectroscopy for the characterization of functional groups.

By using these spectroscopic methods, hydrothermal transformations of humic substances (Nordic fulvic and humic acids) were studied. Two reactions, aromaticity decrease and decarboxylation, were dominant for fulvic acid under hydrothermal conditions. Firstly, the long-term decrease of absorbance at 254 nm (Abs_{254}) of dissolved humic substances in the batch hydrothermal experiments (80% decrease of Abs_{254} during several hundreds of hours at 80-180 °C) correspond mainly to the aromaticity decrease of humic structures with a relatively high activation energy of 85 kJ mol^{-1}. Secondly, the rapid initial Abs_{254} decrease of about 10% during 1-10 hours at 80-180 °C, observed by the in-situ UV spectroscopy with a low activation energy of 29 kJ mol^{-1}, corresponds to the decarboxylation reaction leading to the CO_2 formation (22 kJ/mol) detected by the reaction gas cell FT-IR. The small values of activation energies for these two processes (29 and 22 kJ/mol) indicated that the rate-limiting step for these processes can be attributed to the decarboxylation reaction.

Then interactions of these organics with an iron oxide (goethite) have been studied. These experiments suggest that the fulvic acid is supposed to be decomposed and finally oxidized to CO_2 on the goethite surface following the fast adsorption in aqueous

environments. The first process is the very rapid adsorption of the fulvic acid on goethite within 10 minutes at 25-80 °C (activation energy: 26 kJ mol^{-1}) and the second one is its slower adsorption (activation energy: 30 kJ mol^{-1}). The second adsorption process has similar rates and activation energy to the enhanced CO_2 formation from the fulvic acid in the presence of goethite (activation energy: 32 kJ mol^{-1}). The reaction scheme can be estimated as follows with the obtained stoichiometric relations:

$$FeOOH + RCOO^- + 2H^+ \rightarrow Fe^{2+} + R\cdot + H_2O + HCO_3^-.$$

HCO_3^- formed in micro pore environments (pH 7) on the goethite surface might be diffuse from the micropore to the bulk medium (pH 4), where it was changed to CO_2 by the following reaction:

$$HCO_3^- \Leftrightarrow CO_2 + OH^-$$

The obtained half-lives at 25°C of transformation of the fulvic acid (enhanced CO_2 formation by goethite: 10 hours, decarboxylation leading to CO_2 formation: 1 month and major decomposition mainly by aromaticity decrease: 100 years) are much faster than the age estimates from the ^{14}C dating (several hundred years). The results of this thesis suggest that some parts of humic substances are easily decomposable, especially for their reactive functional groups such as carboxyls, with very short half-lives. Since these reactive groups are important binding sites for environmental pollutants such as heavy metals, their instability, especially in the presence of goethite, should be considered for re-evaluating fate and long-term behavior of environmental pollutants and CO_2 formation.

溶存腐植物質は水環境中の溶存有機物の約半数を占める不定形の高分子物質である．腐植物質は様々な形態と性質を持ち，特にCOOHやOHなどの活性な官能基を持つため，汚染物質との錯体形成や酸化還元反応などを通じて，地球表層物質循環において大きな役割を果たしている．

本研究では，腐植物質特にその官能基構造の分解過程の長期挙動と時間スケールを評価するため，いくつかの分光学的手法を開発して，溶存腐植物質の加熱変化を追跡した．腐植物質の分解によって生成するガス成分の分析には，水熱反応容器とガスセル赤外分光法を組み合わせた分析システムを開発した．また，鉱物存在下での溶存有機物の濃度や官能基構造を直接観察する手段として，紫外可視分光法・減衰全反射赤外分光法を利用した水熱その場観測法を開発した．

腐植標準物質（Nordicフルボ酸，フミン酸）から100 mg/Lの水溶液を作成し，テフロン容器に入れ，80～180℃で数時間から数日間，加熱実験を行なった．その結果，全ての温度・時間範囲で254 nmでの吸光度が最大80%減少し，減少速度は1次反応で近似でき，その活性化エネルギーEは85 kJ/molであった．この吸光度の減少は，主に芳香族度の減少すなわち，腐植物質の主構造である芳香環の分解によると考えられる．また，この吸光度の減少が10%程度までの範囲においては，上記の腐植物質分解反応よりも速い反応（E=29 kJ/mol）が観察された．この初期に進行する254 nmの減少反応は，ガスセル赤外分光によって得られた二酸化炭素の生成反応（E=22 kJ/mol）の速度・変化量と一致しており，脱炭酸反応であると考えられる．

一方，鉄鉱物存在下での溶存腐植物質の挙動を調べるため，ゲーサイト存在下でのフルボ酸の水熱実験を行なった．その結果，フルボ酸はゲーサイト表面に迅速に吸着し，その後，二酸化炭素が生成されることが観察された．この二酸化炭素生成反応（E=32 kJ/mol）は，上記フルボ酸単独での反応と比べ大きい速度を持ち，ゲーサイト存在下で促進されたと考えられる．またこの二酸化炭素生成反応は，十数時間程度でゆっくりと進行するゲーサイトへのフルボ酸の吸着反応が示す速度・活性化エネルギーと同様であり，この吸着過程に律速されていることが示唆された．

ゲーサイト存在下でのフルボ酸の水熱実験において，二酸化炭素，二価鉄の生成量および水素イオンの減少量から，次のような化学反応を化学量論的に確認した．

$$FeOOH + RCOO^- + 2H^+ \rightarrow Fe^{2+} + R\cdot + H_2O + HCO_3^-.$$

ゲーサイトに吸着したフルボ酸のカルボキシル基は，ゲーサイトの三価鉄に電子を与えて酸化されてCO_2を生成し，一方，ゲーサイトの三価鉄は還元されて二価鉄となって溶解する．生成したCO_2は，ゲーサイト近傍のpHが中性のためHCO3-となるが，ゲーサイトの細孔を拡散して溶液に至るとpHが酸性のためCO2となってガスとして放出される．

実験で得られた速度定数と活性化エネルギーから，これらの反応の常温での半減期を予測すると，ゲーサイトの存在により促進される脱炭酸反応は10時間程度，フルボ酸単独の脱炭酸反応は1ヶ月程度であった．これは従来の年代測定法などによって予測されていた腐植物質分解の時間スケール（数百年程度）よりも大幅に短い．一般に分解されにくいと考えられていた腐植物においても，その活性な官能基構造は環境中で比較的容易に変化し，鉄鉱物の存在によってさらにその変化が速くなることが示され，環境汚染などの地球表層物質循環の再評価が必要である．

Acknowledgement

Before anything else, I would like to be grateful to my thesis adviser, Dr. Satoru Nakashima for precise direction, innumerable advise, his big heart and his late to bed & early to rise.

I would also like to thankful to all members of Nakashima laboratory, especially my colleague, Mr. N. Kitadai, Dr. Y. Yamanoi and Dr. M. Igisu. Also to Dr. T. Yokoyama, Dr. M. Katsura, Dr. T. Hirono, Dr. K. (Masuda) Ono, Mr. K. Ishikawa and Dr. A. Tani (Osaka University) for many worthwhile discussion on experiments.

Dr. M. Moriizumi and Ms. R. Fuchiyama (Natural Agricultural Research Center: NARC) helped me for fluorescence spectroscopy and organic carbon analysis. Dr. N. Fujitake (Kobe Univ.) and Dr. R. Ishiwatari gave me helpful advises for the treatment of humic substances. M. Sunose helped me for the technical support for the gas cell FT-IR. I wish express my appreciate to Dr. Y. Takahashi, Mr. S. Mitsunobu, Mr. H. Itai, Mr. Y. Yamamoto (Hiroshima Univ.), Dr. Y. Suzuki (AIST), Dr. T. Matsunaga (NARC), Dr. U. Tsunogai, Dr. H. Shibata (Hokkaido Univ.), Dr. T. Hirata (Tokyo Institute of Technology.) for scientific discussion and encouragement. Mr. S. Kawaguchi, Mr. Y. Konno, Dr. F. Nakagawa (Hokkaido Univ.), Dr. T. Okuda (Keio Univ.) and Dr. K. Koba (Tokyo Univ. Agriculture and Technology) gave me an opportunity to join young committee of Geochemistry. I would also like to thankful to member of Matsuda, Tokunaga and Tsuchiyama laboratory and many other people of Earth & Space Science Department of Osaka University

I would like to be thank for T. Iwamoto, my room mate, and all friends and teachers from ICU days.

Finally, I would sincerely appreciate my family

and Momoko Abe

ABSTRACT

TABLE OF CONTENTS
ACKNOWLEGMENT

CHAPTER 1.

General introduction

General Introduction

The interactions between organic matter and iron are commonly observed in natural surface environments (Stumm and Morgan, 1996). Natural organic matter (NOM) adsorbs onto iron oxide surface, and forms stable complexes with ferric iron. Reducing capacity of NOM is expected and accelerate reductive dissolution of Fe^{III} oxide (LaKind and Stone, 1989; Chorover and Amistadi, 2001; Pullin and Cabaniss, 2003).

Adsorption processes of organics on iron surfaces in aquatic environments have been well studied based on thermodynamic points of view (Gu et al., 1994, Gu et al., 1995, Zhou et al.,2001). NOM makes various types of bonding with iron to in minerals such as hydrogen bond, ionic bond and covalent bonding. These bonding binds electrically charged functional groups of organics and iron (Cabaniss, 1991).

In contract to these sorption studies, much less are known on reactions between NOM and minerals. NOM is reported to accelerate dissolution of iron in minerals such as biotite, hematite and goethite, by reducing insoluble ferric iron to soluble ferrous iron (LaKind, 1989). However, very few data are available on the transformation of NOM (Perdue, 2003). This is because of complex properties of NOM with varying size, chemical composition, molecular weight and functional groups, and other characteristics, depending on their drivers origins and ages (Stevenson, 1994).

Dissolved organic matter (DOM), defined as small organic compounds passing though 0.45μm filter, is common in natural waters such as rivers, lakes, oceans and ground waters. Only 20% of dissolved organic matter (DOM) in the natural aquatic environments is identifiable and the remaining 80% of DOM is dissolved humic substances (Thurman, 1985). Humic substances are high molecular weight organic substances with unknown variable chemical structures. Most of DOM is removed from surface waters as a result of sorption to mineral surfaces and subsequent reactions.

On the other hand, DOM has a key role in biogeochemical cycling (Hedges, 2002). Carbon and nitrogen are fundamental elements for biota. Especially nitrogen is essential for plants. In agriculture, organic nitrogen recycling by soil organic matter (humic substances) is important (Kumada, 1981). Marine chemists and forest ecologists have investigated DOM properties in ocean or forest (Coble, 1996; Berg and McClaugherty, 2003). Despite these extensive studies on DOM at the earth's surface at low temperatures, their behavior under hydrothermal conditions have not been studied in detail (Landais and Gize, 1999).

In order to investigate the behavior of dissolved organic matter under hydrothermal conditions, we have conducted hydrothermal heating experiments of

dissolved humic substances, representative DOM in the natural environment. We have paid particular attention to their functional groups playing key roles of geochemical processes. Volatile compounds formed during these processes have also been studied.

To achieve these objectives, three steps of spectroscopic investigations were performed. The first step is the development of the methodologies to observe the reactions of dissolved humic substances (Chapter 2). The analysis of gas emission from dissolved humic substances during their thermal transformation processes was conducted by using a long-path (10m) gas cell FT-IR method connected to a hydrothermal reaction vessel. The second step is the observation of changes in functional groups of dissolved humic substances under hydrothermal conditions by different analytical methods (Chapter 3). In particular, ultraviolet-visible (UV-VIS) and fluorescence spectroscopies have been employed to study functional groups of humic substances. The third step is studying effects of an iron oxide mineral (goethite) on the hydrothermal transformation of dissolved humic substances (Chapter 4). Finally, I discuss time-scales of transformation of humic substances by using obtained kinetic data.

REFERENCE

Berg B. and McClaugherty C. (2003) Plant litter decomposition, humus formation, carbon sequestation, Berlin; Heidelberg, Springer-Verlag

Cabaniss, S. E. (1991) Carboxylic acid content of a fulvic acid determined by potentiometry and aqueous Fourier transform infrered spectrometry., *Analytica Chimica Acta,* **255**, 23-30

Coble P. G. (1996) Characterization of marine and terrestrial DOM in seawater using excitation-emission matrix spectroscopy, *Marine chemistry*, **51**, 325-346

Chorover J. and Amistadi M. K. (2001) Reaction of forest floor organic matter at goethite, birnessite and smectite surfaces. *Geochimica et Cosmochimica Acta*, **65**, 95-109.

Gu B., Schmitt J., Chen Z., Liang L. and McCathy J. F. (1994) Adsorption and Desorption of natural organic matter on iron oxide: mechanisms and models. *Environmental Science and Technology*, **28**, 38-46.

Gu, B., Schmitt, J., Chen, Z., Liang, L., McCarthy, J. F. (1995) Adsorption and desorption of dirrenet organic-matter ractions on iron-oxide., *Geochimica et Cosmochimica Acta*, **59**, 219-229

Hedges J. I. (2002) Why dissolved organic matter? In *Biogeochemistry of Marine Dissolved Organic Matter* (eds. Hansell D. A. and Carson C. A.) Amsterdam: Academic Press, pp.774

Kumada K. (1981) Dojo-yuukibutu no kagaku 2nd, Tokyo, Japan Scientific Societies Press, 249-268

LaKind J. S. and Stone A. T. (1989) Reductive dissolution of goethite by phenolic reductants. *Geochimica et Cosmochimica Acta*, **53**, 961-971.

Landais P., Gize A. P. (1997) Organic matter in hydrothermal ore deposit, in Barnes H. L. ed., Geochemistry of hydrothermal ore deposits 3rd ed., New York, John Wiley & Sons, p613-656

Perdue E. M. and Ritchie J. D., (2003) Treatise on Geochemistry Vol.5 Surface and ground water, weathering, and soils, Oxford, Elsevier Pergamon, pp273-318

Pullin M. J. and Cabaniss S. E. (2003), The effect of pH, ionic strength, and iron-fulvic acid interactions on the kinetics of non photochemical iron transformations. II. The kinetics of thermal reduction. *Geochimica et Cosmochimica Acta*, **67**, 4079-4089.

Stevenson F. J., Humus chemistry: genesis, composition, reactions 2nd ed., New York: Wiley, 1994

Stumm W. and Morgan J. J. (1996) *Aquatic chemistry: chemical equilibria and rates in natural waters*, 3rd ed., pp. 1022, New York: Willey

Thurman. E. M. (1985) *Organic geochemistry of Natural waters*, Dordrecht, M. Nijhoff, 1-4

Zhou Q. Maurice P. A. and Cabaniss S. E. (2001) Size fractionation upon adsorption of fulvic acid on goethite: equilibrium and kinetic studies, *Geochimica et Cosmochimica Acta*, **65**, 803-812.

CHAPTER 2.

Developments of spectroscopic methods for studying hydrothermal aqueous organic reactions

Chapter 2

2.1. Reaction gas cell FT-IR spectroscopy for tracing volatile species formed from the hydrothermal transformation of humic substances

2.2. *in-situ* UV-VIS spectroscopy for monitoring the hydrothermal transformation of humic substances

2.3. ATR-IR spectroscopy of fulvic acid on the surface of goethite

INTRODUCTION

Humic substances are generally believed to be stable under earth's surface conditions (Stevenson, 1994). Several studies have been conducted on the thermal stability of powdered humic substances in the solid state up to 300 °C (Lu et al., 1997). However, only few works have been conducted on the thermal degradation of humic substances in the dissolved state. In order to understand stability of dissolved humic substances under hydrothermal conditions, in-situ hydrothermal spectroscopic methods were developed here for monitoring hydrothermal organic reactions.

Kinetics of humic substance transformation has been generally studied by conventional batch reaction methods (Nakashima, 1992a,b). The merit of batch experiment is the capability of detailed characterization of reaction products by means of various analytical techniques (e.g., HPLC, GC-MS). However, only a few measurement data can be obtained in the batch methods, and detailed kinetic treatments are limited.

Recently, *in-situ* techniques for aqueous reactions have been developed enabling the kinetic tracing of reaction progress (Brill and Savage; 2004 Masuda, 2005). Previously, conventional heating experiments have been performed by the batch method to obtain a few data points as a function of time. These data can be only fitted by approximate rate laws to obtain rough kinetic parameters. However, by applying advanced in-situ method, numerous data can be acquired and detailed kinetic analyses are possible. In addition, in the case of extrapolating reaction rates at high temperatures to lower temperatures, the kinetic parameters should be determined precisely. Therefore, in-situ method is important for detailed reaction kinetics. In this chapter, three hydrothermal spectroscopic methods have been developed: 1) Gas cell FT-IR for the determination of emitted gases, 2) UV-VIS spectroscopy for the contents and natures of humic substances, and 3) ATR-IR spectroscopy for the characterization of functional groups.

2.1. Reaction gas cell FT-IR spectroscopy for tracing volatile species formed from the hydrothermal transformation of humic substances

2.1.1. INTRODUCTION

Conventionally, dissolved volatile organic compounds (VOCs) in water are measured by means of gas chromatography (GC) or gas chromatography mass spectrometry (GC-MS) equipped with purge and trap system or headspace system (Johnson, 2002). Although these are highly sensitive and precise analytical methods, they require time consuming procedures and delicate maintenance. On the other hand, Fourier transform infrared (FT-IR) spectroscopy has also been applied to trace gas analysis (Hanst et al. 1973). The reaction gas cell FT-IR developed here, a gas cell FT-IR method combined with a reaction vessel, is expected to be a rapid and multi-phase detection method for characterizing general composition of emitted gaseous products. This method was employed here to determine gaseous products emitted from hydrothermal heating of humic substance solutions.

2.1.2. Development of reaction gas cell FT-IR spectroscopy

2.1.2.1. Long-path gas cell FT-IR

The gas cell FT-IR measurement uses infrared absorptions of gaseous compounds contained in a gas cell placed in an FT-IR optics. The characteristics of IR absorption by gaseous compounds are the fine rotational transition absorptions overlapped on the stretching and bending vibrations (Hanst and Hanst, 1990). Therefore, it is possible to identify gaseous molecular species and to determine them quantitatively.

In order to detect trace gas components, a gas cell with a ten-meter path length (10-PA, Infrared analysis Inc.) was set on an FT-IR spectrometer (MB154, Bomem). In the gas cell (25cm path length), reflecting IR mirrors (gold-coated) are set at the both ends to obtain 40 times reflection ($25 \times 40 = 10$m) as shown in Fig.2.1.1. The cell volume was about 2 liter, which was confirmed by measuring a weight of pure water put in the cell with an electric balance.

The FT-IR spectrometer (MB154, Bomem) has an infrared light source (Globar), a CsI beam splitter and a deuterated triglycyl sulfate (DTGS) or a mercury cadmium telluride (MCT) detector. Gaseous sample is introduced into the 10m gas cell by pressure difference with a vacuum pump. (Fig. 2.1.1.A.).

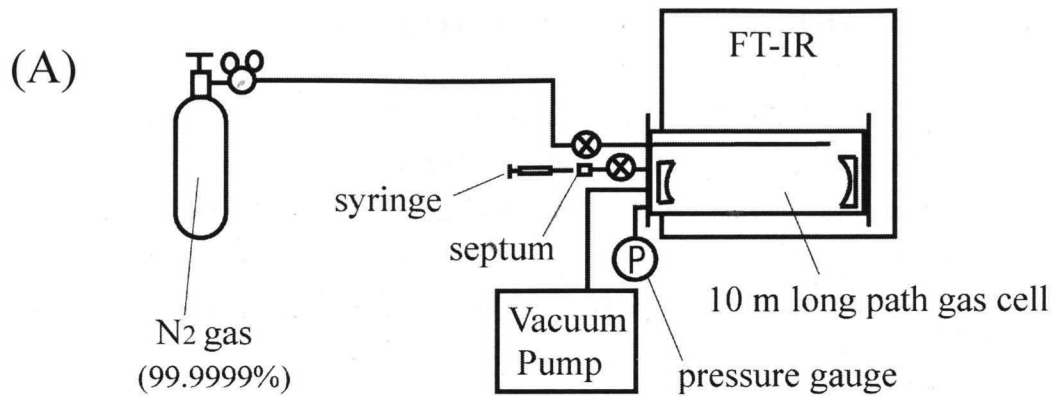

(B)

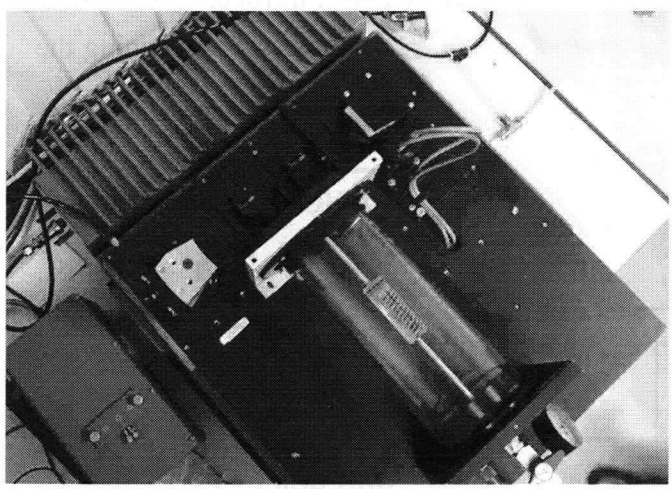

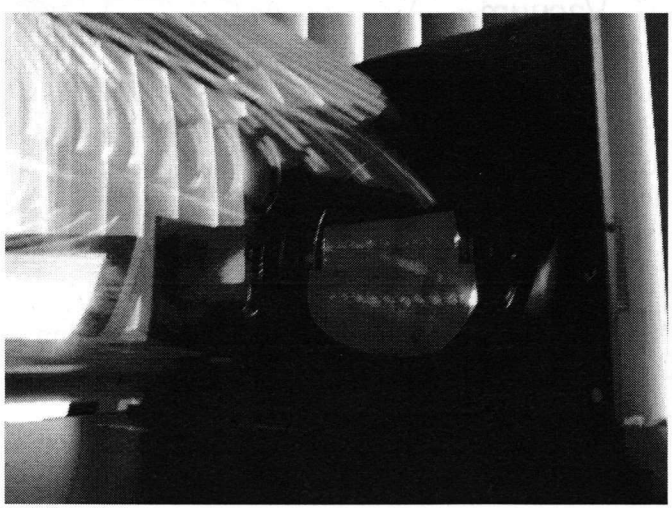

(C)

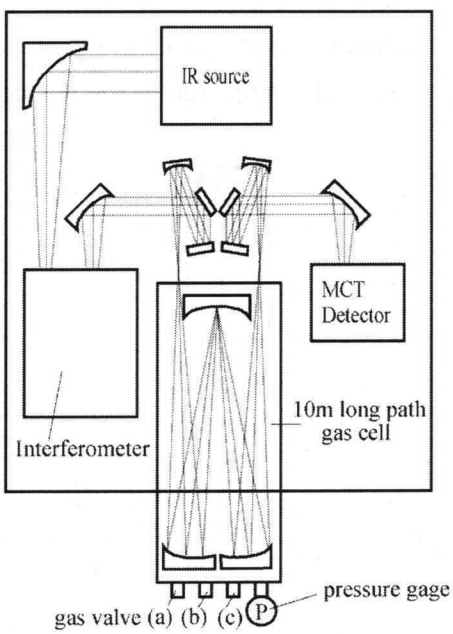

Figure 2.1.1 10 m long path gas cell placed in an FT-IR spectrometer (MB154, Bomem) (A) The schematic configuration of the whole system, (B) the photographs, and (C) schematic configuration of the optics and the gas cell with (a) the sample inlet valve, (b) N_2 gas inlet valve (purity > 99.9999%) and (c) outlet valve for a vacuum pump.

2.1.2.2. Long-path gas cell FT-IR combined with a Tedler® bag

The first stage of reaction gas cell FT-IR system was constructed by using a Tedler® bag, a commercial Teflon bottle as a reaction vessel, a stainless liner and a gas cell FT-IR (Fig2.1.2.). A Tedler® bag have a Teflon valve for gas outlet and was slit up its corner for inlet from the reaction vessel. Then, this bag was connected to the gas cell FT-IR though a stainless liner. A vacuum pump and a N_2 gas bomb (99.9999% purity) are connected to the lines to obtain non-oxidizing atmosphere throughout the whole system.

The sample preparations for emission gas analysis in the reaction vessel were as follows. Firstly, a pre-heated reaction vessel was inserted into a Tedler® bag. The Tedler® bag was sealed by clip and ambient air was replaced with nitrogen gases. After that, emission gases in the reaction vessel were extracted from the vessel by opening the lid and transferred to the gas cell.

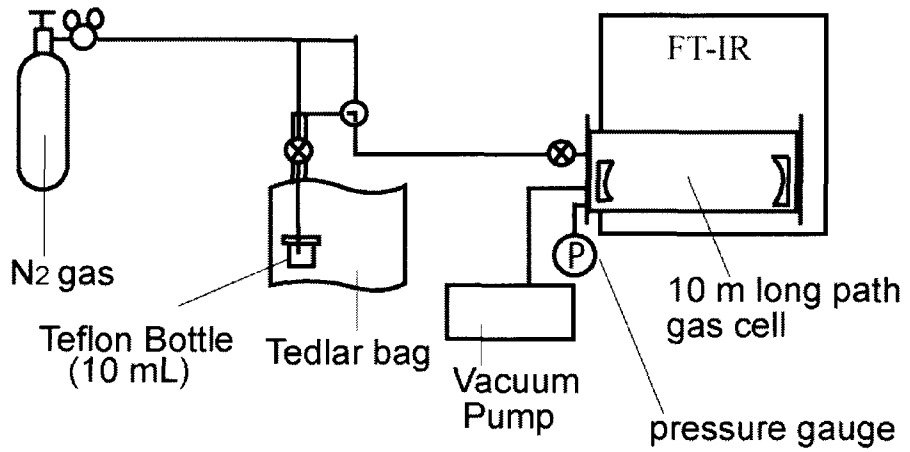

Figure 2.1.2. The schematic configuration of long-path gas cell FT-IR combined with a Tedler® bag.

2.1.2.3. Hydrothermal reaction vessel

An original hydrothermal reaction vessel has been developed for studying hydrothermal transformation of dissolved organic substances (Fig. 2.1.3). The vessel is composed of a Teflon® (PTFE) inner bottle and a stainless (SUS316) outer container (TAIATSU TECHNO Co.). A stainless tube with valves and a pressure gage is used to extract gaseous products from the reaction vessel. A band heater is surrounding the stainless container to heat the vessel. One thermocouple is placed under this band heater to regulate the heater through the temperature controller. Maximum working pressure and temperature are 1 MPa and 180°C, respectively. Pneumatic test (1 MPa) and hydrostatic test (1.5 MPa) confirmed the pressure resistance of the system.

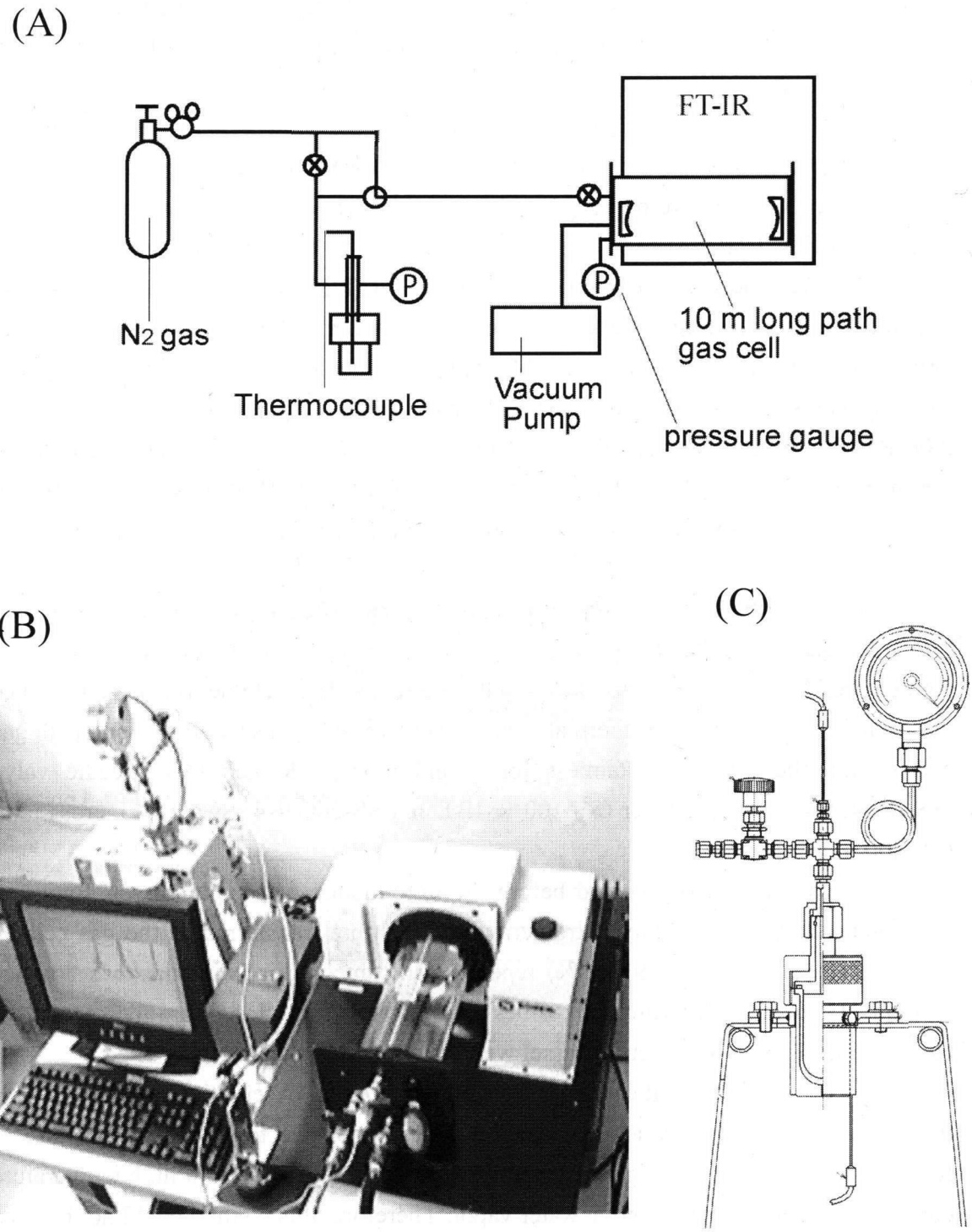

Figure 2.1.3. The reaction gas cell FT-IR system (MB154, Bomem). (A) The schematic configuration of the whole system, (B) the photograph, and (C) schematic configuration of the optics and the hydrothermal reaction vessel

The PTFE inner bottle consists of a cap and a cylindrical main body (Fig.2.1.3). Their junction is sealed by a Viton o-ring to prevent a pressure leak. The temperature of the hydrothermal vessel is maintained by the band heater surrounding the stainless container and is regulated by a temperature control system. The band heater is heated by 100V AC current with an electric power of 300W.

SUS316 sheathed chromel-alumel thermocouple (K-type, 1/8 inch diameter, length: 300mm) was placed inside the Teflon hydrothermal reaction vessel for measuring the temperature of sample solutions (Fig 2.1.3). The temperature controller (DZ1000 series, CHINO) regulates the sample solution temperature measured by the above thermocouple. Another temperature controller (FCS series, Shinko technos Co.) regulates the temperature outside the stainless container and protects the overheating. Temperature precisions are ±1°C both for the thermocouple and controller.

The pressure gage is made of SUS316 with a working pressure range from –0.1 to 2.0MPa. This gage is connected to the stainless reaction vessel and gas outlet and liners via needle valve (SS-IRS4, Swagelok), reducer (SS-100-R-4BT and SS-200-R-4, Swagelok) and cross joint (SS-400-4, Swagelok)(Fig 2.1.4).

2.1.2.4. Long-path gas cell FT-IR combined with the hydrothermal reaction vessel

The steel-lined PTFE (Teflon) reaction vessel was directly connected to a long path gas cell (10 m path length) placed in the FT-IR (MB154, Bomem) (Fig. 2.1.3). The gas outlet line from the hydrothermal reaction vessel was connected to the long path gas cell though the following stainless joints and tubes, 1/8 inch tube, needle valve (SS-IRS4, Swagelok), reducer (SS-100-R-4BT and SS-200-R-4, Swagelok), cross joint (SS-400-4, Swagelok).

The gas cell was evacuated before the introduction of sample gasses. Emission gases generated in the above hydrothermal vessel were transferred to the gas cell by flowing N_2 gas (purify; 99.9999~%) repeating six times. This is similar to headspace method. By means of repeating six times of this gas substitution, more than 99.8% of gas phase initially in the reaction vessel were transferred to the gas cell.

However, this method could not be applied to *in-situ* observation of hydrothermal reactions. The gas cell has a problem with water vapor due to hygroscopic nature of KBr windows. Because of high vapor pressure of aqueous solutions at high temperature condition, it is difficult to remove water vapor. Therefore, this method could not be used to monitor continuously volatiles emitted from the hydrothermal reaction vessel.

2.1.2.5. Continuous analysis of emission gases by reaction gas cell FT-IR

In order to develop, a reaction gas cell FT-IR system which can collect continuously gaseous products from the hydrothermal reaction vessel, a gas filter

(A)

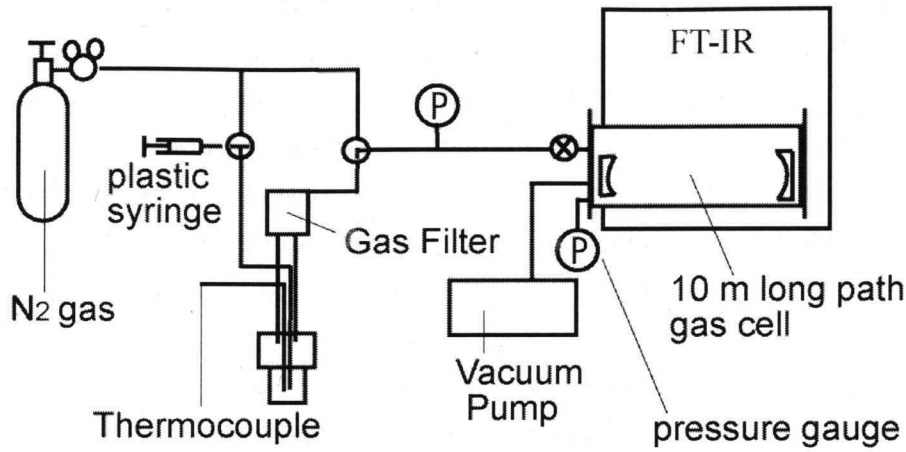

(B)

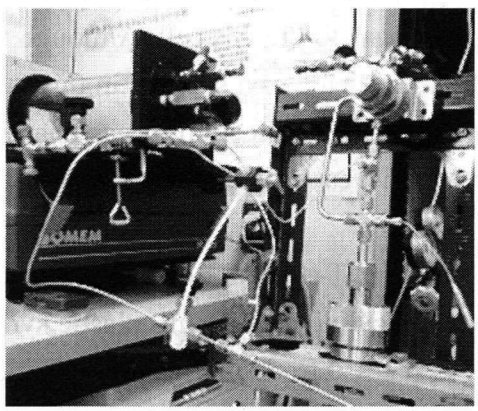

(C)

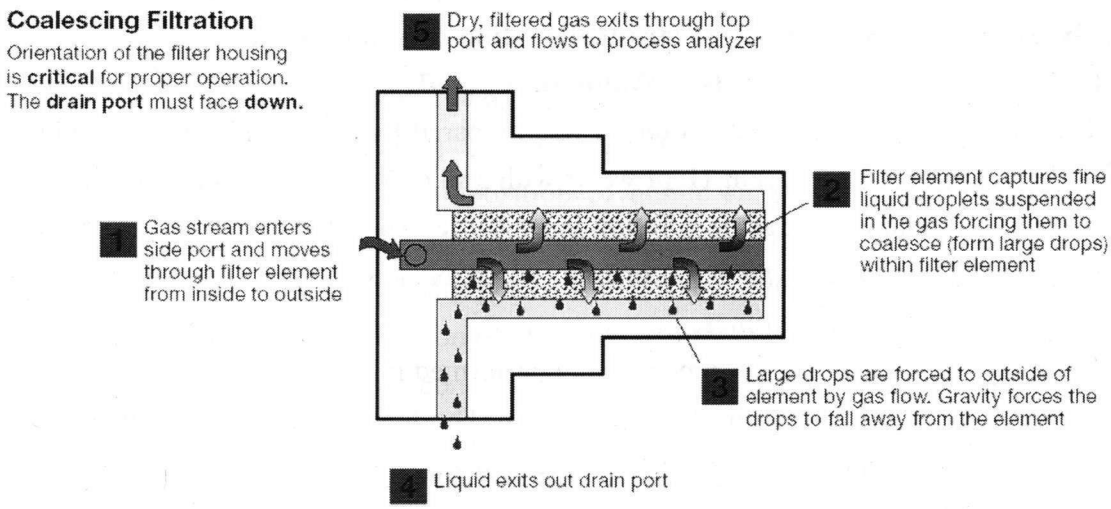

Swagelok homepage: www.swagelok.com MS-02-82

Figure 2.1.4. 10 m long path gas cell FT-IR spectrometer (MB154, Bomem) connected to a steel-lined PTFE (Teflon) hydrothermal reaction vessel. (A) The schematic configuration of the whole system, (B) the photograph of the connecting pats, and © the details of the gas filter.

(SS-FCB, Swagelok) was added in the line (Fig.2.1.4). This filter makes only filtered gas flow to gas cell and makes liquid droplet in the gas form large droplet and exit out from the drain port (Fig. 2.1.4C). Gaseous products during the hydrothermal reactions were extracted by bubbling of the nitrogen gas in the reaction vessel and transferred through the gas filter to the long path gas cell FT-IR (Fig. 2.1.4A) to measure their IR spectra. The gas bubbling tube (1/16 inch, PEEK) was inserted into the bottom of PTFE inner bottle in the vessel. Bubbling volume is regulated by needle valve and pressure gage.

There are two methods, headspace and purge & trap method for extracting emission gas in humic substances solution. Headspace methods are transportation by gas phase in closed system. However, headspace method is unsuitable for dissolved gas fraction. Purge & trap method are transportation by bubbling carrier gas. The purge and trap method can transport dissolved gas to the gas cell. Although the headspace method is only a few volume of gas phase extracted as a sample, in this method all the emission gas were introduced into the gas cell. The collection of gas phase were performed with N_2 gas up to 3 atm in the reaction vessel then transferred to the gas cell at 1 atm pressure.

For the sampling of a solution, T-shaped stopcock was added in a halfway of bubbling tube from the nitrogen gas cylinder. A 20 mL plastic syringe, connected to the side of T-shaped stopcock, is used for introducing sample solutions and for sampling products (Fig.2.1.4A).

2.1.3. Hydrothermal experiments for transformation of humic substances

2.1.3.1. Hydrothermal experiments of Wako humic acid

100 mg L^{-1} Wako humic acid solution was prepared by putting 100mg of humic acid powder reagent (Wako Co.) in 1L of water with 5ml of 0.1M NaOH solution. 30ml of these sample solutions were set in a Teflon inner bottle. Air in the reaction vessel was substituted by N_2 gas (purify; 99.5~%) or high purity N_2 gas (purify; 99.9999~%) by repeating gas injection of three times.

Thermal decomposition experiments were performed in the hydrothermal reaction vessel (Fig.2.1.3) at 140°C during 4 to 100 hours. The temperature of hydrothermal experiments was maintained by a band heater surrounding the stainless container and regulated by the temperature controller with a thermocouple placed inside the Teflon hydrothermal reaction vessel (Fig.2.1.3).

After the heating experiments, reaction vessels were cooled at room temperature. Emission gas was introduced to the gas cell by substitution of N_2 gas (purify; 99.9999~%) repeating six times. More than 99.5% of emission gas is considered to be introduced in the gas cell. This was confirmed by a pilot study that atmospheric CO_2

was introduced from the reaction vessel to the gas cell with a path length of 10 m set in an FT-IR spectrometer. IR spectra were recorded by 128 scans with a wavenumber resolution of 1 cm^{-1}. The gas cell was covered with an aluminum foil to protect from the light exposure during the FT-IR measurement.

2.1.3.2. Hydrothermal experiments of Nordic fulvic acid

100 mg L^{-1} Nordic fulvic acid solution was prepared by putting 100 mg of powder reagent (IHSS reference sample) in 1L of water. The ionic strength of the fulvic acid solution was adjusted to 0.001 M by adding 58.5 mg of NaCl in 1 L of water. 30 mL of these sample solutions were set in a Teflon inner bottle. Air in the reaction vessel was substituted by N_2 gas (purify; 99.5~%) by repeating gas injection of three times and by N_2 gas (purify; 99.9999~%) by repeating gas injection of three times. Thermal decomposition experiment was performed at 140 °C during 4 to 60 hours. The temperature of hydrothermal experiments was maintained by a band heater surrounding the stainless container and regulated by the temperature controller with a thermocouple placed inside the Teflon hydrothermal reaction vessel (Fig.2.1.3). After the heating experiments, reaction vessels were cooled at room temperature. Emission gas was introduced to the gas cell by substitution of N_2 gas (purify; 99.9999~%) repeating six times. IR spectra were recorded by 128 scans with a wavenumber resolution of 1 cm^{-1}. The gas cell was covered with an aluminum foil to protect from the light exposure during the FT-IR measurement.

2.1.4. RESULTS

2.1.4.1 Volatile species from the hydrothermal transformation of humic substances

The following volatile species (CO_2 and CO and unknown ether-like compounds) are detected by thermal decomposition of humic substances (Wako humic acid and Nordic fulvic acid) (Fig.2.1.5). Gaseous CO_2 shows some sharp peaks from 2300 to 2400 cm^{-1}. CO also shows sharp peaks from 2100 to 2200 cm^{-1}. The peak of 1150 cm^{-1} may be C-O stretching vibration of ether-like compounds. The IR absorption intensities of these peaks correspond to concentrations of these compounds.

2.1.4.2. Calibrations for CO and CO_2

CO contents of gaseous products by the gas cell FT-IR method were calibrated by standard gas mixtures of CO in N_2 as shown in Fig.2.1.6. By plotting absorption intensities (peak heights) at 2172 cm^{-1} (C-O stretching vibration) against the introduced volume concentrations of CO with 0.2, 0.4, 0.8, 1.0, 2.0 ppmV, a good linear relation was observed: $y = 0.0075x + 0.0008$, where y is the absorption intensity at 2172 cm^{-1} and x is the concentration of CO (ppmV) (Fig.2.1.6a). This linearity does not hold for

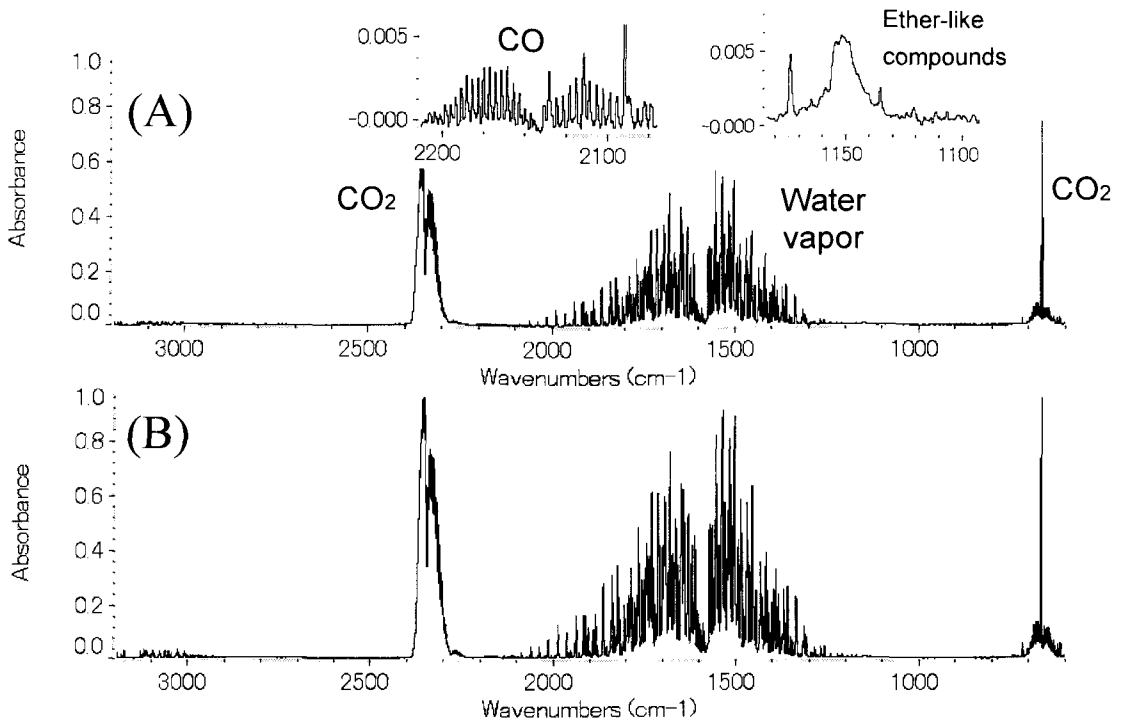

Figure 2.1.5. Typical IR spectra of volatile species emitted from the hydrothermal transformation of humic substances: (A) Wako humic substance heated at 140℃ for 20 hours (B) Nordic fulvic acid heated at 140℃ for 24 hours.

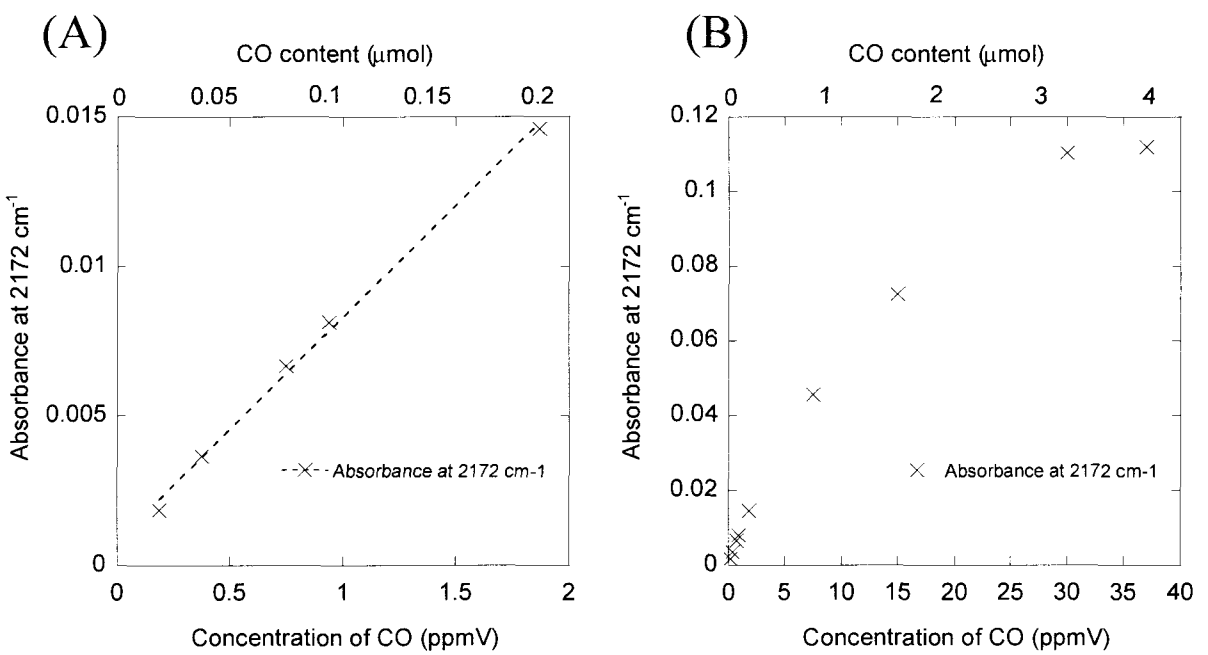

Fig. 2.1.6. Calibration lines for CO concentrations by IR absorbance at 2172 cm^{-1} by means of long-path gas cell FT-IR (A) with 0.2, 0.4, 0.8, 1.0 and 2.0 ppmV CO and (B) with 0.2, 0.4, 0.8, 1.0, 2.0, 7.5, 15, 30 and 37 ppmV CO.

higher concentration of CO (> 2 ppmV) as shown in Fig.2.1.6b. Therefore, the calibration line of CO is only valid from 0.2 to 2 ppmV. The detection limit of CO was about 0.1 μL L^{-1} (0.1 ppmV), but the quantitative measurement can be safely expected for concentrations of 1 ~ 2 ppmV.

CO_2 contents were calibrated by standard gas mixtures of CO_2 in N_2 as shown in Fig.2.1.7. By plotting absorption intensites (peak heights) at 2360 cm^{-1} and 2340 cm^{-1} (C-O stretching vibration) and the peak area from 2200 to 2400 cm^{-1} against the introduced volume concentrations of CO_2 with 1.0, 2.0, 3.0, 4.0 ppmV, good linear relations were obtained for CO_2: $y_{2360} = + 0.0286x + 0.0016$, $y_{2340} = + 0.0231x + 0.0003$ and $y_{area} = + 1.179\ x + 0.017$, where y_{2360} and y_{2340} is the absorption intensity at 2360 cm^{-1} and 2340 cm^{-1}, y_{area} is the peak area from 2200 to 2400 cm^{-1} and x is the concentration of CO_2 (ppmV)(Fig.2.1.7). There linearlities does not extend over about 4 ppmV (Fig. 2.1.7b). The linear calibration lines of CO_2 are then effective from 1 ppm to 4 ppmV. The detection limit of CO_2 was about 0.1 μL L^{-1} (0.1 ppmV), but the quantitative measurement can be safely expected for CO_2 concentrations for 1 to 4 ppmV.

Therefore, the reaction gas cell FT-IR system can be used to determine quantitatively CO and CO_2 concentrations in the gaseous reaction products.

2.1.4.3. Hydrothermal experiments of humic substances

By using the reaction gas cell FT-IR system, CO_2, CO and the peak at 1152 cm^{-1} were detected from the thermal decomposition of humic substances. As shown in Fig.2.1.5, gaseous CO_2 shows fine sharp peaks from 2300 to 2400 cm^{-1}. Experimental data for the increase in CO_2 as a function of time are plotted in Fig.2.1.8 for 140°C heating. The CO_2 contents rapidly increased until 12 hours and the increase became gentle after 12 hours heating. CO also shows fine sharp peaks from 2100 to 2200 cm^{-1} (Fig.2.1.5). Experimental data for the increase in CO as a function of time are plotted in Fig.2.1.9 for 140°C heating. CO emission gradually increased with time.

The peak at 1152 cm^{-1} can be attributed to C-O stretching vibration of ether like compounds (Fig.2.1.11). Experimental data for the increase in absorbance at 1152 cm^{-1} as a function of time are plotted in Fig.2.1.10 for 140°C heating. Absorbance at 1152 cm^{-1} gradually increased with time.

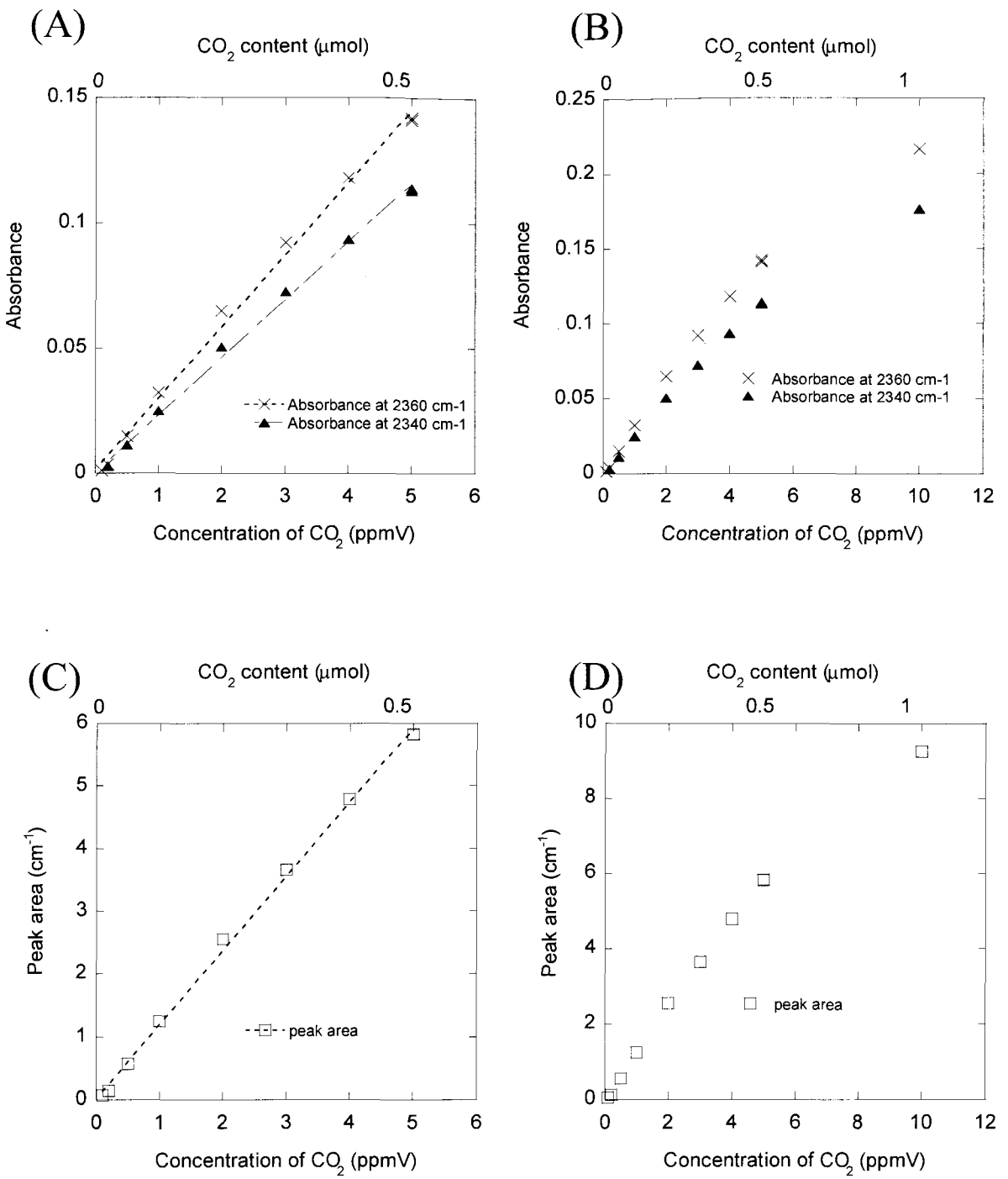

Fig. 2.1.7. Calibration lines for CO_2 concentrations by IR absorbance at 2360 cm^{-1} and 2340 cm^{-1} by means of long-path gas cell FT-IR (A) with 1.0, 2.0, 3.0, 4.0 and 5.0 ppmV CO_2 and (B) with 1.0, 2.0, 3.0, 4.0, 5.0 and 10.0 ppmV CO_2 (C) Peak area with 1.0, 2.0, 3.0, 4.0 and 5.0 ppmV CO_2 and (D) Peak area with 1.0, 2.0, 3.0, 4.0, 5.0 and 10.0 ppmV CO_2

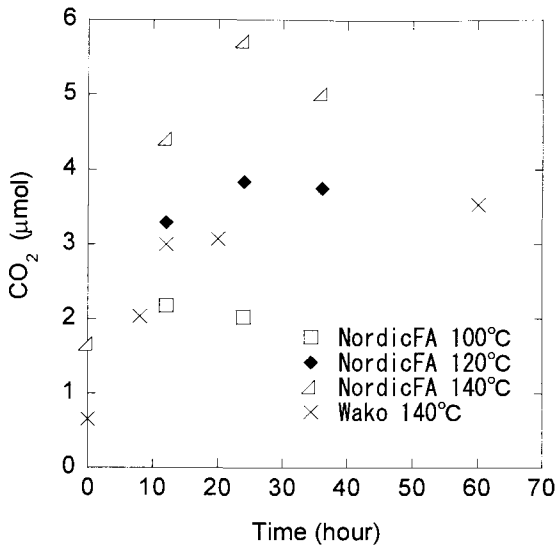

Fig. 2.1.8. Temporal changes in CO_2 emission from Nordic fulvic acid solutions heated at 100 °C, 120 °C and 140 °C and of Wako humic acid heated at 140 °C.

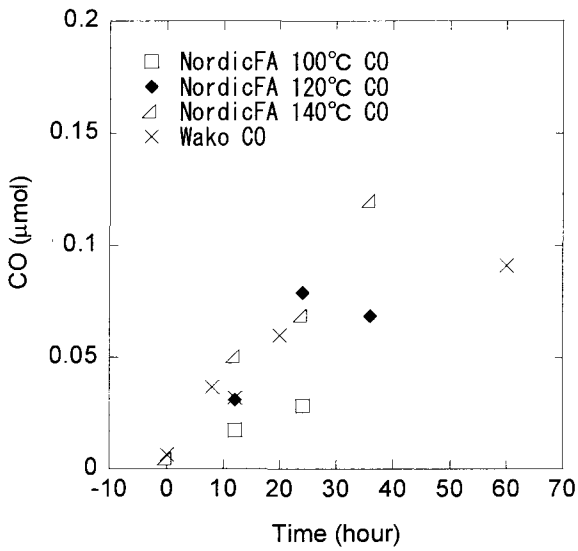

Fig. 2.1.9. Temporal changes in CO emission from Nordic fulvic acid solutions heated at 100 °C, 120 °C and 140 °C and from Wako humic acid heated at 140 °C.

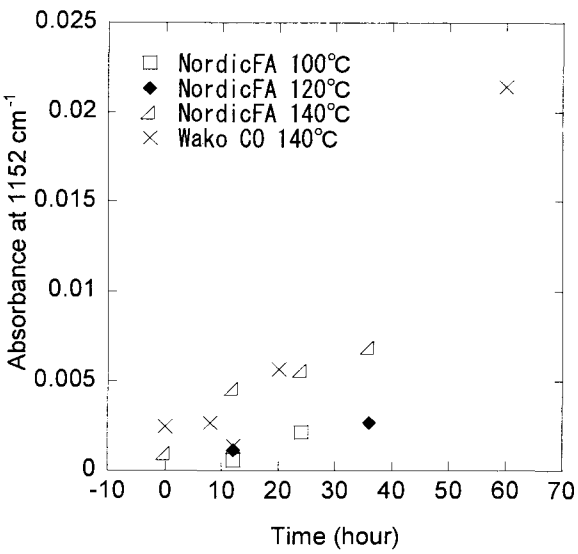

Fig. 2.1.10. Temporal changes in unkown ether-like compound formed from Nordic fulvic acid solutions heated at 100 °C, 120 °C and 140 °C and from Wako humic acid heated at 140 °C.

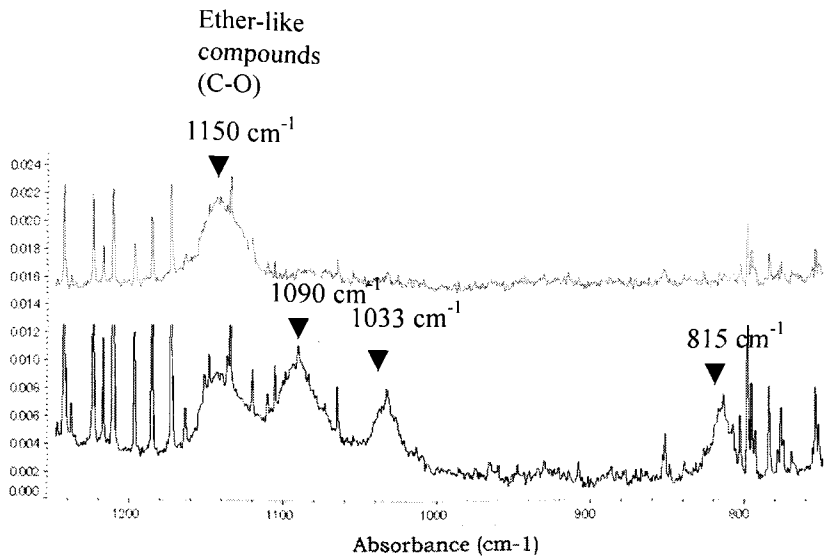

Fig. 2.1.11. IR spectra of emitted gas from Wako humic acid (100 mg L^{-1}, ionic strength: 0.5M) under hydrothermal conditions a) for 24 hours heating at 140 °C and b) for 24 hours heating at 140°C and left for 40 hours at room temperature.

2.1.5.DISCUSSION

2.1.5.1. Emission of gaseous compounds from hydrothermal transformation of humic substances

The emission and increase of CO_2, CO and an unknown C-O compound were observed by a long path (10 m) gas cell FT-IR directly connected to the hydrothermal reaction vessel. CO_2 emission probably originated from carboxyl groups. Therefore, the CO_2 emission is a strong evidence for the occurrence of decarboxylation reaction of humic substances.

The decarboxylation reaction via a carbanion transition state has been described for galic acid (Boles et al., 1988), and is thought to proceed as follows:

$$1)\ ArCOO^- \xrightarrow{k_1} Ar^- + CO_2\ (slow)$$
$$2)\ Ar^- + H_2O \xrightarrow{k_2} Ar\text{-}H + OH^-\ (fast)$$

Ar = aromatic hydrocarbon

Based on the earlier works by Hallem et al. and Li and Brill, the decarboxylation reaction follows the first order reaction. Therefore, CO_2 emission can be written as follows:

$$CO_2\ \text{emission} = C_{COOH}\ (1 - \exp(-k_1 x))$$

Experimental data for the increase in CO_2 as a function of time are plotted in Fig.2.1.8 at 100, 120, 140°C heating. By applying the above first order rate law, the rate

constants for CO_2 were determined to be 3.6×10^{-5} s^{-1} (140°C) in the hydrothermal experiment of Wako humic acid and 3.7×10^{-5} s^{-1} (140°C) for Nordic fulvic acid. Assuming that all the CO_2 emission is derived from the decarboxylation reaction of Nordic fulvic acid, CO_2 was produced from only 5-17% of the initial –COOH.

On the other hand, the increase trend of CO emission was different from that of CO_2 emission (Fig.2.1.9). Although CO_2 emission rapidly increased before 8 hours in Wako humic acid and before 24 hours in Nordic fulvic acid, increase of CO emissions were relatively slow as shown in Fig.2.1.9. The obtained first order rate constants of CO are 1.2×10^{-5} s^{-1} (140°C) in hydrothermal experiment of Wako humic acid and 1.1×10^{-6} s^{-1} (140°C) for Nordic fulvic acid.

The kinetic differences indicated that the CO emission might not be derived from the decarboxylation. However, the origin of CO might be C-O or C=O structure of dissolved humic substances such as ether or carbonyl groups. If CO is derived from carbonyl groups in humic substances, 0.1-0.9% of initial carbonyl groups were decomposed to CO because carbonyl contents was 10% of the total carbon. It is often reported that CO was emitted from decomposition of organic compounds under reducing environments (Krevelen, 1993). The atmosphere of the present experiment was not reducing but without atmospheric oxygen due to substitution of nitrogen gas for the reaction vessel. N_2 substituted atmosphere might be favorable for CO production. It should be noted that the CO emission was much smaller than the CO_2 emission.

Unknown ether like compound (a peak at 1150 cm^{-1}) was observed in all emission gases of hydrothermal experiments of humic substances including Wako humic acid and Nordic fulvic acid (Fig.2.1.11a). The reaction gas was diluted with N_2 gas to obtain a calibration for this ether-like compound. By plotting the absorption intensity (peak heights) at 1150 cm^{-1} against the dilution ratio, a good linear relation was obtained for the unknown ether-like compound. The emission gas was left for 40 hours at room temperature and IR spectrum was again measured. Additional peaks were observed at 1090, 1033 and 815 cm^{-1} (Fig.2.1.11b). The attributions of these bands are not clear yet.

All these results suggest that dissolved humic substances mainly decompose by the decarboxylation reaction leading to the CO_2 formation under hydrothermal conditions.

REFERENCE

Brill. T.B., Savage, P. E. (2004), Aqueous systems at elevated temperatures and pressures, in *physical chemistry in water, steam, and hydrothermal solutions* (eds. Palmer, D. A., Fernandez-Prini, R., Harvey, A. H.), Amsterdam; Boston: Elsevier.

Lumsdom D. G. and Fraser A. R. (2005) Infrared spectroscopic evidence supporting heterogeneous site binding models for humic substances. *Environmental Science Technology*, **39**, 6624-6631

Celi L., Schnitzer M. and Negre M. (1997) Analysis of carboxyl groups in soil humic acids by a wet chemical method, Fourier-transform infrared spectrophotometry, and solution state carbon –13 nuclear magnetic resonance. A comparative study, *Soil Science*, **162**, 189-197

Hanst P. L., Lefohn A. S. and Gay Jr B. W. (1973) Applied Spectroscopy, **27**, 188

Hanst P. L. and Hanst S. T. (1994) in "*Air Monitoring by Spestroscopic Techniques*", (ed. M. W. Sigrist) Chemical Analysis Series 127, New York: John Wiley and Sons, pp.335-470

Johnson G. C. (2002) Water quality of spring in the valley and ridge physiographic province in the upper Tennessee, U. S. geological survey, Water-resources investigations report 02-4180

Lu, X. Q. et al. (1997) Thermal stability of humic substances and their metal forms: an investigation using FTIR emission spectroscopy., *Journal of Analytical Applied Pyrolysis*, **43**, 103-114

Masuda, K. (2005) Development of *in-situ* heating spectroscopic methods for aqueous organic reactions, Doctral thesis, Department of Earth and Space Sciences, Tokyo Institute of Technology

Nakashima, S. (1992a) Complexation and reduction of uranium by lignite., *Science of the Total Environment*, **117/118**, 425-437

Nakashima, S. (1992b) Kinetics and thermodynamics of U reduction by natural and simple organic matter., *Organic Geochemistry*, **19**, 421-430

van Krevelen D. W. (1993) *Coal: typology-physics-chemistry-constitution* 3rd, completely revised edition, Amsterdam; New York, Elsevier Science Pub. B.V.

2.2. *in-situ* UV-VIS spectroscopy for monitoring the hydrothermal transformation of humic substances

2.2.1. INTRODUCTION

Among in-situ spectroscopic methods, UV-VIS spectroscopy (Bennett and Johnston, 1994; Ferry and Fox, 1998; Kawamura, 2002) do not provide detailed information on chemical forms of organics comparing with Raman spectroscopies. (Steeper et al., 1992; Belsky and Brill, 1998; Freitag et al., 2001) and FT-IR (Kieke et al., 1996; Schoppelrei et al., 1996; Ikushima et al., 1999; Brill, 2000; Hoffman et al., 2000; Gorbaty and Bondarenko, 1999; Furutaka and Ikawa, 2000; Kazarian and Martirosyan, 2002; Zhang and Hu, 2004) Nevertheless, UV-VIS spectroscopy is appropriate for the observation of dilute aqueous solutions, because it is sensitive to trace concentrations of organics and also because the solvent water does not interfere with the objective organics on UV absorption spectra in the range of 200-800 nm. As far as I surveyed, if any (Wang et al, 2002), only a few studies have been reported on in-situ UV-VIS spectroscopy for static hydrothermal reactions in the presence of minerals. In the present study, we have newly constructed a real time UV spectroscopy system equipped with a static reactor for hydrothermal solutions up to 200 °C. This system is useful to obtain both kinetic and equilibrium data on hydrothermal reactions of dissolved organics in the presence / absence of minerals.

2.2.2. EXPERIMENTAL METHODS

2.2.2.1 Principles of UV-VIS spectroscopy

Ultraviolet-Visible (UV-VIS) spectroscopy observes electronic excitation of molecules by absorption of ultraviolet or visible light (Heinz-Helmut Perkampus, 1992). UV light induces electronic transition from ground to excited states as shown in Fig 2.2.1. UV excitation of organic compounds are mainly related to $\pi \rightarrow \pi^*$ transition and $n \rightarrow \pi^*$ transitions. The $\pi \rightarrow \pi^*$ transition is derived from conjugated π electron structures such as aromatic structure and unsaturated C=C double bond. This transition is known to have large molar absorption coefficient, $\varepsilon_{max} > 10{,}000$ (Pretsch et al, 2000). The C=O double bond causes $n \rightarrow \pi^*$ transition, which is at relatively longer wavelength with smaller molar absorption coefficient: ε_{max} is about 100 or less (Pretsch et al, 2000).

The $\pi \rightarrow \pi^*$ transition of the π bond in C-C single bond needs high energy corresponding to very short wavelength of UV. This absorption spectrum can be understood by the following detailed explanation of electronic energy levels in benzene molecules from Jaffe and Orchin (1962). Electrons in the ground state (designated as $^1A_{1g}$) may absorb quanta of light and be promoted to π-antibonding orbitals, corresponding to energy levels denoted as $^1E_{2u}$, $^1B_{1u}$ or $^1B_{2u}$ (Fig.2.2.1).

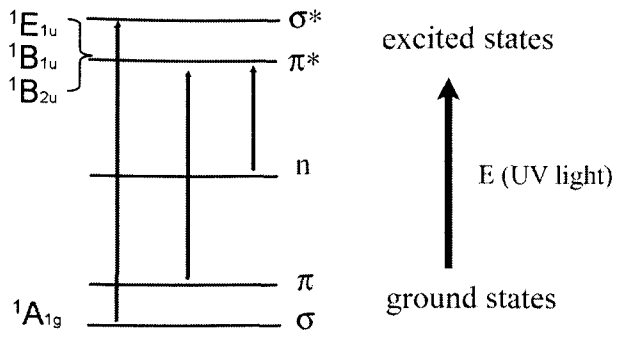

Fig.2.2.1 Schematic diagram of electron energy levels for σ and π bonds in organic compounds and some transitions among them

The Lambert-Beer's law provides a direct link between UV-spectra and the concentration of a solute: Abs = ε c l. Abs is the absorbance in UV-VIS spectra, ε is the molar absorption coefficient, c is the concentration of dissolved substance, l is the optical path length. UV-Visible spectra can therefore be used to determine concentration of solutes.

2.2.2.2. in-situ UV cell

A commercial heatable cell (HARRICK Scientific Corp., Temperature controlled demountable liquid cell) modified by Masuda (2005) was used for in-situ UV monitoring (Masuda, 2005; Fig. 2.2.2, Fig.2.2.3a-f). Calcium fluoride (CaF_2) optical windows of 2 mm thick and 13 mm in diameter (Fig.2.2.3d) are compressed by a piston and a cylinder through Kalrez® O-rings. A Teflon® gasket of 0.5 mm thick and 8 mm inner diameter was sandwiched between these windows to generate 25 μL sample chamber. The maximum temperature of static reactor is 200 °C due to thermal stability of the Teflon® gasket.

2.2.2.3. UV-VIS measurement

Sample solutions were heated at 80 °C for 24 hours using a heatable liquid cell set in an UV-VIS spectrophotometer (Jasco V-530). About 40 μL of 500 mg L^{-1} fulvic acid solution was injected in the sample chamber by a micro syringe (Fig.2.2.3e). UV spectra in the static hydrothermal cell have been measured every 2 minutes at a scanning speed of 1000 nm/min with the resolution of 0.5 nm in the 226-800 nm spectral range. Based on this study, hydrothermal transformation of organic compounds with time and temperature will be discussed (Chapter 3-3).

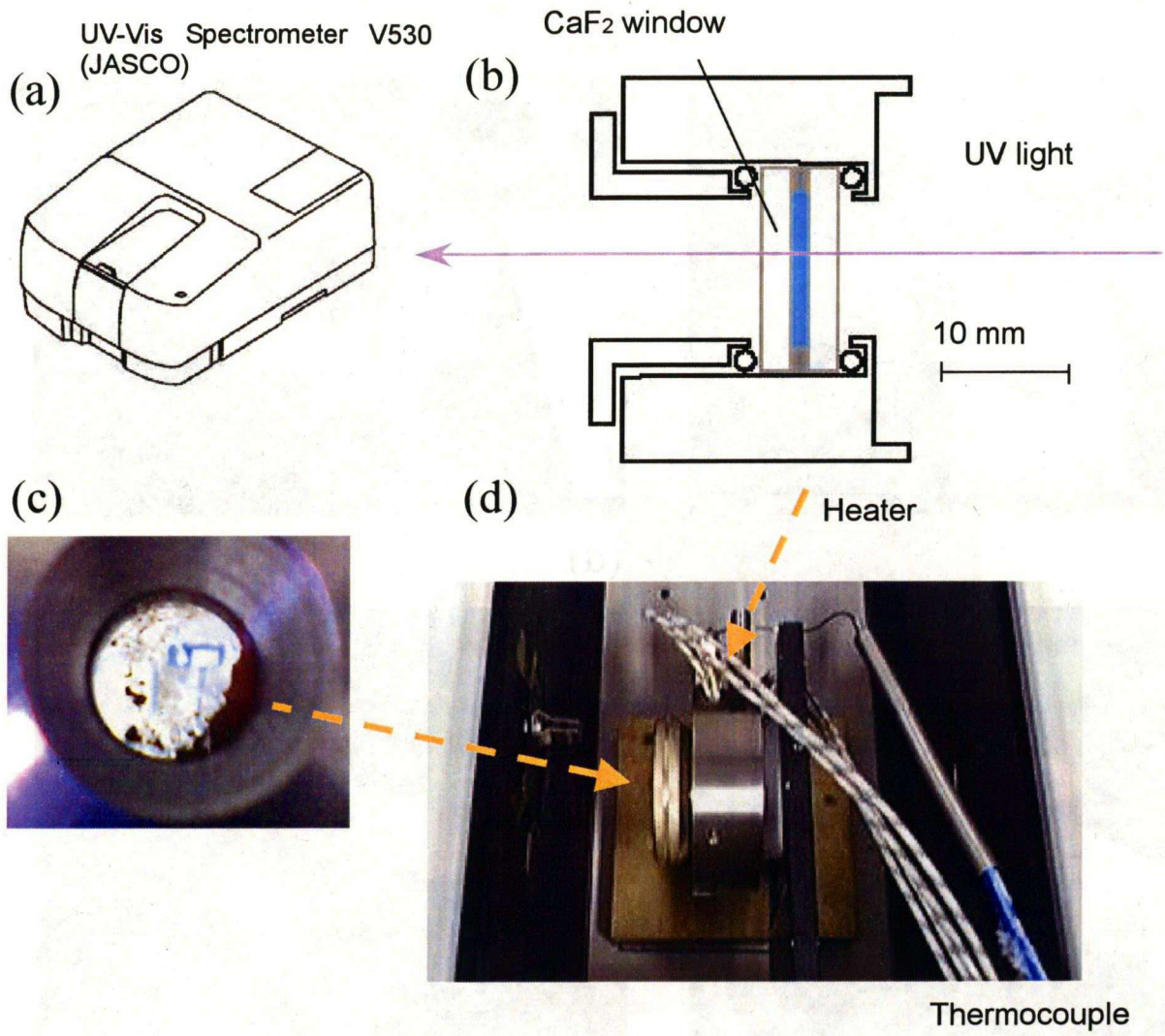

Figure 2.2.2 a) The UV-VIS spectrometer (V530, Jasco) b) Schematic side view of the *in-situ* UV-cell c) photographic view of the CaF_2 window with humic solutions d) photographic view of the *in-situ* UV cell set in the UV-VIS spectrometer.

2.2.2.4. in-situ measurement in the presence of minerals

In situ hydrothermal experiments were conducted at 80 °C for 0 to 24 hours with representative minerals; goethite (synthesized after Cornel and Schwertmann, 1996.), hematite (rare metallic Co.), and two commercial silica gel (Wako Co. WakoSil C-300 and WakoSil 25 Sil) using the heatable liquid cell set in the UV-Vis spectrophotometer (V-530, Jasco). Because the synthesized goethite have alkaline ion adsorbed during precipitation, the sample goethite powder was preliminary re-precipitated at pH 4 avoiding the pH change (Fig 2.2.4a,b). 1.25 mg of mineral powders were added to 25 µL of 500 mg L^{-1} fulvic acid solution in the heatable liquid cell, respectively (Fig.2.2.4

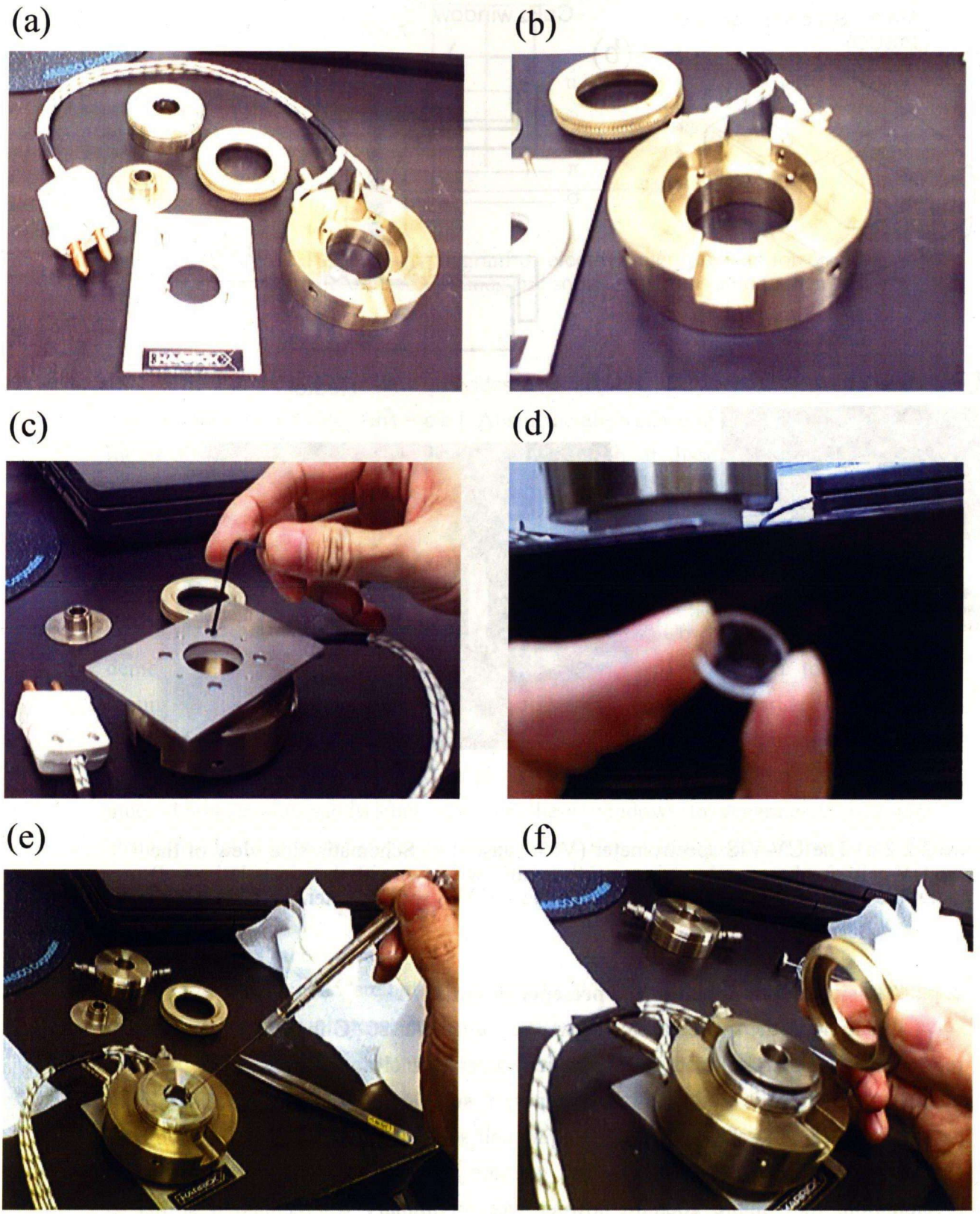

Figure 2.2.3. The photographs for the experimental setting up of the *in-situ* UV cell.

c, d). UV-VIS spectra of the mixture were measured every 2 minutes while heating at 80 °C at a scanning speed of 1000 nm/min with the resolution of 0.5 nm in the 226-800 nm spectral range.

The weight ratio of minerals to fulvic acid was set to 100 for the batch and in situ hydrothermal experiments.

Based on this study, hydrothermal transformation of organic compounds with time and temperature on the surface of goethite will be discussed (Chapter 4).

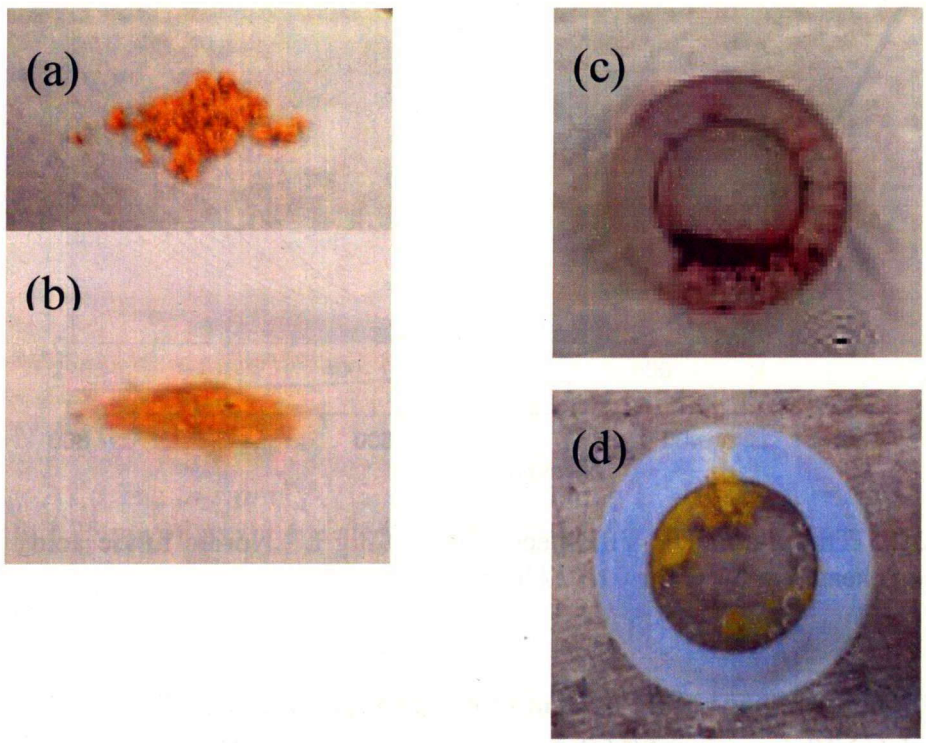

Figure 2.2.4. The hydrothermal cell for *in-situ* UV-VIS spectroscopy. Photographs for the goethite powder (a) synthesized, (b) re-precipitated at pH 4, and photographs for the solution sample with (c) hematite, (d) goethite mounted in the CaF_2 windows

2.2.3. RESULTS

2.2.3.1 in-situ UV-VIS measurement of the fulvic acid

Sample solutions were heated at 80 °C for 27 hours by using in-situ cell. In-situ UV-VIS spectra at every 9 minutes are shown in Fig. 2.2.5. While the spectral changes were successfully measured by the in-situ UV-VIS apparatus, there is no significant change in the spectra during 27 hours.

The absorption intensity (absorbance) at 254 nm of the fulvic acid solution due to π-π^* electron transition originated from substituted aromatic structures is commonly used as a measure of dissolved organic matter contents (Korshin et al, 1997). Therefore, the 254 nm absorbance values of the product solutions were plotted against time in

Figure 2.2.7. The in situ data for the 254 nm absorbance showed a slow slight decrease at 80 °C

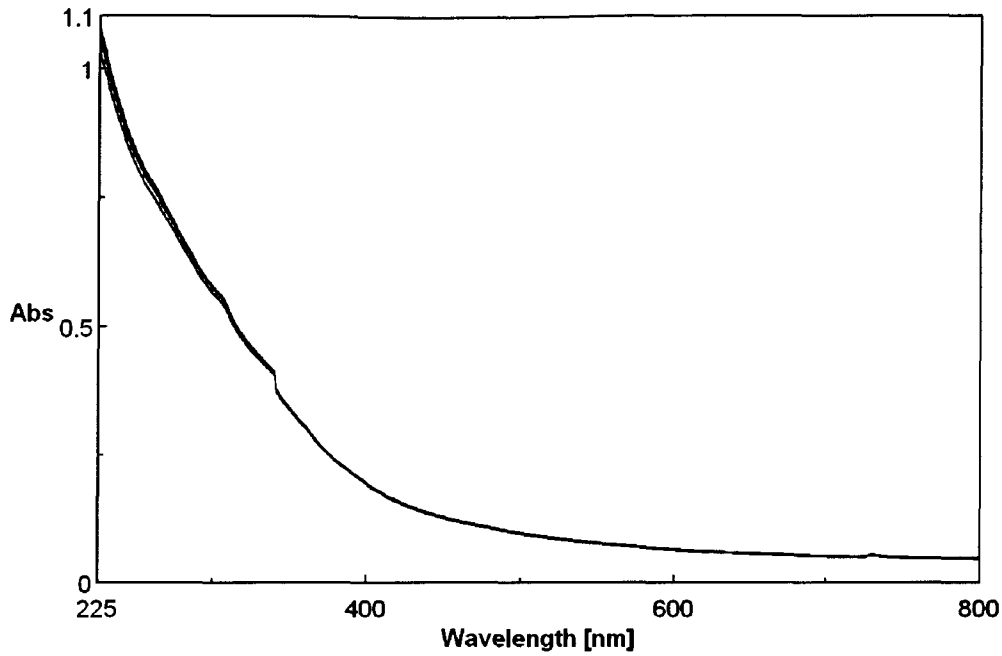

Fig. 2.2.5 The *in-situ* UV-VIS spectra of 500 mg L^{-1} Nordic fulvic acid solutions heated at 80°C for 0 to 27 hours.

2.2.3.2 in-situ measurement of fulvic acid in the presence of minerals

In-situ UV-VIS spectra at 80 °C at every 10 minutes for 27 hours with goethite are shown in Fig. 2.2.6. In the presence of goethite, UV-VIS spectra rapidly decreased. The UV-VIS spectra of product solutions at 80 °C for 14 hours (50000 seconds) with silica gels (WakoSil C-300 and WakoSil 25 Sil) only show small difference from that of the initial Nordic fulvic acid solution (Fig. 2.2.7A). On the other hand, the spectra with hematite and goethite showed drastic decrease in their absorbances already within 3 hours.

In the presence of silica gels, the 254 nm absorbance showed only a slight decrease by heating at 80 °C for 24 hours (Fig.2.2.7A). It decreased to about 0.99 of the initial value of Nordic fulvic acid in the presence of WakoSil C-300 and about 0.9 in the presence of WakoSil-25Sil. On the other hand, they decreased to about 0.8 and 0.2 of the initial value within 3 hours and remain mostly unchanged around 0.7 and 0.1 in the presence of hematite and goethite.

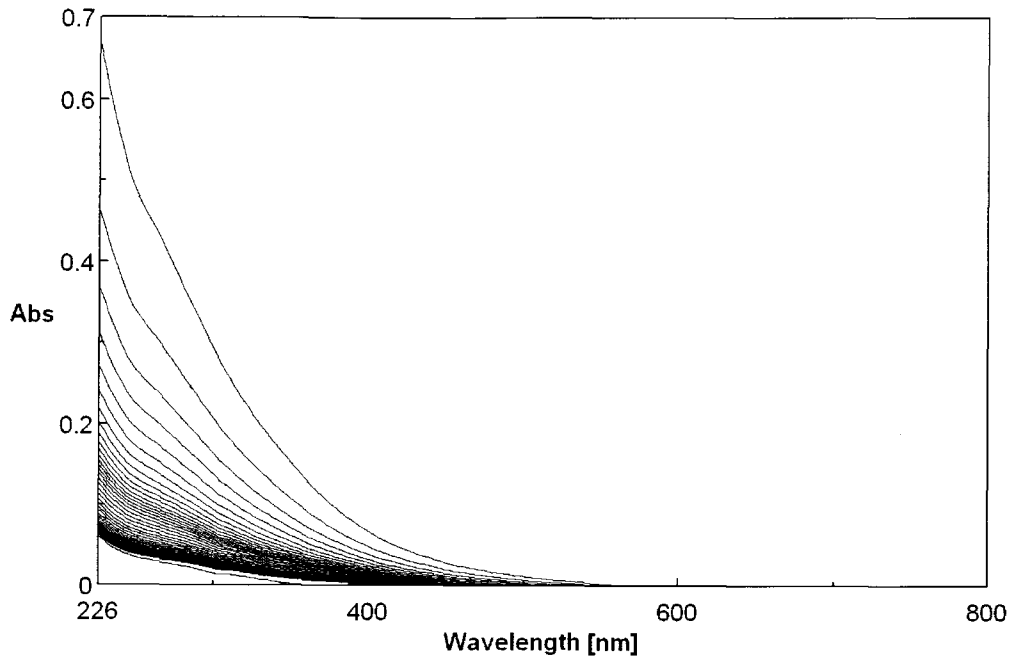

Fig. 2.2.6 The *in-situ* UV-VIS spectra of 500 mg L^{-1} Nordic fulvic acid solutions with 1.25 mg of goethite heated at 80°C for 0 to 27 hours.

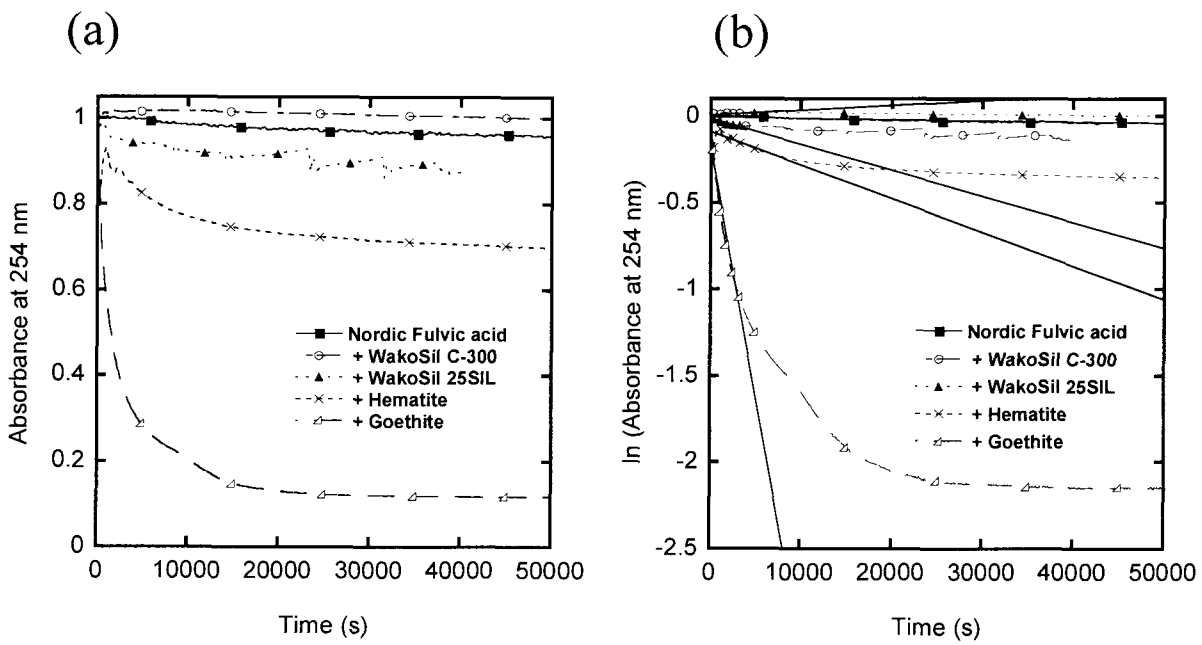

Figure 2.2.7. Changes with time in the (a) absorbance at 254 nm (b) logarithm of absorbance at 254 nm at 80 °C in the presence / absence of silica gels (WakoSil C-300 and 25Sil), hematite and goethite during in situ hydrothermal experiments. The value of the absorbance at 254 nm was derived by the initial value.

2.2.4. DISCUSSION

2.2.4.1 The stability of fulvic acid in hydrothermal solutions with ultraviolet radiation

In the 80 °C condition during 27 hours, there is only small decrease for absorbance at 254 nm. This decrease might be due to degradation of substituted aromatic in the chemical structure of fulvic acid. Comparing to the batch hydrothermal transformation data as shown in Chapter 3.2., The absorbance decrease at 254 nm of in-situ data is in good agreement with the that of batch data. Therefore, effect of ultraviolet radiation, which is continuous for the *in-situ* experiments, can be negligible.

2.2.4.2 The interaction of fulvic acid in the presence of minerals

The 254 nm absorbance decrease with goethite is very rapid at the initial stage but become slow at the later stage leaching to a constant value indicating participation of several processes (Fig.2.2.7A).

These processes can be simulated, for instance, by the sum of two independent first order reactions or the successive three first order reactions. Only the data until 1 hour showing a quasi-linear trend in a semi-logarithmic diagram (Fig.2.2.7B) can be simply fitted by exponential curves to obtain the apparent first order reaction rate constants $k_1^{UV} = 3 \times 10^{-6}$ (s^{-1}) for WakoSil C-300, $k_1^{UV} = 2 \times 10^{-5}$ (s^{-1}) for WakoSil-25Sil, $k_1^{UV} = 2 \times 10^{-5}$ (s^{-1}) for hematite and $k_1^{UV} = 3 \times 10^{-4}$ (s^{-1}) for goethite. Since this value is on the same order as the above complex simulation and the precise kinetic treatment will need further experimental data, we will use these initial stage first order rate constants in this study. This rapid decrease of fulvic acid from solution with goethite suggests its adsorption on goethite. While only small absorbance decrease was observed for WakoSil-25Sil, its first order rate is similar to that of hematite, which shows larger decrease of absorbance at 254 nm than WakoSil-25Sil. This is because the electronic interaction between fulvic acid and hematite may be much larger than that of WakoSil-25Sil due to negative surface charge of WakoSil-25Sil, while positive charge of hematite in this pH condition is expected.

REFERENCES

Belsky, A. J. Brill, T. B. (1998) IR and Raman spectroscopy of hydrolysis and self-reaction of cyanamide and dicyandiamide at 130-270 degrees C and 275 bar., *J. Phys. Chem. A,* **102**, 4509 –4516, Spectroscopy of hydrothermal reactions. 9.

Brill, T. B. (2000), *J. Phys. Chem. A* **104**, 4343-4351, Geothermal vents and chemical processing: The infrared spectroscopy of hydrothermal reactions

Freitag, D., Gotz, C., Luft, G., van der Pol, A., Wierda, K. (2001) In situ Raman spectroscopy of the decomposition of tertiary butyl peroxy pivalate under high pressure and high temperature., *Appl. Spectrosc.*, **55**, 136-141

Furutaka, S.; Ikawa, S. (2000) Infrared study of water-benzene mixtures at high temperatures and pressures in the two- and one-phase regions, *J. Chem. Phys.*, **113**, 1942-1949

Gorbaty, Y. E.; Bondarenko, G. V. (1999) Experimental technique for quantitative IR studies of highly absorbing substances at high temperatures and pressures., *Appl. Spectrosc.*, **53**, 908-913

Hoffman, M. M.; Adleman, R. S.; Fulton, J. L. (2000), *Rev. Sci. Instrum.*, **71**, 1552.

Heinz-Helmut Perkampus, UV-VIS atlas of organic compounds 2nd ed., VCH, 1992

Ikushima, Y., Hatakeda, K., Sato, O., Yokoyama, T., Arai, M. (1999) Noncatalytic organic synthesis using supercritical water: The peculiarity near the critical point. , *Angew. Chem. Int. Ed.*, **38**, 2910-2914

Jaffe, H. H. and Orchin, M., *Theory and Applications of Ultraviolet Spectroscopy.* John Wiley, New York. (1962)

Kazarian, S. G.; Martirosyan, G. G. (2002) ATR-IR spectroscopy of superheated water and in situ study of the hydrothermal, *Phys. Chem. Chem. Phys.*, **4**, 3759-3763

Kieke, M. L.; Schoppelrei, J. W.; Brill, T. B. (1996) Spectroscopy of Hydrothermal Reactions. 1. The CO2-H2O System and Kinetics of Urea Decomposition in an

FTIR Spectroscopy Flow Reactor Cell Operable to 725 K and 335 bar., *J. Phys. Chem.*, **100**, 7455-7462

Korshin. G. V., Li, C. W., and Benjamin, M. M. (1997) Monitoring the properties of natural organic matter through UV spectroscopy: A consistent theory., *Water Research.* **31**, 1787-1795,

Masuda, K. (2005) Development of in-situ heating spectroscopic methods for aqueous organic reactions, Doctral thesis, Department of Earth and Space Sciences, Tokyo Institute of Technology

Pretsch E., Buhlmann P., Affolter C. (2000) Structure determination of organic compounds : tables of spectral data -- 3rd completely revised and enlarged English ed., Berlin: Tokyo: Springer

Schoppelrei, J. W., Kieke, M. L., Wang, E., Klein, M. T., Brill, T. B. (1996) Spectroscopy of hydrothermal reactions .4. Kinetics of urea and guanidinium nitrate at 200-300 degrees C in a diamond cell, infrared spectroscopy flow reactor., *J. Phys. Chem.*, **100**, 14343-14351

Steeper, R. R., Rice, S. F., Brown, M. S. and Johnston, S. (1992) Methane and methanol diffusion flames in supercritical water., *J. Supercrit. Fluits*, **5**, 262-268,

Wang, J.; Heyes, C. D.; El-Sayed, M. A. (2002) Refolding of Thermally Denatured Bacteriorhodopsin in Purple Membrane., *J. Phys. Chem. B*, **106**, 723-729,

Zhang, R.; Hu, S. (2004) Hydrothermal study using a new diamond anvil cell with in situ IR spectroscopy under high temperature and pressures., *J. Supercrit. Fluids*, **29**, 185-202

2.3. ATR-IR spectroscopy of fulvic acid on the surface of goethite

2.3.1. INTRODUCTION

For characterizing the structure of organic compounds, Fourier transform infrared spectroscopy (FT-IR) spectroscopy is a highly effective method due to the information of functional groups (Cabaniss, 1991). In order to measure the liquid (solution) sample, transmittance method and attenuated total reflection (ATR) method have been traditionally used (Kellner R. A., 1997; Schumidt, 2005). In the first method, a spacer of constant thickness is sandwiched by two transparent windows (ex. CaF_2), and then transmission spectra of the thin film liquid sample between two windows were measured (Brill, 2000; Hannah, 2002). The other method is using penetration of evanescent light at the total reflection, which occurs when a light beam approachs the interface between a prism and liquid sample at an appropriate angle (Harrick, 1966). In this situation, a transmittance-like spectrum can be observed by the penetrating light (evanescent wave) to a very short distance into the liquid sample.

This ATR-IR spectroscopy is very useful in characterizing organic functional groups of dissolved organic compounds in solutions and in studying aqueous organic reactions quantitatively by measuring IR absorptions of organic functional groups (Cabaniss, 1991; Hay, 2007). This method use the penetration of evanescent waves less than about 1 micrometer at the total reflection of IR beam at the interface between a prism (ATR crystal) and liquid sample (Harrick, 1966). In this study, for monitoring reactions on the surface of goethite, the goethite film is prepared on the horizontal ATR crystal by drying the goethite suspension. By using this ATR-IR cell with the hydrothermal flow-through system, hydrothermal transformation of organic compounds with time and temperature on the surface of goethite can be investigated (Fig. 2.3.1)

In this study, a newly developed heated ATR-IR cell was employed. As a representative dissolved organic matter, Nordic fulvic acid (a reference sample obtained from International Humic Substance Society = IHSS) aqueous solution was used for the in-situ measurements, and their calibration lines were determined in this chapter. Based on this study, hydrothermal transformation of organic compounds with time and temperature on the surface of goethite will be discussed later (Chapter 4).

2.3.2. EXPERIMENTAL

2.3.2.1. Principles of ATR spectroscopy

The ATR-IR method is using penetration phenomenon in total reflection, which occurs when IR beam approachs the interface between a prism and liquid sample at an enough angle. In this situation, a transmittance-like IR spectrum can be observed by penetrating infrared light to a short distance into the liquid sample.

The total reflection process of a light at the material interface is described by Snell's law, where an incident electromagnetic radiation travels in a transparent medium of higher refractive index (n_1) and strikes an interface with a medium of lower refractive index (n_2) (Fig.2.3.1). For incident angles greater than the critical angle, θ_c ($\theta_c = \sin^{-1}(n_2/n_1)$), reflection of incoming beam becomes total. However, microscopically, the incident wave is not totally reflected at the very interface of the two media but slightly penetrates into the low n_2 sample medium from the interface (called evanescent wave) at a bit deeper point from the interface. The incident waves penetrating into the sample were absorbed by IR active molecular vibration during this reflection process. Therefore, the measurement of the attenuated reflected light against the initial incident light (without the sample) provides an ATR spectrum similar to transmission absorption spectrum.

The Maxwell's equations predicted that standing waves will be established normal to a totally reflecting surface and penetrate into the less dense medium as a result of the superposition of the incoming and reflected waves. The penetrating electromagnetic field maintains the same frequency as the incoming wave, propagates along the surface of the denser medium, and decrease exponentially with the distance from the interface (Fig.2.3.1). The depth of penetration (d_p) of this evanescent wave into the less dense medium, at a single reflection, has been defined as the distance from the interface where the electric field amplitude falls to $1/e$ of its value at the surface and is given by (Harrick, 1966);

$$d_p = \frac{\lambda}{2\pi n_1 (\sin^2\theta - \frac{n_2}{n_1} n_{21}{}^2)^{1/2}}$$

where λ is the wavelength, n_1 and n_2 are the refractive indices of the two media (n_1: optically denser medium; prism, n_2: optically thinner medium; sample), and θ is the incident angle.

Thus, for a fixed incident angle, the penetration depth is dependent on the ratio of the refractive indices of two media and the wavelength of the radiation in the denser medium. For example, the refractive indices of a dense medium (ZnSe crystal) and a less dense medium (water) for visible light at ambient condition are $n_1 = 2.4$ and

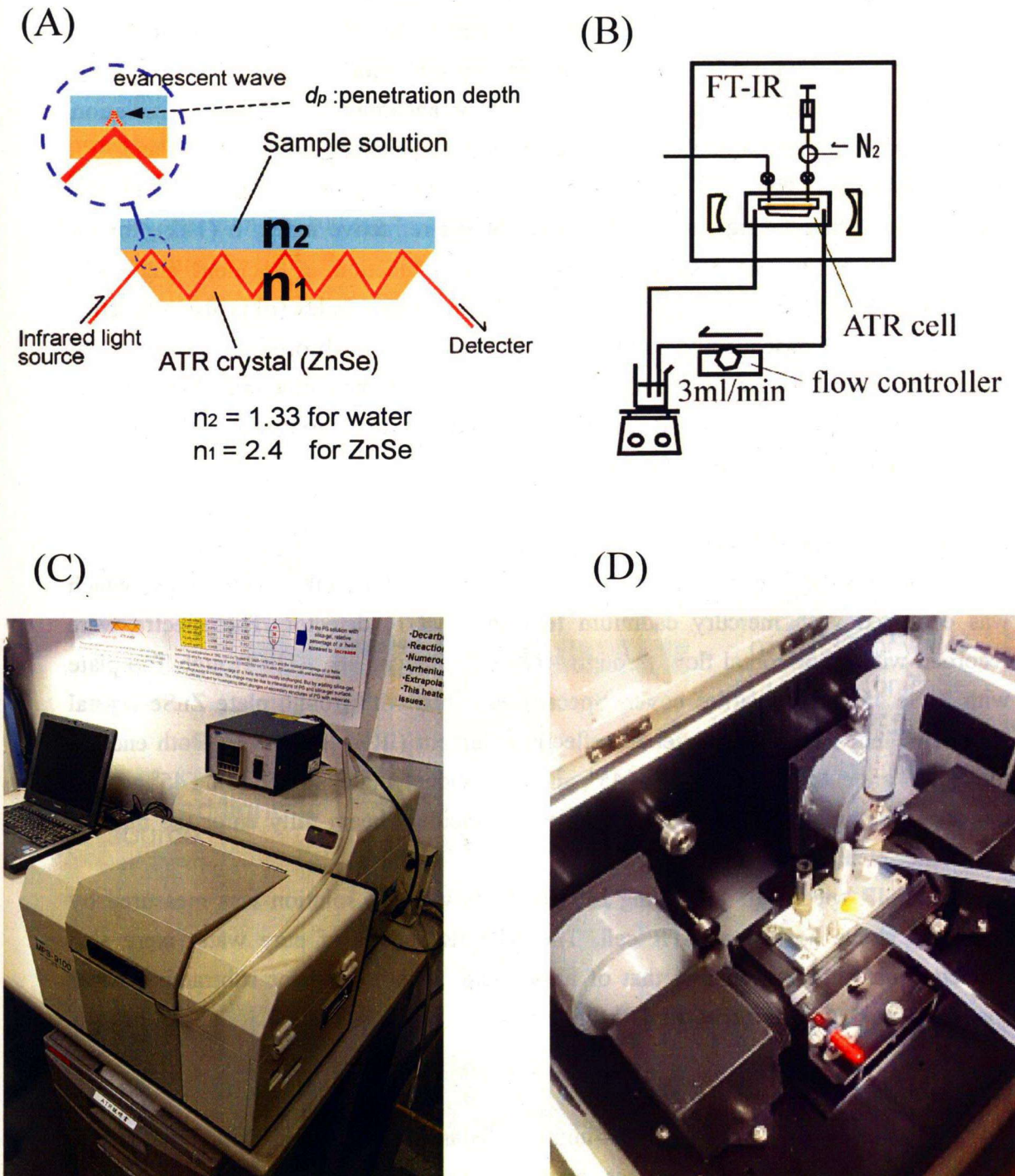

Figure 2.3.1. The horizontal ATR cell spectroscopy with a flow-though system heated solutions. (A) schematic figure of attenuated total reflection (ATR) at the interface of an ATR crystal and a sample solution, (B) schematic figure of the flow-though ATR system heated solutions (C) photograph of the FT-IR (VIR-9500, Jasco) with the heatable IR cell, (C) photograph of the heatable flat IR cell

n_2 = 1.333 respectively, and so the penetration depth for incident light beam of 5000 cm^{-1} (2 μm) is 0.3 μm. Although refractive indices get smaller for longer wavelength of light (IR) or for higher temperature condition, I here assume that the index remains in the same order. The penetration depth is calculated to be 0.6, 1,2, and 1.4 μm for the incident beam of 2300, 1320, and 1000 cm^{-1} for one reflection.

When the less dense medium is capable of absorbing the incoming radiation, energy is lost from the evanescent wave, the reflection becomes less than total, and ATR absorption occurs. This loss in reflectivity can be calculated exactly from the Fresnel reflection equations using the complex form of the refractive index, n (1-ik), for the absorbing medium. The resulting absorption is a function of incident angle (θ), refractive index (n), and attenuation index (k). The refractive index (n) is also a function of wavelength. Consequently, unlike for the transmission absorption spectrum, the quantitative measurement for the ATR spectrum requires some corrections. Nevertheless, in this study, pATR (= -log I / I_0) was empirically used as analogous to absorbance (Abs = -log I / I_0) after Masuda et al. (2003).

2.3.2.2. Horizontal ATR cell

The IR spectra were collected with Jasco VIR-9500 FTIR spectrometer, which was equipped with mercury cadmium telluride (MCT) detector. The spectra were recorded with a horizontal flow through ATR cell (Benchmark ATR Trough Top plate with ZnSe 45° plus volatiles cover, Specac) equipped with trough plate ZnSe crystal (refractive index n_1=2.4) as internal reflection element (IRE) (Fig.2.3.1). Both ends of the crystal are cut off at an angle of 45°, and the incident angle is fixed to be 45° against the crystal-sample interface, which enables the incident beam fully enter the internal reflectance element of ZnSe (Fig.2.3.1).

ATR-IR spectra of 10000 mg L^{-1} Nordic fulvic acid solution was measured by using the above horizontal ATR cell. The ATR-IR spectra of pure water were also collected just before collecting that of fulvic acid. This is used for subtracting water spectra to make different spectrum of fulvic acid.

2.3.2.3. Thin film suspension of goethite

In order to study interactions of humic substances and an iron oxide, goethite by ATR-IR spectroscopy, goethite was evenly deposited onto ZnSe crystal using a technique described by Tededor-Tejedor (1986). First, 1000 μL of pure water was pipetted onto the crystal, and 800 μL was removed to obtain thin water layer evenly across the surface of crystal (Fig.2.3.2). Then, 100 μL of a 10 g L^{-1} goethite suspension was placed into the center of the film with a pipette. The suspension was mixed by using the pipette tip and dried at room temperature during over night. Once deposit was

dried, it was rinsed by pure water to remove excess goethite on the ZnSe surface. After drying, the ATR crystal was rinsed again, and then thin layer of the goethite is attached on the ATR crystal. It was placed into horizontal ATR cell (Fig.2.3.2). To investigate the thickness of goethite layer, laser scanning confocal microscope (LCSM) analysis was applied to thin film suspension of goethite (Fig.2.3.3).

Two types of ATR-IR spectra, in the dry and wet conditions, were obtained by using horizontal ATR cell. 10000 mg L^{-1} Inogashira humic acid was precipitated on the ZnSe ATR crystal. Then, IR spectrum of humic acid in dry condition was collected. ATR-IR spectrum for 100 mg L^{-1} Nordic fulvic acid in the presence of goethite solution was measured by using the above horizontal ATR cell.

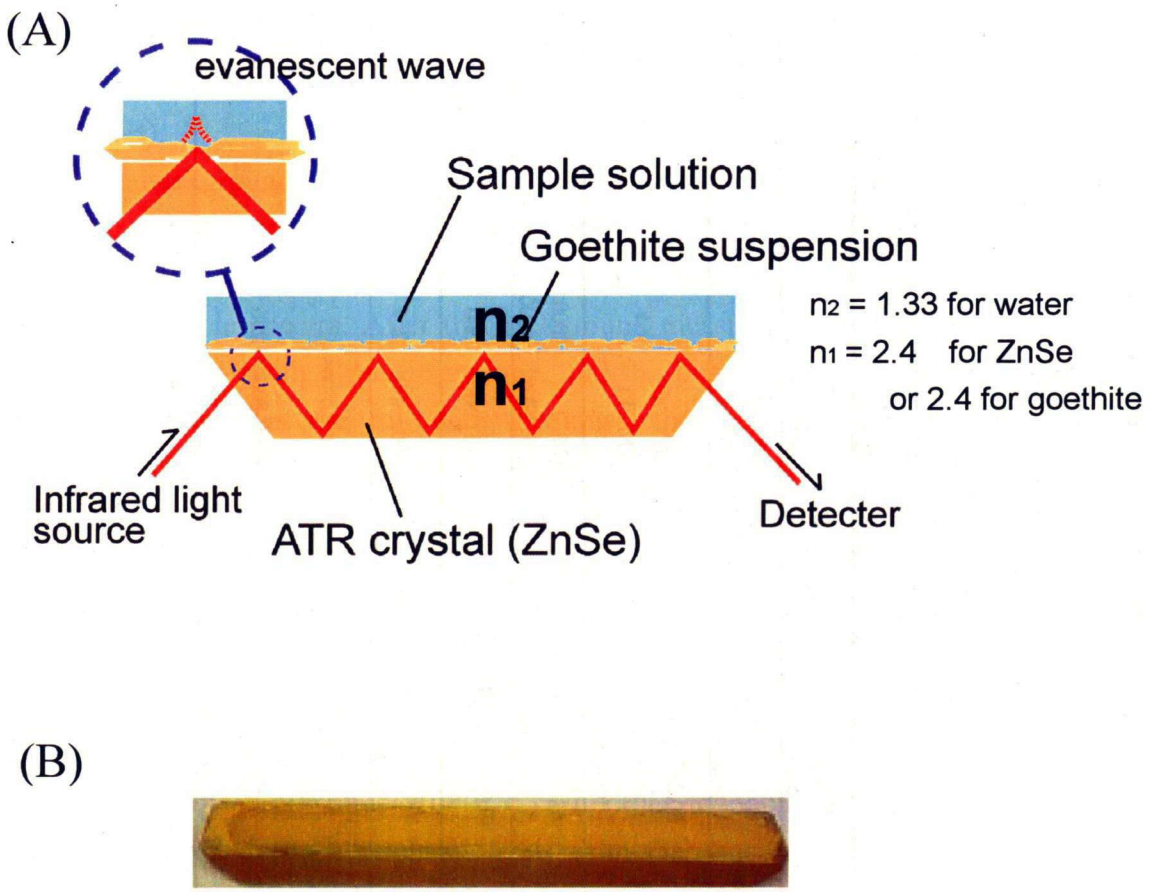

Figure 2.3.2. The horizontal ATR crystal with a goethite suspension and (A) The schematic figures of of the ATR crystal (ZnSe) with a goethite suspension solution., (B) After drying and washing the ATR crystal with the goethite suspension, a thin film layer of goethite remaining on the surface of the ATR crystal.

Table 2.3.1 Summary of ATR-IR studies for adsorption at the iron oxide surface.

Sample	mineral	detail	ATR crystal	Angle (reflec.)	range (cm^{-1}) (Detector)	scan	resolution	others	Author	Journal	page	Vol.	Year
phosphate in D_2O	goethite	80 m^2g^{-1}(BET analysis)	ZnSe	40°(16)	4000-600 (MCT)				Tejedor-Tejedor and Anderson	Langmuir	203	2	1986
Salicylate Complex	goethite	80 m^2g^{-1}(BET analysis)	ZnSe (rod)	39°(16)	4000-700 (MCT)		4		Yost et al.	Environ. Sci. Technol.	822	24	1990
Arsenite (As(III)) and Arsenate(As(V))	goethite	80.2±3.8 m^2g^{-1}(EGME technique)	ZnSe (rod)	39°(16)	4000-700 (MCT)	64	2		Sun and Doner	Soil Sci.	865	161	1996
o-phthalate	goethite	43 m^2g^{-1}(BET analysis)	AMTIR	45°	(MCT or TGS)	4000 or 500	—		Persson et al.	J. Colloid Interface Sci.	252	206	1998
mellitic acid	goethite	49.6 m^2g^{-1}(BET analysis)	diamond	(9)	(TGS)	500	—		Johnson et al.	Langmuir	823	20	2004
oxalate, manolate, succinate	lepidocrocite	130 m^2g^{-1}(BET analysis)	diamond	(9)	4000-400	256	2		Hug and Bahnemann	J. Electron spectrosc.	208	150	2006
phosphate in H_2O	goethite	pH9; $(FeO)_2PO_2$ $5.47x10^{-6}M$											
carbonate	goethite	57 m^2g^{-1} Contamination	ZnSe		4000-800	256	2	Temp. 25 ±2	Luengo et al.	J. Colloid Interface Sci.			2006

2.3.2.4. ATR measurement

The horizontal ATR cell with the thin film goethite on the ZnSe crystal was mounted in the FTIR spectrometer (VIR-9500, Jasco) (Fig.2.3.1, 2.3.2). The sample solutions were placed on the ATR crystal to obtain their IR spectra. All spectra were collected with one hundred interferograms at 4 cm^{-1} resolution to produce a single spectrum from 1000 to 4000 cm^{-1}. The spectra were recorded in absorbance mode aginst air background to obtain pATR spectra.

The FT-IR spectrometer yields the energy of around 19800 (air) and 17500 (water) at the MCT detector with the horizontal ATR cell. In the presence of goethite, spectrometer yields 17000 (air + goethite) and 14000 (water + goethite) at the same setting.

2.3.2.5. Heating ATR-IR measurements

In order to obtain ATR-IR spectra of dissolved humic substances under hydrothermal conditions, hot water was circulated into the flow through ATR cell (Fig.2.3.1B).

The background air spectrum is measured in the blank cell at room temperature. As the air spectrum does not change significantly at higher temperatures of up to 200 °C (Masuda et al., 2003), the air spectrum at room temperature is used as the background for all the sample spectra. After the background measurements, purewater is injected into the ATR cell with a plastic syringe, and the purewater spectrum is measured at same temperature as the following heating experiment (Fig.2.3.1). This will be subtracted from the sample spectra to obtain difference spectra of sample solutes. After pushing off and drying purewater by nitrogen gas flow, the sample humic substances, which is preliminary heated at desired temperature, is injected with another syringe and then the plugs were tightly sealed. The sample spectrum at desired temperature is measured in absorbance mode (pATR spectrum) and the difference spectrum (sample-purewater) was calculated to evaluate the IR signatures of solutes.

The temperature of the ATR cell and fulvic acid solution was preliminary heated at the designed temperature (20-80 °C). In order to obtain spectral changes of the sample solution during the heating experiments, successive measurements were conducted by an interval-measurement program (Spectral manager, Jasco). The isothermal spectral changes could be traced at an interval of every 120 seconds. For the kinetic treatments, the reaction starting time (t=0) was taken as the time when the fulvic acid solution was introduced in the in-situ cell.

2.3.3. RESULTS

2.3.3.1. Thin film suspension of goethite

After removing excess goethite on the ZnSe surface, the goethite thin film was obtained. The LSCM measurement shows average thickness of goethite layer is around 3 μm (Fig.2.3.3). The LSCM mapping data shows the smooth ZnSe surface and relatively flat goethite layer. However, this layer has abundant micron-sized pores. After the interaction of goethite with the fulvic acid, LCSM data shows no significant difference of the goethite film.

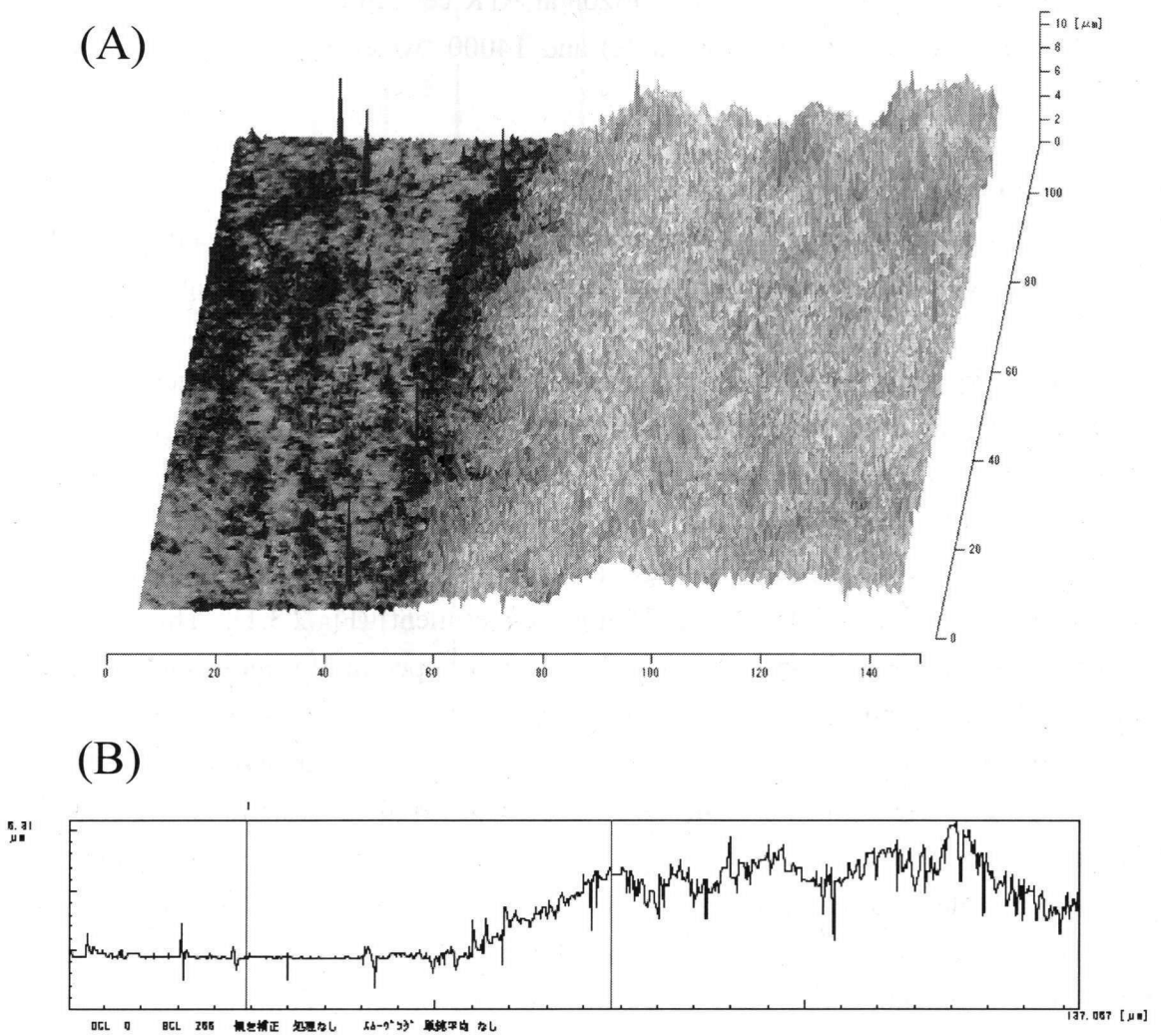

Figure 2.3.3. The Laser Scanning Confocal Microscope (LSCM) of goethite thin film on the ATR crystal. (A) 3 dimensional topographic image of the boundary between the ATR (ZnSe) crystal and the goethite film. (B) typical cross section diagram showing the thick ness of the goethite film of about 3 μm.

2.3.3.2. ATR-IR spectra of goethite

ATR-IR spectra of goethite in a dry condition are shown in Fig. 2.3.4B. Two

sharp bands at 911 and 795 cm^{-1} are derived from the Fe-OH bending band of δ-OH and γ-OH, respectively. A broad band due to bulk hydroxyl stretching vibration is observed at 3138 cm^{-1}.

ATR-IR spectra of goethite in a wet condition are shown in Fig. 2.3.4A. The Fe-OH bending bands at 905 and 801 cm^{-1} are observed with similar positions to the dry goethite. However they are highly overlapped. The OH stretching band of goethite at 3138 cm^{-1} are hidden by absorption of water around at 3600 – 3000 cm^{-1}.

The air spectrum do not change significantly at higher temperatures of up to 200 °C (Masuda et al., 2003). However, in the case of ATR crystal with thin film goethite, the spectrum changed depending on the temperature (Fig.2.3.5). The peaks at 3115, 921 and 800 cm^{-1} decreased with increasing temperature. The band around at 888, 835 and 771 cm^{-1} increased with increasing temperature.

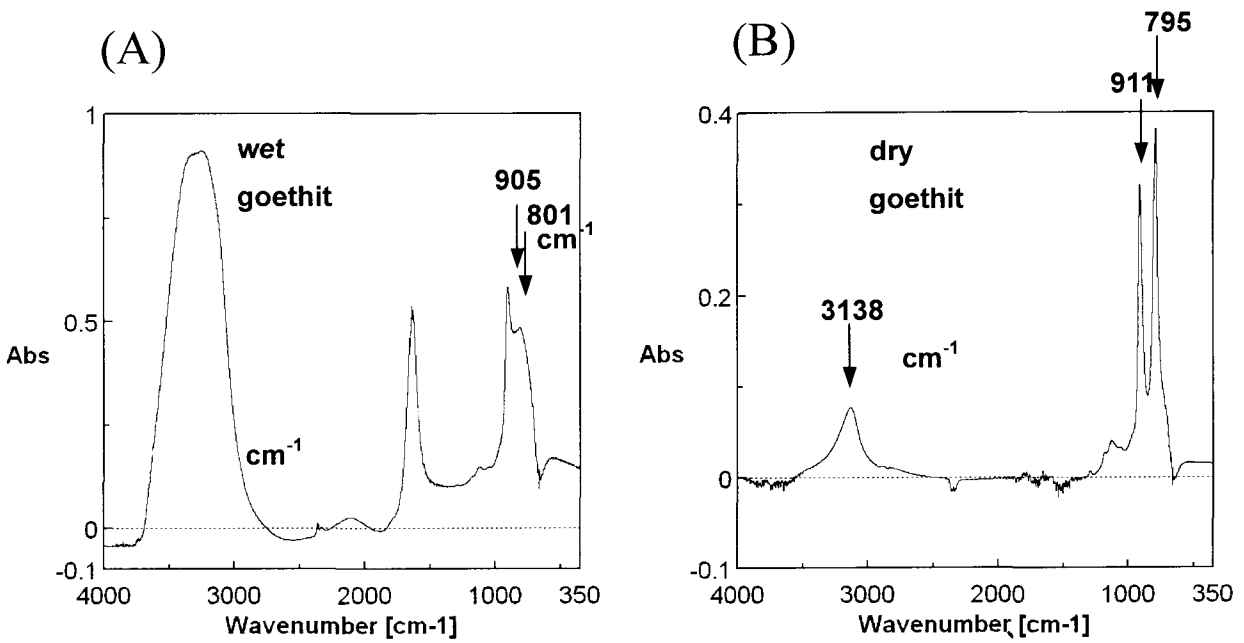

Figure 2.3.4. ATR-IR spectra of goethite film on the ATR crystal at 25°C (A) in the wet condition with goethite suspension solution and (B) in the dry condition without solution.

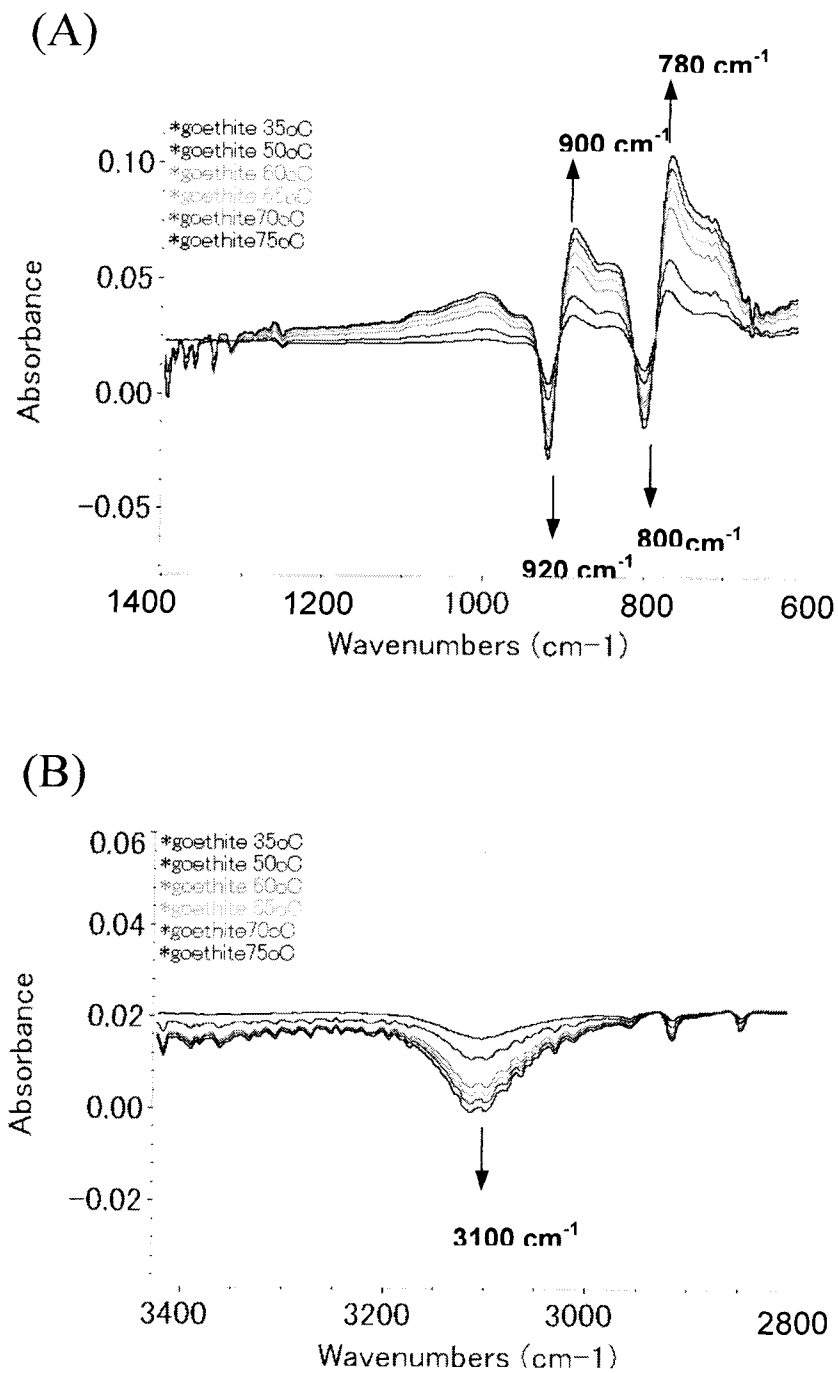

Figure 2.3.5. ATR-IR spectral change with temperature of goethite film at 35°C , 50°C , 60°C , 65°C , 70°C and 75°C in the (A) 1400 – 600 cm^{-1} and (B) 3400 – 2800 cm^{-1} ranges.

2.3.3.3. ATR-IR spectra of humic substances

IR spectrum for 10000 mg L^{-1} (1 %) Nordic fulvic acid solution was measured by the horizontal ATR-IR cell (Fig.2.3.6A). The difference spectrum was made by subtracting the ATR-IR spectrum of pure water collected just before that of fulvic acid solution (Fig.2.3.6B, C). The difference spectrum of the Nordic fulvic acid was obtained as shown in Fig. 2.3.6C. Four major absorption bands are observed at 1710, 1600, 1400, 1220 cm^{-1} in the IR spectrum of Nordic fulvic acid, while Masuda reported two major bands at 1580 and 1380 cm^{-1} in that of Aldrich humic acid. The peaks at 1710 and 1220 cm^{-1} might be derived from C=O stretching of COOH groups and C-O stretching with O-H deformation of COOH groups, respectively. The band centered at 1600 or 1580 cm^{-1} shows superposition of asymmetric stretching of COO^- and aromatic C=C. The 1400 or 1380 cm^{-1} band might be superposition of symmetric stretching of COO^-, O-H deformation and C-O stretching of phenolic OH, and C-H deformation of CH_2 and CH_3 groups.

2.3.3.3. ATR-IR spectra of humic substances on the surface of goethite

IR spectrum for 10000 mg L^{-1} (1 %) Inogashira humic acid in dry condition on the surface of goethite was measured by the horizontal ATR-IR cell (Fig.2.3.7). The spectrum showed major absorption bands due to OH stretching and bending vibrations of goethite at 3115, 902 and 794 cm^{-1}, the asymmetric and symmetric stretching of COO^- at 1582 and 1384 cm^{-1}, and the shoulders at 1720, 1660 and 1240 cm^{-1}.

IR spectrum for 100 mg L^{-1} Nordic fulvic acid solution was measured in the presence of goethite (Fig.2.3.8A). The difference spectrum, subtracted by pure water (Fig.2.3.8B), is shown in Fig. 2.3.8C. Four major absorption bands are observed at 1710, 1600, 1400, 1220 cm^{-1} in the IR spectrum of Nordic fulvic acid, while Masuda reported two major bands at 1580 and 1380 cm^{-1} in that of Aldrich humic acid. The peaks at 1710 and 1220 cm^{-1} might be derived from C=O stretching of COOH groups and C-O stretching with O-H deformation of COOH groups, respectively. The band centered at 1600 or 1580 cm^{-1} shows superposition of asymmetric stretching of COO^- and aromatic C=C. The 1400 or 1380 cm^{-1} band might be superposition of symmetric stretching of COO^-, O-H deformation and C-O stretching of phenolic OH, and C-H deformation of CH_2 and CH_3 groups.

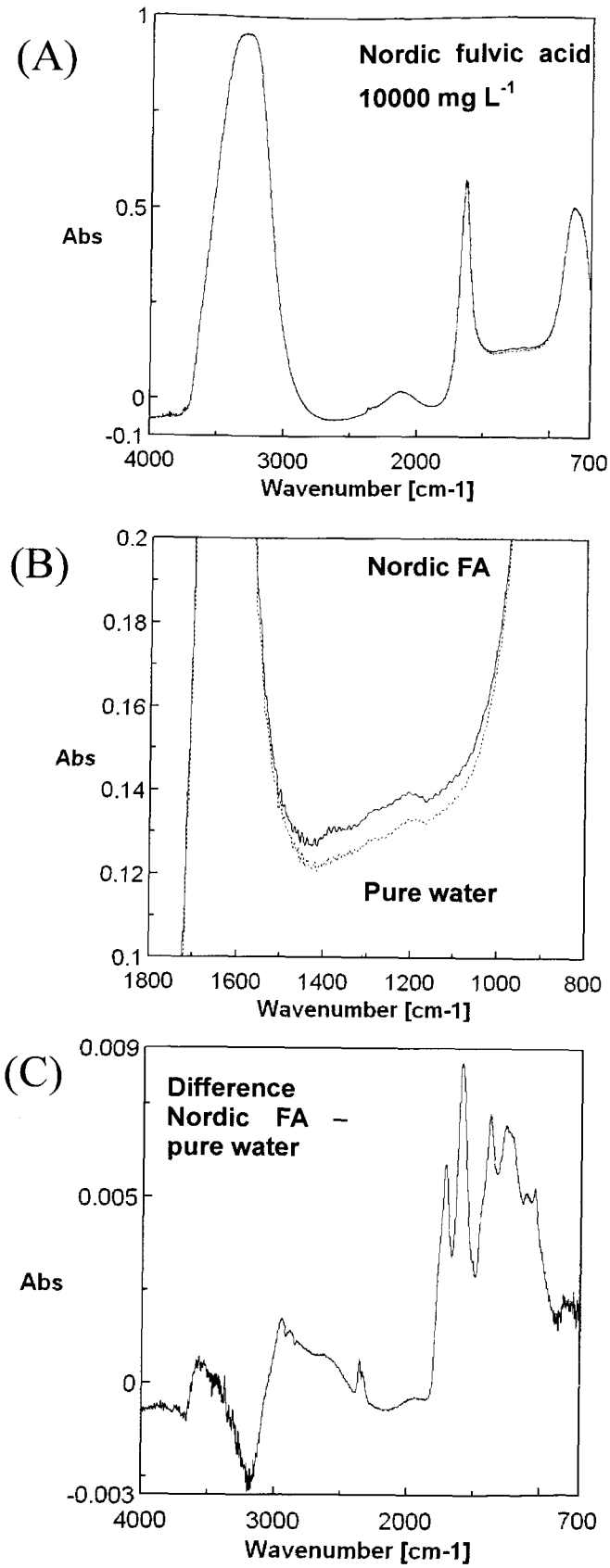

Figure 2.3.6. ATR-IR spectra of 10000 mg L^{-1} Nordic fulvic acid solution (solid curve) and pure water (dotted curve) in the (A) 4000 - 700 cm^{-1}; (B) 1800 - 800 cm^{-1} ranges and (C) the difference spectrum between 10000 mg L^{-1} Nordic fulvic acid and pure water.

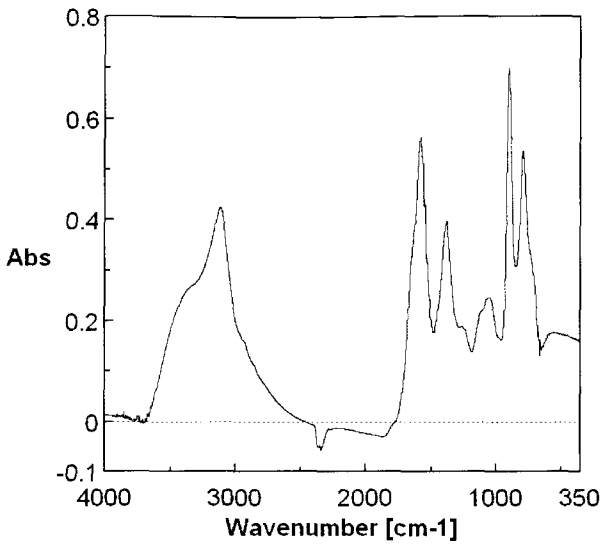

Figure 2.3.7. ATR-IR spectra of 10000 mg L^{-1} Inogashira Humic acid in the dry condition

2.3.4. DISCUSSION

2.3.4.1. ATR-IR spectra of goethite

The obtained ATR-IR spectra of goethite are in good agreement with the literature data (Cornell and Schwertmann, 1996) in their peak positions in the dried film, but shows different peak positions in the wet condition. This is because surface OH groups in the goethite structure may be hydrated with water molecules. Although ATR-IR spectra of goethite in water showed temperature dependences, these can be subtracted at each temperature.

2.3.4.2. ATR-IR spectra of Humic substances

There have been no significant difference in the spectral shape of humic substances with / without goethite. On the other hand, goethite makes the peak heights of fulvic acid larger. This means that the humic substances are concentrated on the goethite surfaces without no significant structural changes. This indicates that the interaction between goethite and humic substances are mainly contributed to the physical adsorption.

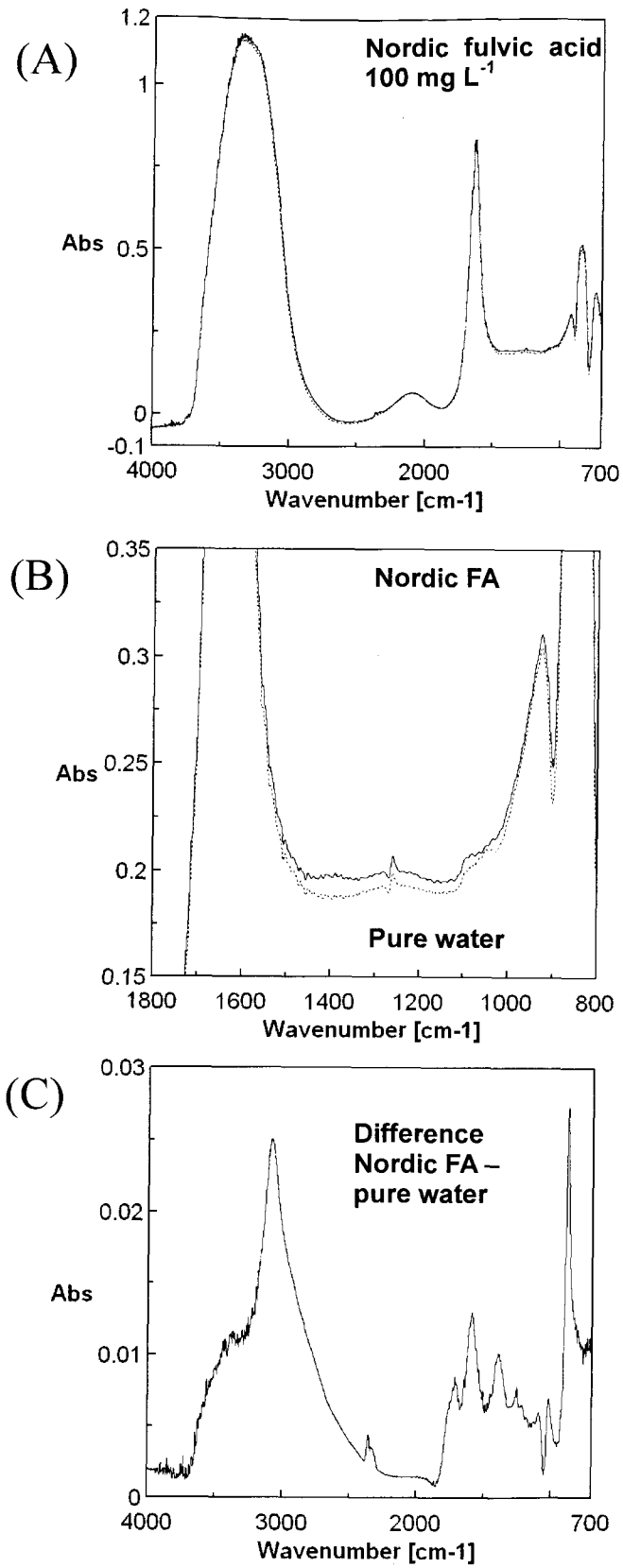

Figure 2.3.8. ATR-IR spectra of 100 mg L^{-1} Nordic fulvic acid solution (straight line) and pure water (dotted line) on the surface of goethite (A) 4000 - 700 cm^{-1}; (B) 1800 - 800 cm^{-1} and (C) the difference spectrum between 10000 mg L^{-1} Nordic fulvic acid and pure water on the surface of goethite

REFERENCES

Brill, T. B. (2000) Geothermal vents and chemical processing: The infrared spectroscopy of hydrothermal reactions, *Journal of Physical Chemistry A* **104**, 4343-4351

Cabaniss, S. E. (1991) Carboxylic acid content of a fulvic acid determined by potentiometry and aqueous Fourier transform infrered spectrometry., *Analytica Chimica Acta,* **255**, 23-30

Hannah R. W. (2002) Standard sampling techniques for infrared spectroscopy, In *Handbook of vibrational spectroscopy*, (eds. Chalmers J. M. and Griffiths P. R.) pp.933-952, Chichester: John Wiley & Sons

Harrick, N. J.; du Pre, K. F. (1966) Effective thickness of bulk materials and of this films for internal reflection spectroscopy., *Applied Optics*. **5**, 1739-1966

Hay M. B. Myneni S. C. B. (2007) Structural environments of carboxyl groups in natural organic molecules from terrestrial systems. Part 1: Infrared spectroscopy, *Geochimica et Cosmochimica Acta*, **71**, 3518-3532

Kellner R. A. (1997) Infrared and Raman Spectroscopy, In *Analytical Chemistry* (eds. Kellner R. A., Mermet J.-M, Otto M. and Widmer H. M.) pp. 541-566, Weinheim: Wiley-VCH

Masuda, K., Haramki, T., Nakashima, S., Habert, B., Martinez, I. and Kashiwabara, S. (2003) Structural change of water with solutes and temperature up to 100 C in aqueous solutions as revealed by ATR-IR spectroscopy., *Applied Spectroscopy*, **57**, 274-281

Schmidt W. (2005) Optics for Spectroscopy, In *Optical Spectroscopy in Chemistry and Life Science*, pp. 55-110, Weinheim: Wiley-VCH

Tejedor-Tejedor M. I. and Anderson M. A. (1986) "In-situ" attenuated total reflection Fourier transform infrared studies of the goethite (α-FeOOH)-aqueous solution interface, **2**, 203-210

APPENDIX A

Quantitative measurements of chlorinated volatile organic compounds for contaminated soils by means of long-path gas cell FT-IR spectroscopy

TAKAHIRO OTSUKA and SATORU NAKASHIMA

Department of Earth and Space Science, Graduate School of Science, Osaka University, 1-1 Machikaneyama-cho, Toyonaka, Osaka, 560-0043, Japan

ABSTRACT

A 10 m long-path gas cell Fourier Transform Infrared (FT-IR) Spectroscopy was applied to determine concentrations of chlorinated volatile organic compounds (VOCs) in contaminated soils. 6 volatile organic standards and their mixture were measured by the gas cell FT-IR for obtaining calibration lines. By selecting a characteristic peak for each compound, all the 6 VOCs showed satisfactory linear trends for concentration ranges of about 0.1 to 10 ppmV (parts per million by volume). A contaminated soil sample was measured by this method and *cis*-1,2-dichloroethylene, trichloroethylene and tetrachloroethylene were detected with concentrations of 0.65, 0.22 and 0.91 ppmV, respectively based on the above calibration lines. This gas cell FT-IR method can therefore be a rapid multi-component analytical technique for VOCs in contaminated soils.

INTRODUCTION

Rapid and simple on-site measurement of volatile organic compounds (VOCs) is needed for assessing environmental pollution in soil and water. Conventionally, VOCs are measured by means of Gas Chromatography (GC) or Gas Chromatography combined with Mass Spectrometry (GC/MS) equipped with purge and trap or headspace systems[1, 2]. Although these are highly sensitive and precise analytical methods, they require time-consuming procedures and delicate maintenance. On the other hand, Fourier Transform Infrared (FT-IR) Spectroscopy has been used to determine trace VOCs in atmosphere[3, 4]. Trace volatiles can be detected by FT-IR using either open-path or long-path method. The open-path measurement of trace compounds in factory atmospheres was reported to be useful for detecting harmful volatile pollutants[5]. However, setting up the measurement systems and appropriate environmental conditions including climates is not easy. The long-path gas cell FT-IR has been used

for measuring volatile pollutants in air[6, 7]. By increasing the optical path up to 10 m or even 100 m, the detection limits of gaseous compounds can be lowered significantly[8]. However, this method has not yet been applied to the analysis of multiple phases of VOCs from soil and water samples, except for FT-IR studies of VOCs in artificially contaminated soils extracted by supercritical fluid [9].

In this study, the long-path (10 m) gas cell FT-IR has been tested for its capability of quantitative measurements of 6 standard chlorinated hydrocarbons and their mixtures as a basis for the new method of rapid multi-component analysis of VOCs in soil and water environments. Then, this method was applied to a contaminated soil gas sample.

EXPERIMENTAL

The long-path gas cell FT-IR

Infrared measurements of the standard VOCs were conducted in an FT-IR spectrometer (Bomem, MB154) equipped with a 10 m long path gas cell (Infrared analysis Inc., 10-PA) as shown in Fig.1a, b. In the gas cell (25 cm path length), reflecting IR mirrors are set at the both ends to obtain 40 times reflection, yielding totally 10 m optical path length (Fig.1c). The cell volume is 2.3 ± 0.1 L. A stainless liner (1/4 inch diameter) is set to an inlet valve (Fig.1c:(1)) and is connected to a volume

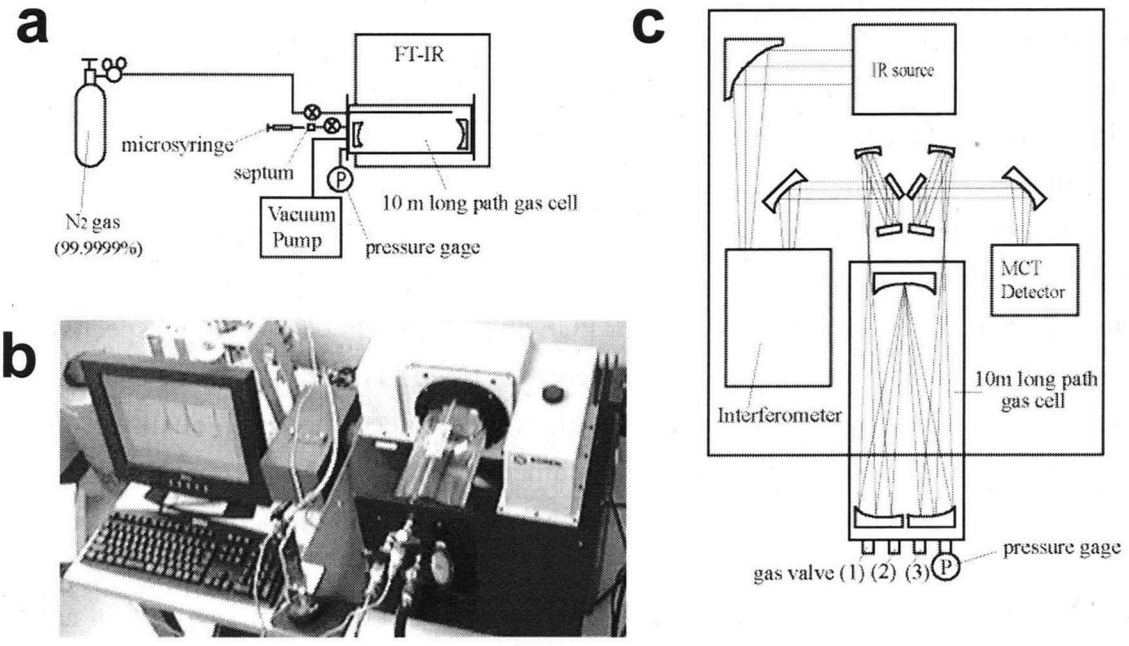

Fig.1 The 10 m long path gas cell FT-IR system (Bomem MB154). The schematic configuration (a) of the whole system, (b) the photograph, and (c) schematic configuration of the optics and the gas cell with (1) the sample inlet valve, (2) N_2 gas inlet valve (purity> 99.9999%) and (3) outlet valve for a vacuum pomp.

-certified container (1 L). Another stainless liner (1/8 inch diameter) from another inlet valve (Fig.1c:(2)) is lined to N_2 gas cylinder (99.9999% purity). An outlet valve (Fig.1c:(3)) is connected to a vacuum pump for cleaning up the gas cell. A pressure gauge (0.0-0.3 MPa) (Fig.1c: P) is placed to monitor the pressure inside the gas cell with a precision of 0.001 MPa.

The spectrometer is equipped with a silicon carbide source (Globar), a CsI beam splitter and a liquid nitrogen cooled mercury-cadmium-telluride (MCT) detector covering the spectral range of 7000-500 cm^{-1}. 128 scans of interferograms are co-added at a wavenumber resolution of 1 cm^{-1} to obtain IR spectra. IR absorption bands by gaseous compounds include fine rotational transition signals overlapped on stretching and bending bands[8]. Therefore, small wavenumber resolution measurements are generally selected for gaseous studies. However, very small wavenumber resolution requires long time period for the measurement and only possible with a high cost spectrometer. For a general use of the present FT-IR method, 1 cm^{-1} resolution is considered to be an optimal one, with a relatively short measurement time (about 10 minutes) and a good linearity in the absorption intensity against concentration[8].

Preparation of standard VOCs and its mixture

1,1-dichloroethylene (1,1-DCE; 99.0% purity), *cis*-1,2-dichloroethylene (*cis*-1,2-DCE; 99.0% purity), *trans*-1,2-dichloroethylene (*trans*-1,2-DCE; 98.0% purity), 1,1,1-trichloroethane (1,1,1-TCA; 98% purity)) were purchased from Tokyo Chemical Industry. Trichloroethylene (TCE; 99.5% purity) and tetrachloroethylene (PCE; 99% purity) were purchased from Kanto Chemical Co.

1000 μL L^{-1} (1000 ppmV: parts per million by volume) of 6 standard VOC gases were prepared by vaporizing the above reagent solutions (Table I). Several μL of the reagent solutions, 4.1 μL for 1,1-DCE, 3.3 μL for *cis*-1,2-DCE, 3.1 μL for *trans*-1,2-DCE, 3.2 μL for TCE, 3.7 μL for PCE and 4.3 μL for 1,1,1-TCA., respectively, according to their molecular weights and densities (Table I) were put in an evacuated container (1 L, volume-certified) with a 10 μL microsyringe. Then high-quality N_2 gas (99.9999% purity) was introduced to the container to obtain 1000 ± 16 ppmV (1000 μL L^{-1}) gas of each VOC. These concentrations include maximum 3.2% of error based on the precision of the syringe (0.1 μL).

A mixture of the above 6 standard VOCs are prepared by vaporizing 4 μL of each VOC in the 1 L evacuated container. The concentrations of each VOC in this standard mixture are 1205 ± 15 ppmV for 1,1-DCE, 1274 ± 16 ppmV for *cis*-1,2-DCE, 1246 ± 16 ppmV for *trans*-1,2-DCE, 1073 ± 13 ppmV for TCE and 941 ± 12 ppmV for PCE, 973 ± 12 ppmV for 1,1,1-TCA, respectively, by using their molecular weights and densities (Table I). These concentrations include 2.5% of error based on the precision of the

syringe (0.1 μL).

Calibration studies for VOCs

VOC gasses of 5, 3, 1, 0.5, 0.3, 0.1 and 0.05 ppmV were prepared by diluting the 1000 ppmV VOC standards. After evacuating the long path gas cell in the FT-IR (Fig.1c), 23 mL of 1000 ppmV each gas standard was introduced to this cell (2.3 ± 0.1 L) by 10 mL syringe in order to obtain 10 ppmV gas. High-quality N_2 gas was then added to the cell until attaining 0.1 MPa on the pressure gauge (Fig.1c: P), in order to obtain a 10 ppmV VOC standard gas sample in pure N_2 gas. The precision of their concentration depends primarily on the minimum reading capability of the pressure gauge (0.001 MPa). Therefore, about 1% of error is included in the final concentration of VOCs together with the above accuracy of the syringe (2.6%) in the concentration.

This procedure is repeated for obtaining concentrations of the VOC of 5, 3, 1, 0.5, 0.3, 0.1 and 0.05 ppmV, respectively by taking 11.5 ± 0.2, 6.9 ± 0.1, 2.3 ± 0.1, 1.15 ± 0.02, 0.69 ± 0.01, 0.23 ± 0.01 and 0.12 ± 0.01 mL of the 1000 ppmV gas. A 1 mL syringe with the minimum reading of 0.01 mL was used for the lower concentrations of 1 to 0.05 ppmV. The maximum error for these concentrations is about 8% for 0.05 ppmV.

The 6 VOC gas mixture with concentrations around 1000 ppmV prepared above was diluted in the gas cell to obtain concentrations around 10, 5, 3, 1, 0.5, 0.3, 0.1 and 0.05 ppmV by the same procedure as above. 23.0 ± 0.3, 11.5 ± 0.2, 6.9 ± 0.1, 2.3 ± 0.1, 1.15 ± 0.02, 0.69 ± 0.01 and 0.23 ± 0.01 mL of the VOC mixture was introduced in the gas cell by 10 or 1 mL syringe. High-quality N_2 gas was then added to the cell until attaining 0.1 MPa on the pressure gauge (Fig.1c: P), in order to obtain VOC mixture gasses in pure N_2 gas.

Environmental quality standard guideline limit values of VOCs in soil and water are in the range of 0.005 to 1 mg/L[10, 11, 12]. If we take 50 mL of sample water containing this concentration range of VOCs which are all evaporated into a 1 L gas container, the volume concentration range will be 0.04 to 9 ppmV. This is the reason of the selection of above concentration ranges for VOCs.

Soil gas sample

A contaminated soil gas was collected in February 2006 from a soil formation at 1 m below the ground of a dry-cleaning shop located in Japan. A stainless liner (100 mm long, 6 mm ID: inner diameter) was inserted into a boring hole (20 mm ID). Then they were sealed with a silicone stopper and a putty for more than a half hour. After pumping 2 to 3 L of stagnant air, fresh soil gas was sampled by difference in pressure between the subsurface area and the sampling bag (1 L, polyvinyl fluoride film) covered with a

vacuumed airtight container.

The sampled soil gas was analyzed on site by gas chromatography (SRI, GC-310) with both photoionization detector (GC-PID) and electrolytic conductivity detector (GC-ELCD). Separation of VOCs was carried out on a NBW-310SS30 column (30 m long, 0.53 mm ID; 3.0 μm thickness). The same gas sample was then measured by gas cell FT-IR. About 1L of the sample gas was introduced from the sample bag to the previously evacuated gas cell. The pressure in the gas cell yielded 0.058 MPa on the pressure gauge and this corresponded to the initial sample gas volume of 1.3 L. N_2 gas was then added to the gas cell (2.3 ± 0.1 L) until attaining 0.1 MPa. FT-IR measurement of the soil gas in pure N_2 gas was conducted with the same conditions as the calibration study of standard VOCs.

RESULTS AND DISCUSSION

Raw spectra of standard VOCs

IR spectra of standard VOCs (1 ppmV) in the 1000 to 680 cm^{-1} region are shown in Fig.2 for 6 chlorinated compounds: 1,1-DCE, *cis*-1,2-DCE, *trans*-1,2-DCE, TCE, PCE and 1,1,1-TCA.

1,1-DCE has (1) a complex band with five peaks at 784, 787, 793 795 and 801 cm^{-1} and (2) a sharp peak at 868 cm^{-1} with a small peak at 862 cm^{-1}. *Cis*-1,2-DCE has (3) a sharp peak at 695 cm^{-1} and (4) a complex band around 870-840 cm^{-1} with a central peak at 848 cm^{-1} with 3 side bands at 856, 858 and 864 cm^{-1}. *Trans*-1,2-DCE has (5) a strong band at 830 cm^{-1} with a large shoulder at 820 cm^{-1} and (6) a weak peak at 898 cm^{-1} with fine features at the both sides around 884 and 914 cm^{-1}. TCE has (7) a sharp peak at 783 cm^{-1} with small side bands around 778 and 788 cm^{-1}, (8) a complex band with a central peak at 849 cm^{-1} and side bands around 845 and 853 cm^{-1} and (9) a broad band at 945 cm^{-1} with a large shoulder at 935 cm^{-1}. PCE has (10) a broad complex band around 782 cm^{-1}, (11) a weak broad complex band around 803 cm^{-1} and (12) a large band around 914 cm^{-1} with a shoulder around 921 cm^{-1}. 1,1,1-TCA has (13) a large broad band around 730 cm^{-1}.

These IR bands between 1000 and 680 cm^{-1} in the "fingerprint" region are due to complex differences in C-Cl stretching vibrations and/or C=C out-of-plane bending vibrations originated from different molecular structures around the C atom of these VOCs[13].

Calibration curves for individual standard VOCs

Among the above IR absorption bands for VOCs, the following peaks are selected for the quantitative analyses of VOC concentrations (Fig.2); the sharp peak at 868 cm^{-1}

(2) with a linear baseline (871-866 cm^{-1}) for 1,1-DCE, the central peak at 864 cm^{-1} (4) with a linear baseline (882-807 cm^{-1}) for *cis*-1,2-DCE, the weak peak at 898 cm^{-1} (6) with a linear baseline (900-894 cm^{-1}) for *trans*-1,2-DCE, the broad band at 945 cm^{-1} (9) with a linear baseline (969-882 cm^{-1}) for TCE, the broad band at 914 cm^{-1} (12) with a linear baseline (969-882 cm^{-1}) for PCE and the broad band at 723 cm^{-1} (13) with a linear baseline (736-708 cm^{-1}) for 1,1,1-TCA. The criteria for this selection of peaks used for their calibration are the large peak height, the narrow full width at half maximum (FWHM) and the least overlapping with other bands of VOCs. The peak 3 at 695 cm^{-1} was not selected for *cis*-1,2-DCE peak, because this region is often masked by atmospheric CO_2 bands.

Two types of calibration curves are shown in Fig.3 for IR absorbance (peak height) against concentration ranges from 0.1 ppmV to 1.0 ppmV (Fig.3a) and from 1.0 ppmV to 10 ppmV (Fig.3b) of each VOC. All the calibration plots of 6 VOC standards showed good linear relationships between the IR peak height and the concentration. By using the Lambert-Beer's law:

$$Abs = \varepsilon\, d\, c,$$

where Abs is the absorbance, ε is the absorption coefficient (L μL^{-1} m^{-1} or $ppmV^{-1}$ m^{-1}), d is the optical path length (10 m) and c is the concentration of a VOC species (ppmV). The absorption coefficients ε of VOC standards can be calculated from the slopes of calibration lines. These values were 1.4×10^{-2}, 7.3×10^{-3}, 2.0×10^{-3}, 7.9×10^{-3}, 1.2×10^{-2} and 1.8×10^{-2} $ppmV^{-1}$ m^{-1} for 1,1-DCE, *cis*-1,2-DCE, *trans*-1,2-DCE, TCE, PCE and 1,1,1-TCA, respectively, in the concentration range of from 0.1 ppmV to 1.0 ppmV (Table II). In the concentration range from 1.0 ppmV to 10 ppmV, they were 1.2×10^{-2}, 7.4×10^{-3}, 2.0×10^{-3}, 8.4×10^{-3}, 1.0×10^{-2} and 1.8×10^{-2} $ppmV^{-1}$ m^{-1} for 1,1-DCE, *cis*-1,2-DCE, *trans*-1,2-DCE, TCE, PCE and 1,1,1-TCA, respectively (Table II). These absorption coefficients show similar values for two different concentration ranges (from 0.1 ppmV to 1.0 ppmV; from 1.0 ppmV to 10 ppmV), maximum difference being 20% (Table II).

Calibration curves for a mixture of 6 standard VOCs

In order to test the applicability of these calibration lines for the mixture of these VOCs, an IR spectrum of a mixture of 6 chlorinated compounds was measured. The measurement conditions are the same as the above calibration study for individual VOCs. The spectrum of 6 VOCs mixture appears to be a sum of each IR spectrum for each compound without severe overlapping of characteristic peaks (Fig.2). The peak heights (absorbance) of these peaks are plotted against their concentrations (Fig.4). They show good linearities both for 0.1 to 1.3 ppmV and 1.0 to 13 ppmV ranges. The differences in absorption coefficients for VOCs in the 6 mixture for the two different

concentration ranges are within about 27% (Table II).

These absorption coefficients for 1,1-DCE, *trans* 1,2-DCE and 1,1,1-TCA in 6 mixture agree well, within 15% of deviation, with those for individual VOCs (Table II). However, those for *cis*-1,2-DCE, TCE, PCE show larger deviations up to 38% for *cis*-1,2-DCE. These differences are considered to be originated from the overlapping of the baselines for *cis*-1,2-DCE, TCE, PCE with absorption bands of *trans*-1,2-DCE.

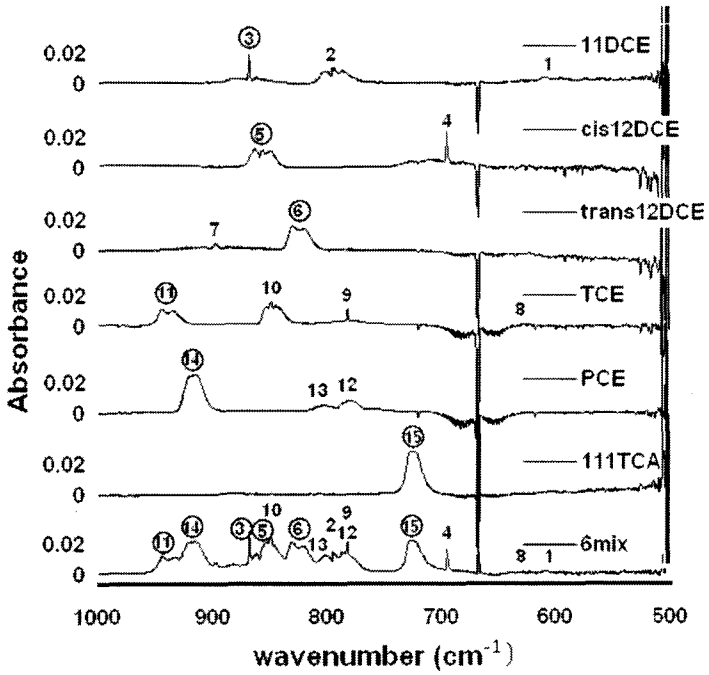

Fig.2 IR spectra for 1ppmV of 1,1-DCE, *cis*-1,2-DCE, *trans*-1,2-TCA, TCE, PCE, 1,1,1-TCA and for a mixture of these 6 compounds. Characteristic absorption peaks for each compound are numbered. The numbers for the selected peaks for calibration are circled.

TABLE II.
Absorption coefficients for 6 chlorinated volatile organic compounds determined from calibration lines for the ranges of 0.1-1.0ppmV and 1.0-10ppmV for the individual VOCs (Fig.3a,b) and for the mixture of 6 VOCs (Fig.4a,b). Their ratios for the mixture/i

VOC	absorption coefficient				ratio (mixture / individual)	
	individual		mixture (6 VOCs)			
Compounds	0.1-1.0 ppmV	1.0-10 ppmV	0.1-1.3 ppmV	1.0-13 ppmV	0.1-1.0 ppmV	1.0-10 ppmV
1,1-Dichloroethylene	1.4×10^{-2}	1.2×10^{-2}	1.4×10^{-2}	1.1×10^{-2}	1.0	0.92
cis-1,2-Dichloroethylene	7.3×10^{-3}	7.4×10^{-3}	4.5×10^{-3}	4.7×10^{-3}	0.62	0.64
trans-1,2-Dichloroethylene	2.0×10^{-3}	2.0×10^{-3}	1.7×10^{-3}	1.9×10^{-3}	0.85	0.95
Trichloroethylene	7.9×10^{-3}	8.4×10^{-3}	6.1×10^{-3}	6.7×10^{-3}	0.77	0.80
Tetrachloroethylene	1.2×10^{-2}	1.0×10^{-2}	8.2×10^{-3}	8.8×10^{-3}	0.68	0.88
1,1,1-Trichloroethane	1.8×10^{-2}	1.8×10^{-2}	1.8×10^{-2}	1.9×10^{-2}	1.0	1.1

Soil gas measurement

The results of the soil gas measurements are shown in Fig. 5 and Table III. Three VOCs, *cis*-1,2-DCE, TCE and PCE, are detected both by GC and FT-IR. In FT-IR measurement, inorganic gases, CO (2200-2100 cm^{-1}), N_2O (2260-2180cm^{-1}) and CO_2 (2400-2220 and 760-590 cm^{-1}), are also detected.

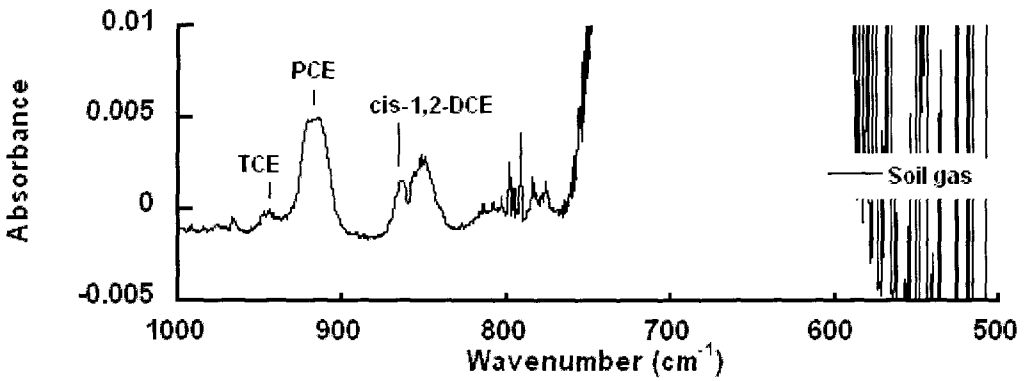

Fig.5 IR spectrum for a contaminated soil gas sample Characteristic IR peaks of TCE (945 cm^{-1}), PCE (914 cm^{-1}) and *cis*-1,2-DCE (898 cm^{-1}) are observed together with a saturated strong band of CO_2.

TABLE III.
The concentrations in ppmV of VOCs in a contaminated soil gas determined by the present 10 m gas cell FT-IR (FT-IR) together with the conventional gas chromatographic methods (GC-PID and GC-ELCD).

VOC	Concentration (ppmV)		
Compounds	GC-PID	GC-ELCD	FT-IR
1,1-Dichloroethylene	ND	ND	ND
cis- 1,2-Dichloroethylene	0.62	0.68	0.65
trans- 1,2-Dichloroethylene	ND	ND	ND
Trichloroethylene	0.12	0.14	0.22
Tetrachloroethylene	0.37	0.44	0.91
1,1,1-Trichloroethane	ND	ND	ND

ND: not detected

The *cis*-1,2-DCE concentration was calculated to be 0.65 ppmV by using the individual absorption coefficient in the range 0.1 to 1.0 ppmV (Table II, Fig.3a). This value is in good agreement with the concentrations determined by GC-PID (0.62 ppmV) and by GC-ELCD (0.68 ppmV).

The TCE concentration was calculated to be 0.22 ppmV by using the individual absorption coefficient in the range 0.1 to 1.0 ppmV (Table II, Fig.3a). This value is somewhat larger than the concentrations determined by GC-PID (0.12 ppmV) and by GC-ELCD (0.14 ppmV). The PCE concentration was calculated to be 0.91 ppmV by

using the individual absorption coefficient in the range 0.1 to 1.0 ppmV (Table II, Fig.3a). This value is about twice as large as the concentrations determined by GC-PID (0.37 ppmV) and by GC-ELCD (0.44 ppmV).

For TCE and PCE, the concentration values obtained by FT-IR were larger than those obtained by GC measurements despite the overlapping band effects for these compounds lowering the VOC concentrations. It is likely that these two compounds have sorbing characters to the sample bag (polyvinyl fluoride film) and they are desorbed from the bag by evacuation. In fact, VOCs can be lost due to sorption on tubing or sampling bag[14, 15]. Only small fractions of the sample gas are introduced to the GC instrument by leaving adsorbed gasses on the sample bag and the VOC concentrations by GC might be underestimated. The FT-IR data using most of the sample gas can therefore be closer to the real VOC concentrations.

All the above results indicate that direct VOC measurements by the present gas cell FT-IR method can successfully detect typical VOCs in contaminated soils in the same range as the environmental protection limits. For example, 0.65, 0.22 and 0.91 ppmV of *cis*-1,2-DCE, TCE and PCE, respectively were detected from a contaminated soil. The Japanese environmental quality standard limits for soil pollution for these 3 VOCs (0.04, 0.03 and 0.01 mg/L), by soaking a soil sample in 50 mL of water, which is then evaporated to a 1 L container, correspond to 0.5, 0.3 and 0.1 ppmV, respectively. Therefore, the present method can be used for screening possible presence of VOCs in soil environments.

CONCLUSION

In order to determine concentrations of chlorinated volatile organic compounds (VOCs) in contaminated soils, a gas cell FT-IR method was tested. 6 volatile organic standards and their mixture were measured by the 10 m long-path gas cell FT-IR for obtaining calibration lines. By selecting a characteristic peak for each compound, all the 6 VOCs showed satisfactory linear trends for concentration ranges of about 0.1 to 1.0 and 1.0 to 10 ppmV, respectively.

A contaminated soil sample was measured by this method. *Cis*-1,2-dichloroethylene, trichloroethylene and tetrachloroethylene were detected by the gas cell FT-IR. Their concentrations were 0.65, 0.22 and 0.91 ppmV, respectively based on the above calibration lines. This gas cell FT-IR method can therefore be a rapid multi-component analytical technique for VOCs in contaminated soils.

ACKNOWLEDGEMENT

The authors wish to express their gratitudes to Masanori Sunose and Satoshi Miwa for

their cooperation. We would like to thank Hironobu Gotoh, Keisho Nakanishi, Kenji Hanno and Masakazu Hayashi for their help in sampling and analysis of the contaminated soils.

References

1. J. W. Hodgeson and A. L. Cohen, "*Method 551 Determination of chlorination byproducts and chlorinated solvents in drinking water by liquid-liquid extraction and gas chromatography with electron capture detection*", (U.S. Environmental protection agency, Washington, DC, 1990), pp. 1-32
2. L. S. Clesceri, A. E. Greenberg and A. D. Eaton, "*Standard methods for the examination of water and wastewater*", 20th ed. (American Public Health Association, Washington, D.C., 1998), pp. 6-18
3. P. L. Hanst, A. S. Lefohn and B. W. Gay Jr, Appl. Spectrosc., **27**, 188 (1973)
4. Z. Bacsik, J. Mink and G. Keresztury, Appl. Spectrosc. Rev., **39**, 295 (2004)
5. T. L. Marshall, C. T. Chaffin, R. M. Hammaker and W. G. Fateley, Environ. Sci. Technol, **28**, 224A (1994)
6. B. Hren, K. Katona, J. Mink, J. Kohan and Gy. Isaak, Analyst, **125**, 1655 (2000)
7. G. M. Russwurm, R. H. Kagann, O. A. simpson, W. A. McClenny and W. F. Herget, J. Air Waste Manage. Assoc., **41**, 1062 (1991)
8. P. L. Hanst and S. T. Hanst, in "*Air Monitoring by Spestroscopic Techniques*", ed. M. W. Sigrist, Chemical Analysis Series 127, (John Wiley and Sons, New York, 1994), pp.335-470
9. C. J. Thompson, R. G. Riley, J. E. Amonette and P. L. Gassman, Appl. Spectrosc., **60**, 914 (2006)
10. EPA 816-F-02-013, "*Current Drinking Water Standards*", (U.S. Environmental Protection Agency, Washington, D.C., 2002), pp. 1-7
11. World Health Organization, "*Guidelines for Drinking-water Quality*", 3rd ed. (World Health Organization, Geneva, 2004), pp. 296-460
12. Environment Agency of Japan, "*Quality of the environment in Japan 1994*", (Environment Agency Government of Japan, Tokyo, 1996), pp. 341
13. G. Socrates, "*Infrared and Raman Characteristic Group Frequencies*", 3rd ed. (John Wiley and Sons, New York, 2001), pp. 198-208
14. E. Kivi-Etelätalo O. Kostiainen and M. Kokko, J. Chromatogr. A, **787**, 205 (1997)
15. Y. Wang, T.S. Raihala, A.P. Jackman and R. St. John, Environ. Sci. Technol., **30**, 3115 (1996)

CHAPTER 3.

Hydrothermal transformation of humic substances

3.2. Hydrothermal transformation of dissolved humic substances

3.3. The decarboxylation of dissolved humic substances under hydrothermal conditions

CHAPTER 3. Hydrothermal transformation of humic substances

INTRODUCTION

Natural organic matter (NOM) is widely distributed in soil, sediment and natural waters (Fig.3.1.1). NOM is classified into two types of organics; one is non-humic substances and the other is humic substances. Non-humic substances are commonly identifiable and are divided into natural polymers (celluloses, carbohydrates, nucleic acids, proteins and etc...) and small organic compounds (sugars, amino acids, fatty acids, dye, hydrocarbons and etc...)(Fig.3.1.2). On the other hand, humic substances are high molecular weight organic substances having brownish color with unknown variable chemical structures. They are considered to be mainly derived from biological constituents of planktons, plants and animals, through complex processes including Mayllard polymerization (Mayllard, 1913; Nissenbaum and Kaplan, 1972). In most natural waters, a major portion of dissolved organic carbon (DOC), defined as small organic compounds passing though 0.45 μm filter, is dominated by dissolved humic substances with 80% contribution of DOC (Fig.3.1.3, Thurman, 1985). In addition, humic substances have abundant hydrophilic functional groups such as –COOH and –OH that gives aqueous solubility, binding sites for metals, buffer capacities and other reactive characteristics (Stevenson, 1994). Because of their high abundance and reactivities, humic substances contribute primarily to the material cycling at the earth's surface.

Many researchers had attempted to characterize dissolved humic substances as sources for fossil fuel production, by-products in water treatments and carriers of material cycling. Thermal transformation (maturation) of humic substances are considered to produce natural gas (methane), petroleum and coals (van Krevelen, 1993). Mining geologists have studied interactions of metals and humic substances both for transportation of metals by complexation and metal deposition by redox processes (Nakashima, 1992, Landais and Gize, 1997). Recently, aqueous environmental geochemist have been interested in dissolved organic compounds as precursors of toxic chlorinated organic compounds such as trihalomethane (Rook, 1977). Marine chemists and forest ecologists have investigated DOM properties in oceans or forests (Coble, 1996; Berg and McClaugherty, 2003). Despite these extensive studies on DOM at the earth's surface at low temperatures, their behavior under hydrothermal conditions have not been studied in detail (Landais and Gize, 1999).

Organic materials in lithosphere are sometimes exposed to high temperatures because of hydrothermal activities (Fisher and Boles, 1990; MacGowan and Surdam, 1990; Martens, 1990; Barth, 1991; Haggerty, 1992 (a), (b); Kawamura and Nissenbaum,

Figure 3.1.1 Distribution of natural organic matter and hydrothermal environments at the earth's surface

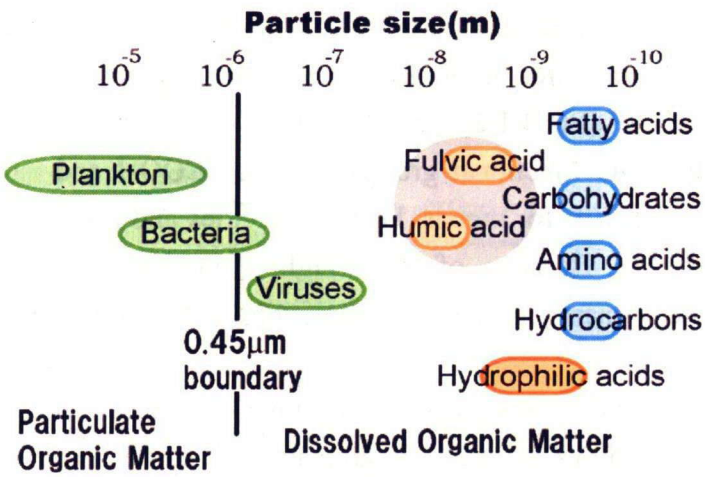

Figure 3.1.2 Classification by particle size of various dissolved organic matters in natural waters after Thurman E. M. (1985)

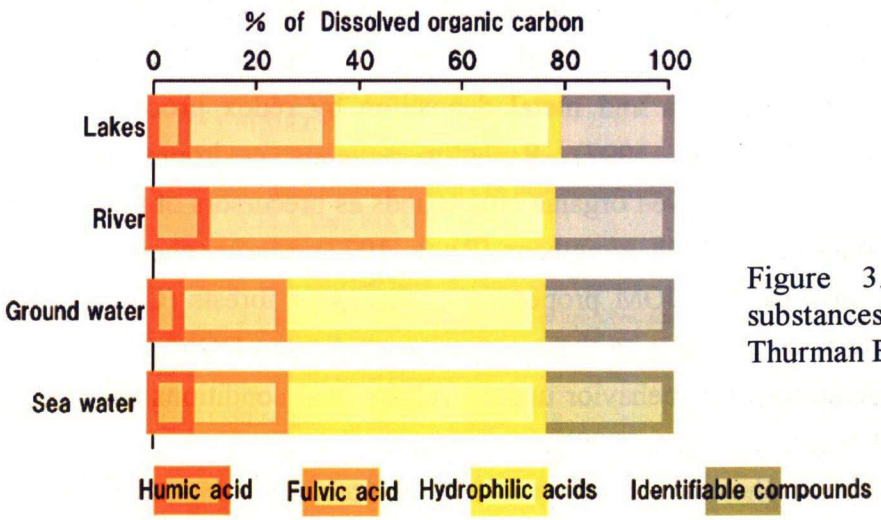

Figure 3.1.3 Distribution of humic substances in natural waters after Thurman E. M. (1985)

1992; Amend et al., 1998; Zeng and Liu, 2000). For example, hydrothermal environments exist often around volcanic activities and provide some hot springs at the earth's surface (Fig.3.1.1) Typical temperatures for hydrothermal solutions and hot springs water are 200-100°C and 90-30°C, respectively (Garven and Raffenspeger, 1997).

In addition, long-term behavior of organics in low temperature aquatic environments should be evaluated by accelerating reactions at higher temperatures, because they are very slow processes. Under these hydrothermal conditions, DOM might be decomposed with possible formation of low molecular weight compounds that are volatile.

In order to investigate the behavior of dissolved organic matter under hydrothermal conditions, we have conducted hydrothermal heating experiments of dissolved humic substances, representative DOM in the natural environment. We have paid particular attention to their functional groups playing key roles of geochemical processes. Volatile compounds formed during these processes have also been studied.

To achieve these objectives, three steps of spectroscopic observations were performed. The first step is the characterization of dissolved humic substances by different analytical methods. In particular, ultraviolet-visible (UV-VIS) and three -dimensional (3D) fluorescence spectroscopies have been employed to study functional groups of humic substances. The second step is the color decrease of dissolved humic substances and aromaticity change examined by UV-VIS spectroscopy and fluorescence index, respectively. The third step is focusing on the changes in functional groups of dissolved humic substances by using UV-VIS spectroscopy combined with the measurement of CO_2 emission monitored by gas cell FT-IR during the hydrothermal condition. Finally, I will discuss time-scales of hydrothermal transformation of humic substance by using obtained kinetic data.

REFERENCES

Berg B. and McClaugherty C. (2003) *Plant litter decomposition, humus formation, carbon sequestation*, Berlin; Heidelberg, Springer-Verlag

Coble P. G. (1996) Characterization of marine and terrestrial DOM in seawater using excitation-emission matrix spectroscopy, *Marine chemistry*, **51**, 325-346

Garven G., Raffenspeger J. P. (1997) Hydrogeology and geochemistry of Ore Genesis in sedimentary Basins, in *Geochemistry of hydrothermal ore deposits* 3rd ed. (Barnes H. L. ed.), New York, John Wiley & Sons, p125-189

Hunt J. M. (1996) *Petroleum geochemistry and geology* 2nd ed., New York, W.H. Freeman

Landais P., Gize A. P. (1997) Organic matter in hydrothermal ore deposit, in *Geochemistry of hydrothermal ore deposits* 3rd ed. (Barnes H. L. ed.), New York, John Wiley & Sons, p613-656

Nakashima S. (1992) Complexation and reduction of uranium by lignite, *The Science Total Environ*ment, **117/118**, 425-437

Maillard, L. C., (1913) Formation de matieres humiques par action de polypeptides sur sucres. *Comptes Rendus del'Académie des Sciences,* **156**, 148–149.

McNight D. M., Hood E. and Klapper L. (2003) Trace organic moieties of dissolved organic matrial in natural water, in Findlay S. E. G. and Sinsabaugh R. L. ed., Aquatic ecosystems interactivity of dissolved organic matter, Sun Diego; London, Academic press, pp.71-96

Nissenbaum, A. and Kaplan, J.R.(1972) Chemical and isotopic evidence for the in situ origin of marine humic substances. *Limnology and Oceanography*, **17**, 570–582.

Rook J. J. (1977) Chlorination reactions of fulvic acids in natural waters, *Environmental Science & Technology*, **11**, 478-482

Stevenson F. J., *Humus chemistry: genesis, composition, reactions* 2nd ed., New York: Wiley, 1994

Thurman. E. M. (1985) *Organic geochemistry of Natural waters*, Dordrecht, M. Nijhoff, 1-4

van Krevelen D. W. (1993) *Coal: typology-physics-chemistry-constitution* 3rd, completely revised edition, Amsterdam; New York, Elsevier Science Pub. B.V.

3.1 Characterization of fulvic acid

3.1.1. INTRODUCTION

3.1.1.1 Definition of humic substances

Dissolved organic matter (DOM), defined as small organic compounds passing though 0.45 μm filter, is common in natural waters such as rivers, lakes, oceans and ground waters. Only 20% of dissolved organic matter (DOM) in the natural aquatic environments is identifiable and the remaining 80% of DOM is dissolved humic substances (Fig.3.1.3, Thurman, 1985). Humic substances are defined as high molecular weight organic substances with unknown variable chemical structures. They are considered to be mainly derived from biological constituents of planktons, plants and animals, through complex processes including Mayllard polymerization (Mayllard, 1913; Nissenbaum and Kaplan, 1972).

Humic substances are operationally divided into 1) fulvic acid, 2) humic acid and 3) humin (Schnitzer and Khan, 1972): The fulvic acid is hydrophilic dissolved humic substance at most of pH conditions. The humic acid is the fraction of humic substances soluble in alkaline solutions, but is precipitated under acidic conditions (pH<2). The humin is insoluble solid phase at all the pH conditions. The international humic substance society (IHSS) defined the standard extraction procedures of humic substances from soils and natural waters and made several standard samples (Swift, 1996)

The majority of DOM is unidentifiable organics represented by dissolved humic substances. Humic substances have infinite forms by combined various chemical structures with abundant hydrophilic functional groups such as –COOH and –OH (Stevenson, 1994)(Fig.3.1.4). In other words, dissolved humic substances are heterogeneous hydrophilic polymers having various functions. DOM plays significant geochemical roles of material transport, reaction and recycling in natural environments (Wood, 1996). Because humic substances are dominant in natural aquatic environment among various dissolved organic substances, humic substances contribute primarily to the material cycling at the earth's surface.

3.1.1.2. The history of characterization of DOM

Because humic substances are heterogeneous unidentifiable polymers, many scientists have attempted to characterize humic substances since early twentieth century (Perdue and Ritchie, 2003). Before 1930s, DOM attracted attention due to their brownish color. Lots of researchers analyze origins of brownish colors and their characteristics. Their colors were often used as index of concentration of DOM. In 1970s, with rising of environmental awareness, researches on DOM explosively increased due to developments of analytical methods. Spectroscopy was the most

common tool for analyzing several properties of humic substances. Chromatography and mass spectrometry were not suitable for humic substances because of their heterogeneous nature.

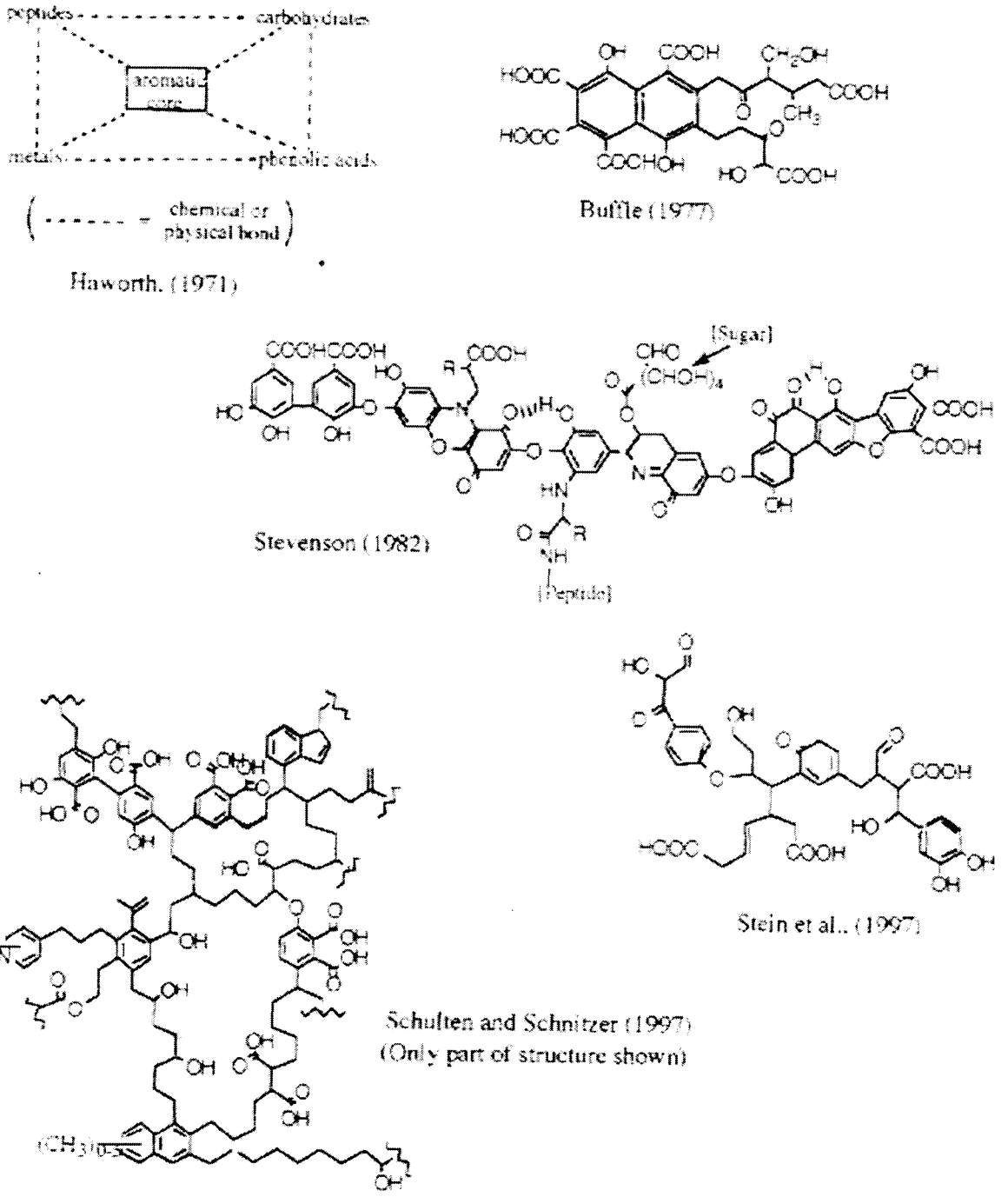

Fig.3.1.4 Chemical structure models of humic substances (Haworth, 1971; Buffle, 1977; Stevenson, 1982; Stein et al, 1997; Schulten and Schnizer, 1997)

3.1.1.3. Chemical structure of humic substances

Various chemical structures of humic substances have been suggested in the literature (Shulten and Schnitzer, 1997; Stevenson, 1982)(Fig.3.1.4). The basic structure model of humic substances is a highly cross-linked carbonaceous polymer constituted by aromatic cores with hydrophilic functional groups. Recently more detailed structure models have been suggested mainly based on NMR analyses (Hertkorn et al., 2002; Nacy et al., 1997). However, since humic substances have infinite forms by combinations of various chemical structural units, vibrational spectroscopy is still a good tool for functional group characterization. In order to understand functions of DOM in natural aquatic environments, the functional group analysis is particularly required. In this chapter, I aim to characterize properties of humic substances with special attentions on their functional groups, by using several spectroscopic methods together with some conventional analytical methods.

3.1.2. EXPERIMENTAL METHODS

3.1.2.1. Materials

As described before, physico-chemical properties of humic substances are heterogeneous depending on their origins. The International Humic Substance Society (IHSS), established in 1981, began to provide standard samples by extracting with a standard procedure (IHSS method) from several source areas. The standard samples make it possible for researchers to compare their experimental results on humic substances. Nordic fulvic acid reference sample and Nordic humic acid reference sample were obtained here from the International Humic Substance Society (IHSS). A small quantity (100 mg) of Nordic HA was used as dilute solutions.

Nordic HS were obtained from a drinking water reservoir at a lake in Norway. The reservoir is at 225 m above sea level and has a maximum depth of about 14 m. The sample was obtained from the intake pipe that draws water from at depth of 10m (pH = 5.6, EC = 2.1 mS m^{-1} and DOC = 10.7 mg L^{-1}). The water temperature was 4 ^{o}C. The detailed chemical properties including element analysis, acidic functional groups (Ritchie and Perdue, 2003), and carbon distribution (Thorn et al., 1989) are listed in Table 3.1.1.

3.1.2.2. Sample preparation

100 mg L^{-1} of these fulvic acid sample solutions were prepared by a volumetric flask. 100.1 mg of the powder sample was weighed by a microbalance and dissolved into 1000mL of deionized distilled water. Ionic strength was adjusted to 0.001 M by adding 58.5 mg of sodium chloride. The initial pH of 100 mg L^{-1} of Nordic fulvic acid was 3.7. For the Nordic fulvic acid solution of pH=3.6, its ionic strength was adjusted to

Table 3.1.1 Elemental compositions and functional group contents of Wako and Nordic humic substances (HA: humic acid; FA: fulvic acid)

							Ash %(w/w)	C (%)	H (%)	N (%)	O (%)	sum(C, H, N, O)	O/C	H/C
wako Humic acid	2003	997.8	66.4	18.4	634.4	286		58.1	3.9	1.1	36.9	100.0	0.48	0.79
Nordic Lake Humic acid	1504	747.5	62.6	15.0	665.8	13	0.86	50.1	4.2	1.0	44.7	100.0	0.67	1.00
Nordic Lake fulvic acid	1497	738.4	61.2	8.1	687.4	2	0.13	49.4	4.1	0.5	46.0	100.0	0.70	0.99
IHSS Nordic Lake HA *	-	-	-	-	-	-	0.31	53.3	4.0	1.2	43.1	101.6	0.61	0.89
IHSS Nordic Lake FA *	-	-	-	-	-	-	0.45	52.3	4.0	0.7	45.1	102.1	0.65	0.91

	Carboxyl group (mmol/g)	phenolic OH (mmol/g)
Nordic Lake Humic acid	9.06	3.23
Nordic Lake fulvic acid	11.16	3.18

Carbonyl	Carboxyl	Aromatic	Acetal	Heteroaliphatic	Aliphatic
220-190ppm	190-165ppm	165-110ppm	110-90ppm	90-60ppm	60-0ppm
10	19	38	7	11	15
10	24	31	7	12	18

* International humi * International humic substance society homepage, http://www.ihss.gatech.edu/
O contents are calcu O contents are calculated from the difference of the total weight minus ash contents and total of C, H, N contents.
* International humic substance society homepage, http://www.ihss.gatech.edu/
O contents are calculated from the difference of the total weight minus ash contents and total of C, H, N contents.

0.001 M by using NaCl.

3.1.2.3. Analyses

Concentration of the fulvic acid was analyzed by an Ultraviolet-visible (UV-VIS) spectrometer (V530 and V570, Jasco) at the wavelength of 254 nm. Two quarts cells were washed three times with pure water and three times with a sample solution. 3mL of 100 mg L^{-1} Nordic fulvic acid solutions for the normal quartz cell and 1 mL of for the quartz micro cell were needed for a path length of 1cm. The Lambert-Beer's law provides a direct link between UV-spectra and the concentration of a solute: Abs = ε c l, where Abs is the absorbance in UV-VIS spectra, ε is the molar absorption coefficient, c is the concentration of dissolved substance and l is the optical path length. UV-VIS spectra can therefore be used to determine concentration of solutes. These quartz cuvettes were placed in the UV-VIS spectrometer for measurement. All spectra were obtained with a spectral range from 600 to 200 nm and with a scan speed of 100 nm/minute. A bandwidth of 2.0 nm was applied with a data acquisition of 0.5 nm step.

Carbon concentrations in solutions were analyzed with a TOC analyzer (TOC-V, Shimadzu) using standard solution of potassium hydrogen phthalate ranging from 0 to 30 mg/L (Fig.3.1.5, Fig.3.1.6). The same sample was measured 2 to 3 times.

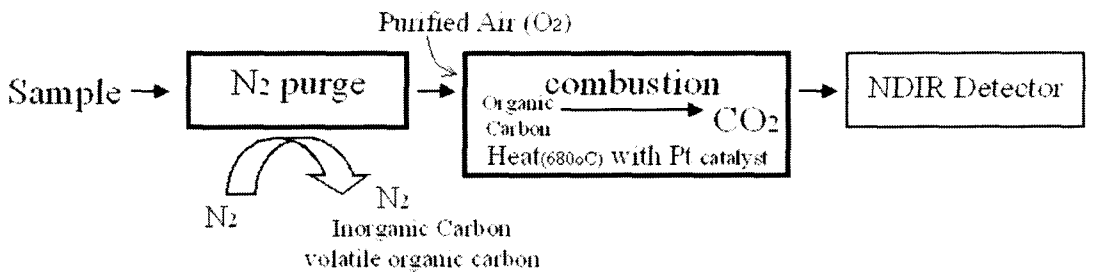

Fig.3.1.5 Conceptual protocol of total organic carbon analysis

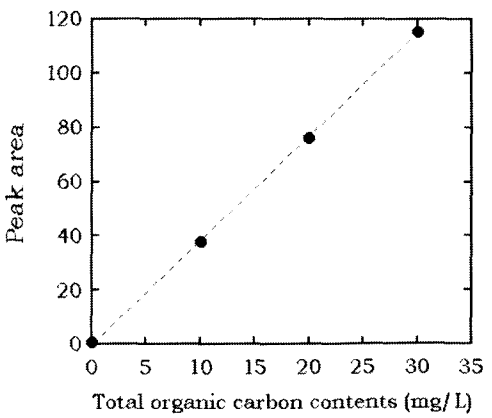

Fig.3.1.6 Calibration line for peak area against total organic carbon contents (concentration of potassium hydrogen phthalate solutions; 0, 10, 20 and 30mg/L)

Infrared (IR) spectroscopy and attenuated total reflectance (ATR) infrared spectroscopy are conducted for functional group analysis of the fulvic acid. The commercial flat ATR cell (Benchmark ATR Trough Top plate with ZnSe 45° plus volatile cover, Specac) was used to measure spectra of the fulvic acid solution. FT-IR spectra were recorded by Fourier transform infrared spectrometer (FT-IR) equipped with a mercury cadmium telluride (MCT) detector (Jasco, VIR-9500). One hundred interferograms at 4 cm^{-1} resolution were co-added to produce a single spectrum from 700 to 4000 cm^{-1}.

The CHN analyzer (CHN corder MT-6, Yanako) is PC-controlled and connected with a sample weighing compartment (microbalance MC-5, Sartorius). 1~2 mg of organic sample was weighed by using the microbalance and was set into a ship-shape sample holder. The sample holder was preliminarily heated at 950℃ during 1 minute for removing organic residues. All the samples were set in the automatic sampler and were measured for their carbon, hydrogen and nitrogen contents. Standard powders of 0, 500, 1000, 1500, 2000 and 2500 μg/L antipyrine ($C_{11}H_{12}N_2O$; C: 70.19% H: 6.43% N: 14.88% O: 8.50%, test sample recommended by the commission of the association of organic elemental analysis, Kishida Chemical Co., lot. No. SMA-SP-9) were weighed and were measured by the CHN analyzer. The carbon, hydrogen and nitrogen contents for these standard samples showed a good linear relations with the prepared carbon, hydrogen and nitrogen contents (Fig.3.1.7), with empirical calibration lines of y = 0.032 x + 19 for C, y = 0.0058 x + 2.4 for H, y= 0.34 x + 39 for N

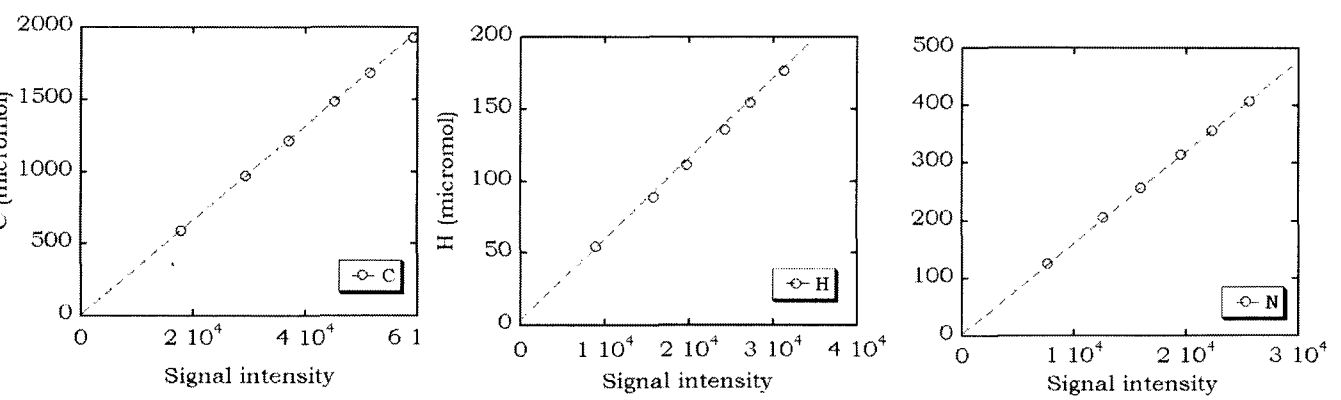

Fig.3.1.7 The calibration lines of C, H and N contents for 0, 500, 2000 and 2500μg/L antipyrine ($C_{11}H_{12}N_2O$).

The fluorescence spectra were recorded on spectrophotometer (FP-6600, Jasco) with a halogen lamp (800-350 nm) and a deuterium lamp (350-190 nm). A series of

emission spectra were collected over a range of excitation wavelength. The 61 individual emission spectra were scanned from 250 to 550 nm at sequential 5 nm increment of excitation wavelength between 200 and 500 nm. These individual spectra were calculated by analysis software (Spectra Manager, Jasco) to generate topographic contour plots. The excitation and emission bandwidths were set to 5 nm and 6 nm, respectively, and the integration time at each wavelength was 0.1 sec. The spectra were calibrated against an external standard, 10 μg L^{-1} quinine sulfate in 0.1N sulfuric acid solution with a known value of 10 QSU (quinine sulfite unit).

The zeta potential for Nordic fulvic acid solution was measured by an Electrophretic Light Scattering Spectrophotometer (Zeecom, microtech nition Co.). This analyzer observes the migration of particles under an optical microscope through an image processing.

3.1.3. RESULTS

3.1.3.1. UV-VIS spectroscopy

UV-VIS spectra in the 200 - 600 nm range of Nordic fulvic acid solutions with the varying concentrations form 10 –100 mg L^{-1} are shown in Figure 3.1.8. Absorption intensities increased in the shorter wavelength region with increasing concentrations of the fulvic acid. A weak shoulder bands is observed at 255-275 nm. Absorbance values at 254 nm are plotted against the concentration of Nordic fulvic acid solutions in Fig 3.1.9. These show a good linear correlation with the fitted line: $y = 0.0237x + 0.0007$, where y is the absorbance at 254nm and x is the concentration of Nordic fulvic acid (mg/L).

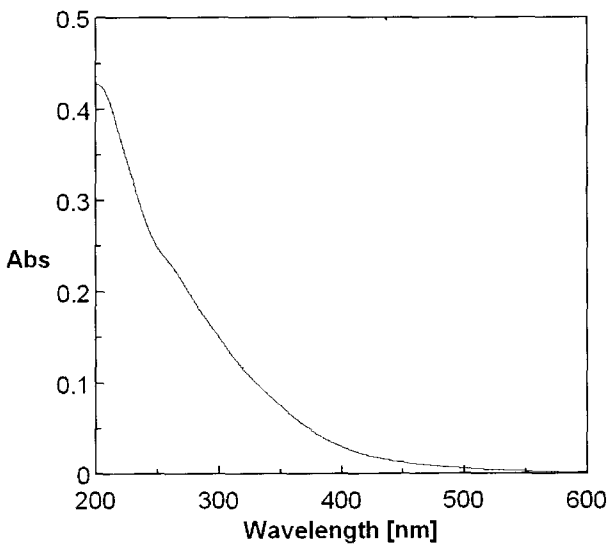

Fig.3.1.8 UV/VIS spectra of 10mg L^{-1} Nordic fulvic acid

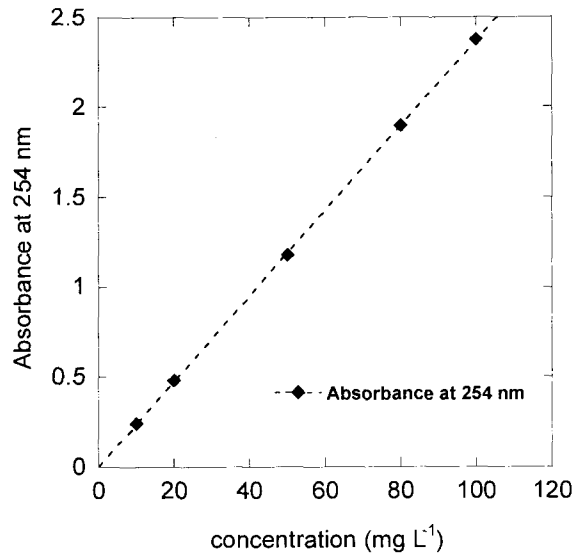

Fig.3.1.9 Calibration line for absorption peak height at 254 nm (Abs_{254}) against concentration of Nordic fulvic acid (d = 1 cm)

3.1.3.2. Total organic carbon (TOC)

The total organic carbon (TOC) content of 10 mg L^{-1} Nordic fulvic acid solution (ionic strength I=0M) was 4.59 ± 0.05 mg L^{-1}. The TOC for Nordic fulvic acid solution with the ionic strength of 0.001M was 4.50 ± 0.06 mg/L. The difference in ionic strength between 0M and 0.001M is found to have no significant effect on the TOC content of the humic substances solutions.

3.1.3.3.Infrared spectroscopy

ATR-IR spectra of Nordic fulvic acid could be measured in the concentration range from 1000 to 14580 mg L^{-1} at pH 4 as shown in Fig. 3.1.10. Major IR absorption bands of fulvic acid were assigned as follows (Table 3.1.2): 2800-2900 cm^{-1} (aliphatic C-H stretching), 1720 cm^{-1} (carboxyl and ketonic carbonyl C=O stretching), 1600 cm^{-1} (aromatic C=C and conjugated carbonyl C=O), 1400 cm^{-1} (symmetrical stretching of COO^-, OH deformation, and C-O stretching of phenolic groups), and 1220 cm^{-1} (C-O stretching and O-H deformation of COOH groups). Fig. 3.1.10B shows their calibration lines for absorption peak heights at 1712, 1590, 1384 and 1215 cm^{-1} against concentration of Nordic fulvic acid.

Table.3.1.2 Major IR observation bands of fulvic acid

Frequency (cm^{-1})	Assignment
3000-2800	stretching vibration of aliphatic C-H
1720-1700	C=O stretching of carboxyl group (-COOH)
1660-1630	quinone C=O stretching and conjugated carbonyl C=O
1620-1600	aromatic C=C and conjugated carbonyl C=O
1590-1517	synmetric stretching vibration of C=O ($-COO^-$), N-H deformation + C=N stretching vibration (amide II band)
1460-1450	bending vibration of aliphatic C-H
1400-1390	OH defromation and C-O streching of phenol OH and asynmetric stretching vibration of -COO-
1280-1200	C-O stretching vibration of OH defromation of carboxyl group (-COOH) , -C-O stretching vibration of aryl ether.
1170-950	C-O stretching vibration of polysaccharide or ether compound, Si-O of silicate impurities

The IR spectra of 10000 mg L^{-1} Nordic fulvic acid with varying pH 3-10 are shown in 3.1.11. The peaks at 1590 and 1384 cm^{-1} shift clearly as the pH increases (Fig.3.1.12A). The peaks at 1712 and 1215 cm^{-1} show no significant change in their peak positions The peak intensities at 1590 and 1384 cm^{-1} increase as the pH increases, while the peak intensities at 1712 and 1215 cm^{-1} decrease as the pH increases as shown in Fig.3.1.12B.

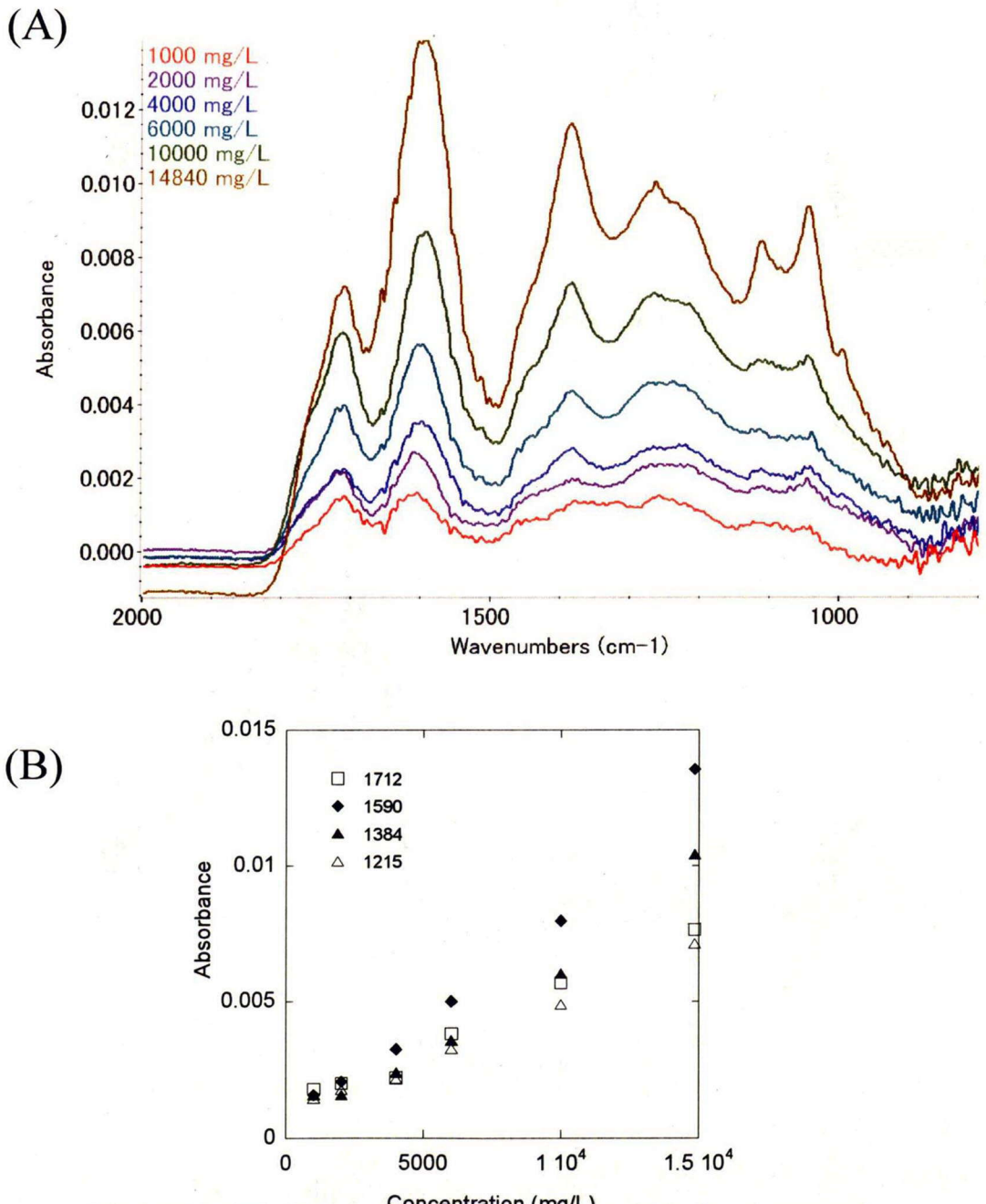

Fig.3.1.10 ATR-IR spectra of Nordic fulvic acid in the concentration range from 1000 - 14840 mg/L and (B) their calibration lines for absorption peak heights at 1712, 1590, 1384 and 1215 cm^{-1} against concentration of Nordic fulvic acid.

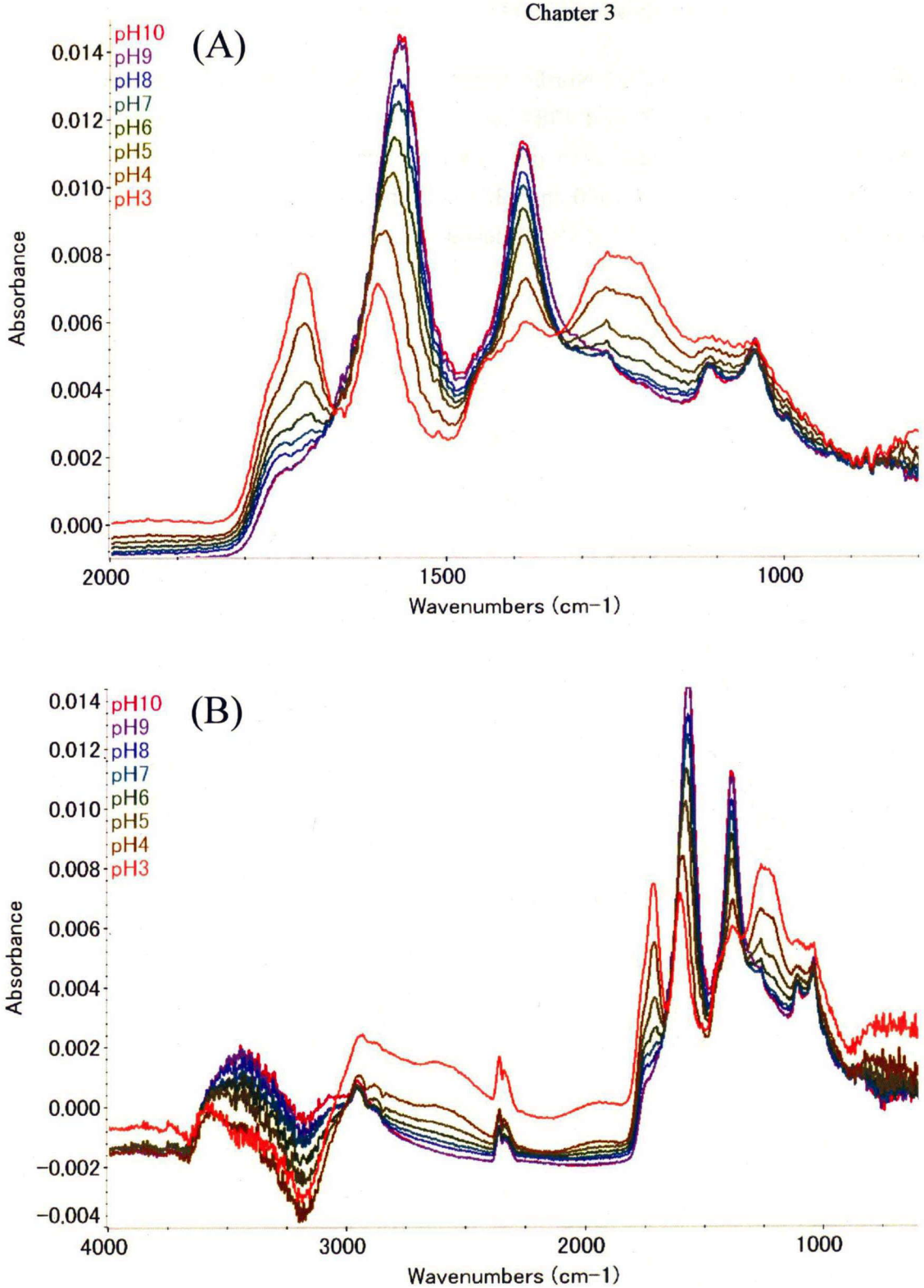

Fig.3.1.11 ATR-IR spectra of 10000 mg/L Nordic fulvic acid for the pH of 3 to 10 (A) 800 – 2000 cm^{-1} and (B) 700 – 4000 cm^{-1}.

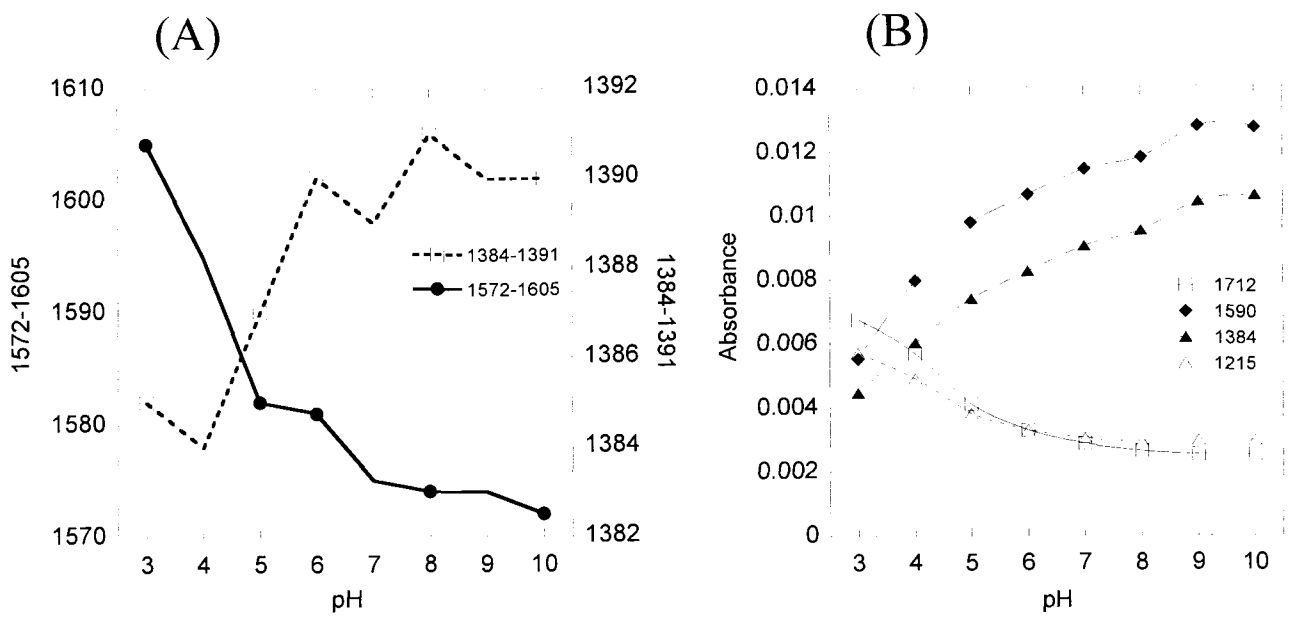

Fig.3.1.12 ATR-IR spectra changes of 10000 mg/L Nordic fulvic acid for the pH of 3 to 10 (A) Changes in peak position with pH (B) Changes in absorbance with pH

3.1.3.4. Organic elemental analysis

Carbon, hydrogen, nitrogen and oxygen contents of studied humic substances are shown in Table 3.1.1. Nordic fulvic acid has 49.4 % of carbon, 4.1 % of hydrogen, 0.5 % of nitrogen and 46.0 % of oxygen. Nordic humic acid has 50.1 % of carbon, 4.2 % of hydrogen, 1.0 % of nitrogen and 44.7 % of oxygen. Published elemental composition data of Nordic fulvic acid and Nordic humic acid show similar results: 52.3 % of carbon, 4.0 % of hydrogen, 0.7 % of nitrogen and 45.1 % of oxygen and 53.3 % of carbon, 4.0 % of hydrogen, 1.2 % of nitrogen and 43.1 % of oxygen (International humic substance society homepage). Compositions of Nordic humic acid and Nordic fulvic acids are similar. However, Nordic fulvic acid has smaller nitrogen and slightly greater oxygen contents than the humic fraction. Therefore, O/C ratio of Nordic fulvic acid is slightly greater than that of Nordic humic acid.

H/C and O/C atomic ratios of Nordic fulvic acid and Nordic humic acid are plotted in the van Krevelen diagram (Fig.3.1.13). Nordic humic substances were found to belong to young Type III kerogen. In typical aquatic humic substances, the range of H/C is 0.9-1.0 and the range of O/C is 0.6-0.7 (IHSS homepage). Nordic fulvic and humic acid are in this typical aquatic range.

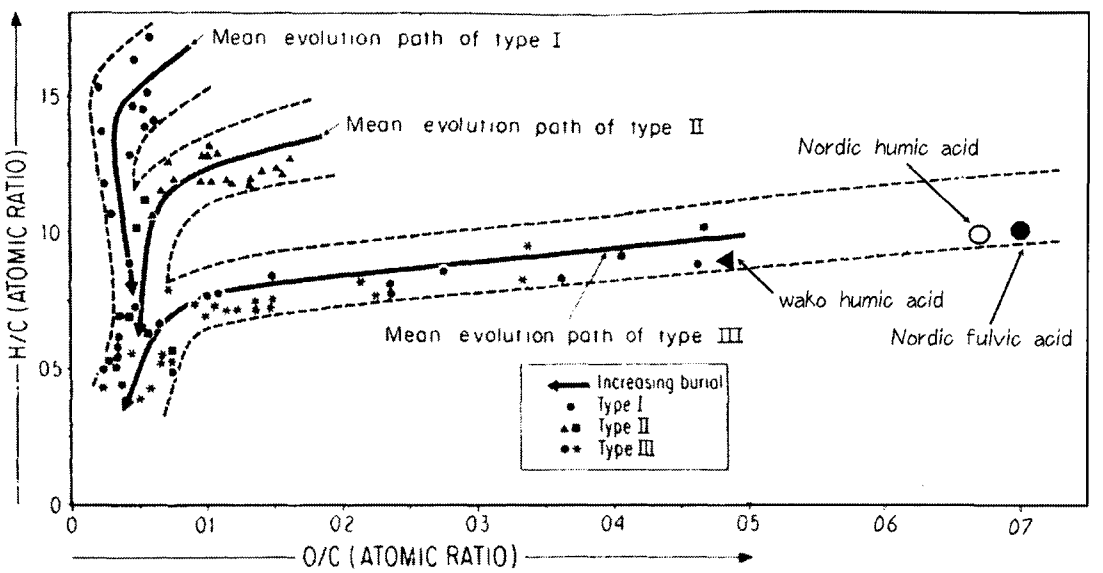

Position in the Van Krevelen diagram of the elemental analysis of selected series of kerogens:

Type I: ● Green River Shales, Uinta Basin, USA

Type II: ▲ Lower Toarcian Shales of the Paris Basin, France
■ Posidonienschiefer (Durand, unpublished).

Type III: • Logbaba wells, Upper Cretaceous, Douala Basin, Cameroon

• Humic coals

Fig.3.1.13 van Krevelen diagram of typical series of kerogens (O/C vs. H/C atomic ratio plot) (Hunt, 1996) with the data of Wako humic and Nordic humic and fulvic acids.

3.1.3.5. 3D-fluorescence spectroscopy

A 3D- fluorescence spectrum of a Nordic fulvic acid solution (10 mg L^{-1}) is shown in Fig.3.3.14. Fluorescence spectra of Nordic fulvic acid show the typical fluorescence signature of humic substance such as fulvic-like component (α and α') and humic-like component (η) in the contour map. The maximum excitation and emission wavelengths of fulvic-like (α and α'), humic-like (η) peaks are at 440 nm (340 nm excitation), 450 nm (250 nm excitation) and 530 nm (485 nm excitation), respectively. The relative intensity change against the concentration is shown in Fig 3.1.15 and Fig 3.1.16. All three peaks, peak α, peak α' and peak η, increase with the concentration. While the relative intensity of peak α is lower than that of peak α' in the lower concentration range (5-20 mg L^{-1}), the relative intensity of peak α is higher than that of peak α' in the higher concentration range (25-50 mg L^{-1}).

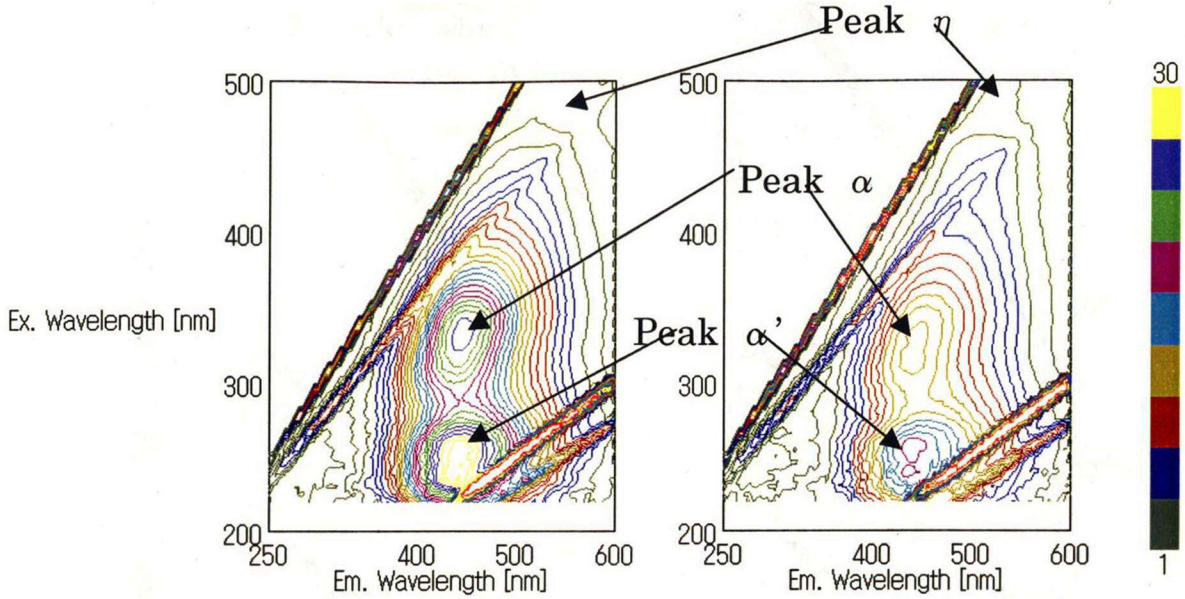

Fig.3.3.14 3D-fluorescence spectra of 10 mg/L Nordic fulvic acid (left)

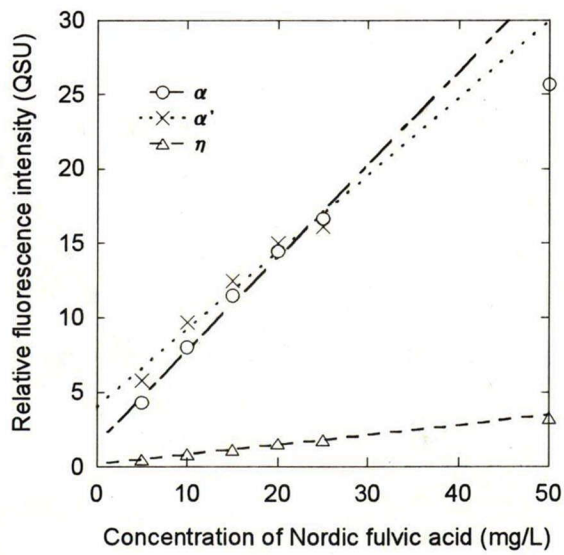

Fig.3.1.15 Calibration lines for relative fluorescence intensities at peak α (fulvic-like), peak α' and peak η (humic-like) against the concentration of Nordic fulvic acid (d = 1 cm)

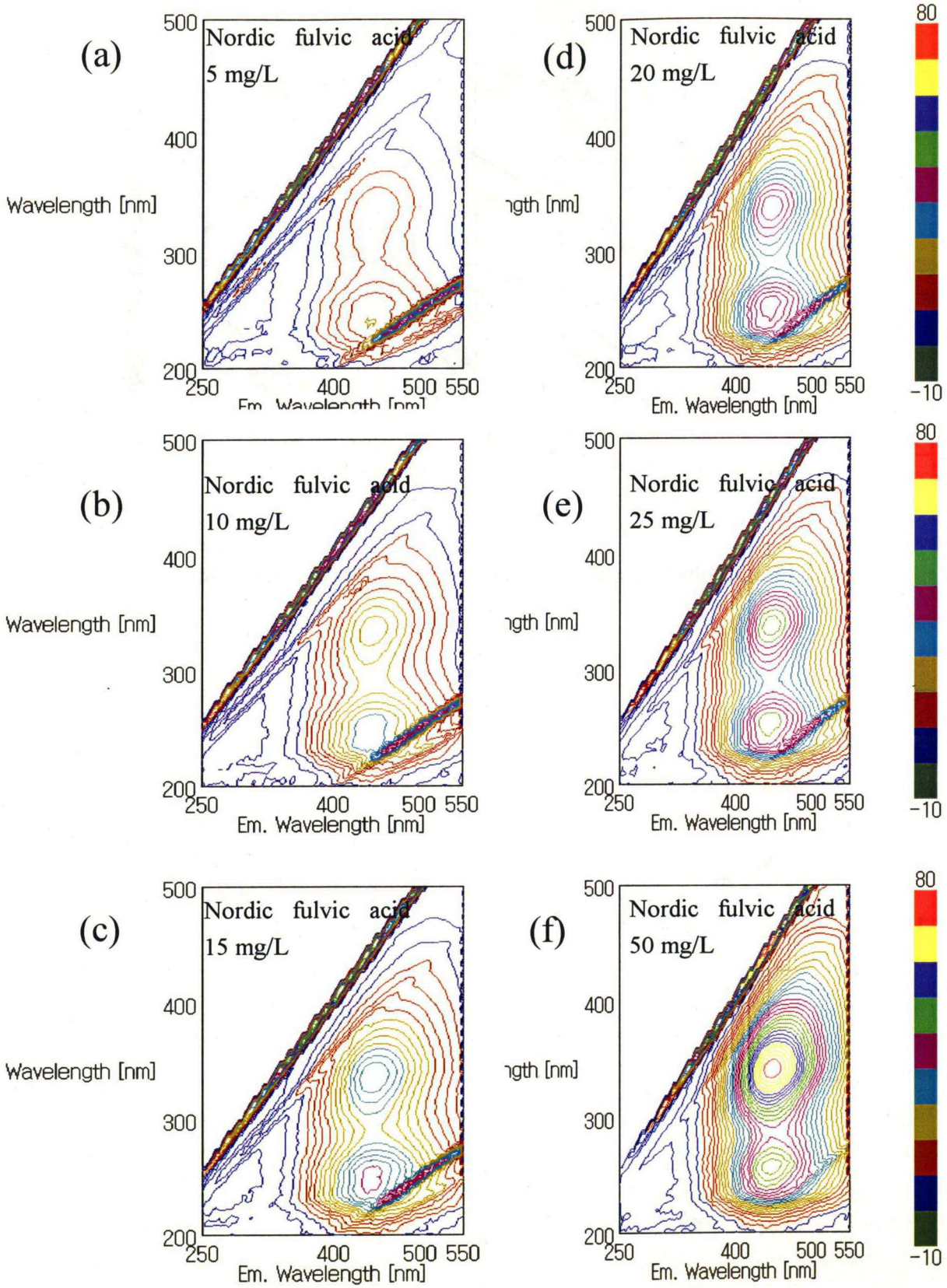

Fig.3.1.16.3D-fluorescence spectra of Nordic fulvic acid solutions (a) 10mg/L, (b) 10 mg/L), (c) 15mg/L, (d) 20mg/L), (e) 25mg/L, (f) 50mg/L

3.1.3.6. Zeta potential

Zeta potential (surface charge) of the Nordic fulvic acid solution (100 mg L^{-1}) was –58.7 ± 4.2 mV at pH = 3.6. This result indicated that the Nordic fulvic acid molecule has negative surface charges originated from acidic functional groups such as COOH and COOH.

3.1.4. DISCUSSION

3.1.4.1. UV-VIS spectrum of humic substance

The UV-VIS spectra of dissolved humic substance show the featureless broad absorption bands in 190-600 nm (Fig.3.1.18). The chemical structure of Humic substance, as a representative of natural organic matter, consists different kinds of chromophores, which make it impossible to identify the exact wavelength with a specific chromophore (Schnitzer and Khan, 1972; Traina et al., 1990; Gu et al., 1995, 1996; Chen et al., 2002; Korshin et al., 1997). Because various organic structures are conjugated in humic substances, these absorption bands are considered to be overlapped. The overall UV spectrum of HS is generated by the superposition of numerous individual bands as in benzene (Fig.3.1.17).

This absorption spectrum can be understood by the following explanation of electronic energy levels in benzene molecules from Jaffe and Orchin (1962). Electrons in the ground state (designated as $^1A_{1g}$) may absorb quanta of light and be promoted to π-antibonding orbitals, corresponding to energy levels denoted as $^1E_{2u}$, $^1B_{1u}$ or $^1B_{2u}$. Korshin (1997) explained UV region of absorption spectra of humic substance consists of three distinctive absorption bands the local-excitation (LE) band, the benzenoid (Bz) band and the electron-transfer (ET) band.

In benzene, the transition $^1A_{1g} \rightarrow {}^1E_{2u}$ occurs by absorption of light at 180 nm. The corresponding spectral band is very intense (molar extinction coefficient ε = 60000 cm^2 mol^{-1}), since there is no quantum-mechanical prohibition of the transition. This band will be referred to as the LE band, as suggested by Scott (1964). The transition $^1A_{1g} \rightarrow {}^1B_{1u}$ generates an absorption band centered at 203 nm for benzene (Fig. 3.1.17). This band is referred to sometimes as the Bz band. It is less intencse (ε = 7400 cm^2 mol^{-1}) than the LE band, since the transition is forbidden, but light absorption takes place because of vibrational perturbations in the π–electron system (Table 3.1.3). The third band, corresponding to the $^1A_{1g} \rightarrow {}^1B_{2u}$ transition in benzene, is centered at 253 nm and has low intensity (ε = 204 cm^2 mol^{-1}) because of very strong quantum-mechanical prohibition (Fig.3.1.17). This band is a distinctive feature of the electronic spectra of aromatic compounds and often is refereed to as the ET band. The intensity of the ET band is greatly affected by the presence of the ring of polar functional groups such as

hydroxyl, carbonyl, carboxyl and ester groups, which increase its molar extinction coefficient from close to 200 cm^2 mol^{-1} for unsubstituted benzene to as high as several thousand cm^2 mol^{-1} (Table 3.1.3, Fig. 3.1.17). By contrast, non-polar aliphatic groups attached to the ring do not increase the intensity of ET transition significantly, with ε generally remaining below 300 cm^2 mol^{-1}. The Bz band is also sensitive to substitution on the ring, but less sensitive than the ET band.

Table 3.1.3 Substituent effect of absorption maxumum wavelenght and molar absorption coefficients (ε: L mol^{-1} cm^{-1}) in UV-VIS spectra of a) mono-substituted benzene and b) di-substituted benzene

mono-substituted benzene

sustitutent	Bz band		ET band	
	λ	ε	λ	ε
H	204	7400	254	204
OH	211	6200	279	1450
COOH	230	11600	273	970

di-substituted benzene (ortho)

sustitutent	Bz band		ET band	
	λ	ε	λ	ε
OH, CHO	256	12600	324	3400
OH, COOH	237	9000	303	3600
N2O, OH	279	6600	351	3200

di-substituted benzene (meta)

sustitutent	Bz band		ET band	
	λ	ε	λ	ε
OH, CHO	255	10100	314	2580
OH, COOH	237	7500	296	2500
N2O, OH	274	6000	333	1960

di-substituted benzene (para)

sustitutent	Bz band		ET band	
	λ	ε	λ	ε
OH, CHO	-	-	284	16000
OH, COOH	-	-	255	13900
N2O, OH	-	-	318	10000

The reason for the common use of absorbance at 254 nm for an index of concentration of dissolved organic matter is originated from molecular explanation for ET band. Jaffe and Orchin (1962) proved that polar functional groups attached to aromatic rings greatly enhance the ET band absorption. Therefore monitoring on the ET band can provide information on the transformation of polar functional groups attached to aromatic rings.

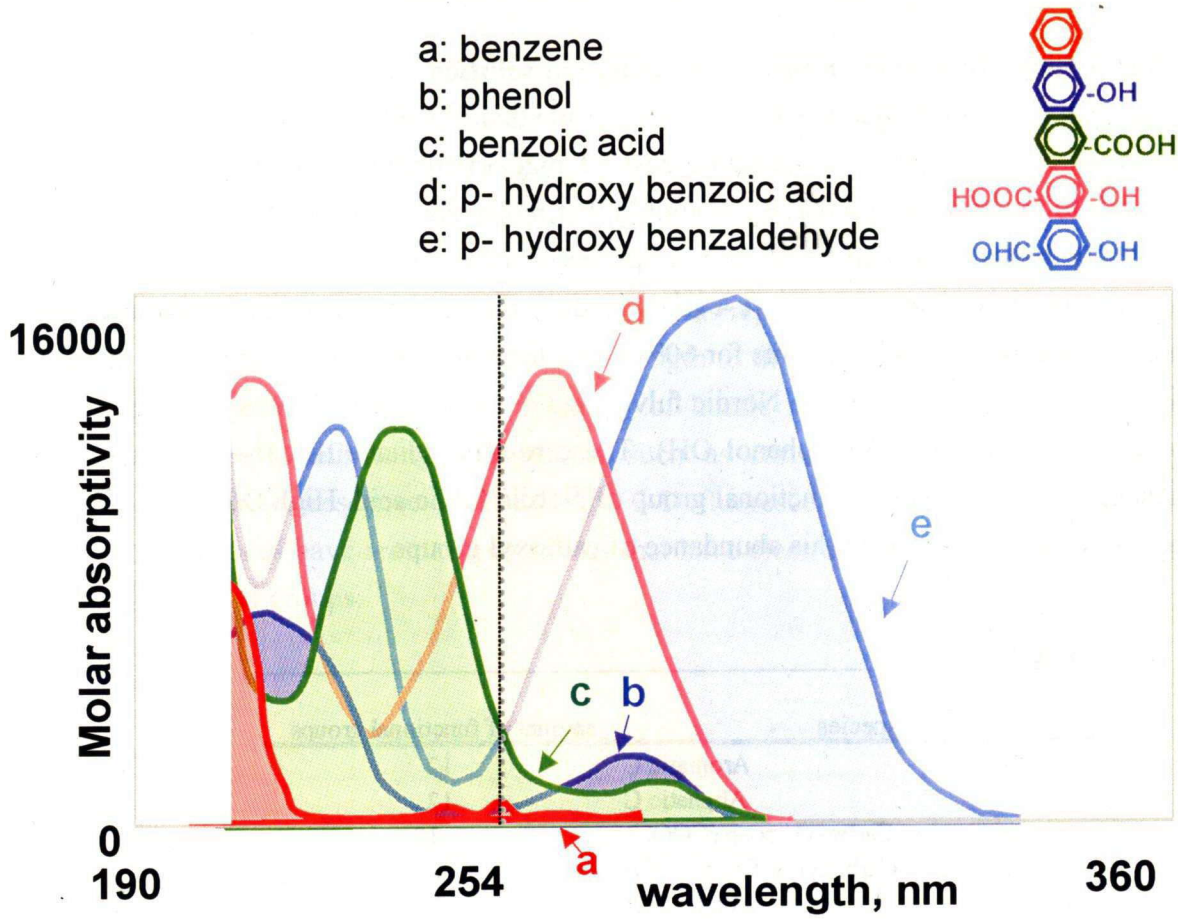

Fig.3.1.17 UV spectra of substituted benzene (Masuda, 2005)

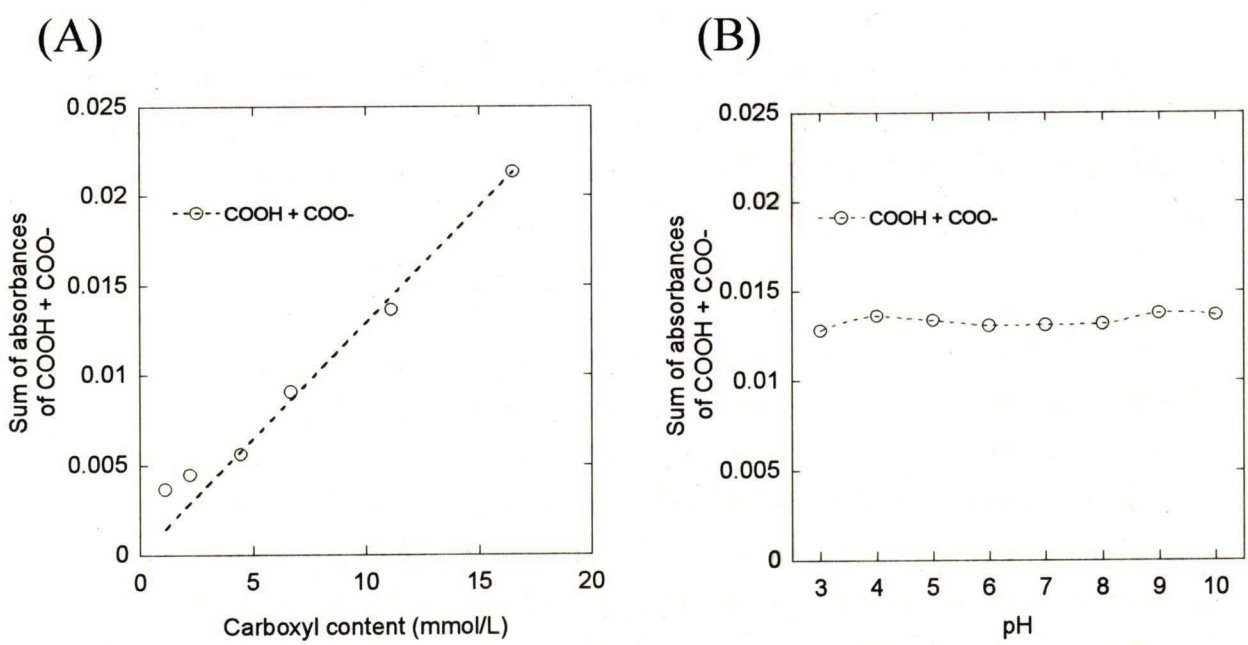

Fig.3.1.18 Calibration line for the sum of IR absorbance of COOH and COO^- against carboxyl content of fulvic acid (d = 1 cm) in (A) different concentration of fulvic acid (1000-14860 mg L^{-1}) and (B) different pH (pH 3-10)

3.1.4.2. Chemical structures of humic substances in solution

The results of total organic carbon (TOC) contents of the humic substances are in agreement with those of organic microanalyses: 4.5 mgC in 10mg of Nordic fulvic acid corresponds to the organic of 45%. By assuming that molecular weight of Nordic fulvic acid is 1000 dalton, distribution of carbon species can be estimated from published NMR and titration data. Table 3.1.4 shows that the carbon skeleton structure (aromatic-C and aliphatic-C) accounts for 60% of the total organic carbon. The ratios of functional groups against carbon in Nordic fulvic acid are about 30 % (carboxyl group), 17% (carbonyl group) and 8% (phenol OH). These results indicate that the carboxyl functional groups are the main functional group of Nordic fulvic acid. High O/C ratio of Nordic fulvic acid also confirm this abundance of carboxyl groups.

Table 3.1.4

species	amount of functional groups
Aromatic C	12
Aliphatic C	12
Carboxyl group (COOH)	5~10
Carbonyl or Ester (C=O)	4
Acetal (C-O)	3
Phenolic -OH	2

Negative surface charges obtained from zeta potential analysis were indicated that Nordic fulvic acid particles have negative charges in water by ionizing their hydrophilic functional groups such as $-COO^-$. These considerations suggest that functional groups observed in IR spectra are only carboxyl groups except for small amount of C-H (Fig. 3.1.10).

To quantify the carboxyl groups in solutions, I will use the sum of IR absorbance COOH and COO^- (Fig.3.1.11). Celi et al (1997) showed the relationship between the content of total COOH groups of fulvic acid and the sum of absorbance at COOH (the maximum absorbance at 1720-1710 cm^{-1}) and COO^- (the maximum absorbance at 1620-1600 cm^{-1}) by using KBr method for soil humic substance powder and 2-hydroxyl benzoic acid. Fig 3.1.18 shows the good relationship between carboxyl content estimated from titration data (11.16 μmol gC^{-1}) and sum of absorbances even in the dissolved state in water and in different pH. This relationship will be applied to the estimation of adsorbed content of carboxyl groups in section 4.1.

The fluorescence spectra of dissolved humic substances show small relative intensities at longer emission wavelengths (Fig.3.3.14). Because aliphatic structures are

fluorescence inactive, fluorescent natures of humic substances are derived from π-π* and n-π* transitions such as aromatic structures or aromatic carboxyl groups. The fluorescence peaks of humic substances are similar to m-hydroxybenzoic acid which has a fluorescence peak at 430 nm (314 nm excitation) (Thommes G. A. and Leinnger E., 1958) (Fig.3.3.14). Fluorescence intensity of substituted benzene with substituted fragments (CH_3, OH, NH_2 and COOH) was reported as shown in Table.3.1.5. Both OH and COOH shifts the emission wavelength to the longer wavelength than benzene. The small relative fluorescence intensity of humic substances are possibly derived from electron withdrawing substituents such as carboxyl groups, which largely reduce relative fluorescence intensity. The 3-D fluorescence spectra suggest that the humic substances have aromatic structures that have electron withdrawing substituents such as carboxyl groups.

REFERENCES

Celi L., Schnitzer M. and Negre M. (1997) Analysis of carboxyl groups in soil humic acids by a wet chemical method, Fourier-transform infrared spectrophotometry, and solution state carbon –13 nuclear magnetic resonance. A comparative study, *Soil Science*, **162**, 189-197

Chen, J., Gu, B., LeBoeuf, E. L., Pan, H., Dai, S. (2002) Spectroscopic characterization of the structural and functional properties of natural organic matter fractions., *Chemosphere*, **48**, 59-68,

Gu, B., Mehlhorn, T. L., Liang, L, and McCarthy, J. F. (1996) Competitive adsorption, displacement, and transport of organic matter on iron oxide .1. Competitive adsorption., *Geochimica et Cosmochimica Acta*, **60**, 1943-1950

Gu, B., Schmitt, J., Chen, Z., Liang, L., McCarthy, J. F., (1995) Adsorption and desorption of dirrenet organic-matter ractions on iron-oxide., *Geochimica et Cosmochimica Acta*, **59**, 219-229,

Hertkorn N., Permin A., Perminova I., Kovalevskii D., Yudov M., Petrosyan V., and Kettrup A. (2002) Comparative Analysis of Partial Structure of a Peat Humic and Fulvic Acid Using One- and Two- dimensional Nuclear Magnetic Resonance Spectroscopy, *Journal of Environmental Quality*, **31**, 375-387

Jaffe, H. H. and Orchin, M. (1962) *Theory and Applications of Ultraviolet Spectroscopy.* John Wiley, New York.

Maillard, L. C., (1913) Formation de matieres humiques par action de polypeptides sur sucres. Comptes Rendus del' Académie des Sciences, **156**, 148–149.

Nanny M. A., Minear R. A. and Leenheer J. A. (1997) *Nuclear magnetic resonance spectroscopy in environmental chemistry*, New York, Oxford University Press

Nissenbaum, A. and Kaplan, J.R. (1972) Chemical and isotopic evidence for the in situ origin of marine humic substances. *Limnology and Oceanography* **17**, pp. 570–582.

Perdue E. M. and Ritchie J. D., (2003) *Treatise on Geochemistry Vol.5 Surface and ground water, weathering, and soils*, Oxford, Elsevier Pergamon, pp273-318

Schnitzer M. and Khan S. U. (1972) *Humic substances in the environment*, New York, M. Dekker, pp.1-7

Schulten H. –R. and Schnitzer M. (1997) Chemical model structures for soil organic matter and soils, *Soil Science*, **162**, 115-130

Stevenson F. J. (1982) *Humus chemistry: genesis, composition, reactions*, New York: Wiley

Stevenson F. J. (1994) *Humus chemistry: genesis, composition, reactions* 2nd ed., New York: Wiley

Stein L.T., Kolla S., Varnum J. M. Davies G. and Jansen S. A. (1997) Conformational modeling of a proposed building block of humic acid: Searching chirally undefined conformational space, in *The Role of humic substances in the ecosystems and in environmental protection* (eds. Drozd J., Gonet S. S., Senesi N. and Weber J.), Polish society of humic substance, 73-77

Thommes G. A. and Leinnger E. (1958) Fluorometric determination of o-and m-hydroxybenzoic acid in mixtures, *Analytical Chemisty*, **30**, 1361-1363

Thorn K. A., Folan D. W., and MacCarthy P. (1989), Characterization of the International Humic Substances Society Standard and Reference Fulvic and Humic Acids by Solution State Carbon-13 (^{13}C) and Hydrogen-1 (^{1}H) Nuclear Magnetic Resonance Spectrometry, U.S. Geological Survey, Water-Resources Investigations Report 89-4196, Denver, CO, pp.93

Thurman. E. M. (1985) *Organic geochemistry of Natural waters*, Dordrecht, M. Nijhoff, 1-4

Traina, S. J., Novak, J., Smeck, N. E. (1990) An ultraviolet absorbance method of estimating the percent aromatic carbon content of humic acids., *Journal of Environmental Quality*, **19**, 151-153

van Krevelen D. W. (1993) *Coal: typology-physics-chemistry-constitution* 3rd, completely revised edition, Amsterdam; New York, Elsevier Science Pub. B.V.

Wood S. A. (1996) The roles of humic substances in the transport and fixation of metal of economic interest (Au, Pt, Pd, U, V), *Ore Geology Reviews*, **11**, 1-31

3.2. Hydrothermal transformation of dissolved humic substances

3.2.1. INTRODUCTION

Humic substance, a representative dissolved organic matter, plays important roles in transportation of toxic chemicals, sources for fossil fuel production, and material cycling in natural waters. Thermal transformations of aquatic humic substances, especially in dissolved state, are essential for evaluating long-term behavior, relevant to environmental issues, of organics in aquatic environment. Because thermal transformations (maturation) of humic substances are considered to produce natural gas (methane), petroleum and coals (van Krevelen, 1993), many researchers have studied thermal stabilities and thermodynamic parameters to predict their formation in geological conditions. However, despite these extensive studies on thermal stabilities of humic substances, the transformation behaviors in dissolved state under hydrothermal conditions have not been studied in detail (Landais and Gize, 1999).

Color is one of the characteristics of humic substances. Yellow-brownish color of humic substances has been used as index of organic concentration in natural water. The color also reflects chemical structures such as functional groups and aromaticity, which are important characters for transformation and release of toxic materials. The hydrothermal condition may induce the transformation of chemical structures of humic substances and may influence color changes.

Light absorption nature of humic substance in the range of ultraviolet and visible light is due to energy transfer of electron configuration derived from their polymeric chemical structures with abundant substituted benzene. Absorbance is assumed to be proportional to corresponding functional group contents in humic substances. Some spectroscopic properties of aquatic humic substances are reported to be correlated to an aromaticity (the percentage of the C accounted for as aromatic C) of these compounds. Several empirical aromaticity indexes are suggested by using florescence spectroscopy (McKnight, 2001) and UV spectroscopy (Chin et al., 1994; Abbt-Braun, 2004), although aromaticity can be directly determined by using ^{13}C NMR spectroscopy.

To investigate the hydrothermal transformations of dissolved humic substances, the color decrease, the carbon concentration decrease and the aromaticity change are examined by UV-VIS spectroscopy, TOC analysis and fluorescence index, respectively. Finally, I discuss time-scale s of transformation of humic substances by using obtained kinetic data.

3.2.2. EXPERIMENTAL METHODS

3.2.2.1. Materials

Two IHSS reference sample solutions (Nordic Nordic fulvic acid and humic acid) were heated in hydrothermal reaction vessels. 100 mg L^{-1} of Nordic fulvic acid and humic acid solutions were prepared by putting 100 mg of powder reagent purchased from IHSS in 1 L of pure water. For the Nordic fulvic acid solution of pH=3.6, its ionic strength was adjusted to 0.001 M by using NaCl.

3.2.2.2. Hydrothermal experiments

The hydrothermal reaction vessel consists of a stainless steel container (SUS316) and a PTFE inner bottle (10 ml inner volume; Flon Industry Co.). The reaction vessels are set into an oven equipped with forced-convection heating system (ISUZU, soyokaze). Temperature of each hydrothermal vessel was measured by chromel-alumel thermocouples (K-type, inner diameter: 0.32 mm). Thermocouples were placed at the bottom of the PTFE inner bottle as shown in Figure 3.2.1. Temperatures during hydrothermal experiments were recorded on a data logger every 30 seconds (Keyence, NR-1000), through the thermocouples. The temperature precision of these hydrothermal vessels were maintained within ±1°C.

8ml of both Nordic fulvic acid and humic acid solutions were introduced into the reaction vessel by pipette. PTFE bottles were weighed before and after the sample introduction, and after the hydrothermal experiment. The pH of solutions were measured before and after the experiment. Temperatures and heating durations are shown as follows. Nordic fulvic acid were heated at 80°C for 0 – 528 hours, 100°C for 0 – 552 hours, 120°C for 0 – 96h hours, 140°C for 0 - 48 hours, 160°C for 0 - 24 hours and 180°C for 0 - 18 hours. Nordic humic acid were heated at 80°C for 0 – 528 hours, 100°C for 0 – 552 hours, 120°C for 0 – 330h hours, 140°C for 0 - 54 hours, 160°C for 0 - 24 hours and 180°C for 0 - 18 hours

After the heating experiments, reaction vessels were taken out from the oven and the PTFE bottles were subjected to ambient cooling. Weights of PTFE inner bottles with sample solutions were measured. Smells, colors and water droplets on PTFE caps were observed for each solution. pH of each sample solution was measured at room temperature. 2ml of sample solution was diluted with 18ml of miliQ water to be used for UV-VIS spectroscopy, fluorescence spectroscopy and total organic carbon analysis. FT-IR spectroscopy and zeta potential analysis were conducted on heated Nordic fulvic acid solutions.

3.2.2.3. UV-VIS Analysis

The sample solutions were analyzed by ultraviolet-visible (UV-VIS) spectrometer (Jasco, V-530 and V-570). 1 mL of heated Nordic fulvic acid solution was diluted with distilled water to 10 mL. The quarts cells, with a path length of 1cm, were washed three times with pure water and three times with a sample solution. The sample solutions in the quartz cell were placed in the UV-VIS spectrometer for measurement. All spectra were obtained with a spectral range from 800 to 190 nm and with a scan speed of 100 nm/minute. A bandwidth of 2.0 nm was applied with a data acquisition of 0.5 nm step.

The absorbance at 254 nm are used as one of the index of the color density and the quantity of humic substances, because the Lambert-Beer's law provides a direct link between UV-spectra and the concentration of a solute: $Abs = \varepsilon\ c\ l$, where Abs is the absorbance in UV-VIS spectra, ε is the molar absorption coefficient, c is the concentration of dissolved substance and l is the optical path length.

3.2.2.4. Total organic carbon (TOC) analysis

Carbon concentrations in solution were analyzed with a TOC analyzer (Shimadzu, TOC-V_{CPH}) using standards prepared by diluting the stock solution of potassium hydrogen phthalate ranging from 0-30 mg L^{-1}. 1.0 mL of 2 mol L^{-1} HCl was added to all the samples. The samples were then purged by nitrogen gases during 4 minute with a flow rate of 150 ml/minutes. The combustion with Pt catalyst at 680 °C of the sample after the acid treatment can therefore determine non-purgeable organic carbon (NPOC), which are taken as organic carbon contents. The same analysis was performed 2 or 3 times for one sample.

3.2.2.5. Fluorescence spectroscopy

The fluorescence spectra were recorded on spectrophotometer (Jasco, FP-6600) with a halogen lamp (800-350 nm) and a deuterium lamp (350-190 nm). The emission spectra were scanned from 250 to 550 nm at sequential 5 nm increment of excitation wavelength between 200 and 500 nm. The excitation and emission bandwidths were set to 5 nm and 6 nm, respectively, and the integration time at each wavelength was 0.1 sec.

The spectra were calibrated against an external standard, 10 μg L^{-1} quinine sulfate in 0.1N sulfuric acid solution, with a known fluorescence intensity value of 10 QSU (quinine sulfate unit).

3.2.2.6. FT-IR analysis

FT-IR spectra were recorded by Fourier transform infrared spectrometer (FT-IR) equipped with a mercury cadmium telluride (MCT) detector (Jasco, FTIR-620 with

IRT-30). The solution samples were dried on the CaF_2 crystal (thickness of CaF_2 is 1mm). The residue on the CaF_2 plate was measured with a 100 × 100 μm aperture. One hundred interferograms at 4 cm^{-1} resolution were co-added to produce a single spectrum from 700 to 4000 cm^{-1}.

3.2.2.7. GC-MS analysis

Trace gases of heated Nordic fulvic acid solution (heated at 140°C in 18 hours) were analyzed by gas chromatography mass spectrometer (SHIMADZU, GCMS QP-2010).

Gas tight syringe (maximum volume: 2.5 mL) was inserted to Teflon-coating silicon rubber plug connected to reaction vessel and collected 1mL of emission gas fraction was collected (Fig 3.2.2.). These gases were immediately injected into a GC capillary column (DB-1 column; 60m × 0.32mm) through an injector port. The components in the gas mixture separate as they pass through the column and detected as they emerge by mass spectrometer.

The settings of GC-MS analysis were as follows. The mobile phase was helium gas that carried the vapors by flow rate of 5.0 mL min^{-1}. The column oven temperature was programmed as 5 min at 35°C and then an increase rate of 10°C min^{-1} from 35°C to 200°C. The mass spectometer was scanned every 0.5 sec over m/z 20 – 300. The temperature of injector port (vaporizing chamber), ion source and interface were maintained at 100°C, 200°C and 150°C, respectively.

3.2.2.8. Zeta potential

The zeta potential for Nordic fulvic acid solution was measured by an imaging analysis system (Zeecom, microtech nition Co.). The electrophoresis migration of particles was observed under an optical microscope.

3.2.3. RESULTS

3.2.3.1. UV-VIS spectroscopy

The color decreases are observed in the all time-range of this experiments (Fig. 3.2.3). During the color decrease, pHs slightly change to acidic condition, organic carbon contents decrease and fluorescence spectroscopy shows the decrease of maturation of organics.

The UV spectra of Nordic fulvic acid and humic acid solutions are shown in Fig.3.2.4. and Fig. 3.4.7. A gradual absorption shoulder is observed from the visible to ultraviolet region. Stevenson (1994) reported that a weak absorption band is often present in the 260-300 nm ultraviolet region. In fact, a weak shoulder at 255-275nm gradually disappeared during the heating of Nordic fulvic acid solution. Absorption

intensities throughout the 600-190 nm range decreased with time. Temporal changes with time at each temperature of Nordic fulvic acid and humic acid in absorbances at 254 nm are listed in Table 3.2.1 and Table 3.2.2 and plotted in Fig. 3.2.5. and Fig. 3.2.8., respectively. These absorbances decreased gradually with time. The UV-VIS spectra shows 80% decrease of Abs_{254}, which is proportional to the concentration of humic substances, following the initial small decrease of Abs_{254} (Fig. 3.2.5 and Fig. 3.2.8).

3.2.3.2. Carbon concentration

The total organic carbon (TOC) content of 10 mg L^{-1} Nordic fulvic acid and humic acid solution (ionic strength I = 0 M) was 4.55 ± 0.01 mg L^{-1}. The TOC for Nordic fulvic acid solution with the ionic strength of 0.001 M was 4.50 ± 0.06 mg L^{-1}. The difference in ionic strength between 0 M and 0.001 M is found to have no significant effect on the organic carbon content of the humic substances solutions.

The TOC values for heated Nordic fulvic acid and humic acid solutions, listed in Table 3.2.1 and Table 3.2.2, gradually decreased with time at each temperature during the hydrothermal experiments (Fig.3.2.11 and Fig. 3.2.12). These results are in agreement with the decrease in 254 nm absorbance of the fulvic acid and humic acid.

3.2.3.3 Fluorescence spectra

The Fluorescence spectra of Nordic fulvic acid and humic acid solutions are shown in Fig.3.2.13 and Fig. 3.2.14. Fluorescence intensities throughout the 380-600 nm range decreased with time. A small peak around 420 nm is due to Raman effect of water.

3.2.3.4. The FT-IR spectra

The FT-IR spectra at the initial stage (at 180°C for 0 and 1.5 hour) are obtained as shown in Fig. 3.2.15. Two absorption bands existed near 1710 and 1600 cm^{-1} for C=O and C=C stretching vibrations, respectively. The 1575 cm^{-1} band was derived from COO^- symmetric stretching vibration. The 1400 cm^{-1} band was OH deformation and C-O stretching of phenolic OH and/or COO^- asymmetric stretching vibration. The 1455 and 1356 cm^{-1} band were due to CH bending vibration. The broad band occurred in the 1000-1200cm^{-1} for C-O stretching vibration.

3.2.3.5.GC-MS analysis

Fig.3.2.16 Shows a gas chromatogram of compounds released from heated Nordic fulvic acid solution (heated at 140°C in 18 hours). A total of 9 peaks was identified as shown in Fig. 3.2.18., and compound names corresponding to these peaks are listed in Table 3.2.3: difluorodimetyl-silane (Retention time (Rt): 2.88 min), Chloromethane (Rt:

3.050 min), acetaldehyde (Rt: 3.27 min), 2-methyl-1-propene (Rt: 3.61min), methyl isocyanide (Rt: 5.18 min), acetone (Rt: 5.67 min), carbon disulfide (Rt: 7.51 min), benzene (Rt: 11.6 min), 2,4,4-trimethyl-1-pentene (Rt: 13.29 min). These compounds were identified by comparison with mass spectra of Shimadzu library database.

Although difluorodimetyl-silane and carbon disulfide were also detected, these compounds might be contaminant from column and GC system. Silane (C-Si) is component of a stationary phase on the inside surface of a coiled capillary tube. Carbon disulfide is often detected by GC-MS analysis as contaminant.

3.2.3.6 Zeta potential

Zeta potential (surface charge) of the initial Nordic fulvic acid solution (100 mg L^{-1}) was –58.7 ± 4.3 mV at pH = 3.6. Zeta potentials of heated Nordic fulvic acid solutions are shown in Table 3.2.4. and Fig.3.2.17. They are -57.1 ± 5.2 mV (12 hour at 120°C), –51.3 ± 6.3 mV (25 hour at 120°C), –54.5 ± 6.8 mV (30 hour at 120°C) and –52.7 ± 4.6 mV (72 hour at 120°C). Zeta potential of the heated Nordic fulvic acid did not change significantly.

3.2.4. DISCUSSON

3.3.4.1. Decrease rates of 254nm absorbance of the fulvic acid solution

By plotting the data in semi logarithmic diagram, the 254 nm absorbance showed linear decrease (Fig.3.2.9), suggesting the first order reaction. The rate of Abs_{254} can be simulated by the first order kinetics by using the following integrated rate equation:

$$\ln [a]_{t_{uv}} = \ln [a]_0 - k^{UV} t$$

, where α is the normalized absorbance at 254 nm and k^{uv} is the rate constant of Abs_{254} decrease. Except for the small initial decrease, this decrease can be simulated by the first order reaction and the rates of Nordic fulvic acid are k^{UV}_{fulvic} = 4.8 × 10^{-8} s^{-1} at 80 °C, 1.1 × 10^{-7} s^{-1} at 100 °C, 1.2 × 10^{-6} s^{-1} at 120 °C, 3.2 × 10^{-6} s^{-1} at 140 °C, 1.0 × 10^{-5} s^{-1} at 160 °C and 2.1 × 10^{-5} s^{-1} at 180 °C. Similarly, the rates of Nordic humic acid are k^{UV}_{humic} = 1.1 × 10^{-7} s^{-1} at 80 °C, 1.6 × 10^{-7} s^{-1} at 100 °C, 6.6 × 10^{-6} s^{-7} at 120 °C, 4.4 × 10^{-6} s^{-1} at 140 °C, 2.1 × 10^{-5} s^{-1} at 160 °C and 5.4 × 10^{-5} s^{-1} at 180 °C.

The effect of the temperature on the rate constant can be described as the Arrhenius equation:

$$\ln k^{UV} = \ln A - \frac{E_a}{RT}$$

, where Ea is the activation energy, R is the gas constant (8.31 J K^{-1}), T is the absolute temperature, and A is the frequency factor. By introducing the obtained rate constants to

this equation, the activation energy of this decrease of Nordic fulvic acid and humic acid is 85 kJ mol^{-1} and 88 kJ mol^{-1}, respectively (Fig.3.2.10).

3.2.4.2. Transformation of functional groups

Nordic fulvic acid solution has 11.12 mmol/g of carboxyl functional group in their structure (IHSS homepage, http://www.ihss.gatech.edu/). Because carbon contents of Nordic fulvic acid is 52% of the total weight, carboxyl carbon correspond to about the 26% of total organic carbon of Nordic fulvic acid (11.12 mmol g^{-1} ÷ 0.52 gC g^{-1} × 12 gC mol^{-1}). The result of ^{13}C NMR on the same sample also reported 24% of carboxylic contents (Thorn, 1989). On the other hand, the carbon skeleton structure (aromatic-C and aliphatic-C) accounts for 60% of the total organic carbon based on the same ^{13}C NMR result. These results indicate that the carboxyl functional groups are the main functional group of Nordic fulvic acid.

The UV absorption band around at 254 nm corresponds to a peak position of certain substituent functional groups such as aromatic carboxyl groups (Buffle et al., 1982). Therefore decrease of UV absorbance at 254 nm might be derived from decrease of substituents for aromatic rings or from transformation to different substituents that have a weak absorption around at 254 nm.

The major released compounds were carbon dioxide and carbon monoxide based on the gas cell FT-IR results (Chapter.3). Acetaldehyde and acetone detected by GC/MS are considered to be oxidized fragments of the fulvic acid. These are fragments of functional groups and/or oxygen-containing hydrocarbonaceous components, such as ketone, quinone and hydroxyl aromatic carbon. Chloromethane detected by GC/MS may be released by natural chlorination (Keppler et al, 2000). Chloride ion and/or chloride radical might have reacted with methyl cation and/or methyl radical.

Zeta potential for heated Nordic fulvic acid at 120°C did not show significant changes with the heating time. The negative surface charges of the humic substances are considered to be originated from carboxyl anion ($-COO^-$) and phenolic anion ($-O^-$). Because $-O^-$ has –OH form in acidic conditions, the origins of negative charge of Nordic fulvic acid would be $-COO^-$. The ratio $-COO^-$/–COOH is generally constant at a fixed pH, according to their dissociation constant. Therefore, the surface charge of the fulvic acid might be similar for heated products.

Since the carboxyl content is suggested to decrease in heated humic substance solutions, humic substance particles might have decreased their surface area keeping similar carboxyl contents.

3.2.4.3. Aromaticity

The spectroscopic properties of dissolved organic matter or aquatic humic

substances are often related to aromaticity (the percentage of the C accounted for as aromatic C) of these compounds. Several empirical aromaticity indices are suggested by using florescence (Mcknight et al., 2001) and UV adsorption (Chin et al., 1994; Abbt-Braun, 2004).

Mcknight et al. (2001) discussed the relationship between the aromaticity and the ratio of the fluorescence emission intensity at a wavelength of 450nm to that at 500nm, obtained with 370nm excitation. A quasi-linear relation has been found between the 450/500nm intensity ratio, called the fluorescence index (y), and aromaticity (x): $y = -0.027x + 2.1$ ($r^2 = 0.85$), and its power function regression was $y = 3.94x^{-0.316}$. By using this equation, the aromaticity of the fulvic acid was 10-30%.

Chin et al. (1994) reported relation between aromaticity and UV absorbance at 280nm. They argued that this correlation for a fulvic acid (aromaticity = $0.05\varepsilon + 6.74$; ε= absorption coefficient at 280nm) is much better than the E4/E6 ratio-aromaticity relation. The obtained aromaticity for the fulvic acid was 12~28%.

Abbt-Braun (2004) reported a correlation of ^{13}C NMR spectroscopic data (aromaticity) with the specific UV absorption coefficients (Abs254nm/DOC in L/mg·m at pH=11). The linear fitting function is as follows: $y = 6.3\ x + 1.4$, where x is absorption coefficient at 254nm and y = aromaticity. The obtained aromaticity of the fulvic acid from this relation was 18-50%.

Based on the above reports, the aromaticity of heated Nordic Fulvic acids were calculated by fluorescence index 450nm/500nm (Mcknight et al., 2001) as shown in Table 3.2.5., Table 3.2.6, Fig. 3.2.19 and Fig 3.2.21., by absorption coefficient at 254nm (Abbt-Braun, 2004) as shown in Table 3.2.5., Table 3.2.6., Fig. 3.2.23 and Fig 3.2.24, and by molar absorptivity at 280nm (Chin et al., 1994) in Table 3.2.7, Table 3.2.8., Fig. 3.2.25 and Fig 3.2.26.

Aromaticity of the initial Nordic fulvic acid were about 30% (linear equation) or 35% (power function) of the total carbon calculated from the fluorescence index, about 38% calculated from absorbance at 254nm and about 35% calculated from absorbance at 280nm. Three different methods gave a similar aromaticity around 35%.

According to the calculation by using fluorescence index and linear fitting (Mcknight et al., 2001), almost all the heated sample showed stable aromaticity around 30% (maximum 10% decrease) except for the experiments at 180°C and the later half of 160°C experiments (Fig.3.2.19, Fig.3.2.21). Aromaticity at 180°C decreased by maximum 47%. Aromaticity calculated by using the power law function also showed that almost all the sample have 33 ± 5 % of aromaticity except for the experiments at 180°C and the latter of 160°C. Aromaticity at 180°C dropped by maximum 53%.

The aromaticity calculated by the absorbance at 254nm (Abbt-Braun, 2004) showed stable aromaticity of 35-39% (maximum 10% decrease) for the experiments of

former half of 180°C and 160°C, and throughout the 140°C and 120°C (Fig.3.2.23). The latter of 180°C and 160°C marked maximum 55% decrease and 32% decrease for their aromaticity, respectively. In the case of the 80°C heating, the aromaticity showed a maximum 20% increase.

Aromaticity calculated by the absorbance at 280nm (Chin et al. 1994) showed a stable aromaticity 33-35% (maximum 10% decrease) for the experiments of the former half of 180°C and 160°C, and throughout 140°C and 120°C (Fig.3.2.25). The latter half of 180°C and 160°C marked maximum 51% decrease and 30% decrease for their aromaticity, respectively. In the case of the 80°C heating, aromaticity showed a maximum 20% increase.

Three types of aromaticity estimation performed above suggest that the aromaticity of Nordic fulvic acid gradually decrease with the first order degradation tendency. At higher temperatures (160°C to 180°C) and for longer durations, the aromaticity clearly appeared to decrease. By introducing the obtained first order rate constants (Fig.3.2.20, 22, 23, 24, 25, 26) to the above equation, the average activation energy of this decrease of Nordic fulvic acid and humic acid is 76 kJ mol^{-1} (67, 68, 95 kJ mol^{-1}) and 80 kJ mol^{-1} (56, 92 and 91 kJ mol^{-1}), respectively (Fig.3.2.29). These values are similar to those for the decrease of Abs_{254}. The color decrease of dissolved humic substances indicated by Abs_{254} can be correlated to the aromaticity decrease examined here.

The decrease of aromatic structure indicates a fragmentation of these structures. 2-methyl-1-propene and 2,4,4-trimethyl-1-pentene, detected by GC-MS, which have carbon double bonds, may be originated from ring opening reaction (Larson and Weber, 1994) and/or thermal cracking of aliphatic carbon structure such as random cracking (Kodera and McCoy, 2003).

3.2.4.4. Molecular weight

Chin et al. (1994) reported a relation between molecular weight (Mw) and UV absorption coefficient at 280nm (ε) for fulvic acid solutions: $M_w = 3.99\varepsilon + 490$. The UV absorption coefficient at 280nm (ε) is determined as L/mg·m by using the organic carbon contents (mg/L) and optical path length (10^{-2}m). The range of molecular weight determined for the fulvic acids are 500-4000.

The molecular weights of Nordic Fulvic acid solutions were determined by the above method (Table 3.2.7., Table 3.2.8., Fig. 3.2.27 and Fig 3.2.28). The initial solution has a molecular weight of around 2700. Molecular weights decreased greatly with time for 180°C and 160°C heating until about 1300. They are almost constant at lower temperatures (140°C and 120°C). These results indicate the loss of carbonaceous compounds from the humic substances, especially at higher temperatures, during the

hydrothermal transformations.

GC-MS analysis indicates molecular weight decrease by fragmentation of carbon structure. 4 hydrocarbons; 2-methyl-1-propene, methyl isocyanide, benzene and 2,4,4-trimethyl-1-pentene, are considered to be released from carbon structure. Especially, benzene is the main component of humic substance structure. Methyl isocyanide may be originated from heterocyclic compounds.

3.2.4.5. Additional processes

The absorption at 254nm of the samples heated at 160 and 180°C for 0 hour already greatly decreased from the initial solutions. However, the absorbance at 254 nm of the samples heated at 80°C for 0 hour is unchanged or slightly increased from the initial solution. Therefore, additional processes might occur at the initial stage at higher temperatures. Their origins are not yet known.

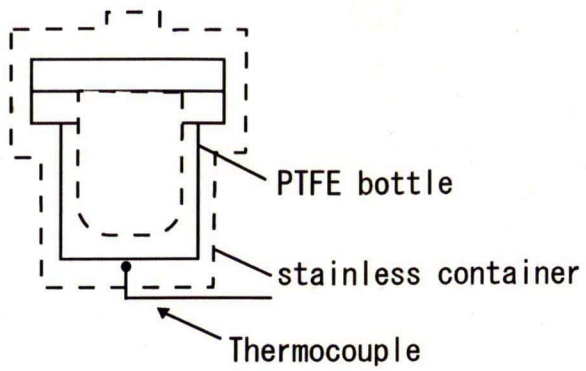

Fig. 3.2.1. Thermocouples at the bottom of the PTFE inner bottle of the reaction vessel

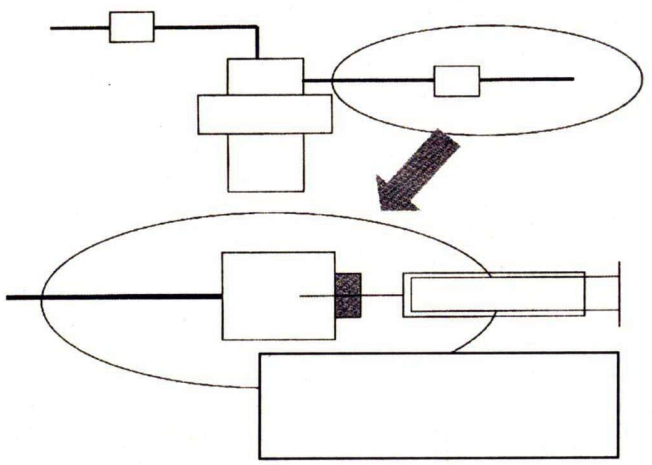

Fig. 3.2.2. Gas tight syringe (maximum volume: 2.5 mL) was inserted to Teflon-coating silicon rubber plug connected to the reaction vessel

Fig. 3.2.3. Color changes of Nordic fulvic acid solution (100mg/L) at 180°C for 0 - 18 hours.

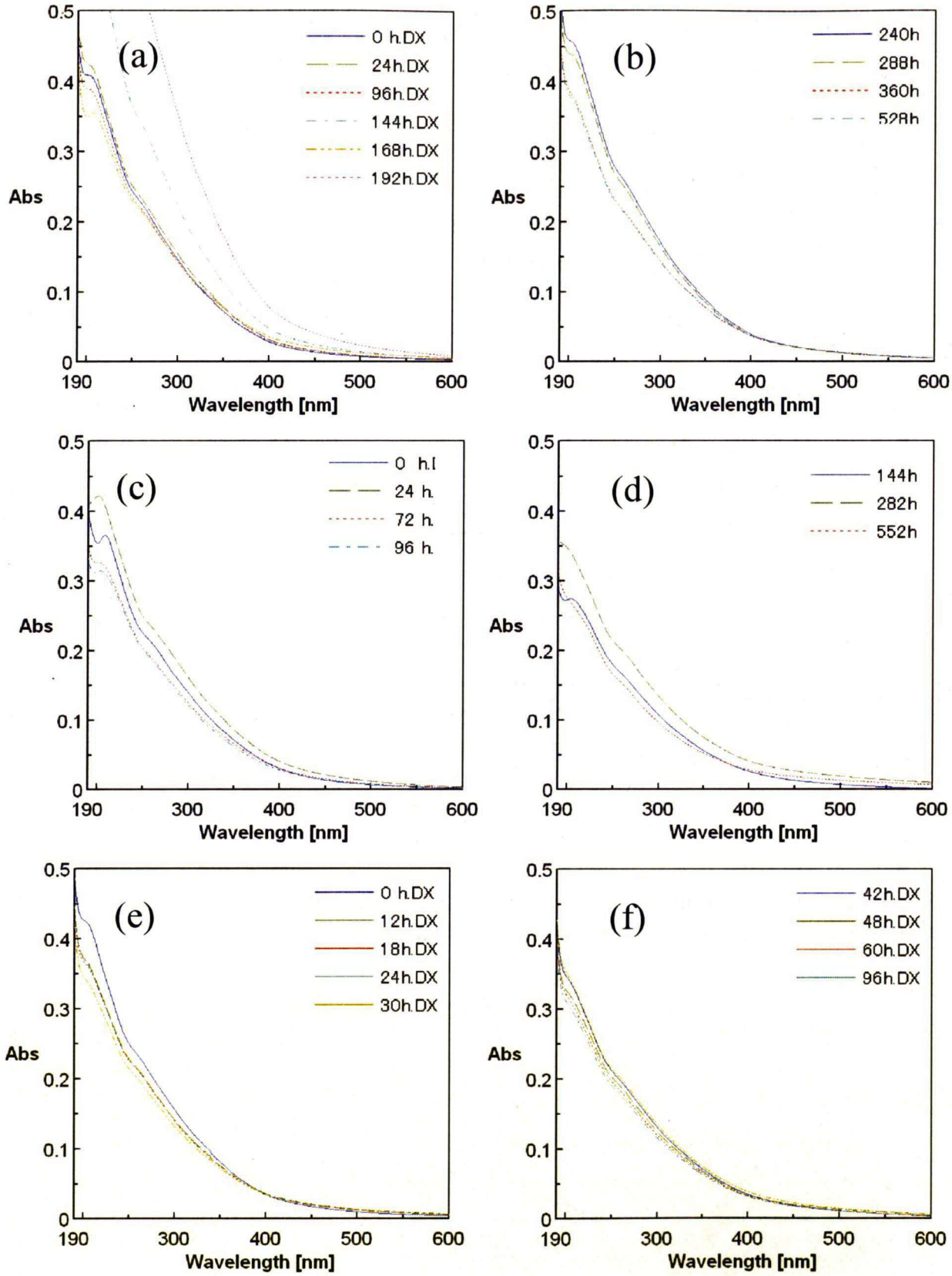

Fig. 3.2.4. UV-VIS spectral changes of heated Nordic fulvic acid solutions (100mg/L) at (a) 80° C for 0 - 192 hours, (b) 80° C for 240 - 528 hours, (c) 100° C for 0 – 96h, (d) 100° C for 144 - 552 hours, (e) 120° C for 0 - 30 hours and (f) 120° C for 42 - 96 hours

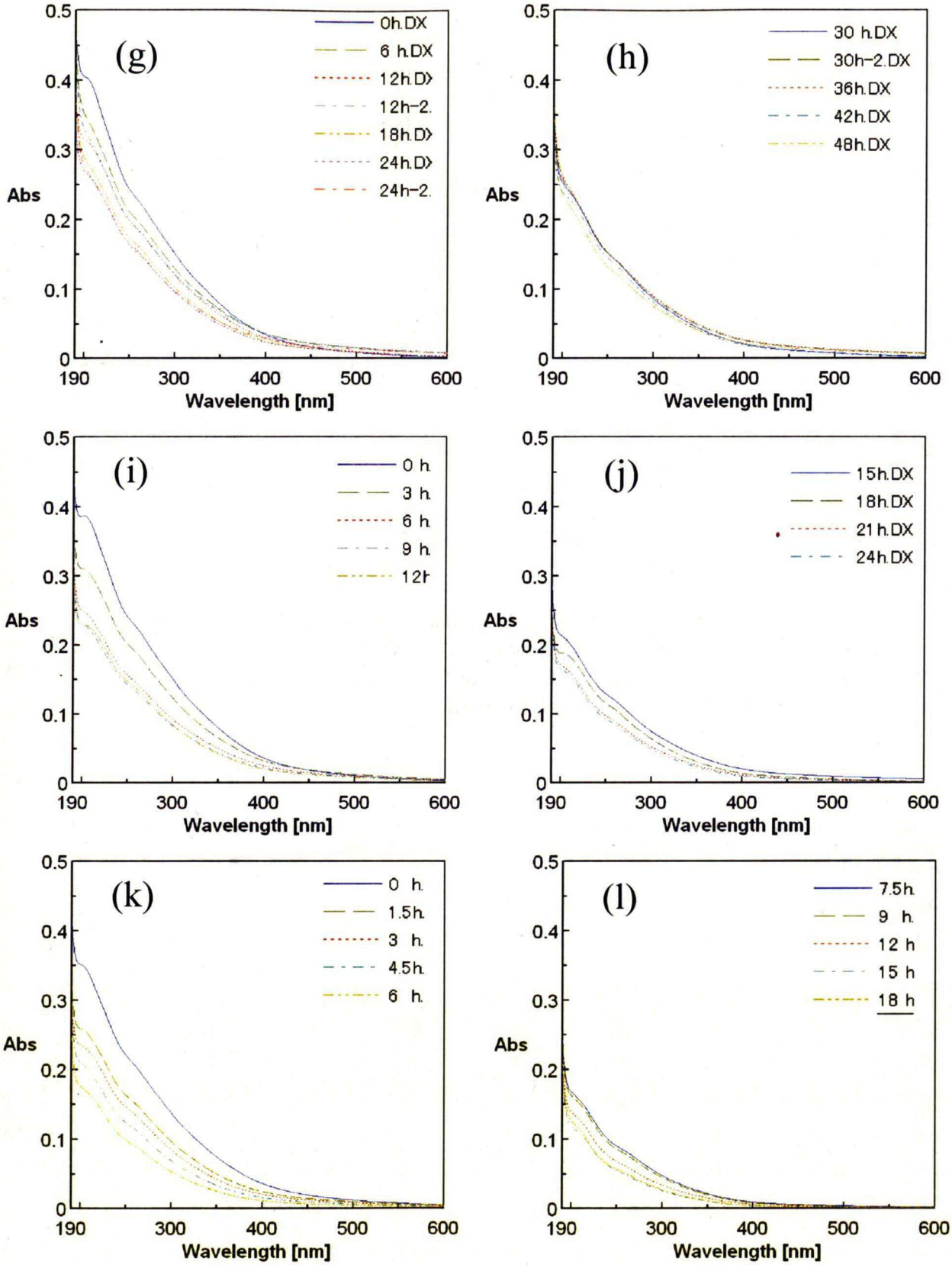

Fig. 3.2.4. UV-VIS spectral changes of heated Nordic fulvic acid solutions (100mg/L) at (g) 140° C for 0 - 24 hours, (h) 140° C for 30 - 48 hours, (i) 160° C for 0 -12 hours, (j) 160° C for 15 -24 hours, (k) 180° C for 0 - 6 hours and (l) 180° C for 7.5 - 18 hours

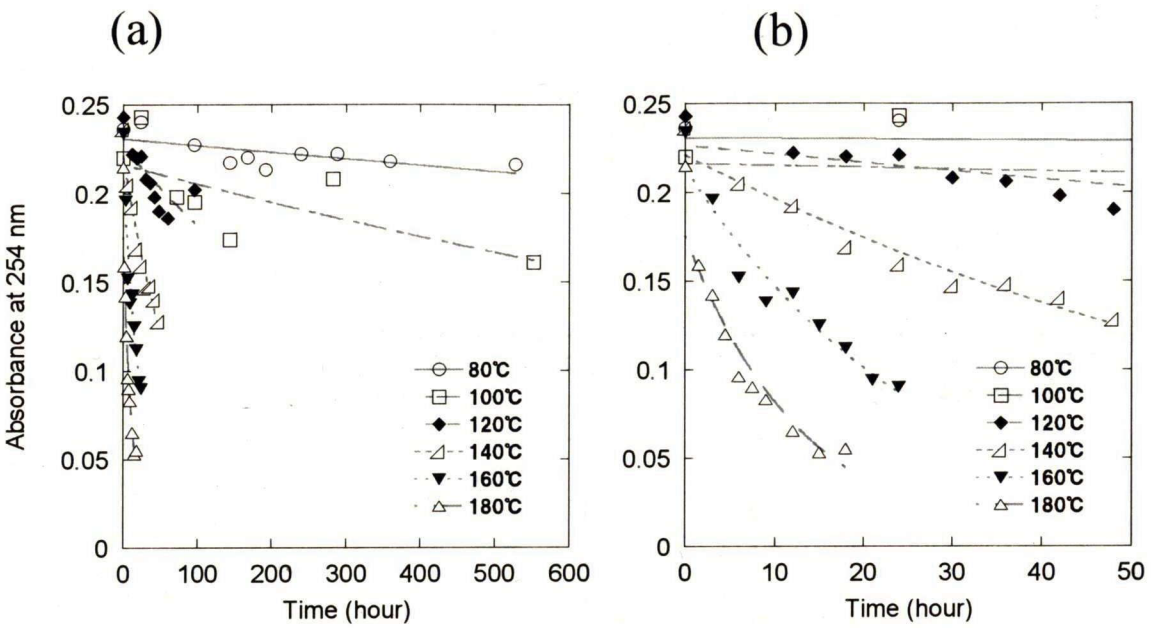

Fig. 3.2.5. Temporal changes in UV-VIS 254 nm absorbances of Nordic fulvic acid solutions heated at 80° C for 0 – 528 hours, 100° C for 0 – 552 hours, 120° C for 0 – 96h hours, 140° C for 0 - 48 hours, 160° C for 0 - 24 hours and 180° C for 0 - 18 hours: a) from 0 to 550 hours; b) from 0 to 50 hours

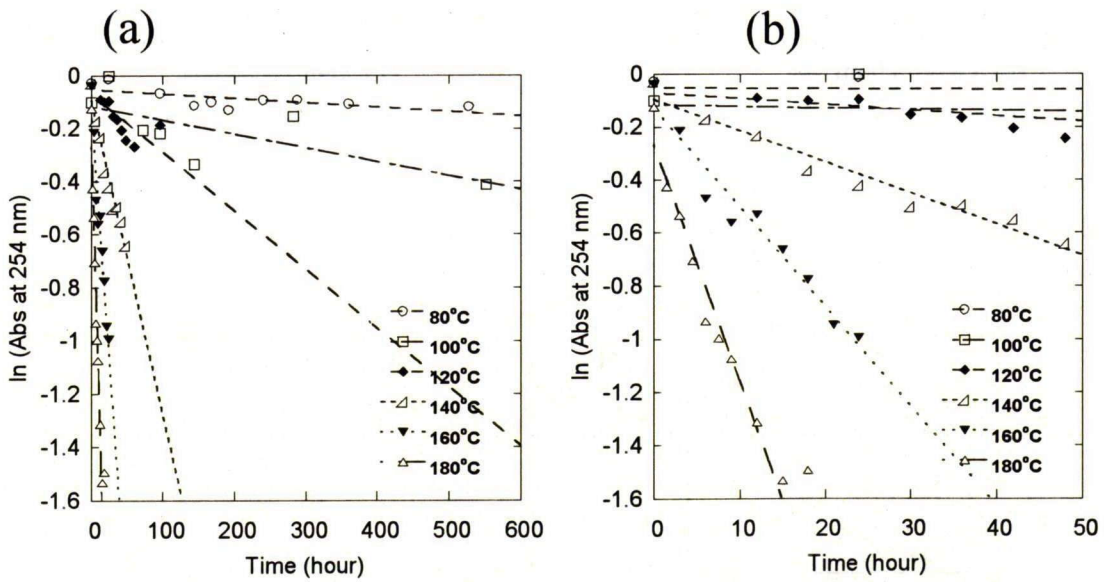

Fig. 3.2.6. Temporal changes in of logarithm of 254nm absorbance of Nordic fulvic acid solutions heated at 80° C for 0 – 528 hours, 100° C for 0 – 552 hours, 120° C for 0 – 96h hours, 140° C for 0 - 48 hours, 160° C for 0 - 24 hours and 180° C for 0 - 18 hours

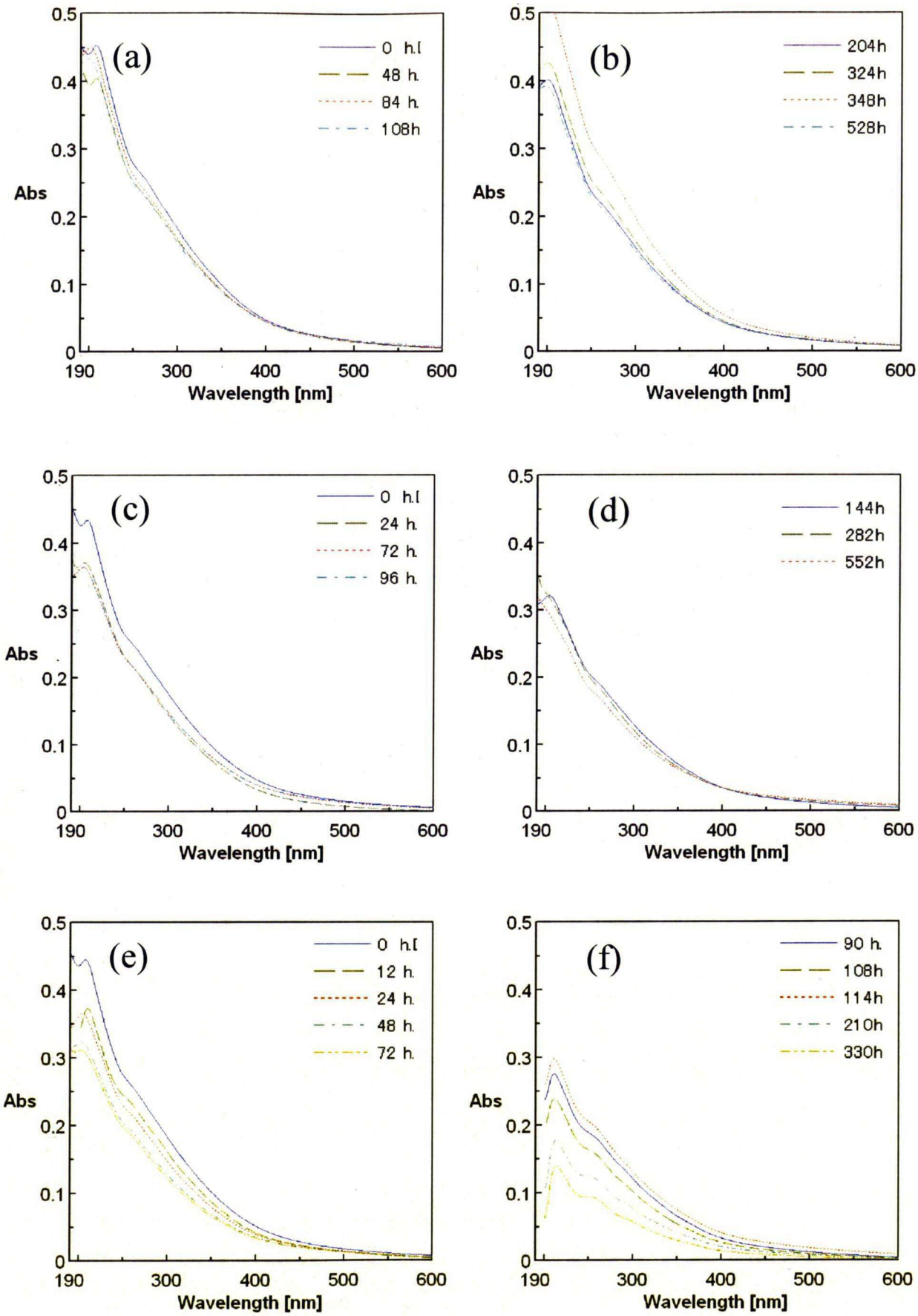

Fig. 3.2.7. UV-VIS spectral changes of heated Nordic humic acid solutions (100mg/L) at (a) 80° C for 0 - 108 hours, (b) 80° C for 204 - 528 hours, (c) 100° C for 0 – 96h, (d) 100° C for 144 - 552 hours, (e) 120° C for 0 - 72 hours and (f) 120° C for 90 - 330 hours

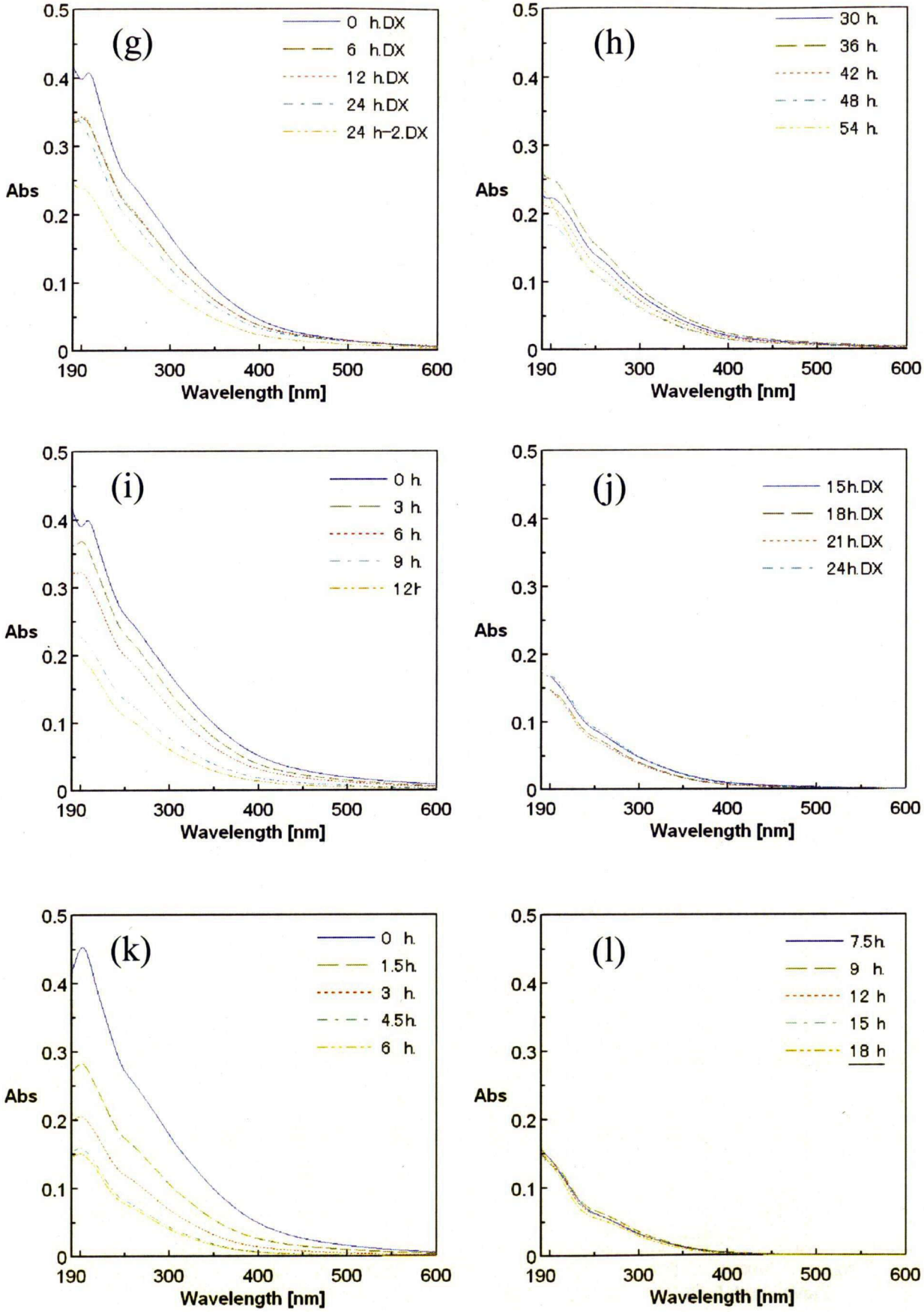

Fig. 3.2.7. UV-VIS spectral changes of heated Nordic humic acid solutions (100mg/L) at (g) 140° C for 0 - 24 hours, (h) 140° C for 30 - 48 hours, (i) 160° C for 0 -12 hours, (j) 160° C for 15 -24 hours, (k) 180° C for 0 - 6 hours and (l) 180° C for 7.5 - 18 hours

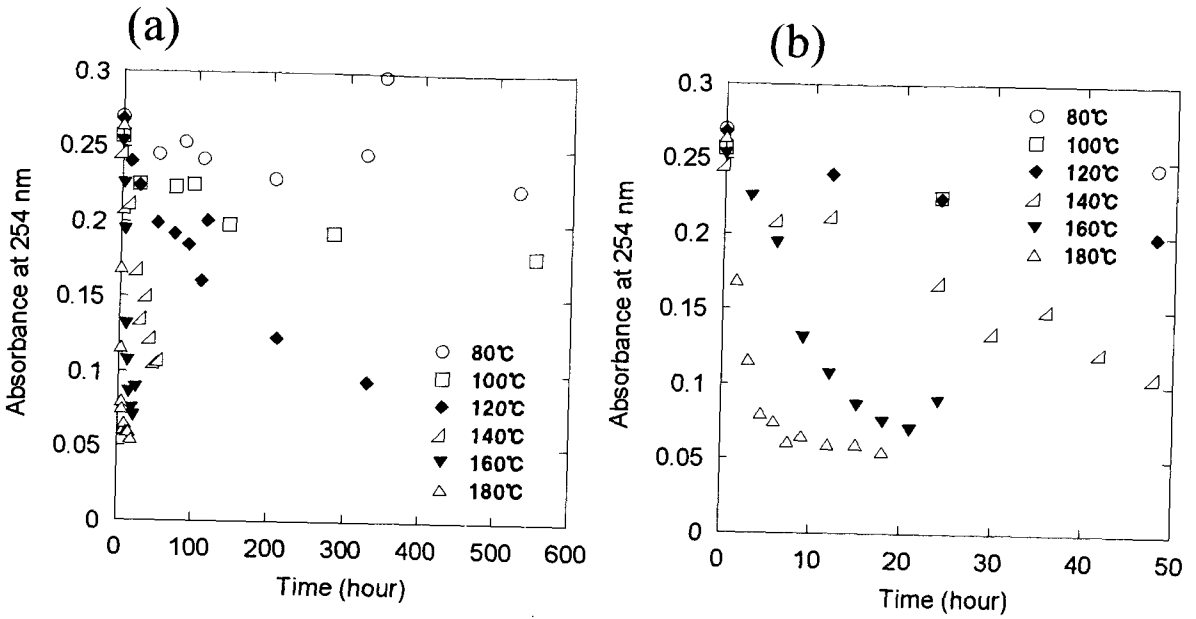

Fig. 3.2.8. Temporal changes in UV-VIS 254 nm absorbances of Nordic humic acid solutions heated at 80° C for 0 – 528 hours, 100° C for 0 – 552 hours, 120° C for 0 – 330h hours, 140° C for 0 - 54 hours, 160° C for 0 - 24 hours and 180° C for 0 - 18 hours: a) from 0 to 600 hours; b) from 0 to 50 hours

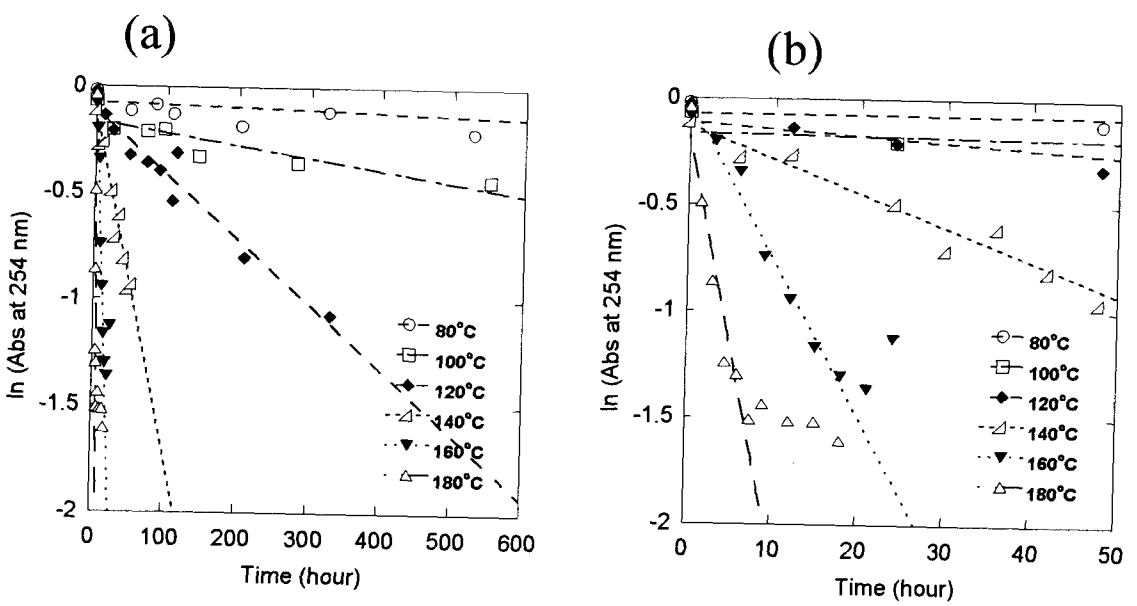

Fig. 3.2.9. Temporal changes in logarithm of 254nm absorbance of Nordic fulvic acid solutions heated at 80° C for 0 – 528 hours, 100° C for 0 – 552 hours, 120° C for 0 – 96h hours, 140° C for 0 - 48 hours, 160° C for 0 - 24 hours and 180° C for 0 - 18 hours: a) from 0 to 600 hours; b) from 0 to 50 hours

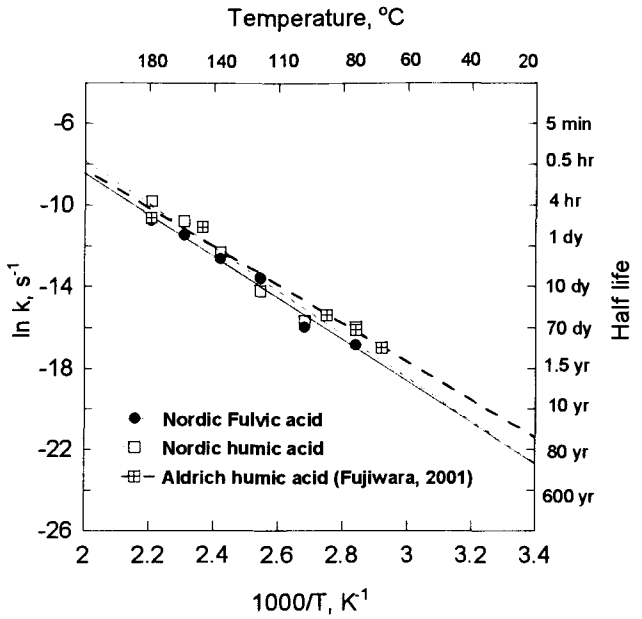

Fig 3.2.10 Arrhenius diagram for decrease rates of UV absorbance at 254nm

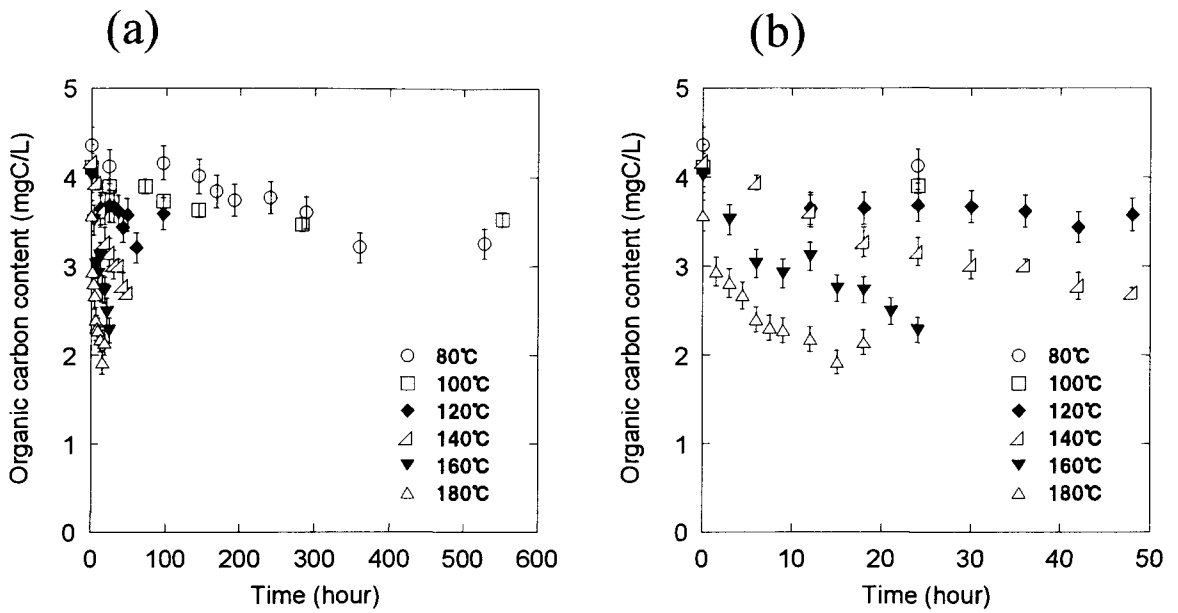

Fig. 3.2.11. Temporal changes in organic carbon contents of Nordic fulvic acid solutions heated at at 80° C for 0 – 528 hours, 100° C for 0 – 552 hours, 120° C for 0 – 96h hours, 140° C for 0 - 48 hours, 160° C for 0 - 24 hours and 180° C for 0 - 18 hours: a) from 0 to 550 hours; b) from 0 to 50 hours

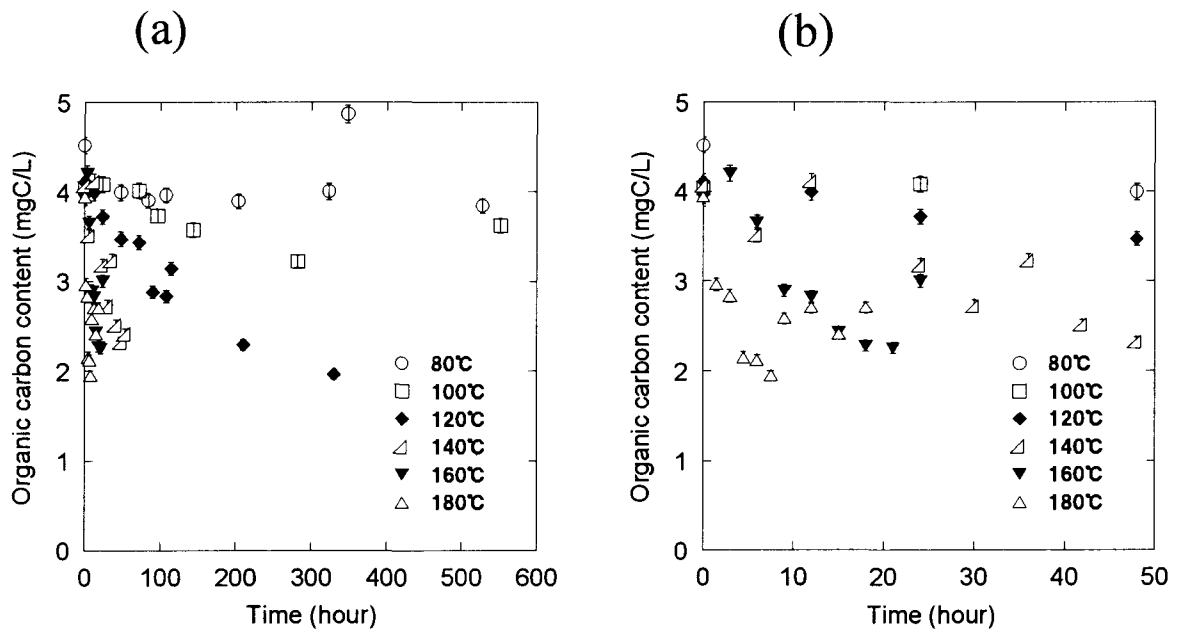

Fig. 3.2.12 Temporal changes in organic carbon contents of Nordic humic acid solutions heated at 80° C for 0 – 528 hours, 100° C for 0 – 552 hours, 120° C for 0 – 330h hours, 140° C for 0 - 54 hours, 160° C for 0 - 24 hours and 180° C for 0 - 18 hours: a) from 0 to 600 hours; b) from 0 to 50 hours

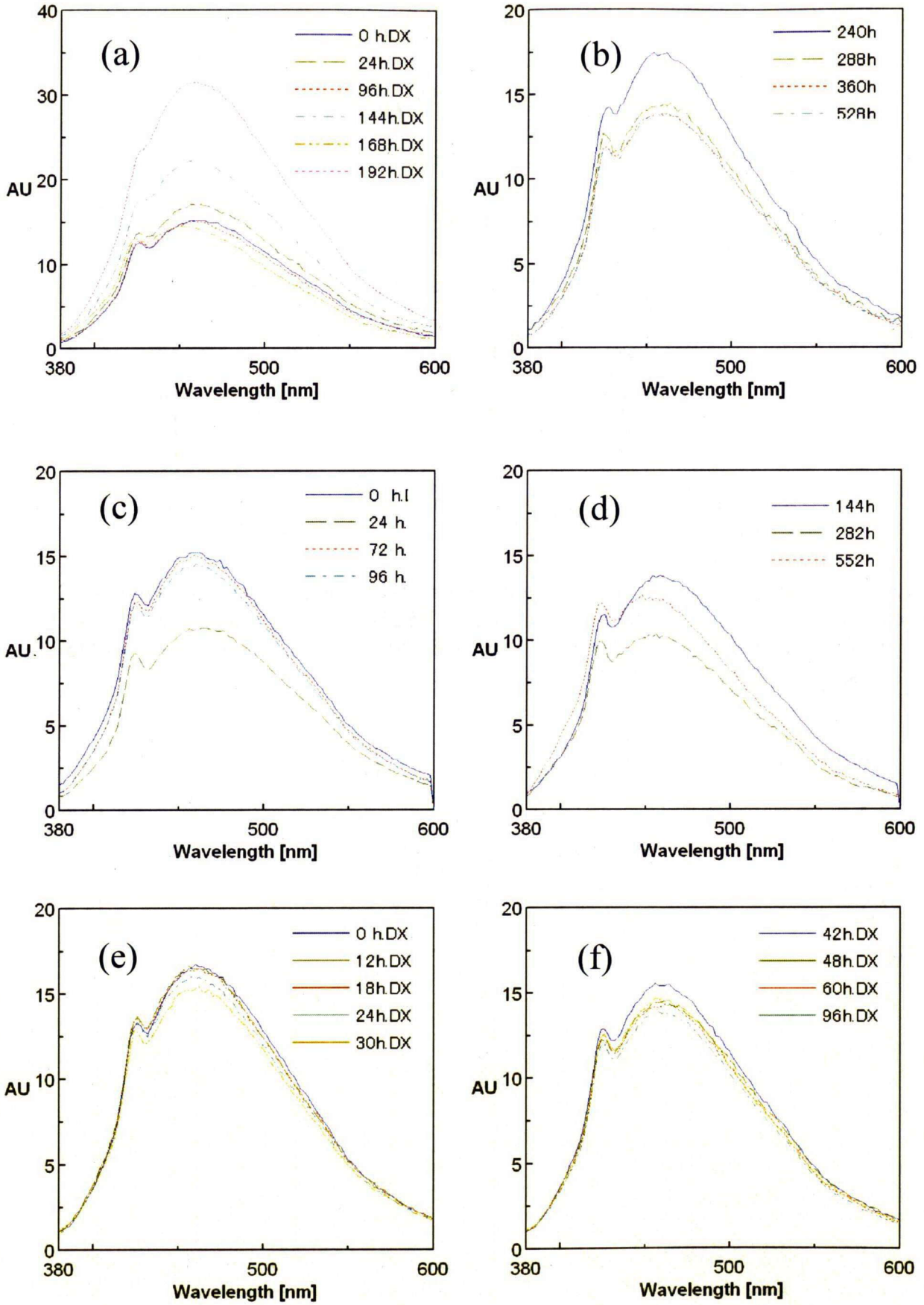

Fig. 3.2.13. Fluorescence spectral changes of heated Nordic fulvic acid solutions (100mg/L) at (a) 80° C for 0 - 192 hours, (b) 80° C for 240 - 528 hours, (c) 100° C for 0 – 96h, (d) 100° C for 144 - 552 hours, (e) 120° C for 0 - 30 hours and (f) 120° C for 42 - 96 hours

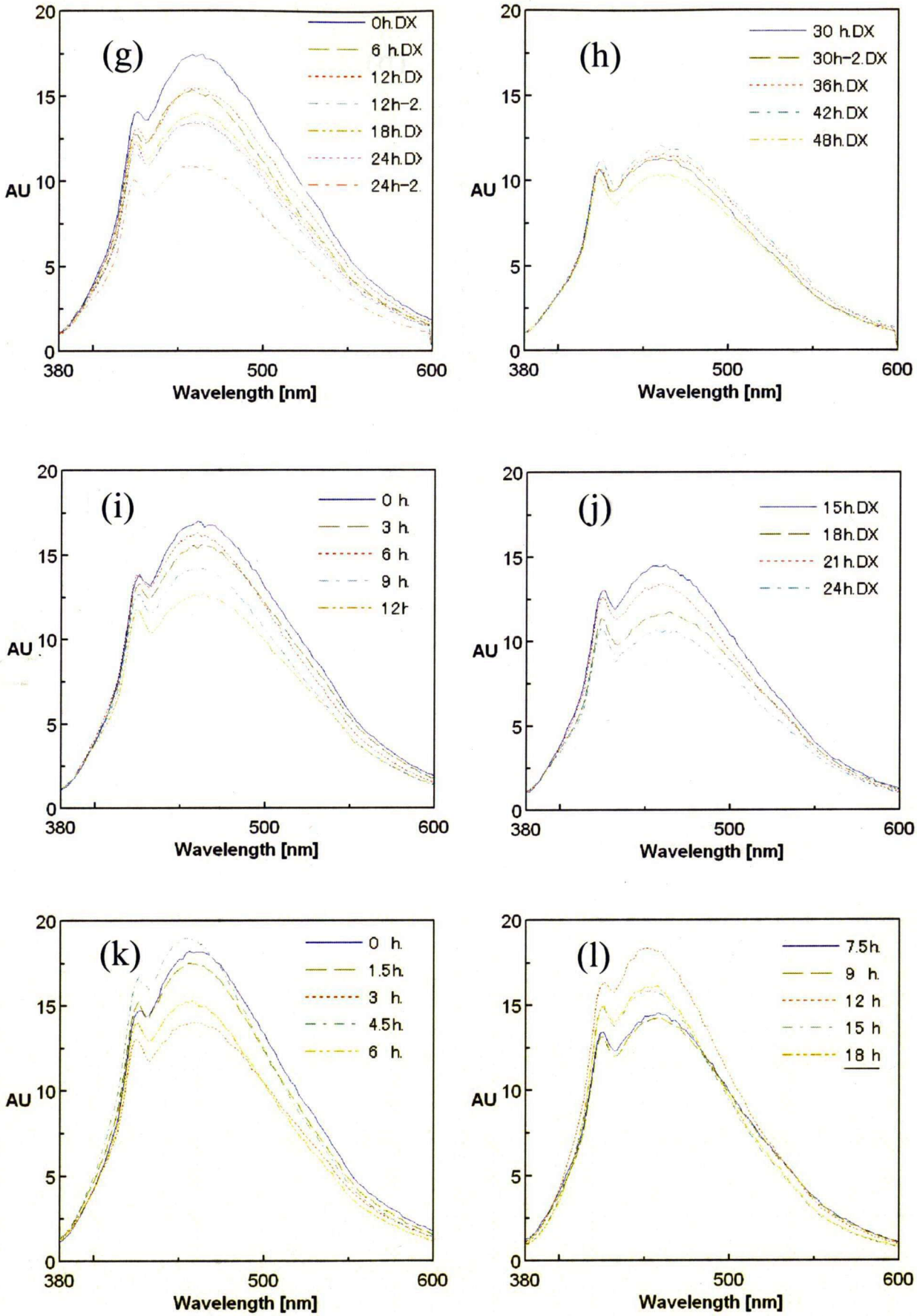

Fig. 3.2.13. Fluorescence spectral changes of heated Nordic humic acid solutions (100mg/L) at (g) 140° C for 0 - 24 hours, (h) 140° C for 30 - 48 hours, (i) 160° C for 0 -12 hours, (j) 160° C for 15 -24 hours, (k) 180° C for 0 - 6 hours and (l) 180° C for 7.5 - 18 hours

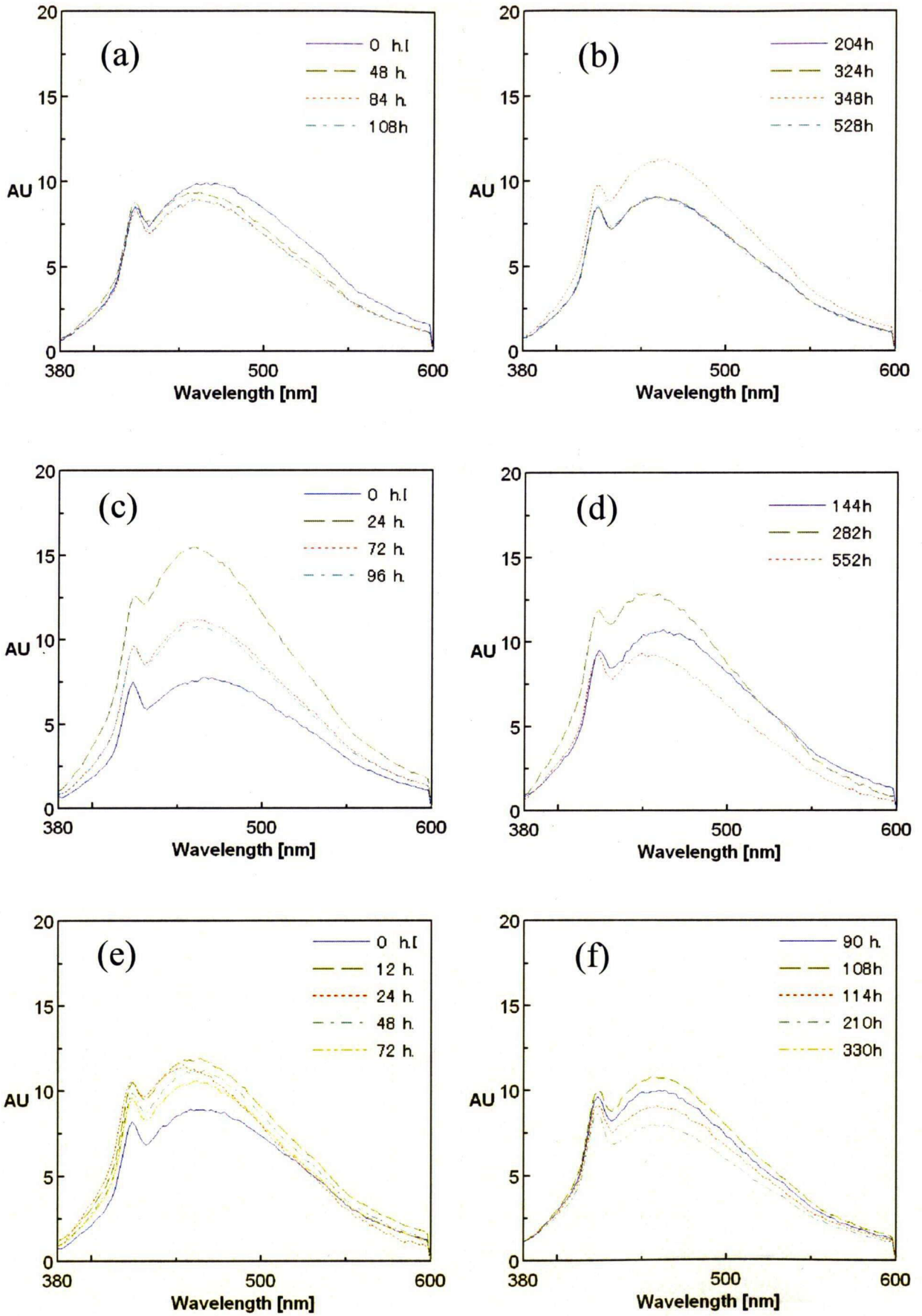

Fig. 3.2.14. Fluorescence spectral changes of heated Nordic fulvic acid solutions (100mg/L) at (a) 80° C for 0 - 192 hours, (b) 80° C for 240 - 528 hours, (c) 100° C for 0 – 96h, (d) 100° C for 144 - 552 hours, (e) 120° C for 0 - 30 hours and (f) 120° C for 42 - 96 hours

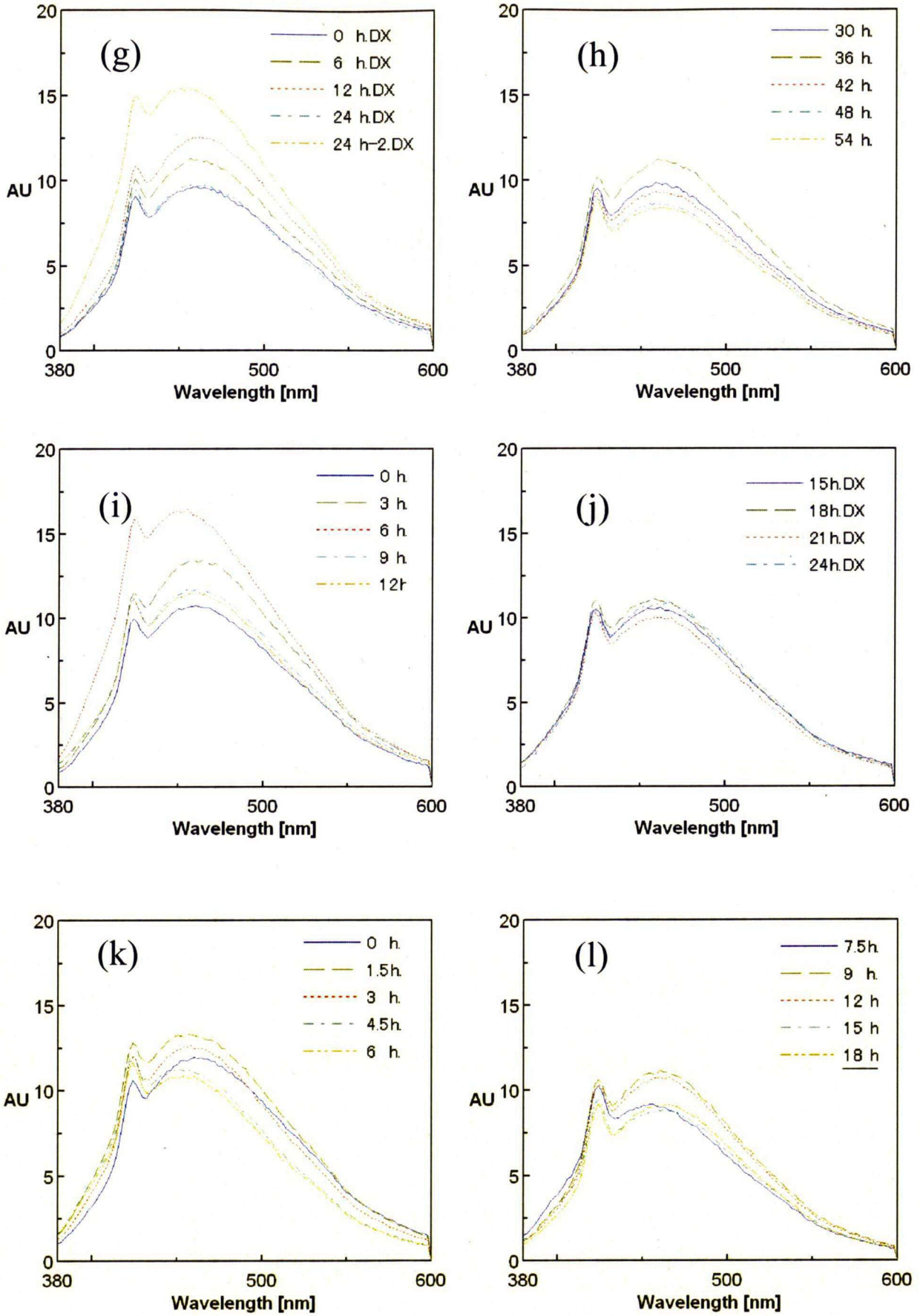

Fig. 3.2.14. Fluorescence spectral changes of heated Nordic humic acid solutions (100mg/L) at (g) 140° C for 0 - 24 hours, (h) 140° C for 30 - 48 hours, (i) 160° C for 0 -12 hours, (j) 160° C for 15 -24 hours, (k) 180° C for 0 - 6 hours and (l) 180° C for 7.5 - 18 hours

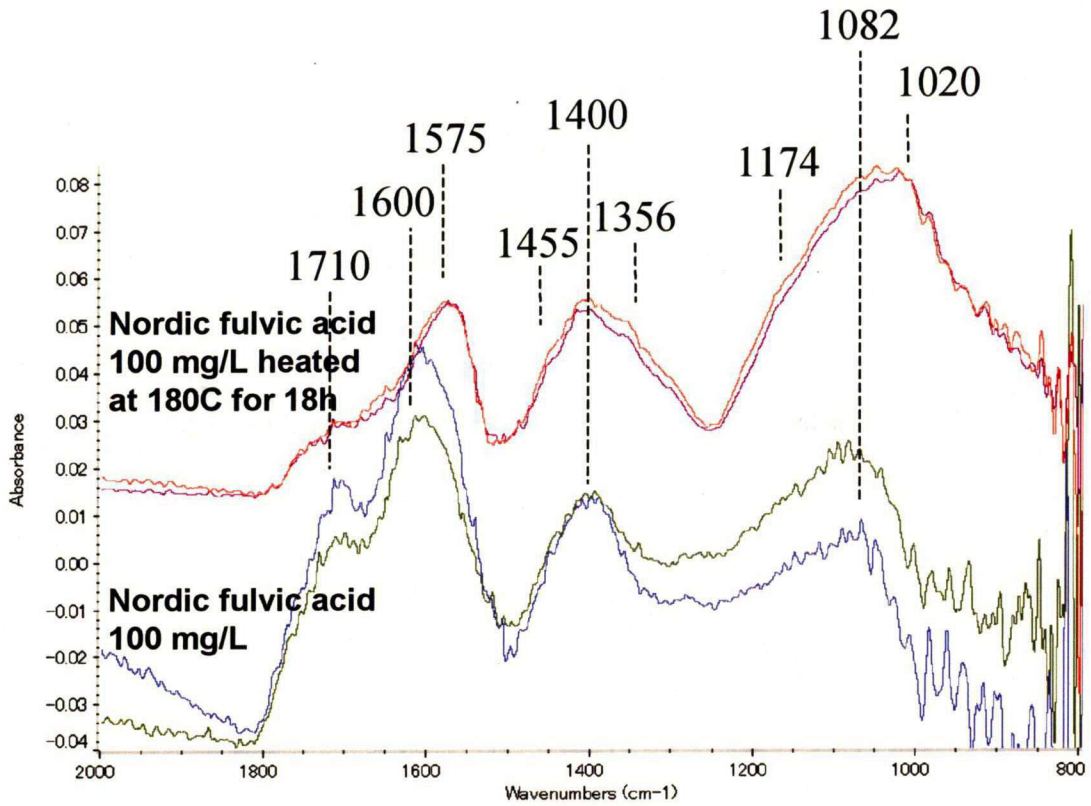

Fig. 3.2.15. FT-IR spectra of heated Nordic fulvic acid solution (100mg/L) at 180° C for 18 hour and the initial fulvic acid solution (100mg/L) on CaF_2 disk.

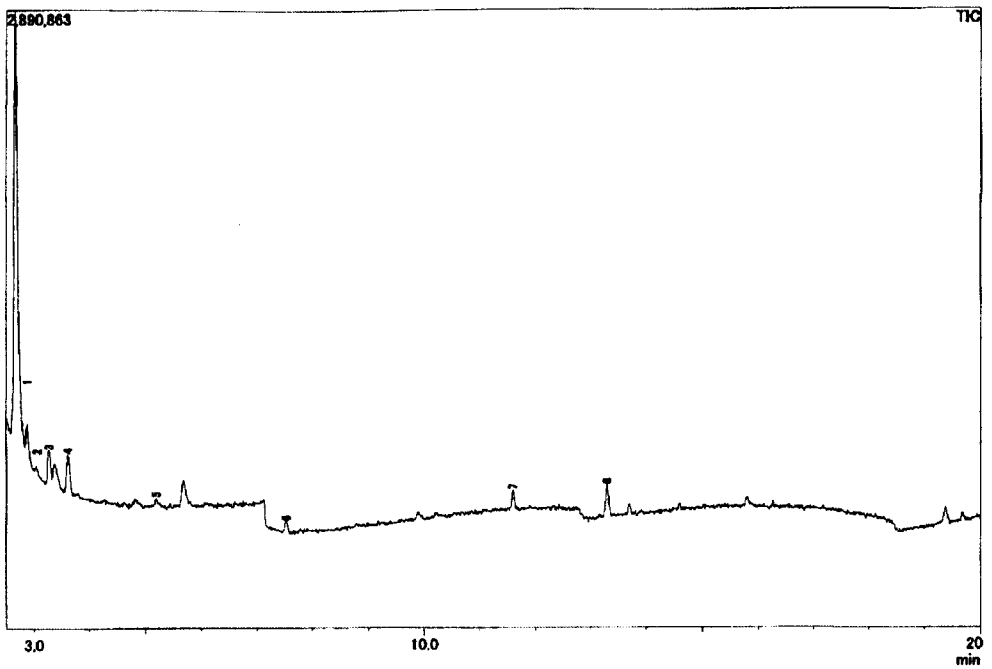

Fig 3.2.16 GC-MS chromatogram (total ion chromatogram) of compounds released from heated Nordic fulvic acid solution (heated at 140° C for 18 hours)

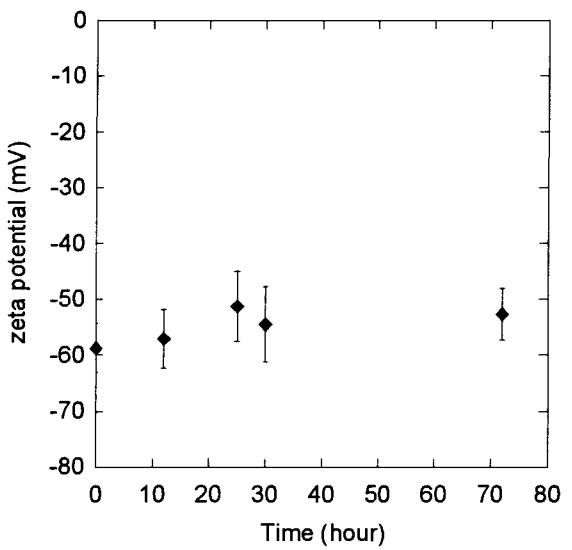

Fig 3.2.17 The zeta potential of heated Nordic fulvic acid at 120°C for 12-72 hours

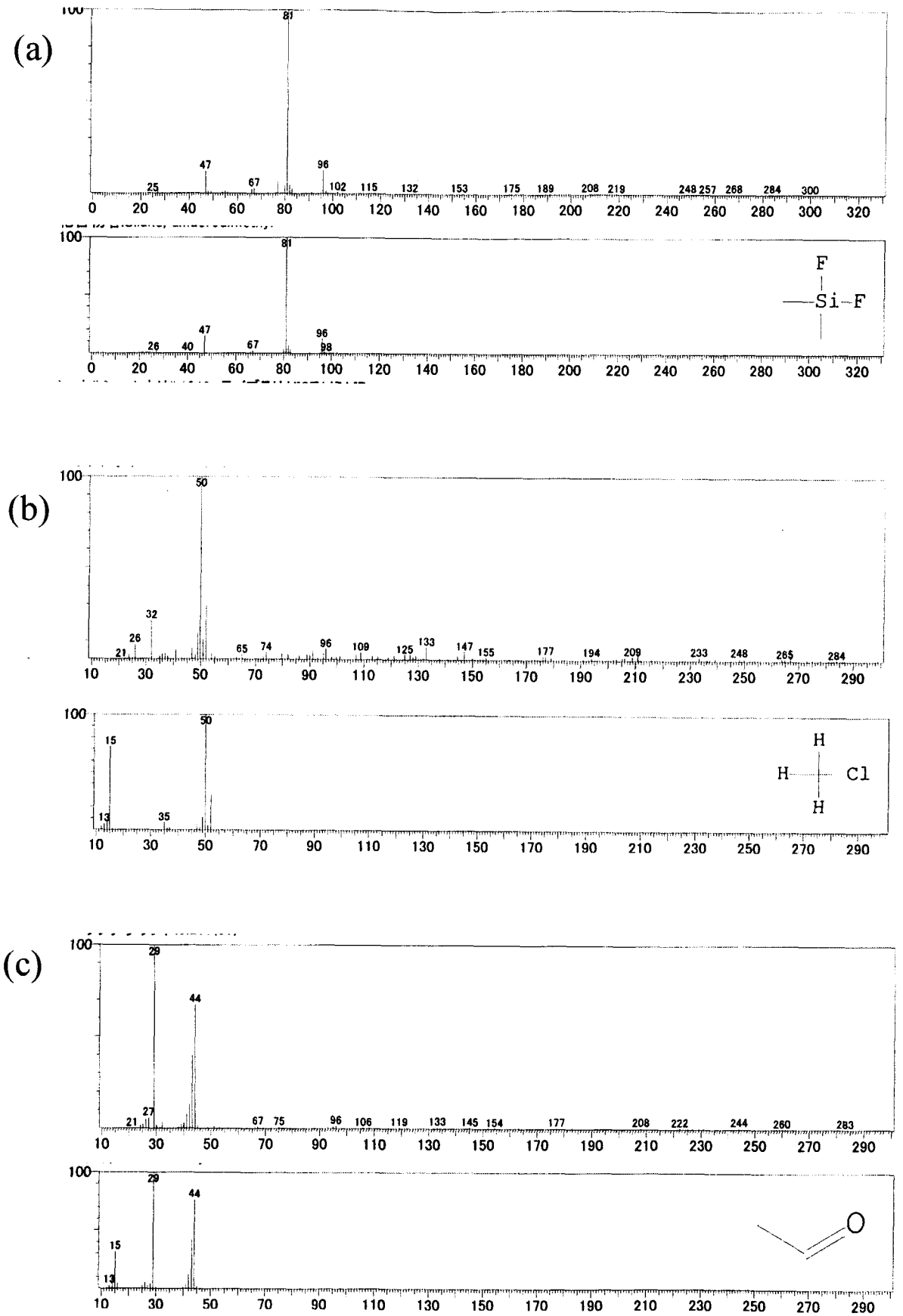

Fig 3.2.18. MS spectra of GC-MS chromatogram (total ion chromatogram) at (a) 2.875 min, (b) 3.050 min and (c) 3.267 min (Nordic fulvic acid solution heated at 140° C for 18 hours)

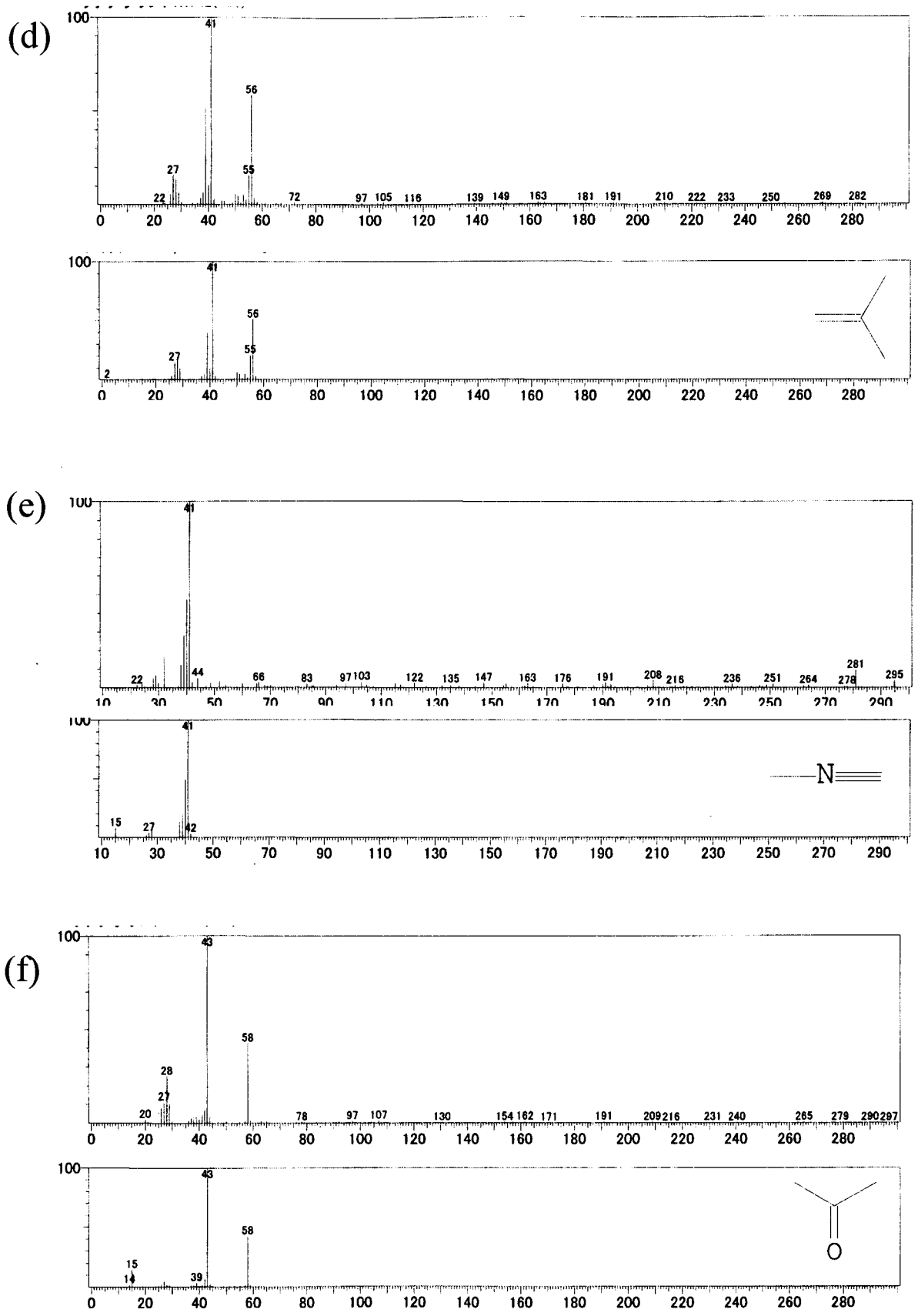

Fig 3.2.18. MS spectra of GC-MS chromatogram (total ion chromatogram) at (d) 3.608 min, (e) 5.183 min and (f) 5.667 min (Nordic fulvic acid solution heated at 140° C for 18 hours)

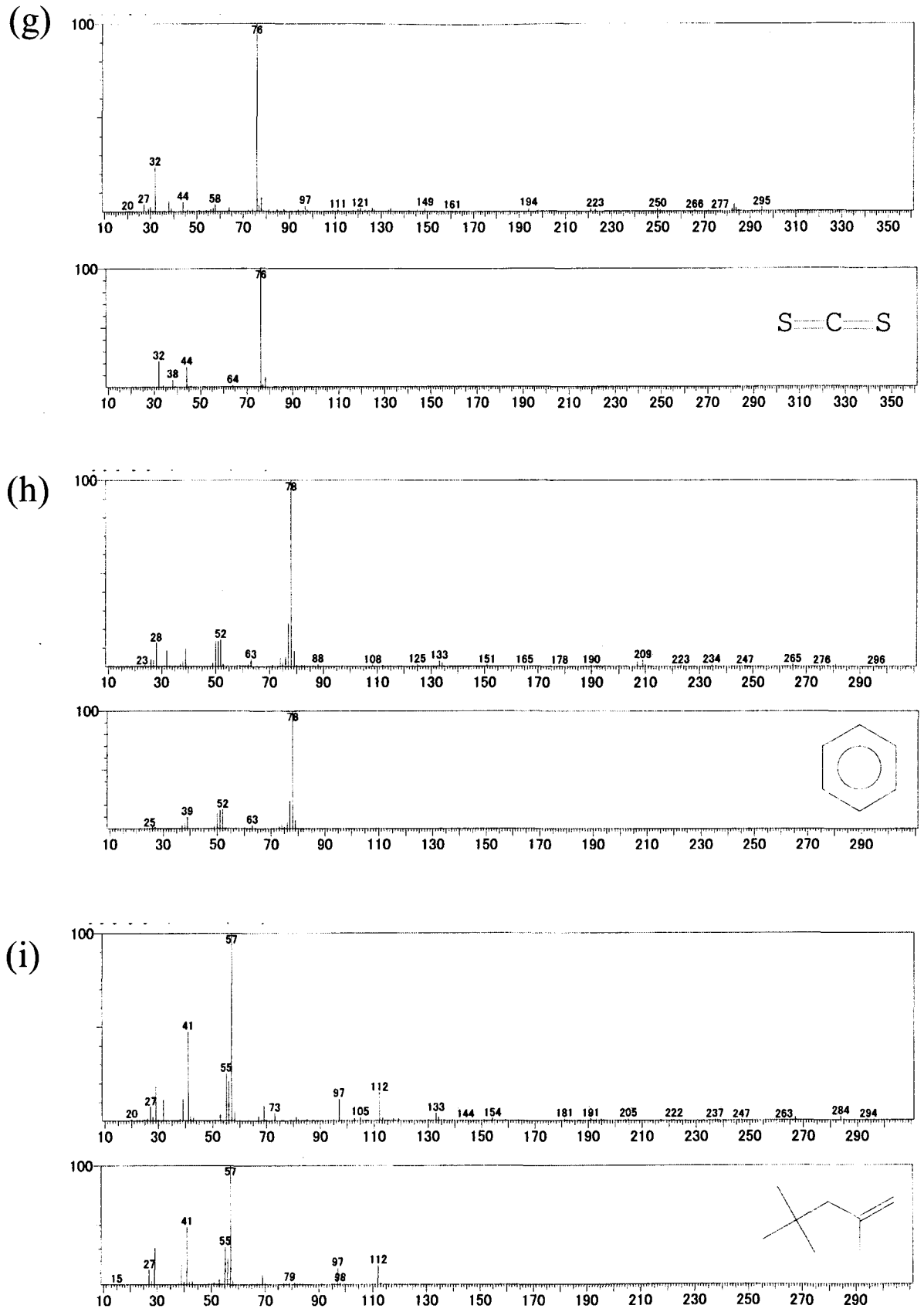

Fig 3.2.18. MS spectra of GC-MS chromatogram (total ion chromatogram) at (g) 7.525 min (h) 11.600 min and (i) 13.292 min (Nordic fulvic acid solution heated at 140° C for 18 hours)

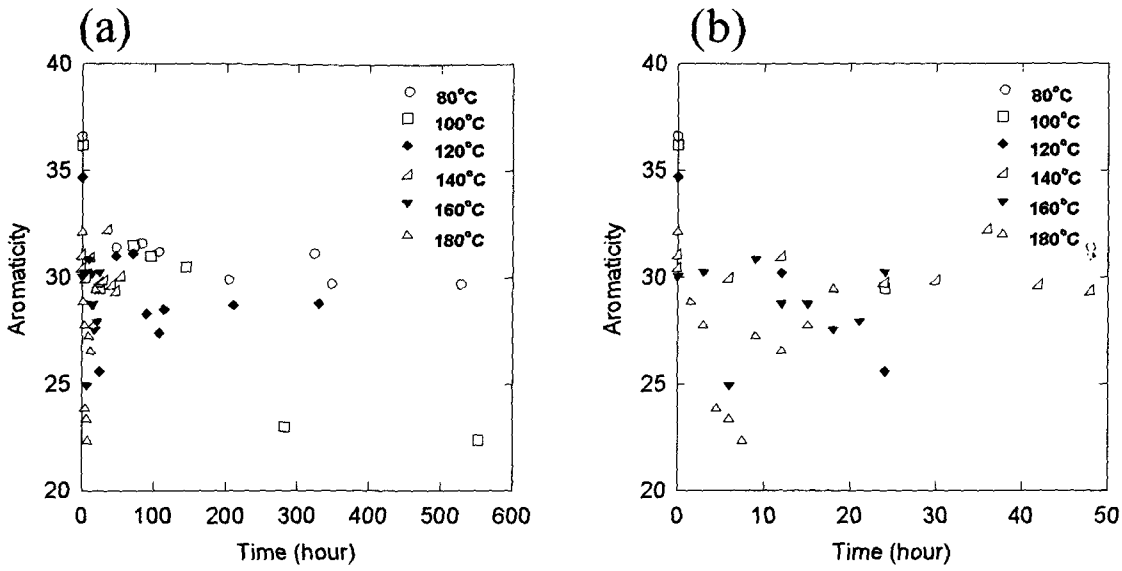

Fig. 3.2.19. Temporal changes in aromaticity, calculated from fluorescence index linear fitting of Nordic fulvic acid solutions heated at 80° C for 0 – 528 hours, 100° C for 0 – 552 hours, 120° C for 0 – 330h hours, 140° C for 0 - 54 hours, 160° C for 0 - 24 hours and 180° C for 0 - 18 hours: a) from 0 to 550 hours; b) from 0 to 50 hours

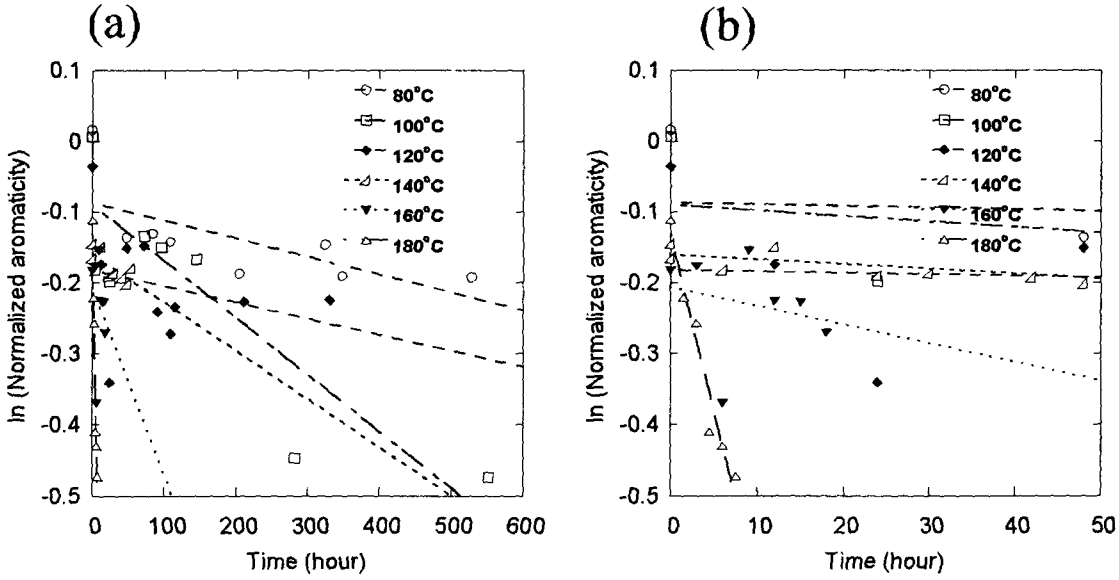

Fig. 3.2.20. Temporal changes in logarithm of aromaticity, calculated from fluorescence index linear fitting , of Nordic fulvic acid solutions heated at 80° C for 0 – 528 hours, 100° C for 0 – 552 hours, 120° C for 0 – 96h hours, 140° C for 0 - 48 hours, 160° C for 0 - 24 hours and 180° C for 0 - 18 hours

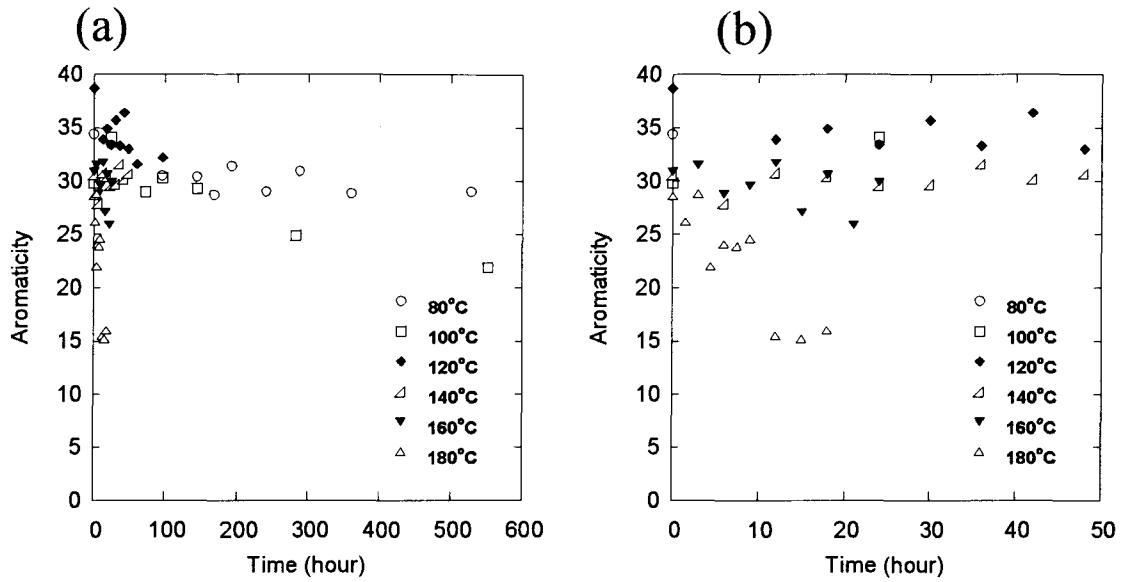

Fig. 3.2.21. Temporal changes in aromaticity, calculated from fluorescence index linear fitting, of Nordic humic acid solutions heated at 80° C for 0 – 528 hours, 100° C for 0 – 552 hours, 120° C for 0 – 330h hours, 140° C for 0 - 54 hours, 160° C for 0 - 24 hours and 180° C for 0 - 18 hours: a) from 0 to 550 hours; b) from 0 to 50 hours

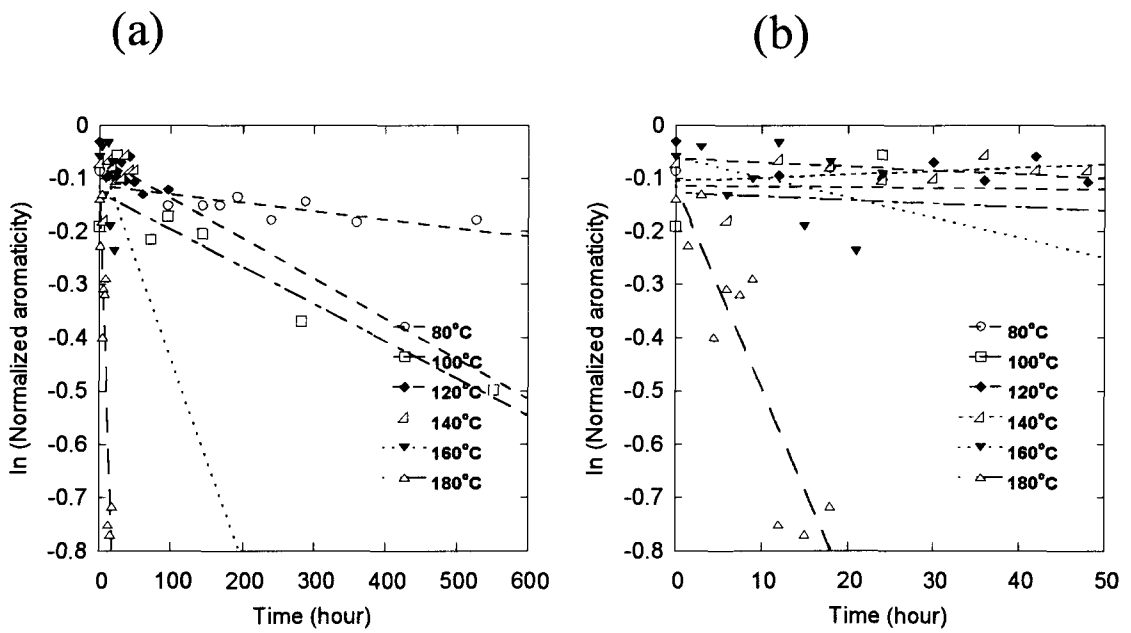

Fig. 3.2.22. Temporal changes in logarithm of aromaticity, calculated from fluorescence index linear fitting , of Nordic humic acid solutions heated at 80° C for 0 – 528 hours, 100° C for 0 – 552 hours, 120° C for 0 – 96h hours, 140° C for 0 - 48 hours, 160° C for 0 - 24 hours and 180° C for 0 - 18 hours

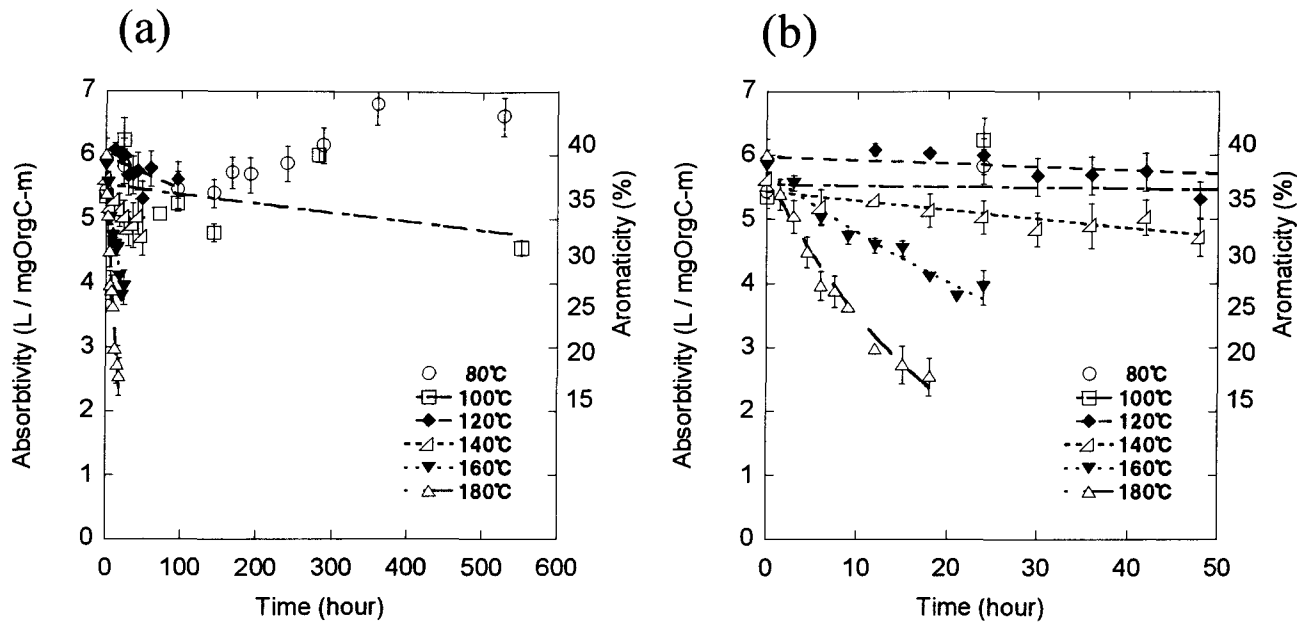

Fig. 3.2.23. Temporal changes in specific UV absorbance (absorbtivity) of Nordic fulvic acid solutions heated at 80° C for 0 – 528 hours, 100° C for 0 – 552 hours, 120° C for 0 – 96h hours, 140° C for 0 - 48 hours, 160° C for 0 - 24 hours and 180° C for 0 - 18 hours: a) from 0 to 600 hours; b) from 0 to 50 hours

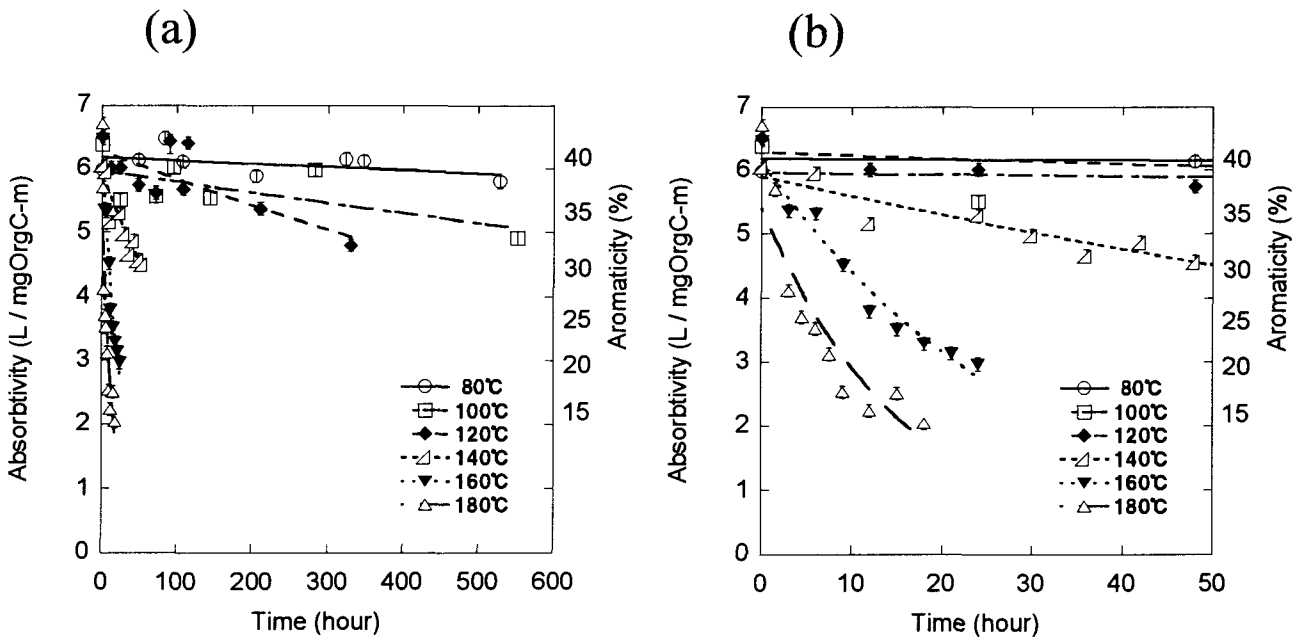

Fig. 3.2.24 Temporal changes in specific UV absorbance (absorbtivity) of Nordic humic acid solutions heated at 80° C for 0 – 528 hours, 100° C for 0 – 552 hours, 120° C for 0 – 330h hours, 140° C for 0 - 54 hours, 160° C for 0 - 24 hours and 180° C for 0 - 18 hours: a) from 0 to 600 hours; b) from 0 to 50 hours

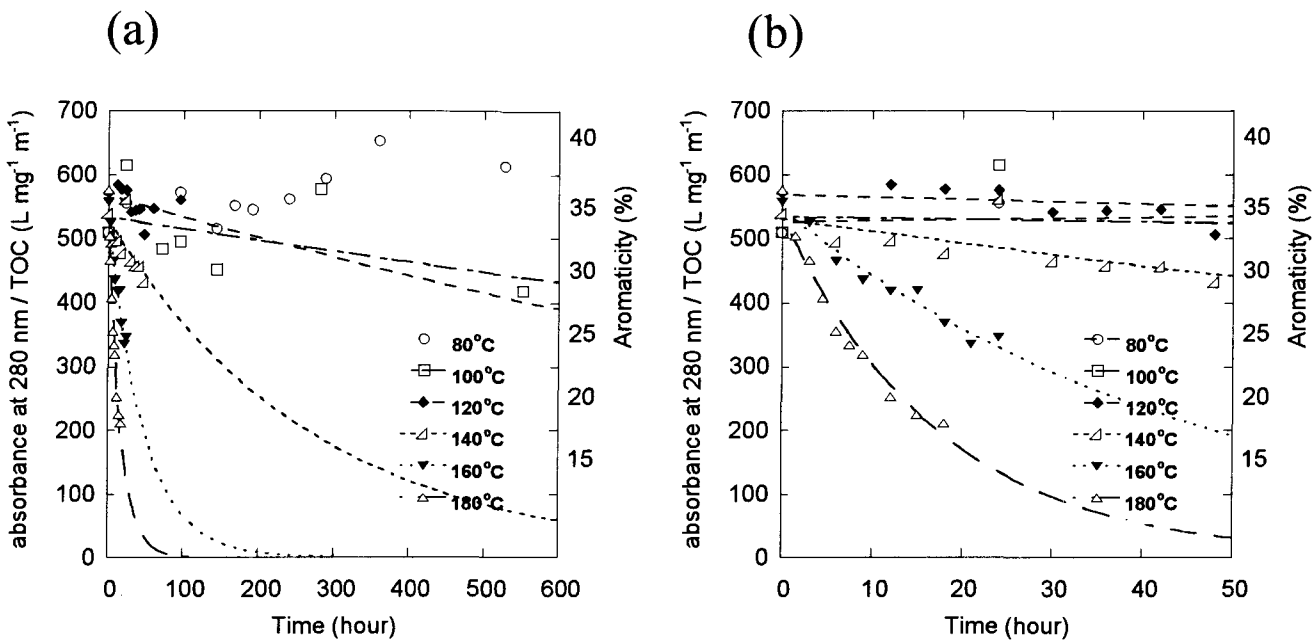

Fig. 3.2.25. Temporal changes in specific UV absorbance at 280 nm divided by total organic carbon (absorbtivity) of Nordic fulvic acid solutions heated at 80° C for 0 – 528 hours, 100° C for 0 – 552 hours, 120° C for 0 – 96h hours, 140° C for 0 - 48 hours, 160° C for 0 - 24 hours and 180° C for 0 - 18 hours: a) from 0 to 600 hours; b) from 0 to 50 hours

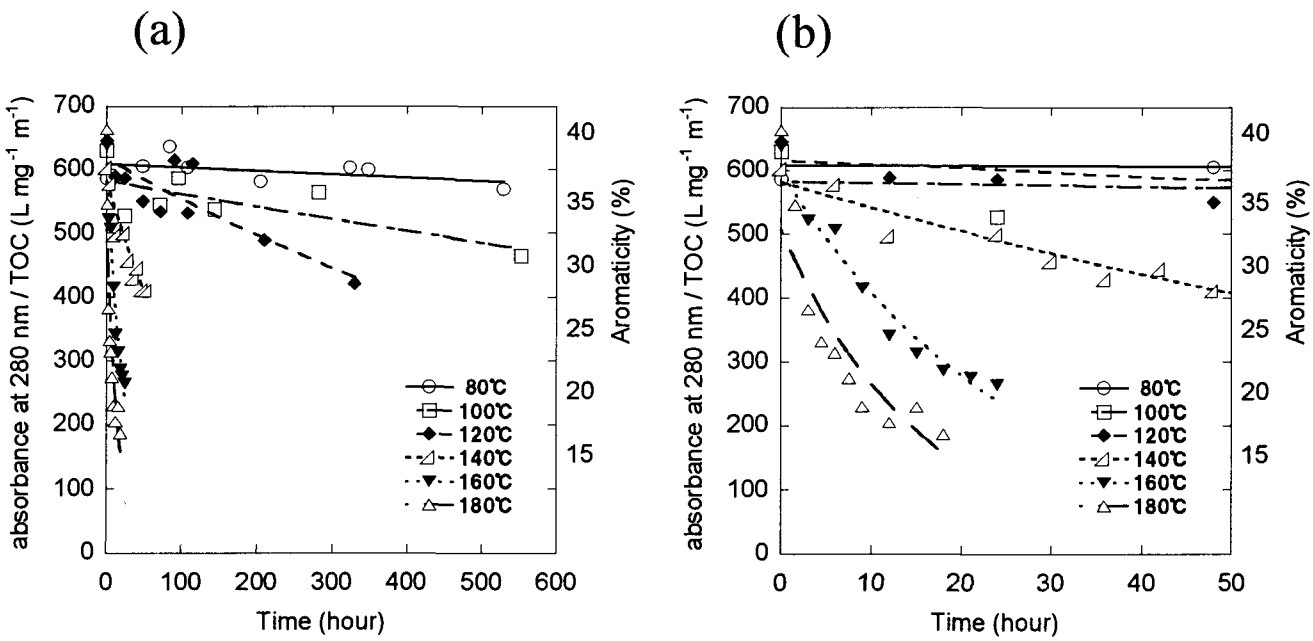

Fig. 3.2.26 Temporal changes in specific UV absorbance at 280 nm divided by total organic carbon (absorbtivity) of Nordic humic acid solutions heated at 80° C for 0 – 528 hours, 100° C for 0 – 552 hours, 120° C for 0 – 330h hours, 140° C for 0 - 54 hours, 160° C for 0 - 24 hours and 180° C for 0 - 18 hours: a) from 0 to 600 hours; b) from 0 to 50 hours

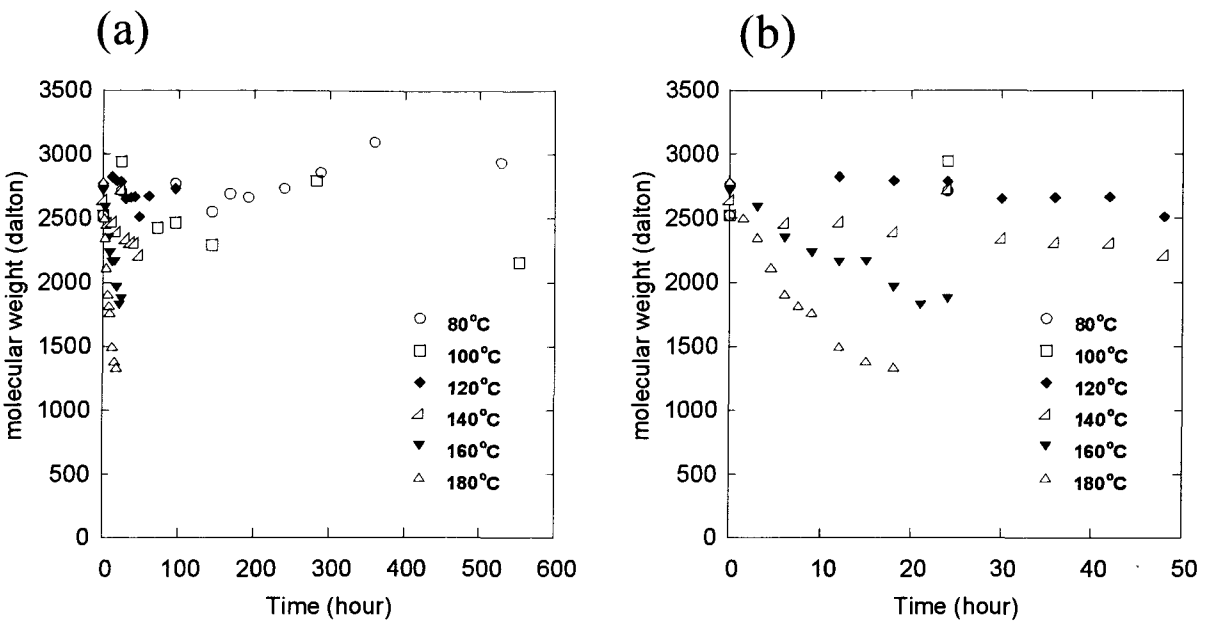

Fig. 3.2.27. Temporal changes in molecular weight of Nordic fulvic acid solution heated at 80° C for 0 – 528 hours, 100° C for 0 – 552 hours, 120° C for 0 – 96h hours, 140° C for 0 - 48 hours, 160° C for 0 - 24 hours and 180° C for 0 - 18 hours: a) from 0 to 600 hours; b) from 0 to 50 hours

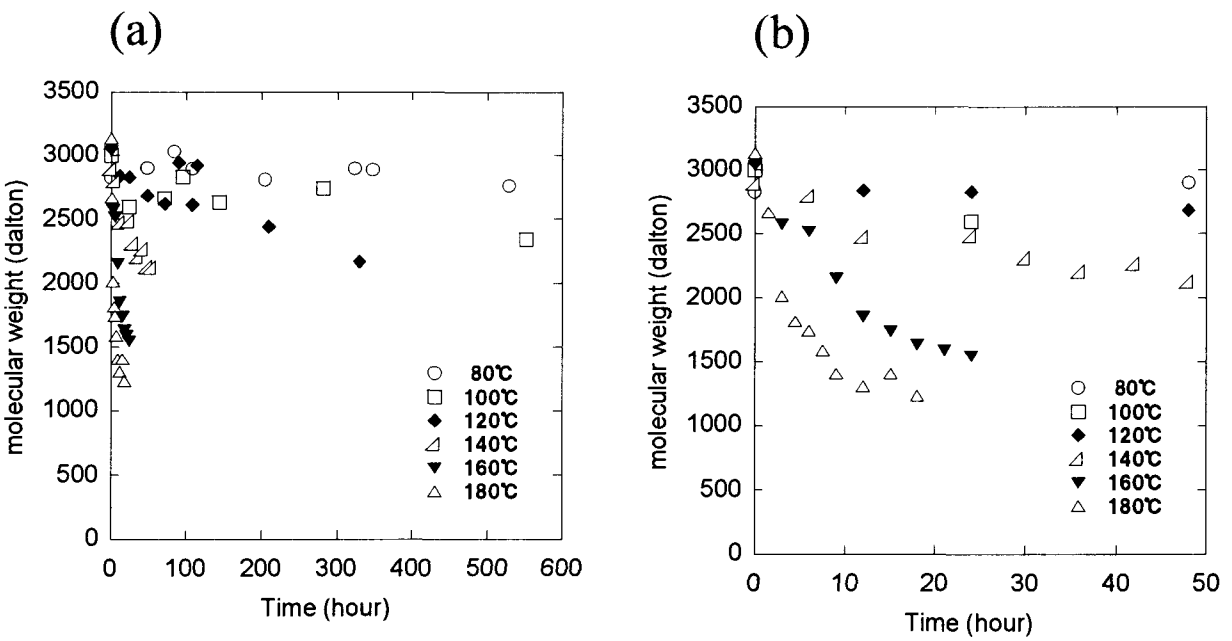

Fig. 3.2.28 Temporal changes in molecular weight of Nordic humic acid solution heated at 80° C for 0 – 528 hours, 100° C for 0 – 552 hours, 120° C for 0 – 330h hours, 140° C for 0 - 54 hours, 160° C for 0 - 24 hours and 180° C for 0 - 18 hours: a) from 0 to 600 hours; b) from 0 to 50 hours

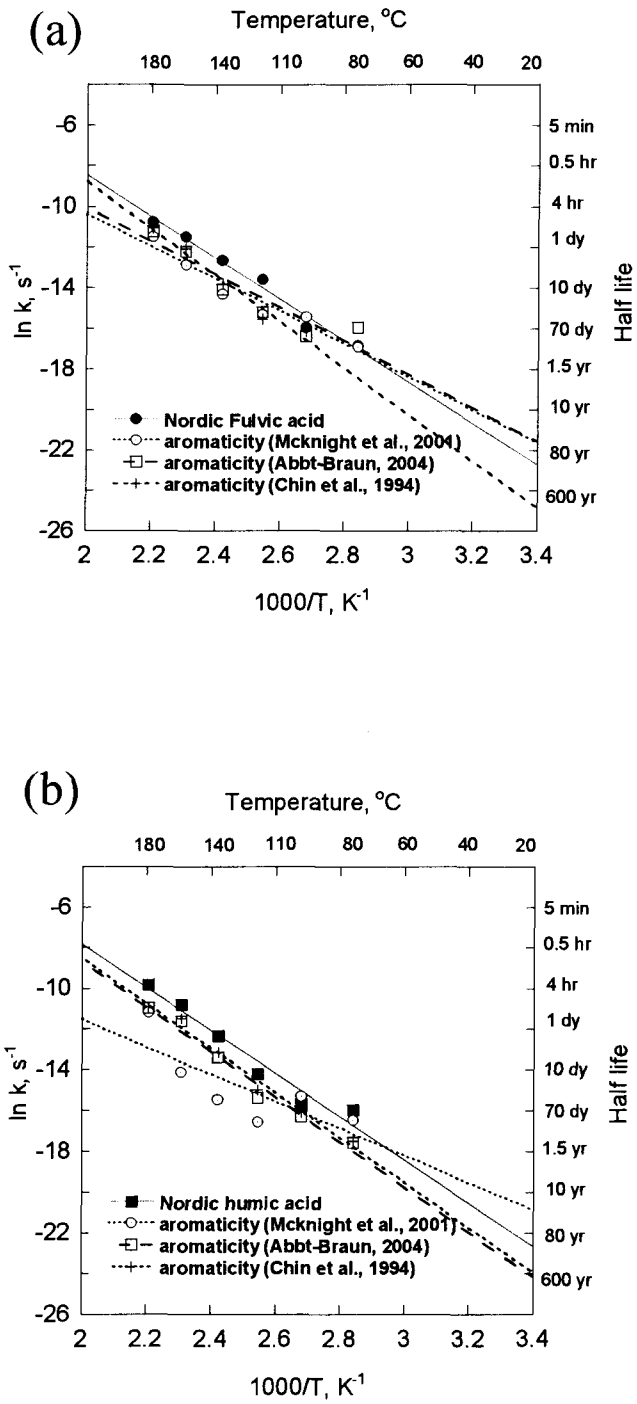

Fig 3.2.29 The Arrhenius diagram for the decrease rates of absorbance at 254 nm and aromaticity decrease rates of (A) Nordic fulvic acid and (B) Nordic humic acid

Table 3.2.1

	Sample	Temperature	Time hour	Time sec	Ave Conc. mgOC/L	error	abs 254nm cm^{-1}	ln (abs 254 nm)
	Nordic FA	100 mg/L			4.55		0.245	0.006
					4.64		0.241	-0.007
	Nordic FA	80℃	0	0	4.36	0.20	0.236	-0.028
			24	86400	4.12	0.19	0.240	-0.012
*			96	345600	4.16	0.19	0.227	-0.067
			144	518400	4.01	0.19	0.217	-0.113
			168	604800	3.84	0.18	0.220	-0.099
			192	691200	3.74	0.18	0.213	-0.130
			240	864000	3.77	0.18	0.222	-0.092
*			288	1036800	3.60	0.18	0.222	-0.091
			360	1296000	3.21	0.17	0.218	-0.107
*			528	1900800	3.26	0.17	0.216	-0.118
	Nordic FA	100℃	0	0	4.11	0.09	0.220	-0.100
			24	86400	3.90	0.08	0.243	0.000
			72	259200	3.90	0.08	0.198	-0.205
			96	345600	3.73	0.08	0.195	-0.218
			144	518400	3.63	0.08	0.174	-0.334
			282	1015200	3.47	0.08	0.208	-0.154
			552	1987200	3.53	0.08	0.161	-0.413
	Nordic FA	120℃	0	0	4.08	0.19	0.243	0.001
			12	43200	3.65	0.18	0.222	-0.089
			18	64800	3.65	0.18	0.220	-0.099
			24	86400	3.68	0.18	0.221	-0.095
			30	108000	3.67	0.18	0.208	-0.153
			36	129600	3.62	0.18	0.206	-0.164
			42	151200	3.44	0.17	0.198	-0.206
			48	172800	3.58	0.18	0.190	-0.244
			60	216000	3.21	0.17	0.186	-0.268
			96	345600	3.59	0.18	0.202	-0.185
	Nordic FA	140℃	0	0	4.18	0.19	0.236	-0.030
			6	21600	3.94	0.08	0.205	-0.171
*			12	43200	3.62	0.18	0.192	-0.233
			18	64800	3.27	0.17	0.169	-0.365
*			24	86400	3.16	0.16	0.159	-0.421
*			30	108000	3.02	0.16	0.147	-0.503
			36	129600	3.01	0.07	0.148	-0.495
			42	151200	2.78	0.15	0.140	-0.551
			48	172800	2.70	0.06	0.128	-0.642
	Nordic FA	160℃	0	0	4.02	0.19	0.234	-0.037
			3	10800	3.52	0.17	0.196	-0.214
			6	21600	3.03	0.16	0.152	-0.470
			9	32400	2.92	0.16	0.138	-0.562
			12	43200	3.11	0.16	0.143	-0.530
			15	54000	2.75	0.15	0.125	-0.662
			18	64800	2.73	0.15	0.112	-0.775
			21	75600	2.49	0.15	0.094	-0.946
			24	86400	2.28	0.14	0.090	-0.994
	Nordic FA	180℃	0	0	3.57	0.17	0.215	-0.124
			1.5	5400	2.94	0.16	0.159	-0.426
			3	10800	2.81	0.16	0.142	-0.535
			4.5	16200	2.67	0.15	0.120	-0.705
			6	21600	2.40	0.14	0.096	-0.933
			7.5	27000	2.31	0.14	0.090	-0.997
			9	32400	2.28	0.14	0.083	-1.075
			12	43200	2.18	0.14	0.065	-1.313
			15	54000	1.92	0.13	0.053	-1.532
			18	64800	2.14	0.14	0.055	-1.494

Table 3.2.2

Sample	Temperature	Time		Ave Conc.	error	abs 254nm	ln (abs 254 nm)
		hour	sec	mgOC/L		cm^{-1}	
Nordic HA	100 mg/L			4.75	0.10	0.281	0.021
				4.04	0.09	0.269	-0.022
Nordic HA	80°C	0	0	4.52	0.09	0.270	-0.017
		48	172800	3.99	0.09	0.245	-0.115
		84	302400	3.90	0.08	0.253	-0.085
		108	388800	3.96	0.08	0.242	-0.126
		204	734400	3.89	0.08	0.229	-0.184
		324	1166400	4.00	0.09	0.246	-0.113
		348	1252800	4.87	0.10	0.298	0.082
		528	1900800	3.84	0.08	0.223	-0.210
Nordic HA	100°C	0	0	4.04	0.09	0.257	-0.066
		24	86400	4.08	0.09	0.225	-0.201
		72	259200	4.01	0.09	0.223	-0.210
		96	345600	3.73	0.08	0.225	-0.202
		144	518400	3.57	0.08	0.198	-0.327
		282	1015200	3.22	0.07	0.193	-0.354
		552	1987200	3.62	0.08	0.178	-0.436
Nordic HA	120°C	0	0	4.11	0.09	0.268	-0.026
		12	43200	3.99	0.09	0.240	-0.135
		24	86400	3.72	0.08	0.224	-0.206
		48	172800	3.47	0.08	0.199	-0.323
		72	259200	3.43	0.08	0.192	-0.357
		90	324000	2.88	0.07	0.185	-0.395
		108	388800	2.83	0.07	0.161	-0.537
		114	410400	3.14	0.07	0.201	-0.311
		210	756000	2.29	0.06	0.123	-0.803
		330	1188000	1.96	0.05	0.094	-1.072
* Nordic HA	140°C	0	0	4.07	0.09	0.246	-0.110
		6	21600	3.51	0.08	0.209	-0.275
		12	43200	4.11	0.09	0.212	-0.261
*		24	86400	3.18	0.07	0.168	-0.490
		30	108000	2.72	0.07	0.135	-0.710
		36	129600	3.23	0.07	0.150	-0.606
		42	151200	2.51	0.06	0.122	-0.811
		48	172800	2.32	0.06	0.106	-0.957
		54	194400	2.41	0.06	0.108	-0.932
Nordic HA	160°C	0	0	3.92	0.08	0.253	-0.081
		3	10800	4.20	0.09	0.225	-0.199
		6	21600	3.65	0.08	0.194	-0.346
		9	32400	2.89	0.07	0.131	-0.744
		12	43200	2.82	0.07	0.107	-0.944
		15	54000	2.43	0.06	0.086	-1.167
		18	64800	2.27	0.06	0.075	-1.302
		21	75600	2.25	0.06	0.070	-1.363
		24	86400	3.00	0.07	0.089	-1.127
Nordic HA	180°C	0	0	3.94	0.08	0.264	-0.039
		1.5	5400	2.96	0.07	0.169	-0.487
		3	10800	2.83	0.07	0.116	-0.861
		4.5	16200	2.15	0.06	0.080	-1.241
		6	21600	2.12	0.06	0.075	-1.300
		7.5	27000	1.95	0.05	0.061	-1.509
		9	32400	2.58	0.06	0.065	-1.438
		12	43200	2.70	0.06	0.060	-1.517
		15	54000	2.41	0.06	0.060	-1.518
		18	64800	2.70	0.06	0.055	-1.607

Table 3.2.3

Retention time (min)	Compound
2.88	difluorodimetyl-silane
3.05	Chloromethane
3.27	acetaldehyde
3.61	2-methyl-1-propene
5.18	methyl isocyanide
5.67	acetone
7.51	carbon disulfide
11.60	benzene
13.29	2,4,4-trimethyl-1-pentene

Table 3.2.4 Temporal changes in zeta potential of Nordic fulvic acid solution (100mg/L, 120°C for 0-72 hours)

No.	0	12(hour)	25(hour)	30(hour)	72(hour)
1	-61.08	-64.13	-56.45	-61.92	-47.70
2	-53.79	-68.02	-58.14	-60.72	-50.18
3	-57.53	-51.03	-45.24	-47.76	-56.68
4	-61.13	-57.43	-54.98	-45.72	-61.42
5	-60.78	-55.23	-37.32	-57.25	-53.90
6	-59.27	-62.59	-47.55	-64.72	-47.66
7	-60.71	-58.75	-57.10	-53.51	-60.03
8	-52.97	-53.25	-47.29	-46.14	-58.81
9	-58.28	-55.11	-51.42	-47.72	-49.61
10	-57.13	-51.15	-52.56	-45.86	-45.53
11	-59.50	-54.91	-53.09	-44.77	-48.31
12	-57.56	-61.49	-52.50	-58.53	-51.25
13	-64.22	-60.20	-50.54	-62.84	-59.26
14	-61.80	-67.16	-54.18	-56.95	-48.25
15	-57.79	-62.74	-54.70	-54.82	-52.61
16	-57.85	-58.67	-49.26	-56.95	-49.79
17	-57.86	-52.60	-42.43	-50.79	-49.99
18	-55.69	-54.15	-60.96	-59.96	-52.51
19	-65.37	-60.72	-53.41	-40.09	-55.15
20	-55.19	-57.19	-61.28	-51.37	-52.52
21	-53.66	-54.18	-51.66	-42.81	-54.57
22	-59.03	-54.95	-55.29	-57.89	-59.23
23	-61.78	-69.18	-35.72	-66.24	-44.43
24	-56.42	-53.27	-38.37	-55.10	-53.35
25	-65.57	-46.05	-63.90	-54.81	-57.80
26	-59.21	-47.14	-42.14	-55.54	-62.96
27	-58.03	-52.36	-56.32	-66.98	-40.72
28	-51.76	-55.68	-47.31	-56.71	-51.40
29	-62.44	-50.03	-49.04	-58.12	-53.88
30	-60.36	-56.93	-41.40	-57.61	-48.38
31	-54.84	-55.48	-52.63	-42.19	-55.94
32	-62.66	-60.08	-51.97	-60.09	-57.51
33	-56.78	-51.38	-58.33	-51.24	-57.42
34	-52.42	-60.18	-48.12	-53.28	-48.16
35	-67.87	-58.09	-52.46	-56.70	-51.67
36	-52.80	-62.63	-58.07	-46.73	-53.59
37	-63.91	-51.58	-39.08	-57.71	-50.80
38	-66.44	-51.43	-58.19	-53.11	-59.25
39	-53.34	-55.33	-54.67	-41.86	-49.92
40	-57.25	-61.35	-51.83	-57.46	-52.13
41	-52.01	-61.95	-56.04	-55.72	-48.10
42	-50.30	-58.34	-50.45	-56.78	-55.86
43	-54.71	-59.82	-52.70	-48.92	-52.24
44	-67.31	-63.64	-48.84	-44.83	-53.24
45	-56.59	-53.78	-49.15	-58.91	-47.60
46	-57.47	-56.67	-56.03	-59.18	-52.39
47	-61.97	-53.74	-49.54	-59.93	-53.63
48	-60.64	-61.01	-53.41	-57.81	-50.61
49	-57.39		-52.85	-56.04	-51.31
50	-62.10			-66.28	-56.12
Ave	-58.7	-57.1	-51.3	-54.5	-52.7

Table 3.2.5

	Sample	Temperature	Time hour	Time sec	UV / TOC L mgOC^{-1}m^{-1}	error +	error -	aromaticity (%)	Em 450 nm (Ex 370nm)	Em 500 nm (Ex 370nm)	Fluorescence index	aromaticity (%)	Normalized FL index	ln(FL index)
	Nordic FA	100 mg/L							16.3	13.7	1.19	33.7	1.01	
									14.7	12.2	1.21	33.0	0.99	
	Nordic FA	80℃	0	0	5.426	0.2	0.3	35.6	14.8	11.5	1.29	34.4	1.03	-0.086
			24	86400	5.829	0.3	0.3	38.1	16.3	12.5	1.30	33.4	1.00	-0.102
*			96	345600	5.460	0.2	0.3	35.8	12.8	9.5	1.34	30.5	0.91	-0.151
			144	518400	5.407	0.2	0.3	35.5	21.7	16.2	1.34	30.4	0.91	-0.152
			168	604800	5.733	0.3	0.3	37.5	30.9	23.3	1.33	28.7	0.86	-0.151
			192	691200	5.701	0.3	0.3	37.3	18.9	14.3	1.33	31.4	0.94	-0.135
			240	864000	5.877	0.3	0.3	38.4	16.9	12.4	1.36	29.0	0.87	-0.179
*			288	1036800	6.160	0.3	0.3	40.2	16.2	12.2	1.33	30.9	0.93	-0.144
			360	1296000	6.797	0.3	0.4	44.2	13.2	9.7	1.36	28.8	0.86	-0.183
*			528	1900800	6.620	0.3	0.4	43.1	14.1	10.3	1.36	29.0	0.87	-0.179
	Nordic FA	100℃	0	0	5.350	0.1	0.1	35.1	14.9	11.5	1.30	29.8	0.89	-0.190
			24	86400	6.231	0.1	0.1	40.7	10.3	8.7	1.18	34.1	1.02	-0.050
			72	259200	5.076	0.1	0.1	33.4	14.7	11.2	1.32	29.0	0.87	-0.220
			96	345600	5.240	0.1	0.1	34.4	14.0	10.9	1.28	30.3	0.91	-0.170
			144	518400	4.792	0.1	0.1	31.6	13.5	10.3	1.31	29.3	0.88	-0.210
			282	1015200	6.002	0.1	0.1	39.2	10.2	7.1	1.43	24.9	0.75	-0.370
			552	1987200	4.556	0.1	0.1	30.1	12.4	8.2	1.51	21.9	0.66	-0.500
	Nordic FA	120℃	0	0	5.965	0.3	0.3	39.0	15.9	12.8	1.24	38.7	1.16	-0.030
			12	43200	6.089	0.3	0.3	39.8	16.0	12.4	1.29	33.9	1.02	-0.094
			18	64800	6.030	0.3	0.3	39.4	15.9	12.4	1.28	34.9	1.05	-0.080
			24	86400	5.994	0.3	0.3	39.2	15.5	11.9	1.30	33.4	1.00	-0.101
			30	108000	5.679	0.3	0.3	37.2	14.9	11.7	1.27	35.7	1.07	-0.069
			36	129600	5.695	0.3	0.3	37.3	15.0	11.5	1.30	33.3	1.00	-0.104
			42	151200	5.749	0.3	0.3	37.6	13.9	11.0	1.27	36.4	1.09	-0.059
			48	172800	5.320	0.2	0.3	34.9	13.8	10.6	1.30	33.0	0.99	-0.107
			60	216000	5.787	0.3	0.3	37.9	13.5	10.2	1.32	31.6	0.95	-0.130
			96	345600	5.618	0.3	0.3	36.8	13.9	10.6	1.32	32.2	0.97	-0.121
	Nordic FA	140℃	0	0	5.637	0.2	0.3	36.9	16.9	13.3	1.27	30.6	0.92	-0.069
			6	21600	5.198	0.1	0.1	34.1	15.0	11.1	1.35	27.9	0.84	-0.178
*			12	43200	5.310	0.2	0.3	34.9	15.0	11.8	1.27	30.8	0.92	-0.063
			18	64800	5.152	0.3	0.3	33.9	13.6	10.6	1.28	30.4	0.91	-0.077
*			24	86400	5.040	0.2	0.3	33.2	13.2	10.1	1.30	29.6	0.89	-0.102
*			30	108000	4.860	0.2	0.3	32.0	12.4	9.5	1.30	29.7	0.89	-0.098
			36	129600	4.918	0.1	0.1	32.4	11.2	9.0	1.25	31.6	0.95	-0.054
			42	151200	5.047	0.3	0.3	33.2	11.5	8.9	1.28	30.2	0.91	-0.083
			48	172800	4.736	0.1	0.1	31.2	10.0	7.9	1.27	30.7	0.92	-0.083

		0	0	5.827	0.3	0.3	38.1	16.5	13.0	1.27	30.9	0.93	-0.059
		3	10800	5.573	0.3	0.3	36.5	15.1	12.1	1.25	31.5	0.94	-0.041
		6	21600	5.013	0.3	0.3	33.0	15.8	11.9	1.32	28.8	0.86	-0.132
		9	32400	4.734	0.2	0.3	31.2	13.8	10.6	1.30	29.6	0.89	-0.101
Nordic FA	160°C	12	43200	4.590	0.2	0.3	30.3	12.3	9.9	1.24	31.7	0.95	-0.033
		15	54000	4.553	0.2	0.3	30.1	14.1	10.3	1.37	27.1	0.81	-0.190
		18	64800	4.099	0.2	0.2	27.2	11.3	8.9	1.27	30.6	0.92	-0.069
		21	75600	3.796	0.2	0.2	25.3	13.1	9.4	1.40	25.9	0.78	-0.237
		24	86400	3.937	0.2	0.3	26.2	10.3	8.0	1.29	29.9	0.90	-0.092
		0	0	6.006	0.3	0.3	39.2	17.8	13.4	1.33	28.6	0.86	-0.138
		1.5	5400	5.400	0.3	0.3	35.4	17.1	12.3	1.39	26.2	0.79	-0.226
		3	10800	5.057	0.3	0.3	33.3	13.8	10.4	1.32	28.8	0.86	-0.129
		4.5	16200	4.501	0.2	0.3	29.8	18.7	12.4	1.51	22.0	0.66	-0.399
Nordic FA	180°C	6	21600	3.982	0.2	0.3	26.5	15.1	10.4	1.45	24.1	0.72	-0.307
		7.5	27000	3.890	0.2	0.3	25.9	14.3	9.8	1.46	23.9	0.72	-0.318
		9	32400	3.640	0.2	0.2	24.3	14.0	9.8	1.44	24.6	0.74	-0.288
		12	43200	2.992	0.2	0.2	20.3	18.2	10.8	1.68	15.5	0.46	-0.751
		15	54000	2.739	0.2	0.2	18.7	15.7	9.3	1.69	15.2	0.46	-0.769
		18	64800	2.553	0.2	0.2	17.5	15.9	9.5	1.67	16.0	0.48	-0.716

Table 3.2.6

Sample	Temperature	Time		UV / TOC	error			Em 450 nm	Em 500 nm	Fluorescence		Normalized	ln
		hour	sec	L $mgOC^{-1}m^{-1}$	+	-		(Ex 370nm)	(Ex 370nm)	index	aromaticity	aromaticity	(aromaticity)
Nordic HA	100 mg/L			5.670	0.1	0.1	37.1	8.0	7.1	1.13	36.0	1.00	
		0	0	5.980	0.1	0.1	39.1	9.3	8.4	1.11	36.6	1.02	0.020
		48	172800	6.140	0.1	0.1	40.1	9.1	7.3	1.25	31.4	0.87	-0.140
		84	302400	6.480	0.1	0.1	42.2	8.6	6.9	1.25	31.6	0.88	-0.130
Nordic HA	80°C	108	388800	6.113	0.1	0.1	39.9	8.6	6.8	1.26	31.2	0.87	-0.140
		204	734400	5.884	0.1	0.1	38.5	8.9	6.8	1.29	29.9	0.83	-0.190
		324	1166400	6.148	0.1	0.1	40.1	8.7	6.9	1.26	31.1	0.86	-0.150
		348	1252800	6.124	0.1	0.1	40.0	11.0	8.5	1.30	29.7	0.83	-0.190
		528	1900800	5.801	0.1	0.1	37.9	8.8	6.8	1.30	29.7	0.82	-0.190
		0	0	6.370	0.1	0.1	41.5	7.3	6.5	1.12	36.2	1.01	0.010
		24	86400	5.511	0.1	0.1	36.1	15.0	11.5	1.30	29.5	0.82	-0.200
		72	259200	5.564	0.1	0.1	36.5	10.8	8.6	1.25	31.5	0.87	-0.130
Nordic HA	100°C	96	345600	6.024	0.1	0.1	39.4	10.5	8.3	1.26	31.0	0.86	-0.150
		144	518400	5.546	0.1	0.1	36.3	10.4	8.2	1.28	30.5	0.85	-0.170
		282	1015200	5.986	0.1	0.1	39.1	12.8	8.7	1.48	23.0	0.64	-0.450
		552	1987200	4.911	0.1	0.1	32.3	9.3	6.3	1.49	22.4	0.62	-0.470

		0	0	6.508	0.1	0.1	42.4	8.5	7.3	1.16	34.7	0.96	-0.040
		12	43200	6.013	0.1	0.1	39.3	11.6	9.0	1.28	30.2	0.84	-0.170
		24	86400	6.015	0.1	0.1	39.3	11.3	8.0	1.41	25.6	0.71	-0.340
		48	172800	5.743	0.1	0.1	37.6	10.9	8.6	1.26	31.0	0.86	-0.150
	Nordic HA	72	259200	5.617	0.1	0.1	36.8	10.2	8.1	1.26	31.1	0.86	-0.150
	120°C	90	324000	6.436	0.1	0.2	41.9	10.5	7.9	1.34	28.3	0.79	-0.240
		108	388800	5.681	0.1	0.1	37.2	9.9	7.3	1.36	27.4	0.76	-0.270
		114	410400	6.409	0.1	0.1	41.8	10.6	7.9	1.33	28.5	0.79	-0.230
		210	756000	5.370	0.1	0.1	35.2	8.9	6.7	1.33	28.7	0.80	-0.230
		330	1188000	4.801	0.1	0.1	31.6	7.8	5.9	1.32	28.8	0.80	-0.220
*		0	0	6.048	0.1	0.1	39.5	10.5	8.3	1.28	30.5	0.85	-0.170
		6	21600	5.948	0.1	0.1	38.9	9.4	7.5	1.26	31.1	0.87	-0.140
		12	43200	5.156	0.1	0.1	33.9	10.9	8.4	1.29	30.0	0.83	-0.180
*		24	86400	5.291	0.1	0.1	34.7	12.1	9.6	1.26	31.0	0.86	-0.150
	Nordic HA	30	108000	4.978	0.1	0.1	32.8	9.5	7.4	1.30	29.8	0.83	-0.190
	140°C	36	129600	4.650	0.1	0.1	30.7	9.5	7.3	1.29	29.9	0.83	-0.190
		42	151200	4.861	0.1	0.1	32.0	10.5	8.6	1.23	32.3	0.90	-0.110
		48	172800	4.558	0.1	0.1	30.1	9.1	7.0	1.30	29.7	0.82	-0.190
		54	194400	4.492	0.1	0.1	29.7	8.4	6.4	1.31	29.4	0.82	-0.200
		0	0	6.473	0.1	0.1	42.2	10.6	8.2	1.29	30.0	0.83	-0.180
		3	10800	5.363	0.1	0.1	35.2	13.2	10.2	1.29	30.2	0.84	-0.180
		6	21600	5.322	0.1	0.1	34.9	16.4	11.4	1.43	24.9	0.69	-0.370
		9	32400	4.521	0.1	0.1	29.9	11.4	9.0	1.27	30.8	0.86	-0.150
	Nordic HA	12	43200	3.795	0.1	0.1	25.3	11.3	8.5	1.32	28.7	0.80	-0.230
	160°C	15	54000	3.515	0.1	0.1	23.5	10.3	7.8	1.33	28.7	0.80	-0.230
		18	64800	3.287	0.1	0.1	22.1	10.9	8.0	1.36	27.5	0.76	-0.270
		21	75600	3.130	0.1	0.1	21.1	9.9	7.3	1.35	27.9	0.78	-0.250
		24	86400	2.968	0.1	0.1	20.1	10.6	8.2	1.28	30.2	0.84	-0.180
		0	0	6.707	0.1	0.1	43.7	11.6	9.4	1.23	32.2	0.89	-0.110
		1.5	5400	5.700	0.1	0.1	37.3	13.3	10.0	1.32	28.9	0.80	-0.220
		3	10800	4.113	0.1	0.1	27.3	12.4	9.2	1.35	27.8	0.77	-0.260
		4.5	16200	3.703	0.1	0.1	24.7	11.2	7.7	1.45	23.9	0.66	-0.410
	Nordic HA	6	21600	3.526	0.1	0.1	23.6	10.8	7.3	1.47	23.4	0.65	-0.430
	180°C	7.5	27000	3.117	0.1	0.1	21.0	9.1	6.1	1.49	22.4	0.62	-0.470
		9	32400	2.527	0.1	0.1	17.3	10.8	8.0	1.36	27.3	0.76	-0.270
		12	43200	2.232	0.1	0.1	15.5	10.5	7.6	1.38	26.6	0.74	-0.300
		15	54000	2.506	0.1	0.1	17.2	8.7	6.4	1.35	27.8	0.77	-0.260
		18	64800	2.039	0.0	0.1	14.2	8.8	6.7	1.30	29.5	0.82	-0.200

Hydrothermal transformation of humic substances

Table 3.2.7

	Sample	Temperature	Time hour	Time sec	Ave Conc. mgOC/L	UV Abs. 280nm	Abs280/TOC (L/mg m)	Aromaticity (%)	molecular weight
		100 mg/L			4.72	0.1912	486.4	31.1	2430.6
					4.64	0.1888	488.1	31.1	2437.5
	Nordic FA	80℃	0	0	4.36	0.1851	510.0	32.2	2524.8
			24	86400	4.12	0.1907	555.7	34.5	2707.3
*			96	345600	4.16	0.1825	571.9	35.3	2772.0
			144	518400	4.01	0.1723	515.5	32.5	2546.8
			168	604800	3.84	0.1761	550.7	34.3	2687.5
			192	691200	3.74	0.1699	544.7	34.0	2663.5
			240	864000	3.77	0.1763	561.3	34.8	2729.8
*			288	1036800	3.60	0.1780	593.2	36.4	2857.0
			360	1296000	3.21	0.1745	652.2	39.3	3092.2
*			528	1900800	3.26	0.1721	613.9	37.4	2939.4
	Nordic FA	100℃	0	0	4.11	0.1743	509.2	32.2	2521.6
			24	86400	3.90	0.1996	614.1	37.4	2940.4
			72	259200	3.90	0.1573	484.0	30.9	2421.0
			96	345600	3.73	0.1538	495.1	31.5	2465.6
			144	518400	3.63	0.1365	451.1	29.3	2289.9
			282	1015200	3.47	0.1671	577.6	35.6	2794.6
			552	1987200	3.53	0.1228	417.7	27.6	2156.5
	Nordic FA	120℃	0	0	4.08	0.1944	571.9	35.3	2772.1
			12	43200	3.65	0.1777	584.5	36.0	2822.2
			18	64800	3.65	0.1755	576.9	35.6	2791.7
			24	86400	3.68	0.1770	576.2	35.6	2789.2
			30	108000	3.67	0.1657	541.6	33.8	2650.9
			36	129600	3.62	0.1643	544.1	33.9	2661.1
			42	151200	3.44	0.1566	546.4	34.1	2670.1
			48	172800	3.58	0.1511	506.6	32.1	2511.2
			60	216000	3.21	0.1464	547.1	34.1	2673.0
			96	345600	3.59	0.1680	560.9	34.8	2727.9
	Nordic FA	140℃	0	0	4.18	0.1881	540.0	33.7	2644.4
			6	21600	3.94	0.1626	495.4	31.5	2466.4
*			12	43200	3.62	0.1520	497.2	31.6	2473.6
			18	64800	3.27	0.1303	477.9	30.6	2397.0
*			24	86400	3.16	0.1226	561.2	34.8	2729.4
*			30	108000	3.02	0.1114	465.2	30.0	2346.1
			36	129600	3.01	0.1148	457.7	29.6	2316.1
			42	151200	2.78	0.1055	456.3	29.6	2310.8
			48	172800	2.70	0.0973	432.6	28.4	2216.0
	Nordic FA	160℃	0	0	4.02	0.1867	557.7	34.6	2715.1
			3	10800	3.52	0.1542	525.5	33.0	2586.8
			6	21600	3.03	0.1174	465.3	30.0	2346.6
			9	32400	2.92	0.1062	435.9	28.5	2229.1
			12	43200	3.11	0.1084	417.7	27.6	2156.6
			15	54000	2.75	0.0963	419.5	27.7	2163.9
			18	64800	2.73	0.0839	368.6	25.2	1960.8
			21	75600	2.49	0.0693	334.7	23.5	1825.4
			24	86400	2.28	0.0660	346.8	24.1	1873.7
	Nordic FA	180℃	0	0	3.57	0.1714	575.6	35.5	2786.5
			1.5	5400	2.94	0.1235	504.3	32.0	2502.0
			3	10800	2.81	0.1092	465.8	30.0	2348.4
			4.5	16200	2.67	0.0907	408.0	27.1	2117.9
			6	21600	2.40	0.0711	355.3	24.5	1907.6
			7.5	27000	2.31	0.0642	334.1	23.4	1823.1
			9	32400	2.28	0.0605	318.8	22.7	1762.2
			12	43200	2.18	0.0461	253.2	19.4	1500.1
			15	54000	1.92	0.0359	224.6	18.0	1386.2
			18	64800	2.14	0.0377	211.6	17.3	1334.3

Table 3.2.8

Sample	Temperature	Time hour	Time sec	Ave Conc. mgOC/L	UV Abs. 280nm	Abs280/TOC (L/mg m)	Aromaticity (%)	molecular weight
Nordic HA	100 mg/L			4.75	0.2201	556.7	34.6	2711.2
Nordic HA	80℃	0	0	4.52	0.2210	586.9	36.1	2831.6
		48	172800	3.99	0.2012	605.0	37.0	2904.0
		84	302400	3.90	0.2067	636.5	38.6	3029.7
		108	388800	3.96	0.1991	602.8	36.9	2895.4
		204	734400	3.89	0.1883	581.5	35.8	2810.3
		324	1166400	4.00	0.2010	603.7	36.9	2898.6
		348	1252800	4.87	0.2436	600.1	36.7	2884.4
		528	1900800	3.84	0.1823	569.4	35.2	2762.1
Nordic HA	100℃	0	0	4.04	0.2121	629.7	38.2	3002.5
		24	86400	4.08	0.1793	527.5	33.1	2594.6
		72	259200	4.01	0.1818	544.5	34.0	2662.6
		96	345600	3.73	0.1823	586.8	36.1	2831.5
		144	518400	3.57	0.1597	536.3	33.6	2629.7
		282	1015200	3.22	0.1515	564.2	34.9	2741.1
		552	1987200	3.62	0.1398	463.8	29.9	2340.6
Nordic HA	120℃	0	0	4.11	0.2213	645.5	39.0	3065.5
		12	43200	3.99	0.1959	588.9	36.2	2839.5
		24	86400	3.72	0.1818	586.4	36.1	2829.7
		48	172800	3.47	0.1590	550.4	34.3	2686.2
		72	259200	3.43	0.1524	533.9	33.4	2620.3
		90	324000	2.88	0.1474	614.6	37.5	2942.4
		108	388800	2.83	0.1253	531.8	33.3	2612.0
		114	410400	3.14	0.1597	609.5	37.2	2922.1
		210	756000	2.29	0.0935	489.1	31.2	2441.5
		330	1188000	1.96	0.0688	421.3	27.8	2171.2
* Nordic HA	140℃	0	0	4.07	0.2048	603.6	36.9	2898.5
		6	21600	3.51	0.1692	578.2	35.6	2796.9
		12	43200	4.11	0.1703	497.3	31.6	2474.3
*		24	86400	3.18	0.1326	500.0	31.7	2485.0
		30	108000	2.72	0.1034	456.8	29.6	2312.5
		36	129600	3.23	0.1155	429.6	28.2	2204.2
		42	151200	2.51	0.0933	445.4	29.0	2267.3
		48	172800	2.32	0.0794	411.0	27.3	2129.7
		54	194400	2.41	0.0823	409.7	27.2	2124.8
Nordic HA	160℃	0	0	3.92	0.2083	638.6	38.7	3038.0
		3	10800	4.20	0.1828	522.2	32.9	2573.7
		6	21600	3.65	0.1545	507.7	32.1	2515.6
		9	32400	2.89	0.1003	416.6	27.6	2152.2
		12	43200	2.82	0.0801	341.1	23.8	1850.8
		15	54000	2.43	0.0635	312.9	22.4	1738.3
		18	64800	2.27	0.0543	286.6	21.1	1633.7
		21	75600	2.25	0.0516	275.7	20.5	1589.9
		24	86400	3.00	0.0663	265.0	20.0	1547.2
Nordic HA	180℃	0	0	3.94	0.2180	663.3	39.9	3136.7
		1.5	5400	2.96	0.1348	545.9	34.0	2668.2
		3	10800	2.83	0.0899	382.0	25.8	2014.0
		4.5	16200	2.15	0.0594	332.2	23.3	1815.3
		6	21600	2.12	0.0556	314.2	22.4	1743.6
		7.5	27000	1.95	0.0447	274.9	20.5	1586.8
		9	32400	2.58	0.0495	230.1	18.2	1407.9
		12	43200	2.70	0.0463	205.5	17.0	1309.9
		15	54000	2.41	0.0459	229.2	18.2	1404.6
		18	64800	2.70	0.0420	186.4	16.1	1233.5

REFERENCE

Abbt-Braun G., Lankes U. and Frimmel F. H. (2004) Structural characterization of aquatic humic substances – The need for a multiple method approach, *Aquatic Science*, **66**, 151–170

Buffile J., Deladoey P., Xumstein J. and Haerdi W. (1982) Analysis and characterization natural organic matters in freshwaters I. Study of analytical tequniques. *Schwei. Z. Hydrol.* **44/2**, 325-362

Chin Y., Aiken G., O'Loughlin E. (1994) Molecular weight, polydispersIty, and Spectroscopic properties of aquatic humic substances. *Environmental Science Technology*, **28**, 1853-1858

Davidson E. A. and Janssens I. A. (2006) Temperature sensitivity of soil carbon decomposition and feedbacks to climate change. *Nature*, **440**, 165-173

Malcolm R. L. (1990) Variations between humic substances isolated from soils, stream waters, and groundwaters as revealed by 13CNMR spectroscopy. In *Humic substances in soil and crop sciences; selected Readings*, (eds P. MacCarthy, C. E. Clapp, R. L. Malcolm, P. R. Bloom) pp. 13-35. Madison, Wisconsin: American Society of Agronomy and Soil Science Society of America,

Garven G. and Raffenspeger J. P. (1997) Hydrogeology and geochemistry of Ore Genesis in sedimentary Basins, In *Geochemistry of hydrothermal ore deposits*, 3rd ed. (ed. Barnes H. L.) pp. 125-189, New York: John Wiley & Sons

Keppler F., Eiden R., Niedan V., Pracht J. and Schöler H. F. (2000) Halocarbon produced by natural oxidation processes during degradation of organic matter, *Nature*, **403**, 298-301

Kodera Y. and McCoy B. J. (2003) Distribution kinetics of plastic decomposition, *Journal of the Japan Petroleum Institute*, **46**, 155-165

Larson R. A. and Weber E. J. (1994) *Reaction mechanisms in environmental organic chemistry*, pp. 433, Boca Raton: Lewis publishers

3.3. The decarboxylation of dissolved humic substances under hydrothermal conditions

3.3.1. INTRODUCTION

Hydrothermal environments exist often around volcanic activities and provide some hot springs at the earth's surface (Fig.3.1.1) Typical temperatures for hydrothermal solutions and hot springs waters are 200-100°C and 90-30°C, respectively (Garven and Raffenspeger, 1997). Under these hydrothermal conditions, DOM might be decomposed with possible formation of low molecular weight compounds that are volatile. In order to investigate the behavior of dissolved organic matter under hydrothermal conditions, I have conducted hydrothermal heating experiments of dissolved humic substances, representative DOM in the natural environment. We have paid particular attention to their functional groups playing key roles of geochemical processes. Volatile compounds formed during these processes have also been studied.

Thermal transformation of fulvic acid contains several reaction processes such as oxidation, reduction, hydrolysis, demethoxylation and decarboxylation. Absorbance at 254 nm (Abs_{254}) decrease is mainly derived from ring opening reaction. However, the initial decrease was too fast to be understood by aromaticity decrease.

Several possible reaction mechanisms can be considered. Since carboxyl groups are the most dominant substituents of aromatic rings, and the removal of carboxylic groups from aromatic ring can be correlated with the Abs_{254} decrease, the decarboxylation reaction is the most probable candidate reaction. Decarboxylation could occur via three major pathways: anionic (reaction 1), cationic (reaction 2) and free radical (reaction 3) (Artok and Schobert, 2000; Britt et al. 1999).

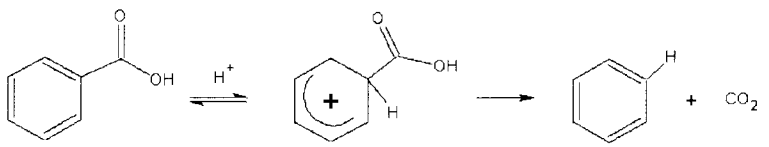

(1)

$$RCOO^- \rightarrow R^- + CO_2 \qquad (2)$$

$$RCOO^- \rightarrow R\cdot + CO_2 + e^- \qquad (3)$$

The aim of this study is to clarify a contribution of decarboxylation reaction to the thermal transformation processes of humic substances. To achieve these objectives, the changes in functional groups of dissolved humic substances are observed by using UV-VIS spectroscopy and compared to CO_2 emission monitored by gas cell FT-IR. In

order to study the rapid changes in the 254 nm absorbance, in situ UV-VIS experiments were conducted. Finally, we discuss time-scales of degradation of humic substance by using obtained kinetic data.

3.3.2. EXPERIMENTAL

3.3.2.1. Sample preparation

One of standard fulvic acids, Nordic aquatic fulvic acid powder, was obtained from the International Humic Substances Society (IHSS). Their elemental composition is C:52.3, H:4.0, O:45.1, N:0.7 weight percents. The functional group contents are: COOH 11.2 mmol gC^{-1} (13.4wt% of the carbon is in the form of COOH) and OH 3.2 mmol gC^{-1} (Ritchie and Perdue, 2003). The stock solutions of 500 mg/L Nordic fulvic acid were prepared with pure water. pHs of these solutions were adjusted to 4 using 0.01 M HCl and 0.01 M NaOH solutions.

3.3.2.2. Continuous analysis of volatiles from heating of the fulvic acid by gas cell FT-IR

A steel-lined PTFE (Teflon) reaction vessel was connected to a long path gas cell (10 m path length) placed in a Fourier transform infrared spectrometer (FT-IR)(Bomem MB154) (Fig. 2.1.4). Reflecting IR mirrors are set at the both ends of the 25 cm long cell to obtain 40 times reflection, yielding totally 10 m optical path length. A 20 mL plastic syringe is used for introducing sample solutions and for sampling products (Fig.2.1.4). A vacuum pump and a N_2 gas bombe (99.9999% purity) are connected to the lines to obtain non-oxidizing atmosphere throughout the whole system.

30 mL of 100 mg/L fulvic acid solution were set in the above hydrothermal reaction system purged by ~99.9999% nitrogen atmosphere. Hydrothermal experiments were conducted at 25, 50 and 80 °C for 25 hours. The product gaseous compounds were collected at 0.5, 1 2, 3, 4, 5, 6, 7, 8, 9, 10, 12, 24 hours. Gaseous products during the hydrothermal reactions were introduced by the nitrogen gas to the long path gas cell FT-IR to measure their IR spectra.

3.3.2.3. In situ UV monitoring of hydrothermal experiments

A commercial high temperature cell (HARRICK Scientific Corp., Temperature controlled demountable liquid cell) modified by Masuda (2005) was used for in-situ UV monitoring (Masuda, 2005; Fig. 3.3.1). Calcium fluoride (CaF_2) optical windows of 2 mm thick and 13 mm in diameter are compressed by a piston and a cylinder through Kalrez® O-rings. A Teflon® gasket of 0.5 mm thick and 8 mm inner diameter was sandwiched between these windows to generate 25 μl sample chamber.

Sample solutions were heated at 25, 80, 120, 140, 160 and 180 °C for 24 hours

using a heatable liquid cell set in an UV-VIS spectrophotometer (Jasco V-530). The experiment at 100 °C for 5 hours was also conducted. Sample solution at room temperature (25 °C) was also analyzed for a blank measurement. About 40 μL of 500 mg/L fulvic acid solution was injected in the sample chamber by a micro syringe. UV spectra in the static hydrothermal cell have been measured every 2 minutes at a scanning speed of 1000 nm/min with the resolution of 0.5 nm in the 200-800 nm spectral range.

3.3.2.4. FT-IR analysis

FT-IR spectra were recorded by Fourier transform infrared spectrometer (FT-IR) equipped with a mercury cadmium telluride (MCT) detector (Jasco, FTIR-620 with IRT-30). The solution samples were dried on the CaF_2 crystal (thickness of CaF_2 is 1mm). The residue on the CaF_2 plate was measured with a 100 × 100 μm aperture. One hundred interferograms at 4 cm^{-1} resolution were co-added to produce a single spectrum from 700 to 4000 cm^{-1}.

3.3.3. RESULTS

3.3.3.1. Decrease rates of 254nm absorbance of the fulvic acid solution

Sample solutions were heated at 80 °C for 24 hours, 100 °C for 5 hours, 120, 140, 160 and 180 °C for 24 hours. The yellowish brown starting solution became gradually colorless with time. A representative in-situ UV-VIS spectra are shown in Fig. 3.3.2. The spectral changes were successfully measured by the in-situ UV/VIS apparatus.

The absorption intensity (absorbance) at 254 nm of the fulvic acid solution due to π-π^* electron transition originated from substituted aromatic structures is commonly used as a measure of dissolved organic matter contents (Korshin et al, 1997). Therefore, the 254 nm absorbance values of the product solutions were plotted against time in Figure 3.3.3. The continuous changes in absorbance at 254 nm (Abs_{254}) at 25 °C, 80 °C, 100 °C, 120 °C, 140 °C, 160 °C, 180 °C are illustrated in Fig. 3.3.3, where the absorbance is normalized to the Abs_{254} value at the beginning. Discontinuities of data originated from the freezing of the interval measuring software program.

The in situ data for the 254 nm absorbance showed a slow decrease at 80 °C, 100 °C, 120 °C and 140 °C in good agreement with the batch data conducted at the same temperature conditions (Fig. 3.3.3 a, b, c, d). On the other hand, the changes in 254 nm absorbance of in situ data at 160 and 180 °C are much slower than those of batch data (Fig. 3.3.3 e, f). This difference might be due to bubble formation and different reaction conditions such as oxygen concentration. The in situ data at 25 °C did not show significant difference from that of the initial Nordic fulvic acid solution during 24 hour (Fig. 3.3.3 g).

Two individual steps (namely I and II) can be recognized. In the first stage (I), the absorbance at 254 nm decreases quasi-exponentially (Fig. 3.3.4). In the second stage (II), the Abs_{254} decrease becomes slower. The boundary between these two steps is defined as the first 10% decrease of Abs_{254} and/or until 10 hours.

3.3.3.2. Formation rates of CO_2 from the fulvic acid solution

Gaseous products during the batch hydrothermal experiments analyzed by gas cell FT-IR spectroscopy indicated only CO_2 as recognizable species. Carbon monoxide and other incomplete combustion gases were not detected.

The cumulative amount of formed CO_2 gradually increased with time (Fig. 3.3.5). This amount of CO_2 formed during 24 hour is only about 3%, 5%, 11%, 12%, 23% and 33% of the initial carboxyl content at 25°C, 50°C, 80°C, 100°C, 120°C and 140°C, respectively.

3.3.3.3. The FT-IR spectra

The FT-IR spectra at the initial stage decrease (at 180°C for 0 and 1.5 hour) are obtained as shown in Fig. 3.3.6. Two absorption bands existed near 1710 and 1600 cm^{-1} for C=O and C=C stretching vibrations, respectively. The 1400 cm^{-1} band was OH deformation and C-O stretching of phenolic OH and/or COO^- asymmetric stretching vibration. The 1455 and 1356 cm^{-1} bands were due to CH bending vibration. The broad band occurred in the 1000 – 1200 cm^{-1} for C-O stretching vibration.

3.3.4. DISCUSSION

3.3.4.1. Decrease rates of 254nm absorbance of the fulvic acid solution

The first stage I decrease rates of Abs_{254} can be simulated by the first order kinetics by using the following integrated rate equation:

$$\ln[a]_{t\,uv} = \ln[a]_0 - k^{UV} t \qquad (4)$$

, where a is the normalize absorbance at 254 nm and k^{uv} is the rate constant of Abs_{254} decrease. The initial decrease of 254 nm absorbance of the fulvic acid can be used to determine the first order reaction rate constants by fitting the data of the first 10% decrease of Abs_{254} and/or until 10 hours with linear trends (Fig.3.3.4a). The first order decrease rate of Abs_{254} were then $k^{uv} = 1.6 \times 10^{-7}$ s^{-1} at 25°C, 1.0×10^{-6} s^{-1} at 80°C, 1.4×10^{-6} s^{-1} at 100°C, 2.4×10^{-6} s^{-1} at 120°C, 5.0×10^{-6} s^{-1} at 140°C, 9.0×10^{-6} s^{-1} at 160°C, 4.5×10^{-5} s^{-1} at 180°C.

The effect of the temperature on the rate constants can be described the Arrhenius equation:

$$\ln k^{UV} = \ln A - \frac{E_a}{RT} \qquad (5)$$

, where Ea is the activation energy, R is the gas constant (8.31 J K^{-1}), T is the absolute temperature, and A is the frequency factor. By introducing the obtained rate constants to this equation, the activation energy for the Abs_{254} decrease is determined to be 29 kJ mol^{-1} (Fig.3.3.7).

3.3.4.2. Formation rates of CO_2 from the fulvic acid solution

By assuming that the maximum CO_2 formation is limited by the initial carboxylic content of the fulvic acid: $C_0 = 1.75 \times 10^{-5}$ mol for 3 mg fulvic acid, the CO_2 formation rate can be simulated by the first order kinetics by using this C_0 value (Fig.3.3.5): [$C = C_0$ (1- exp (k_0^{CO2} t))]. The first order CO_2 formation rates were then $k_0^{CO2} = 3.2 \times 10^{-7}$ s^{-1} at 25°C, 6.1×10^{-7} s^{-1} at 50°C, 1.2×10^{-6} s^{-1} at 80°C, 1.8×10^{-6} s^{-1} at 100°C, 2.4×10^{-6} s^{-1} at 120°C, 3.7×10^{-6} s^{-1} at 140°C. By using obtained rate constants to the Arrhenius equations, the activation energy of the CO_2 formation is calculated to be 22 kJ mol^{-1} (Fig.3.2.7). The first order CO_2 formation rate from the fulvic acid is on the same order as the above initial first order rate of the decrease in 254 nm absorbance. This indicates that CO_2 formation mechanism might be related to the decrease of 254 nm absorbance of the fulvic acid.

3.3.4.3. Reaction mechanisms

In aqueous solutions, ionic decarboxylation is often catalyzed by acid and base. The cationic mechanism needs a proton attack by strong acids. The present experiment was conducted at weak acidic conditions. So, the cationic mechanism can be ignored. Therefore, the decarboxylation reaction of the fulvic acid in aqueous solution can be considered as the anionic decarboxylation:
, or radical decarboxylation

$$RCOO^- \rightarrow R^- + CO_2 \qquad (3)$$

$$RCOO^- \rightarrow R\cdot + CO_2 + e^- \qquad (3)$$

In addition, dissolved CO_2 is assumed to be in equilibrium with hydrogen carbonate ions (HCO_3^-).
This equilibrium is greatly affected by the pH conditions of these experiments, which were acidic at all the reaction time (at 25°C). The major proportion of carbon dioxide is

$$CO_2 + OH^- \Leftrightarrow HCO_3^- \quad (6)$$

in the form of CO_2 at pH 4.

3.3.4.4. Reaction kinetics

The anionic decarboxylation reaction via a carbanion transition state has been described for gallic acid (Boles et al., 1988), and is thought to proceed as follows:

$$ArCOO^- \rightarrow Ar^- + CO_2 \qquad \text{(slow process)}$$

$$Ar^- + H_2O \rightarrow Ar\text{-}H + OH^- \qquad \text{(fast process)}$$

The rate determination step of anionic decarboxylation is cleavage of C-C bond of carboxylate (equation 4). In agreement with earlier works by Boles et al. (1988) and Li and Brill (2003), the decarboxylation reaction follows the first order reaction.

If the reaction is the first order, the reaction rate equation is given in the form of:

$$\frac{d[ArCOO^-]}{dt} = -k\,[ArCOO^-]$$

The integrated form of this equation gives:

$$\ln[ArCOO^-] = \ln[ArCOO^-]_0 - kt$$

Therefore, if natural logarithm of measured concentration of $ArCOO^-$ plotted against time show a linear decrease, the reaction can be considered to be the first order and gradients of the regression lines gives the reaction constants.

Nordic fulvic acid has abundant acidic functional groups, which are mainly originated from absorbance at 254 nm. The relationship between the initial decrease of absorbance at 254 nm and the formation of carbon dioxide can be understood by the above decarboxylation reaction. Although π-π^* transition of Nordic fulvic acid are highly conjugated, initial decrease of absorbance at 254 nm was considered to be due to decarboxylation from carboxyls substituted to aromatic ring.

The rate constant data were plotted in an Arrhenius diagram, which gave an apparent activation energy value of 29 and 22 kJ/mol (Fig. 3.3.7). Activation energy values for decarboxylation reactions of organic acids are generally in the 80~120 kJ/mol range (Brill, 2000; Li and Brill, 2003). Empirically, it is around 90 ±5 kJ/mol for anionic decarboxylation of OH substituted benzoic acid. On the other hand activation energy values for radical mechanism decarboxylation reaction of organic acid are generally in the 30-40 kJ/mol range (Chateauneuf et al., 1988). The low apparent activation energies (29 and 22 kJ/mol) might have similar values to these. Although previous radical reactions are rapid, the reaction rates depends on the stability of R·

radical produced. The rate can differ several orders of magnitude according to the stability.

In addition, a similar reaction has been observed at coal liquefaction reaction (Artok and Schobert, 2000). The mechanisms of decarboxylation are very simple, however, are dependent on the chemical structure of the reactants and reaction conditions. Therefore, the initial decomposition reaction determined by Abs_{254} decrease and CO_2 gas emission analysis can be attributed mainly to the decarboxylation reaction.

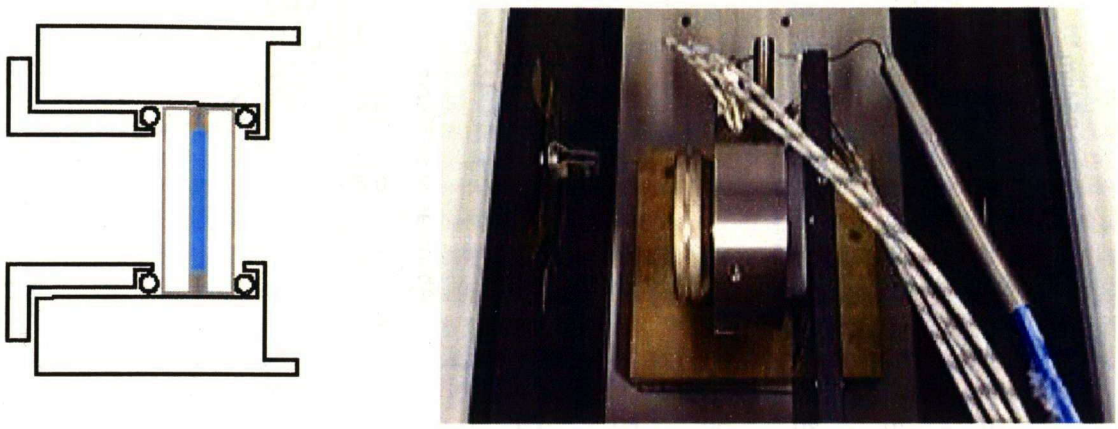

Fig. 3.3.1. The in-situ UV spectroscopy (A) The schematic configuration of the heatable liquid cell, and (B) the photograph,

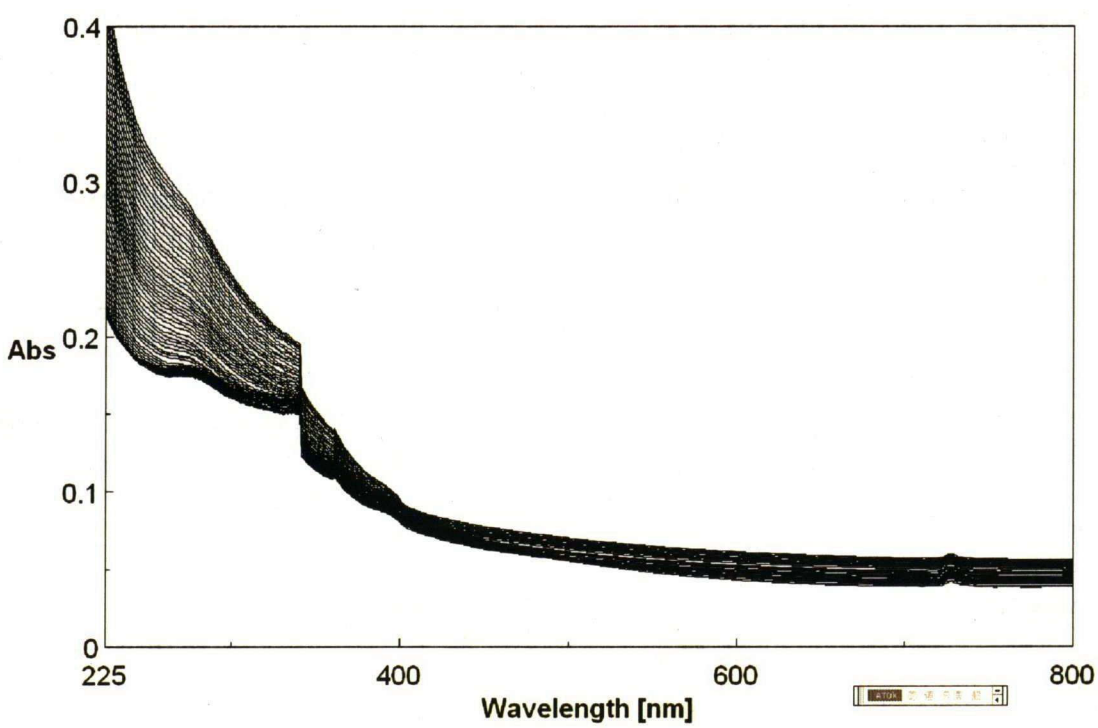

Fig. 3.3.2. The *in-situ* UV-VIS spectra of Nordic fulvic acid heated at 120C for 24 hour.

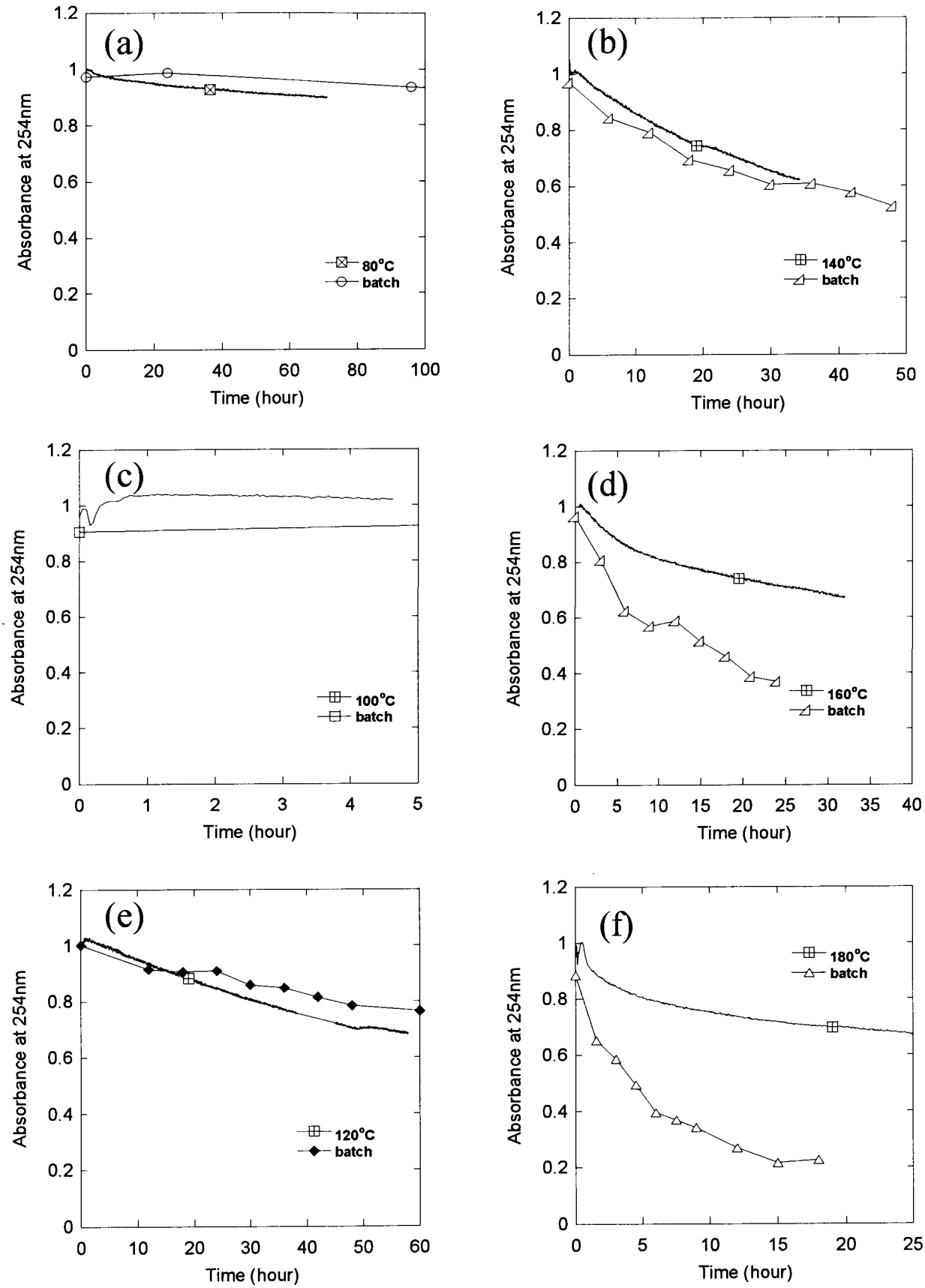

Figure . 3.3.3. The temporal changes in 254 nm absorbances of Nordic fulvic acid solution both by in-situ and batch experiment at (a) 80° C for 70 hour, (b) 100° C for 5 hour, (c) 120° C for 60 hour, (d) 140° C for 50 hour, (a) 160° C for 40 hour and (e) 180° C for 25 hour.

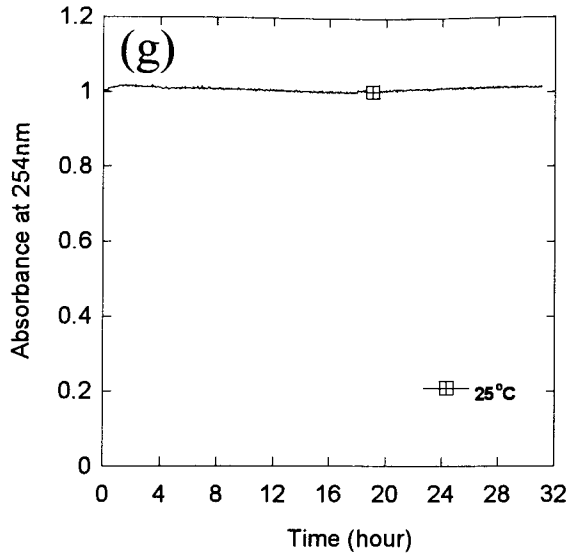

Fig. 3.3.3. The temporal changes in 254 nm absorbances of Nordic fulvic acid solution both by in-situ and batch experiment at (g) 25° C for 30 hour

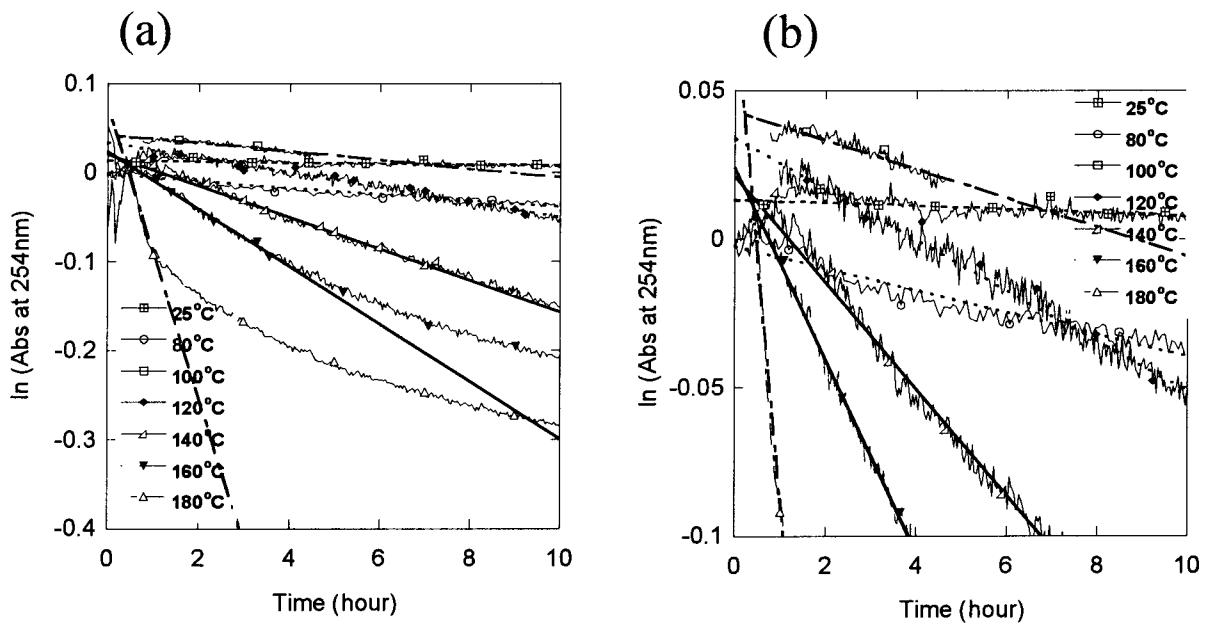

Fig. 3.3.4. The temporal changes in 254 nm absorbances of Nordic fulvic acid solution heated at 80-180° C during initial stage (a) ranged from -0.4 to 0.1 and (b) from -0.1 to 0.05 for natural logarithm of absorbance at 254 mn.

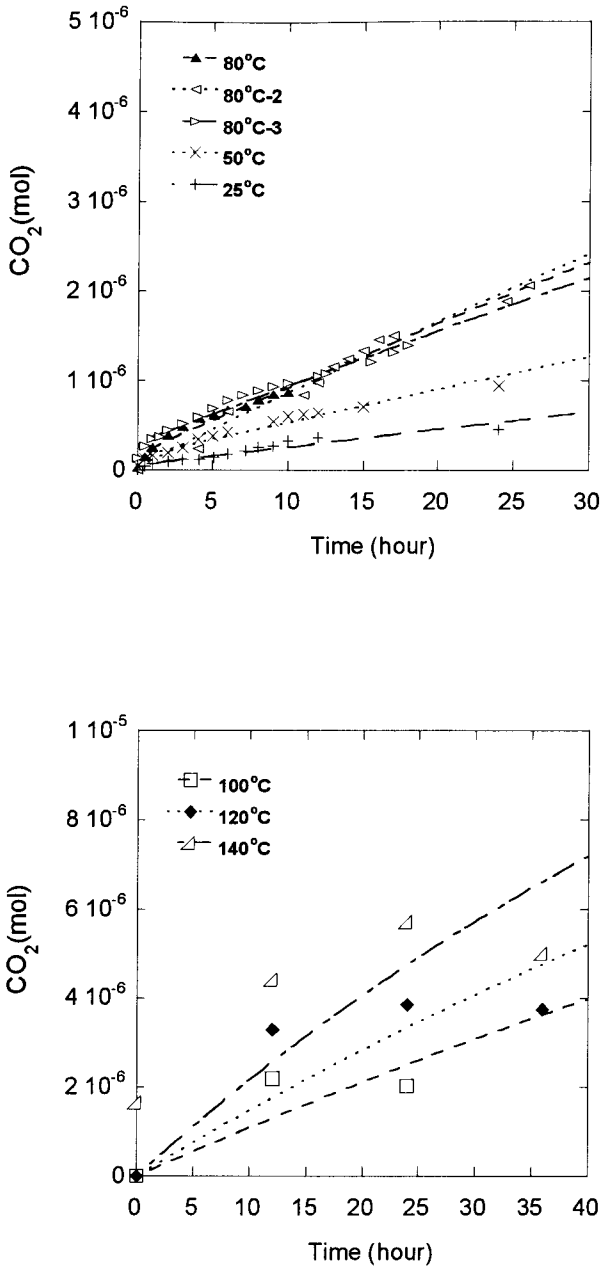

Fig. 3.3.5. Temporal changes in CO_2 formation at (a) 25 - 80 ° C and (b) 100 - 140 ° C

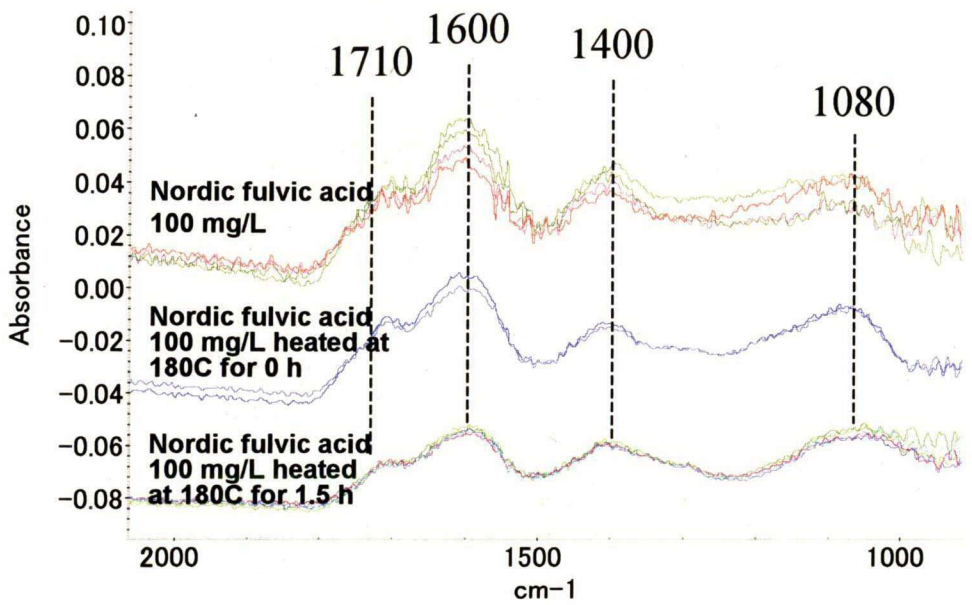

Fig. 3.3.6. FT-IR spectra of heated Nordic fulvic acid (100mg/L) at 180° C for 0, 1.5 hours and no heat fulvic acid (100mg/L).

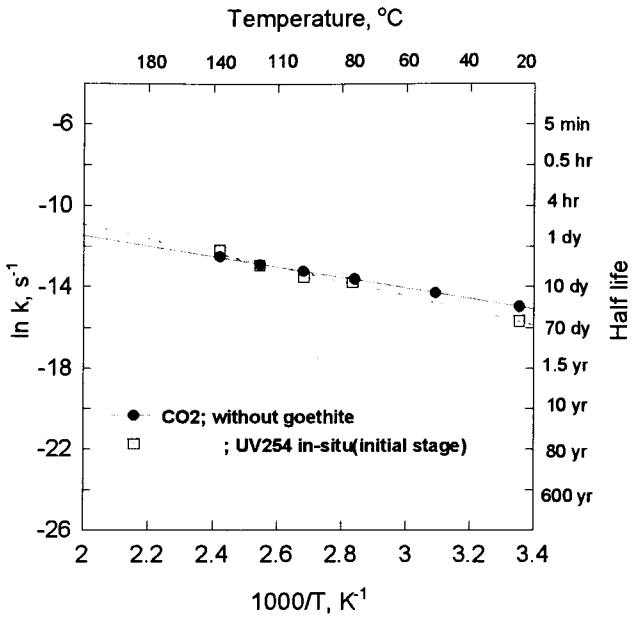

Fig. 3.3.7. The Arrhenius diagram of the initial decrease of absorbance at 254 nm and CO_2 formation

REFERENCES

Artok L. and Schobert H. H. (2000) Reaction of carboxylic acid under coal liquefaction conditions 1. Under nitrogen atmosphere. *Journal of Analytical and Applied Pyrolysis,* **54**, 215-233

Britt P. F., Buchanan III A. C., Eskay T. P. and Mungall W. S. (1999) Mechanistic investigation into the decarboxylation of aromatic carboxylic acids. *Invited Paper for presentation at the American Chemical society National Meeting, New Orleans, LA,*

Boles J. S., Crerar D. A., Grissom G. and Key T. C. (1988) Aqueous thermal degradation of galic acid, *Geochimica et Cosmochimca acta*, **52**, 341-344

Chateauneuf J., Lusztyk J. and Ingold K. U. (1988) Spectroscopic kinetic characteristics of aroyloxyl radicals. 1. The 4-methoxylbenzoyloxyl radical. *Journal of American Chemical Society*, **54**, 2877-2885

Garven G. and Raffenspeger J. P. (1997) Hydrogeology and geochemistry of Ore Genesis in sedimentary Basins, In *Geochemistry of hydrothermal ore deposits*, 3rd ed. (ed. Barnes H. L.) pp. 125-189, New York: John Wiley & Sons

Kawamura and Kaplan (1987) Dicarboxylic acids generated by thermal alternation of kerogen and humic acid, *Geochimica et Cosmochimica Acta*, **51**, 3201-3207

Li J. Brill T. B. (2003) Spectroscopy of hydrothermal reaction 23: the effect of OH substituent on the rates and mechanism of decarboxylation of benzoic acid, *Journal of Physical Chemistry A*, **107**, 2667-2673

Ritchie J. D. and Perdue E. M. (2003) Proton binding study of standard and reference fulvic acid and humic acid, and natural organic matter ,*Geochimica et Cosmochimica Acta*, **67**, 85-96

CHAPTER 4.

Hydrothermal interaction of fulvic acid and goethite

Chapter 4

4.1. Adsorption of fulvic acid on the surface of goethite in hydrothermal condition

4.2. The formation of CO_2 by fulvic acid on the surface of goethite studied using ultraviolet and infrared spectroscopy

4.3. Transformation of fulvic acid and goethite in hydrothermal condition

INTRODUCTION

Common dissolved organic compounds in the environment such as fulvic acids generally co-exist with iron oxides in natural environments (Maranger and Pullin, 2003). Minerals are known to be effective in the adsorption of humic substances and many adsorption studies have been engaged previously (Gu et al, 1994; Filius et al, 2000; Zhou et al, 2001). In this context, minerals and dissolved organics in water have been examined in complex forming reaction, colloid formation and organic induced mineral dissolution. Biodegradation reaction mechanisms of humic substances may change greatly depending on the regional variety of microbes.

The interactions between humic substances and minerals are primarily determined by their active functional groups. Although functional group analyses of humic substances have been often conducted their changes with temperature and time are mostly unknown. If humic substances loose their reactive functional groups (OH, COOH) with decomposition of their chemical structure, their reactivity with surrounding materials can be decreased greatly. Therefore, the investigation of transformation of functional groups in geochemical environments is necessary.

In this Chapter 4, I will first study the adsorption of the fulvic acid on the surface of goethite. Secondly, the formation of CO_2 by the fulvic acid on the goethite surface are studied by means of UV-VIS spectroscopy and IR spectroscopy. Thirdly the transformation of the fulvic acid and goethite is investigated under hydrothermal conditions.

REFERENCES

Filius J. D., Lumsdon D. G., Meeussen J. C. L., Hiemstra T. and van Riemsduk W. H. (2000). Adsorption of fulvic acid on goethite. *Geochimica et Cosmochimica Acta*, **64**, 51-60.

Gu B., Schmitt J., Chen Z., Liang L. and McCathy J. F. (1994) Adsorption and Desorption of natural organic matter on iron oxide: mechanisms and models. *Environmental Science and Technology*, 28, 38-46.

Maranger R. and Pullin M. J. (2003) Elemental complexation by dissolved organic matter in lakes: Implications for Fe speciation and the bioavailability of Fe and P, In *Aquatic ecosystems interactivity of dissolved organic matter*, (eds. Findlay S. E. G. and Sinsabaugh R. L.) pp.186-214, Sun Diego, London: Academic press

Zhou Q. Maurice P. A. and Cabaniss S. E. (2001) Size fractionation upon adsorption of fulvic acid on goethite: equilibrium and kinetic studies, *Geochimica et Cosmochimica Acta*, **65**, 803-812.

4.1. Adsorption of fulvic acid on the surface of goethite under hydrothermal conditions

4.1.1. INTRODUCTION

Common dissolved organic compounds in the environment such as fulvic acids have been reported to be adsorbed on oxide minerals such as goethite (Gu et al, 1994; Filius et al, 2000; Zhou et al, 2001, Table 4.1.1). On the other hand, ferric iron in the iron hydroxides are often found to be reduced to ferrous iron in the presence of organic matter (LaKind and Stone, 1989; Chorover and Amistadi, 2001; Pullin and Cabaniss, 2003).

Interaction experiments between a representative dissolved organic compound, a fulvic acid, and a representative iron hydroxides, goethite, have been conducted in this study. The interaction experiments were conducted at 80 °C to accelerate the reactions. The adsorbed fulvic acid on the surface of goethite were monitored by ultraviolet-visible spectroscopy by means of absorption intensity at 254 nm, which is commonly used as a measure of dissolved organic carbon content (Korshin et al., 1997). To observe fast adsorption process, two type of in-situ observation were employed here to quantify the decrease of fulvic acid in solution by using UV-VIS spectroscopy and to quantify adsorbed fulvic acid onto goethite by using ATR-IR spectroscopy. By using these spectroscopic methods, adsorption kinetics of the fulvic acid on goethite have been investigated.

4.1.2. EXPERIMENTAL

4.1.2.1. Goethite and fulvic acid solution

Goethite samples were prepared after Schwertmann and Cornell (2000). Iron hydroxides were precipitated in a polyethylene vessel by adding 180 mL of 5 M potassium hydroxide to 100 mL of 0.1 M $Fe(NO_3)_3$ solution. The suspension was immediately diluted to 2 L with pure water (MilliQ-UV) and incubated at 70 °C for 60 hours. Yellowish brown precipitates were centrifuged and washed (Fig.4.1.1a). These products were identified to be goethite by X-ray diffraction and FT-IR spectroscopy (Nagano et al., 1992). Surface area of goethite is 29.2 $m^2\ g^{-1}$ by BET analysis. Particle size is mainly distributed in the 0.5-5 μm range by particle size distribution analysis and laser scanning confocal microscopy (LSCM) (Fig.4.1.1b). Synthesized goethite is mainly by {101} faces (Fig.4.1.1d; Schwertmann and Cornell, 2002).

One of standard fulvic acids, Nordic aquatic fulvic acid powder, was obtained from the International Humic Substances Society (IHSS). Their elemental composition is C:52.3, H:4.0, O:45.1, N:0.7 weight percents. The functional group

contents are: COOH 11.2 mmol gC^{-1} (13.4wt% of the carbon is in the form of COOH) and OH 3.2 mmol gC^{-1} (Ritchie and Perdue, 2003). The stock solutions of 200 and 500 mg/L Nordic fulvic acid were prepared with pure water. pHs of these solutions were adjusted to 4 using 0.01 M HCl and 0.01 M NaOH solutions.

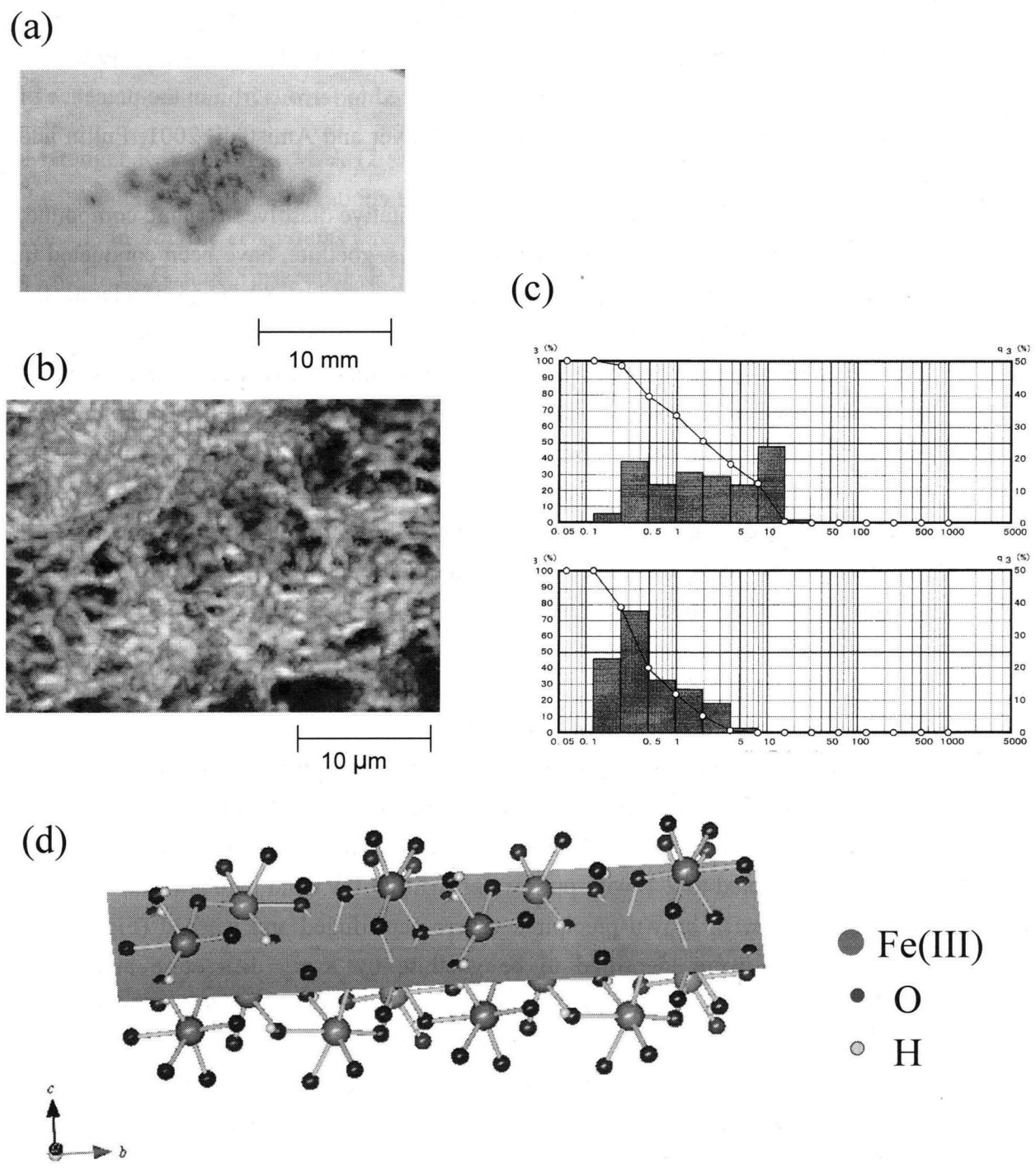

Fig.4.1.1. The synthesized goethite; (A) Its photograph; (B) Laser Scanning Confocal Microscope (LSCM) image of goethite; (C) size distribution by of particle distribution analysis of goethite; (D) atomic geometry by a drawing software BICS-II

4.1.2.2. Batch Adsorption experiments

Adsorption experiments were conduced at pH 4.0 in polycarbonate centrifuge tubes at 22 °C with 1 g L^{-1} of goethite. The goethite suspension were prepared by adding 20 mg of goethite powder to 10 mL of pure water and adjusting pH to 4.0 by using NaOH and HCl. The stock solutions of Nordic fulvic acid (20 mg L^{-1} and 200 mg L^{-1}) are prepared by adding freeze-dried powder into pure water and by adjusting pH to 4.0. Adsorption experiments were conducted by adding 10 mL of fulvic acid stock solution into the goethite suspension. Samples were made up to 20 mL volume with 10 or 100 mg L^{-1} Nordic fulvic acid with 1 g L^{-1} goethite suspension (goethite: fulvic acid ratio were 10:1 and 100:1). The blank samples (without goethite) were prepared at each concentration.

The samples, collected at 15 min, 30 min, 2, 3, 6, 9, and 12 hours of interaction experiments, were centrifuged 15 min at 13500 rpm (Zhou et al., 2001). 15 ml of supernatant were removed and filtered though 0.2 μm cellulose acetate membrane. The concentration of the organic absorbate in the supernatant was determined by absorbance at 254 nm of the compound in the UV-VIS spectra.

4.1.2.3. ATR-IR spectroscopic experiments on fulvic acid-goethite interaction

The IR spectra were collected with an FTIR spectrometer (Jasco, VIR 9500) equipped with a mercury cadmium telluride (MCT) detector. The spectra were recorded with a horizontal ATR cell (Flow Though, Thermostabilised and Injection Top plate, Specac) equipped with trough plate ZnSe crystal (refractive index n_1=2.4) as internal reflection element (IRE) (Fig.2.3.2). One hundred interferograms at 4 cm^{-1} resolution were co-added to produce a single spectrum from 700 to 4000 cm^{-1}. All spectra were recorded in absorbance mode aginst air background to obtain pATR spectra.

In-situ adsorption experiments of fulvic acid on goethite were at conducted at 25°C, 50°C and 80°C at pH 4.0 by means of ATR-IR spectroscopy. The preparation of goethite film on the ZnSe IRE was described in section 2-3. The fulvic acid solution was heated at the designed temperature (20-80°C, in surrounded by a band heater). In order to obtain spectral changes of the sample solution during the heating experiments, successive measurements were conducted by an interval-measurement program (spectral manager, JASCO). The isothermal spectral changes could be traced at an interval of every 120 seconds. For the kinetic treatments, the reaction starting time (t=0) was taken as the time when the fulvic acid solution was introduced in the in-situ cell.

The background air spectrum is measured in the blank cell at room

temperature. After the background measurements, pure water is injected into the ATR cell with a plastic syringe, and the pure water spectrum is measured. This will be subtracted from the following sample spectra to obtain difference spectra of sample solutes. Then, after drying off water by 99.5% of nitrogen gas, the sample organic solution is injected with syringe and the plugs were tightly sealed.

4.1.3. RESULTS

4.1.3.1. Batch adsorption experiment of fulvic acid on goethite

The UV-VIS spectra of supernatant at 25°C for 15 min, 30 min, 2, 3, 6, 9, and 12 hours showed drastic decrease in their absorbances already within 15 minutes. The quantity of adsorbed fulvic acid did not show significant difference in all the reaction time (Fig. 4.1.2). The 60 – 90 % of fulvic acid are absorbed for 10 mg L^{-1} fulvic acid with 1 g L^{-1} goethite suspension and the 20 % of fulvic acid are absorbed for 100 mg L^{-1} fulvic acid with 1 g L^{-1} goethite suspension.

4.1.3.2. *In-situ* measurement of fulvic acid adsorption on the surface of goethite

In-situ observations of the fulvic acid adsorption on the goethite are conducted by using ATR-IR spectroscopy. The infrared absorption spectra were successfully observed and increased in their intensity with time as shown in Fig.4.1.3. IR spectra of Nordic fulvic acid on the goethite film were shown in Fig. 4.1.3. Because Nordic fulvic acid has high carboxyl contents, the IR absorption peaks are due to carboxyl groups at 1720, 1585, 1400 and 1260 cm^{-1}. These peaks are also overlapped with aromatic C=C stretching at 1600 cm^{-1}, aliphatic C-H bending at 1460 and 1370 cm^{-1}, C-O stretching of phenol-OH around at 1400 cm^{-1}, and C-O stretching of ether compounds. However obtained spectra after adsorption to goethite did not show these peaks. The spectral shape of adsorbed fulvic acid did not significantly change from the initial spectrum of fulvic acid (Fig 3.1.10).

The changes in absorption intensity of functional groups are plotted in Fig 4.1.3B. While the peak of COOH at 1720 cm^{-1} appeared to stop increasing their intensity, the peak at 1585 cm^{-1} kept increasing. The carboxyl contents rapidly increase within 1 minute and keep a gradual increase. The observed carboxyl groups are 0.15 mol L^{-1}. This is 150 times of the initial carboxyl groups. This means that concentrated layers of the fulvic acid are produced on the surface of goethite. The measurement ranges of ATR-IR methods depend on penetration depth of evanescent wave.

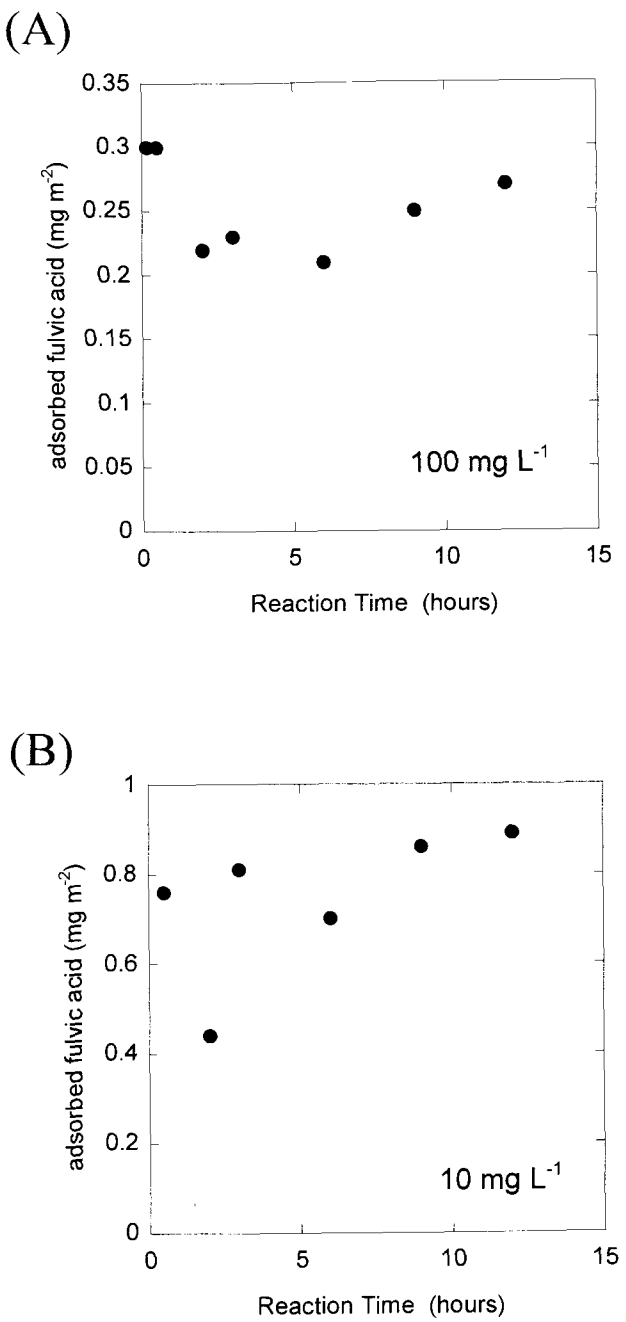

Fig.4.1.2. Changes with time (15 min. to 12 hours) in the adsorbeed Nordic fulvic acid on 20 mg of goethite at 25°C, pH =4. (A) Nordic fulvic acid: 100 mg L^{-1}, (B) Nordic fulvic acid: 10 mg L^{-1}.

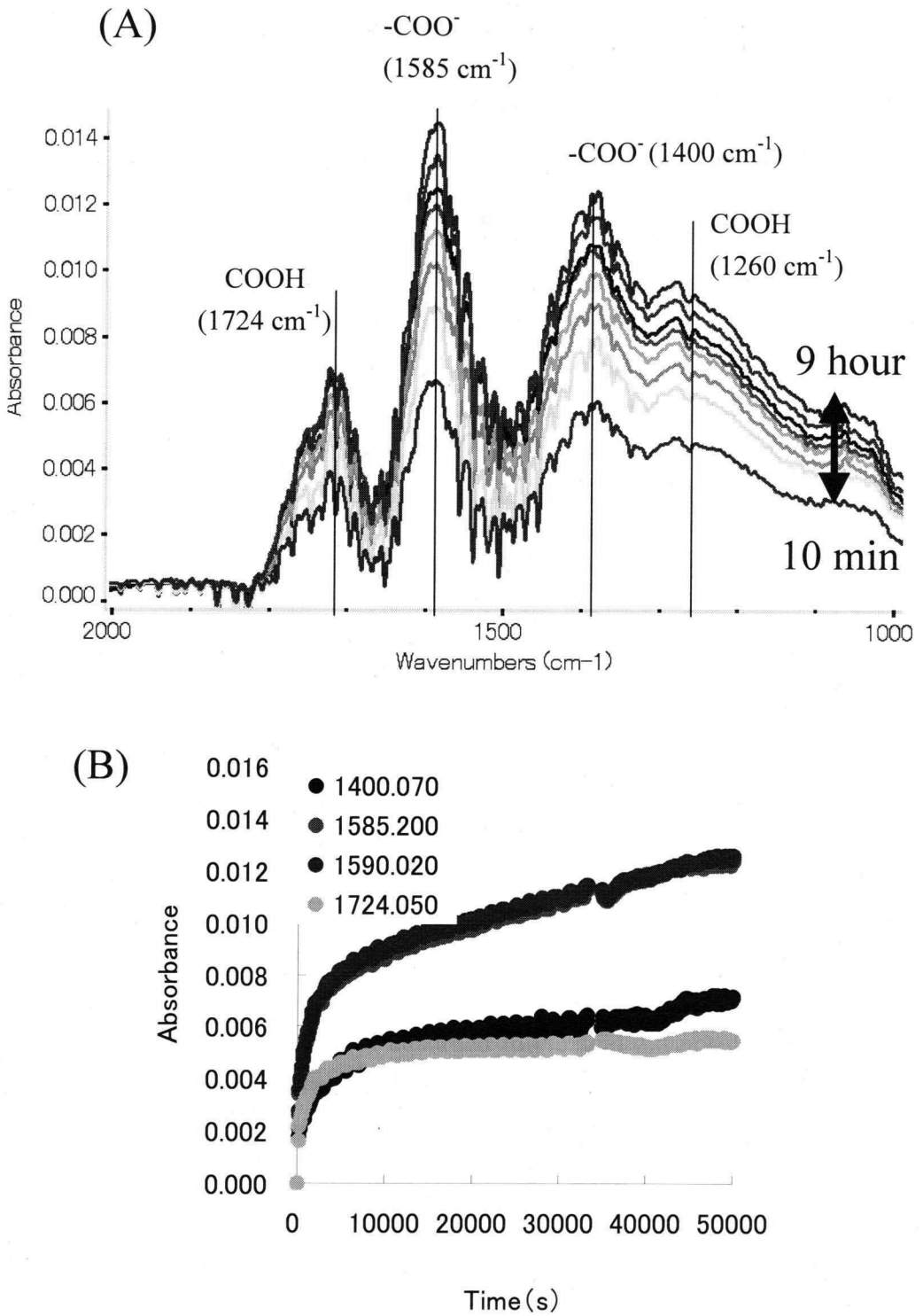

Fig. 4.1.3. The ATR-IR spectral changes with time of Nordic fulvic acid on the goethite at 25°C for 10 min. to 12 hours (A) IR spectra in the 2000- 1000 cm^{-1} range (B) Changes with time of absorption intensities at 1400, 1585, 1590 and 1724 cm^{-1}.

Absorption of the fulvic acid on goethite at pH 4 is mainly due to the interaction between hydroxyl groups on the surface of goethite and carboxyl groups in the fulvic acid. For evaluating the increase of absorbance of the fulvic acid, the carboxyl content on the surface of goethite are quantified by using the relationship described in section 2.3. The sum of absorbance of COOH (1720 cm^{-1}) and COO^- (1600 cm^{-1}) are empirically correlated to carboxyl contents after Celi et al. (1997).

4.1.3.3. Adsorption rates of fulvic acid on the goethite surface

The carboxyls of the fulvic acid on the goethite showed a rapid increase at the initial stage, and then they continued to increase gradually with time (Fig. 4.1.4). Assuming that the fulvic acid was adsorbed by two independent first order reactions [$C = C_1$ (1- exp ($k_1 t$)) + C_2 (1- exp ($k_2 t$))], the first order adsorption rates at 25 °C are obtained by fitting the data until 12 hours by the above equation (Fig.4.1.4.)(k_1 = 1.4×10^{-3} s^{-1}; $k_2 = 1.7 \times 10^{-5}$ s^{-1}; with $C_1 = 9.2 \times 10^{-3}$ and $C_1 = 7.4 \times 10^{-3}$).

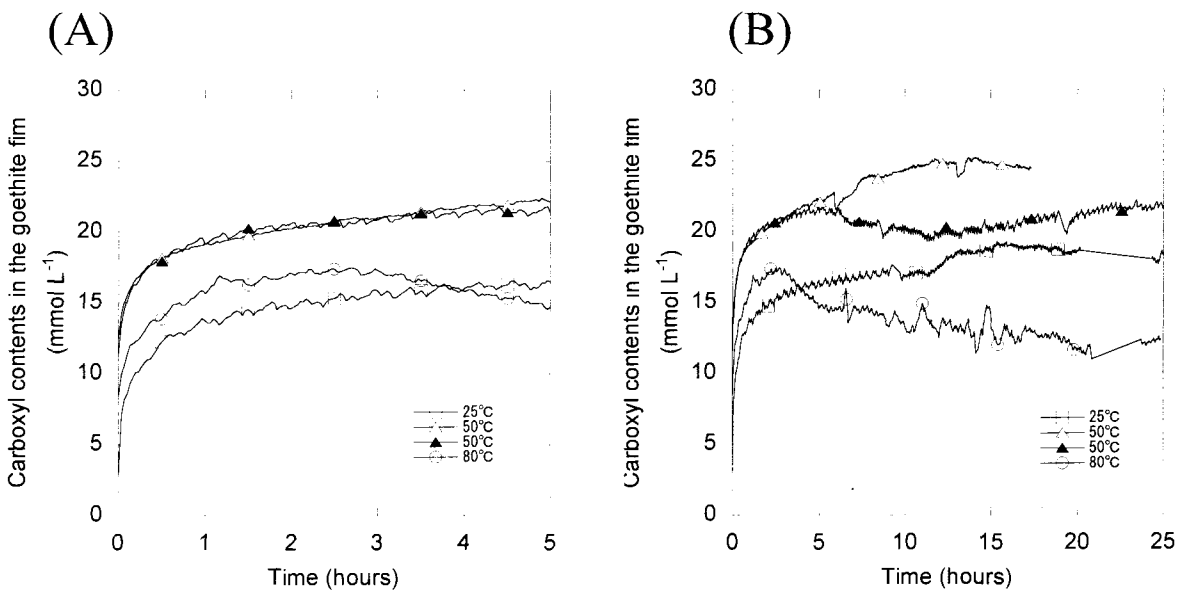

Fig. 4.1.4. Changes with time of carboxyl contents absorbed on the goethite at 25°C, 50°C and 80°C. (A) for 10 min. to 5 hours (B) for 10 min. to 25 hours

4.1.4. DISCUSSION

4.1.4.1. Adsorption quantity of the fulvic acid on the goethite surface

Because the fulvic acid and goethite attract each other with an electric force that depend on negative charges of the fulvic acid derived from carboxyl and hydroxyl groups and positive charges of goethite originated from Fe(III) molecule on the surface of goethite. The quantity of carboxyl groups and phenolic hydroxyl groups are 11.16 mmol gC^{-1} and 3.18 mmol gC^{-1}, respectively (Ritchie and Perdue, 2003). The elemental analysis showed 52.3% of total weight is carbon contents of Nordic fulvic acid. In the case of adsorption experiment, 20 mL of 10 mg L^{-1} fulvic acid contain 0.2 mg of Nordic fulvic acid in each interaction experiment. Therefore, carboxyl and phenolic hydroxyl contents of Nordic fulvic acid are 17.5μmol and 5.0 μmol, respectively. On the other hand, BET analysis showed the surface area of goethite is 29.2 m^2 g^{-1}. By using density of ferric atom, ferric atoms are 5 molecule nm^{-2}:

This estimation shows that the quantity of Fe(III) molecule on the surface of goethite is 3 times more than the sum of carboxyl and hydroxyl groups in the fulvic acid. Because goethite surface are excess supply for absorbing agents, nearly 80% of fulvic acid can be adsorbed on the surface of goethite.

$$\text{quantity of carboxyl group} = 11.16\,\text{mmol}\,gC^{-1} \times 0.523\,gC\,g^{-1} \times 0.20\,\text{mg}$$
$$= 1.2\,\mu\text{mol}$$

$$\text{quantity of phenolic OH} = 3.18\,\text{mmol}\,gC^{-1} \times 0.523\,gC\,g^{-1} \times 0.20\,\text{mg}$$
$$= 0.33\,\mu\text{mol}$$

$$\text{quantity of } Fe^{3+} \text{ on the goethite surface}$$
$$= 29.2\,m^2\,g^{-1} \times 5\,\text{molecule}\,nm^2 \times 20\,\text{mg}$$
$$= 4.9\,\mu\text{mol}$$

4.1.4.2. Adsorption rates of fulvic acid on the goethite surface

Absorbance at 254 nm of the fulvic acid solution rapidly decreased. This is considered to be due to the adsorption on the goethite surface. The result of ATR-IR spectroscopy shows that the rapid initial increase of the fulvic acid occurred within 1 minutes and the following second stage of adsorption proceeded for 5 hours. This rapid initial adsorption is also observed in several previous studies (Table 4.1.2). Cornelissen et al (1997) is

Table 4.1.1 Summary of adsorption studies of organic compounds on iron oxide surface

Mineral & their amount	Organics	Organic Conc.	ratio	Equilibrium constant	Max quantity of NOM adsorption (mg C m^{-2})	Gibbs free energy of (kJ mol^{-1})	pH	Temperature	Atomosphere	Author		journal
Hematite (2 g L^{-1}; BET 10.1 m^2 g^{-1})	Goergetown Natural Organic matter (NOM)	0-60 mg L^{-1}	33-	1.47 - 1.5 (m^3 g^{-1})	0.33-0.18	-35.2	4.1 - 6.5	Room Temp.	------	— Gu et al.	1994	Environ. Sci. Technol.
	Suwannee river Fulvic Acid	0-60 mg L^{-1}	33-	1.13-1.14 (m^3 g^{-1})	0.29-0.20	-34.5	4.3 - 6.3					
Hematite (2 g L^{-1}; BET 10.1 m^2 g^{-1})	HbA NOM	0-60 mg L^{-1}	33-	3.81	0.40	-38	4.3	23±1 °C	----	Gu et al.	1995	Geochim. Cosmochim. Acta
				2.71	0.29	-37	6.3		----			
	HL NOM			1.76	0.28	-36	4.3		----			
				0.64	0.21	-33	6.3		----			
	phthalic acid			----	0.28 (1.7 μmol m^{-2})		4		purged with N_2			
	Salicylic acid			----	0.14 (1.0 μmol m^{-2})							
	p-hydroxybenzoic acid			----	0.08 (0.6 μmol m^{-2})							
	catechol	0-60 mg L^{-1}		----	0.19 (1.7 μmol m^{-2})		9.5					
	resorcinol			----	0.02 (0.2 μmol m^{-2})							
Goethite (5 g L^{-1}; BET 94 m^2 g^{-1})	Soil fulvic acid (IHSS method)	25 mg L^{-1}	200	----	0.58	----	4	Room Temp.	N_2 spaged (to avoid CO_2 contamination)	Filius et al.	2000	Geochim. Cosmochim. Acta
		125 mg L^{-1}	40	----	0.33	----	7					
		120 mg L^{-1}	42	----	0.07	----	10					
Goethite (0.75 g L^{-1}; BET 27 m^2 g^{-1})	McDonald Fulvic Acid	30-50 mg L^{-1}	15-25	1.6	0.52	-35	3.5	22±1 °C	----	Zhou et al.	2001	Geochim. Cosmochim. Acta
		0-35 mg L^{-1}	21-	2.0	0.32	-36	5.5		----			
		0-30 mg L^{-1}	25-	2.0	0.23	-36	7.5		----			

Table 4.1.2 Summary of kinetic studies on adsorption of organic compounds at the iron oxide surface

Mineral & their amount	Organics	Organic Conc.	molar ratio	adsorption rate	desorption rate	pH	Temperature	Author		journal
Sediment	PAH	1mM (110 mg L^{-1})		1st order + 1st order	k_{slow} 8.2 - 1.1*10^{-6} s^{-1} k_{slow} 7.3 - 1.1*10^{-6} s^{-1}	k_{slow} 0.8 - 1.1*10^{-6} s^{-1} k_{slow} 3.6 - 5.1*10^{-5} s^{-1}		20 °C 60 °C	Cornelissen et. al.	1997	Environ. Sci. Technol.
Goethite (0.75 g L^{-1}; BET 27 m^2 g^{-1})	McDonald Fulvic Acid	23 mg C L^{-1}		1.39 (mg C m^{-2} h^{-1}) 0.57 (mg C m^{-2} h^{-1}) 0.12 (mg C m^{-2} h^{-1})	first 15 min	3.5 5.5 7.5	22 °C	Zhou et al.	2001	Geochim. Cosmochim. Acta
Goethite (360 mg/L; BET 44 m^2 g^{-1})	Red water Creek NOM	10 mg L^{-1}	36:1	very rapidly (minutes)		3, 5, 9	20±2 °C	Day et al.	1994	Colloids and Surfaces A
Aluminum Oxide (100 mg; 120 m^2 g^{-1})	DOC in lake water	9.4 mg L^{-1}	11:1	2-3 hour (sufficient time to reach equilibrium)		4.5-9.5	20 °C	Davis and Gloor	1981	Environ. Sci. Technol.
Fe_2O_3	purified Aldrich Humic acid	6 - 50 mg L^{-1}		20-80 sec (the absorption rates becomes very slow)		3.9± 0.1	25 °C	Avena and Koopal	1999	Environ. Sci. Technol.
Fe_2O_3	purified Aldrich Humic acid	50 mg L^{-1}		rapidly occur in the first 100-200 sec*	slow (cannot reached equilibrium in practice)	3.25	22 °C	Avena and Koopal	1998	Environ. Sci. Technol.
iron-oxide-coated quartz (100 mg; 0.496 m^2 g^{-1})	Suwannee River Fulvic Acid (SRFA)	10 - 200 ppm		high (the initial stage) but decrease (the later stage)	slow or irreversible	6	room Temp.	Chi and Amy	2004	Journal of Colloid and Interface Sci.

* after the fast process, there is a decrease in the absorption rate and it increases slowly with time over a much large time range (up to several hours)

REFERENCES

Avena M. J. and Koopal L. K. (1998) Desorption of humic acid from an iron oxide surface. *Environmental Science and Technology*, **32**, 2572-2577

Avena M. J. and Koopal L. K. (1999) Kinetic of humic acid adsorption at solid-water interface. *Environmental Science and Technology*, **33**, 2739-2744

Celi L., Schnitzer M. and Negre M. (1997) Analysis of carboxyl groups in soil humic acids by a wet chemical method, Fourier-transform infrared spectrophotometry, and solution state carbon –13 nuclear magnetic resonance. A comparative study, *Soil Science*, **162**, 189-197

Chi F.-H. and Amy G. L. (2004) Kinetic study on the sorption of dissolved natural organic matter onto different aquifer materials: the effects of hydrophobicity and functional groups. *Journal of Colloid and Interface Science*, **274**, 380-391

Chorover J. and Amistadi M. K. (2001) Reaction of forest floor organic matter at goethite, birnessite and smectite surfaces. *Geochimica et Cosmochimica Acta*, **65**, 95-109.

Cornelissen G., van Noort P. C. M., Parsons J. R. and Govers H. A. J. (1997) Temperature dependence of slow adsorption and desorption kinetics of organic compounds in sediments, *Environmental Science and Technology*, **31**, 454-460

Day G. M., Hart B. T., McKelvie I. D. and Beckett R. (1994) Adsorption of natural organic matter onto goethite. *Colloids and Surfaces A*, **89**, 1-13

Davis J. A. and Gloor R. (1981) Adsorption of dissolved organics in lake water by aluminum oxide. Effect of molecular weight. *Environmental Science and Technology*, **15**, 1223-1229

Filius J. D., Lumsdon D. G., Meeussen J. C. L., Hiemstra T. and van Riemsduk W. H. (2000). Adsorption of fulvic acid on goethite. *Geochimica et Cosmochimica Acta*, **64**, 51-60.

Gu B., Schmitt J., Chen Z., Liang L. and McCathy J. F. (1994) Adsorption and Desorption of natural organic matter on iron oxide: mechanisms and models. *Environmental Science and Technology*, 28, 38-46.

Koopal L. K. and Avena M. J (2001) A simple model for adsorption kinetics at charged solid-liquid interface. *Colloids and Surfaces A*, **192,** 93-107

Korshin G. V., Li C. and Benjamin M. M. (1997) Monitoring the properties of natural organic matter through UV spectroscopy: a consistent theory. *Water Research*,

31, 1787-1795.

LaKind J. S. and Stone A. T. (1989) Reductive dissolution of goethite by phenolic reductants. *Geochimica et Cosmochimica Acta*, **53**, 961-971.

Nagano T., Nakashima S., Nakayama S., Osada K. and Senoo M. (1992) Color variations associated with rapid formation of goethite from proto-ferrihydrite at pH 13 and 40°C. *Clays and Clay Minerals*, **40**, 600-607.

Pullin M. J. and Cabaniss S. E. (2003), The effect of pH, ionic strength, and iron-fulvic acid interactions on the kinetics of non photochemical iron transformations. II. The kinetics of thermal reduction. *Geochimica et Cosmochimica Acta*, **67**, 4079-4089.

Schwertmann U. and Cornell R. M. (2000) *Iron oxides in the laboratory: preparation and characterization*, 2nd ed., pp. 188, New York: Wiley-VCH

Zhou Q. Maurice P. A. and Cabaniss S. E. (2001) Size fractionation upon adsorption of fulvic acid on goethite: equilibrium and kinetic studies, *Geochimica et Cosmochimica Acta*, **65**, 803-812.

4.2. The formation of CO_2 by fulvic acid on the surface of goethite studied using ultraviolet and infrared spectroscopy

4.2.1. Abstract

Changes in absorption intensity (absorbance) at 254 nm of a fulvic acid solution in the presence of goethite powders were monitored in situ in a heatable liquid cell at 80 °C in an ultraviolet - visible (UV-Vis) spectrometer. The 254 nm absorbance decreased rapidly with time at the initial stage in the presence of goethite (the first order rate constant $k_1^{UV} = 3 \times 10^{-4}$ s^{-1}), while without goethite it decreased slowly (the first order rate constant $k_0^{UV} = 6 \times 10^{-7}$ s^{-1}). A hydrothermal vessel was connected to a long path gas cell infrared (IR) spectrometer to monitor volatile compounds formed during the fulvic acid heating at 80 °C. CO_2 was formed gradually with time from the fulvic acid without goethite ($k_0^{CO2} = 1.5 \times 10^{-6}$ s^{-1}). The CO_2 formation with goethite could be simulated by the sum of two first order reactions. The obtained initial first order rate constant of CO_2 formation from the fulvic acid in the presence of goethite ($k_1^{CO2} = 3.2 \times 10^{-4}$ s^{-1}) is on the same order as the above 254 nm absorbance decrease rate. The CO_2 formation rate with goethite in the second stage ($k_2^{CO2} = 1.8 \times 10^{-6}$ s^{-1}) agrees with the rate without goethite. These results suggest that the CO_2 formation from the fulvic acid is greatly accelerated by the presence of goethite possibly through the adsorption of the fulvic acid on the goethite surface and subsequent redox reactions.

Keywords: CO_2 formation, organic-inorganic reaction, fulvic acid, goethite

4.2.2. INTRODUCTION

4.2.2.1. Batch interaction experiments on a dissolved organic matter (fulvic acid) and a mineral (goethite)

Organic compounds are supposed to be decomposed and finally oxidized to CO_2 in surface geological environments: $CH_2O + O_2 \rightarrow CO_2 + H_2O$ (Berner, 1980). On the other hand, various interactions of organic matter with minerals are commonly observed in earth's surface environments (Stumm and Morgan, 1996; Blesa et al., 2000). Recently, enhanced CO_2 formation from organic matter was found on oxide minerals (Dec et al., 2001, Majcher et al., 2000; Wang and Huang, 2000; Table 4.2.1). However mechanisms and rates of CO_2 formation on oxide minerals are not known.

Common dissolved organic compounds in the environment such as fulvic acids have been reported to be adsorbed on oxide minerals such as goethite (Gu et al, 1994; Filius et al, 2000; Zhou et al, 2001). Ferric iron in the iron hydroxides are often

Table 4.2.1 Summary of previous studies on CO_2 formation from organic compounds in the presence of minerals

Mineral & their amount	Organics		ratio	CO_2 at 10h (mmol L^{-1})	pH	Temperature	Atomosphere	Author	year	journal
Birnessite (1.0 g/L)	Catechol	2.3 mmol/L (253 mg/L)	4:1	1	4	room temp.	cintinuous aeration by drawing a vacuum	Majcher et al.	2000	Soil Sci. Soc. Am. J.
Birnessite (33.3 g/L)	catechol	5 mM (550 mg/L)	61:1	0.035	6	25 °C	air	Dec et al.	2001	Soil Sci.
	4-hydroxy benzoic acid	5 mM (690 mg/L)	48:1	1.47						
	Vanillic acid	5 mM (841 mg/L)	40:1	2.74						
	p-Coumaric acid	5 mM (821 mg/L)	41:1	0.89						
	Ferulic acid	5 mM (971 mg/L)	34:1	0.94						
					CO_2 at 24h (mmol L^{-1})					
Mn(IV) oxide (3.3 g/L)	pyrogallol	16.7 mM (2.1 g/L)	1.6:1	15.46	6	25 °C	air	Wang and Huang	2000	Soil Sci.
Fe(III) oxide (3.3 g/L)			1.6:1	4.13						
Al oxide (3.3 g/L)			1.6:1	1.76						
Si oxide (3.3 g/L)			1.6:1	0.95						
No Catalyst				0.82						
					CO_2 at 90h (mmol L^{-1})					
Mn(IV) oxide (3.3 g/L)	pyrogallol	16.7 mM (2.1 g/L)	1.6:1	0.46	6	25 °C	N_2	Wang and Huang	2000	Soil Sci.
Fe(III) oxide (3.3 g/L)			1.6:1	0.71						
Al oxide (3.3 g/L)			1.6:1	0.61						
Si oxide (3.3 g/L)			1.6:1	0.09						
No Catalyst				0						
					CO_2 at 90h (mmol L^{-1})					

found to be reduced to ferrous iron in the presence of organic matter (LaKind and Stone, 1989; Chorover and Amistadi, 2001; Pullin and Cabaniss, 2003). Although the organic compounds are supposed to be oxidized in turn and have a possibility of forming CO_2, details of these redox reactions are not yet understood.

In order to investigate the possible formation of CO_2 from organic matter in the presence of iron hydroxides, interaction experiments between a representative dissolved organic compound, a fulvic acid, and a representative iron hydroxides, goethite, have been conducted in this study. The interaction experiments were conducted at 80 °C to accelerate the reactions. The decrease of the fulvic acid in solution was monitored by an in situ ultraviolet-visible spectroscopy by means of absorption intensity at 254 nm, which is commonly used as a measure of dissolved organic carbon content (Korshin et al., 1997). A long path gas cell infrared spectroscopy (Ishikawa et al., 2007) was employed here to quantify gaseous products including CO_2 from the fulvic acid. By using these spectroscopic methods, reaction kinetics of the fulvic acid in the presence of goethite have been investigated.

4.2.3. MATERIALS AND METHODS

4.2.3.1. Goethite and fulvic acid solution

Goethite samples were prepared after Schwertmann and Cornell (2000). Iron hydroxides were precipitated in a polyethylene vessel by adding 180 mL of 5 M potassium hydroxide to 100 mL of 0.1 M $Fe(NO_3)_3$ solution. The suspension was immediately diluted to 2 L with pure water (MilliQ-UV) and incubated at 70 °C for 60 hours. Yellowish brown precipitates were centrifuged and washed. These products were identified to be goethite by X-ray diffraction and FT-IR spectroscopy (Nagano et al., 1992).

One of standard fulvic acids, Nordic aquatic fulvic acid powder, was obtained from the International Humic Substances Society (IHSS). Their elemental composition is C:52.3, H:4.0, O:45.1, N:0.7 weight percents. The functional group contents are: COOH 11.2 mmol/gC (13.4wt% of the carbon is in the form of COOH) and OH 3.2 mmol/gC (Ritchie and Perdue, 2003). The stock solutions of 200 and 500 mg/L Nordic fulvic acid were prepared with pure water. pHs of these solutions were adjusted to 4 using 0.01 M HCl and 0.01 M NaOH solutions.

4.2.3.2. Continuous analysis of fulvic acid-goethite interaction by Gas cell FT-IR

A steel-lined PTFE (Teflon) reaction vessel was connected to a long path gas cell (10 m path length) placed in a Fourier transform infrared spectrometer (FT-IR)(Bomem MB154) (Fig.4.2.1). Reflecting IR mirrors are set at the both ends

of the 25 cm long cell to obtain 40 times reflection, yielding totally 10 m optical path length. A 20 mL plastic syringe is used for introducing sample solutions and for sampling products (Fig.4.2.1). A vacuum pump and a N_2 gas bombe (99.9999% purity) are connected to the lines to obtain non-oxidizing atmosphere throughout the whole system.

15 mL of 200 mg/L fulvic acid solution and 15 mL of 20 g/L goethite suspension were purged by ~99.9999% nitrogen gas in advance. The fulvic acid solution was added to the goethite suspension in the above hydrothermal reaction system under nitrogen atmosphere.

Hydrothermal experiments were conducted at 80 °C for 0 and 24 hours without goethite and for 0, 2, 4, 6, 9, 12, 18 and 24 hours with goethite. The product solutions were filtered by 0.45 μm MF-membrane™ filter. Ultraviolet – visible (UV-Vis) spectra of the filtered solutions were collected by a spectrophotometer (Jasco V-570) using 1.0 cm quartz cells.

Gaseous products during the hydrothermal reactions were introduced by the nitrogen gas to the long path gas cell FT-IR (Fig.4.2.1) to measure their IR spectra.

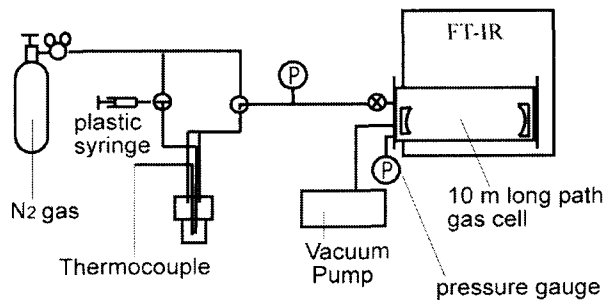

Fig. 4.2.1. The 10-m long path gas cell Bomem MB154 FT-IR spectrometer connected to the steel-lined PTFE (Teflon) hydrothermal reaction vessel.

4.2.3.3. *In situ* UV monitoring of hydrothermal experiments

In situ hydrothermal experiments were conducted at 80 °C for 0 to 24 hours with or without goethite using a heatable liquid cell set in an UV-Vis spectrophotometer (Jasco V-530). 1.25 mg of goethite powder was added to 25 μL of 500 mg/L fulvic acid solution in the heatable liquid cell. UV-Vis spectra of the mixture were measured every 2 minutes while heating at 80 °C.

The weight ratio of goethite to fulvic acid was set to 100 for the batch and in situ hydrothermal experiments.

4.2.4. RESULTS

4.2.4.1. Decrease rates of 254nm absorbance of the fulvic acid with/without goethite

The UV-Vis spectra of product solutions at 80 °C for 0 and 24 hours without goethite did not show significant difference from that of the initial Nordic fulvic acid solution (Fig.4.2.2). On the other hand, the spectra with goethite showed drastic decrease in their absorbances already within 2 hours.

The absorption intensity (absorbance) at 254 nm of the fulvic acid solution due to π-π^* electron transfer originated from substituted aromatic structures is commonly used as a measure of dissolved organic matter contents (Korshin et al, 1997). Therefore, the 254 nm absorbance values of the product solutions were plotted against time in Fig.4.2.3. Without goethite, the 254 nm absorbance showed only a slight decrease by heating at 80 °C for 24 hours, while it decreased to about 0.1 of the initial value within 2 hours and remain mostly unchanged around 0.05 in the presence of goethite.

In order to study the rapid changes in the 254 nm absorbance, in situ UV-Vis experiments were conducted. The in situ data for the 254 nm absorbance showed a slow decrease at 80 °C without goethite (Fig.4.2.3). The batch data for 24 hours without goethite is close to this trend. On the other hand, the in situ data at 80 °C with goethite appeared to decrease very rapidly (Fig.4.2.3). The batch data with goethite are about 0.1 lower than these in situ data. This difference might be due to light scattering and absorption by goethite particles in the in-situ experiments and loss of adsorbed fulvic acids on goethite during filtering in the batch experiment.

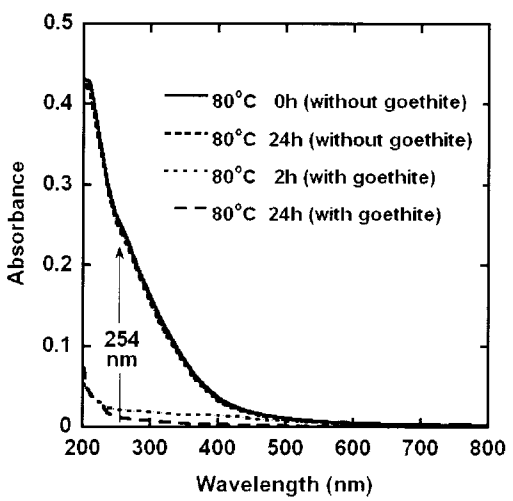

Fig. 4.2.2. Ultraviolet-visible spectra obtained from the product solutions at 80 ° C for periods of 0 and 24 h in the absence of goethite, and for periods of 2 and 24 h in the presence of goethite, taken using the batch hydrothermal experimental apparatus shown in Fig. 4.2.1.

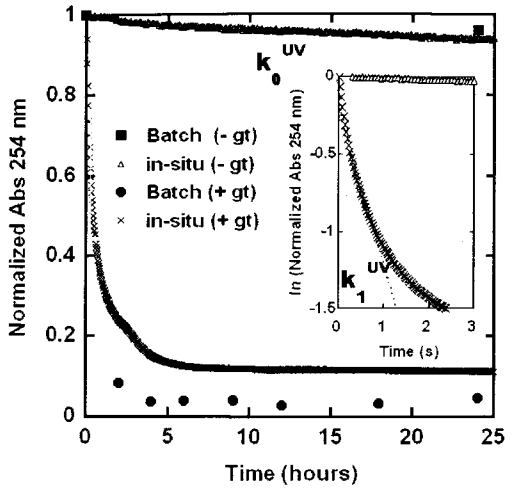

Figure 4.2.3. Change in the absorbance at 254 nm with time at 80 ° C in the presence / absence of goethite during the batch and in situ hydrothermal experiments. The value of the absorbance at 254 nm was devided from the initial value. The in situ data in the initial stage up to a period of 3 h are shown in the inset as a semi-logarithm plot. Consult the main text for the curve fitting information used to obtain the first-order rate constants of $k_0^{UV} = 6 \times 10^{-7}$ s^{-1} and $k_1^{UV} = 3 \times 10^{-4}$ s^{-1}.

4.2.4.2. Formation rates of CO_2 from the fulvic acid with/without goethite

Gaseous products during the batch hydrothermal experiments analyzed by gas cell FT-IR spectroscopy indicated only CO_2 as recognizable species. Carbon monoxide and other incomplete combustion gases were not detected.

In the absence of goethite, the cumulative amount of formed CO_2 gradually increased with time (Fig.4.2.4). By assuming that the maximum CO_2 formation is limited by the initial carboxylic content of the fulvic acid: $C_0 = 1.75 \times 10^{-5}$ mol for 3 mg fulvic acid, the CO_2 formation rate can be simulated by the first order kinetics by using this C_0 value: $[C = C_0 (1- \exp (k_0^{CO2} t))]$. The first order CO_2 formation rate was then $k_0^{CO2} = 1.5 \times 10^{-6}$ s^{-1}.

On the other hand, formed CO_2 with goethite showed a rapid increase at the initial stage, and then the CO_2 emission continued gradually with time (Fig.4.2.4). Assuming that the CO_2 was formed by two independent first order reactions $[C = C_1 (1- \exp (k_1^{CO2} t)) + (C_0 - C_1)(1- \exp (k_2^{CO2} t))]$, the first order CO_2 formation rates are obtained by fitting the data until 24 hours by the above equation (Fig.4.2.4)($k_1^{CO2} = 3.2 \times 10^{-4}$ s^{-1}; $k_2^{CO2} = 1.8 \times 10^{-6}$ s^{-1}; with $C_1 = 1.1 \times 10^{-6}$ mol). This amount of CO_2

formed with goethite (C_1) is only about 6% of the initial carboxyl content (C_0).

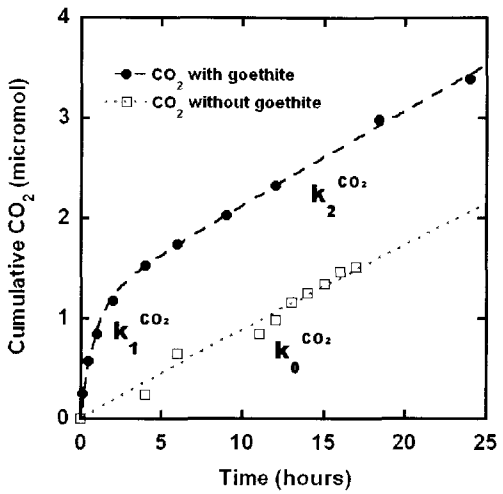

Figure 4.2.4 The cumulative formation of CO_2 with time from fulvic acid at 80 ° C in the presence / absence of goethite during the batch hydrothermal experiments. Consult the main text for the curve fitting information used to obtain the first-order rate constants of $k_0^{CO2} = 1.5 \times 10^{-6}$ s^{-1}, $k_1^{CO2} = 3.2 \times 10^{-4}$ s^{-1}, and $k_2^{CO2} = 1.8 \times 10^{-6}$ s^{-1}.

4.2.5. DISCUSSION

4.2.5.1. Decrease rates of 254nm absorbance of the fulvic acid with/without goethite

The slow decrease of 254 nm absorbance of the fulvic acid without goethite can be used to determine the first order reaction rate constant ($k_0^{UV} = 6 \times 10^{-7}$ s^{-1}) by fitting the data until 24 hours with an exponential curve. The 254 nm absorbance decrease with goethite is very rapid at the initial stage but become slow at the later stage leaching to a constant value indicating participation of several processes. These processes can be simulated, for instance, by the sum of two independent first order reactions or the successive three first order reactions. These simulations gave the rate constant for the initial stage k_1^{UV} to be from 2 to 5 $\times 10^{-4}$ (s^{-1}). Alternatively, only the data until 1 hour showing a quasi-linear trend in a semi-logarithmic diagram (Fig.4.2.3 inset) can be simply fitted by an exponential curve to obtain the apparent first order reaction rate constant $k_1^{UV} = 3 \times 10^{-4}$ (s^{-1}). Since this value is on the same order as the above complex simulation and the precise kinetic treatment will need further experimental data, we will use this initial stage first order rate constant in this

study. This rapid decrease of fulvic acid from solution suggests its adsorption on goethite.

4.2.5.2. Formation rates of CO_2 from the fulvic acid with/without goethite

The first order CO_2 formation rate from the fulvic acid in the presence of goethite ($k_1^{CO2} = 3.2 \times 10^{-4}$ s^{-1}) is on the same order as the above initial first order rate of the decrease in 254 nm absorbance ($k_1^{UV} = 3 \times 10^{-4}$ s^{-1}). This indicates that CO_2 formation mechanism might be related to the adsorption of fulvic acid on goethite. The first order CO_2 formation rate with goethite in the second stage ($k_2^{CO2} = 1.8 \times 10^{-6}$ s^{-1}) agrees with the rate without goethite ($k_0^{CO2} = 1.5 \times 10^{-6}$ s^{-1}).

These results suggest that the hydrothermal transformation of the fulvic acid producing CO_2 is greatly accelerated by the presence of goethite possibly through the adsorption of the fulvic acid on the goethite surface and subsequent redox reactions. Further studies are needed to clarify mechanisms of this surface interaction of fulvic acid and goethite.

REFERENCES

Berner R. A. (1980) *Early diagenesis a theoretical approach*, pp. 241, Princeton: Princeton University Press

Blesa M. A., Weisz A. D., Morando P. J., Salfity J. A., Magaz G. E. and Regazzoni A. E. (2000) The interaction of metal oxide surfaces with complexing agents dissolved in water. *Coordination Chemistry Reviews*, **196**, 31-63.

Chorover J. and Amistadi M. K. (2001) Reaction of forest floor organic matter at goethite, birnessite and smectite surfaces. *Geochimica et Cosmochimica Acta*, **65**, 95-109.

Dec.J., Haider K. and Bollag J.-M. (2001) decarboxylation and demethoxylation of naturally occurring phenols during coupling reactions and polymerization, *Soil Science*, **166**, 660-671.

Filius J. D., Lumsdon D. G., Meeussen J. C. L., Hiemstra T. and van Riemsduk W. H. (2000). Adsorption of fulvic acid on goethite. *Geochimica et Cosmochimica Acta*, **64**, 51-60.

Gu B., Schmitt J., Chen Z., Liang L. and McCathy J. F. (1994) Adsorption and Desorption of natural organic matter on iron oxide: mechanisms and models. *Environmental Science and Technology*, 28, 38-46.

Ishikawa K., Tani A., Otsuka T. and Nakashima S., (2007) Transformation of γ–ray-formed methyl radicals in methane hydrate at 10MPa. *Japanese Journal of Applied Physics*, **46**, 455-460.

Korshin G. V., Li C. and Benjamin M. M. (1997) Monitoring the properties of natural organic matter through UV spectroscopy: a consistent theory. *Water Research*, **31**, 1787-1795.

LaKind J. S. and Stone A. T. (1989) Reductive dissolution of goethite by phenolic reductants. *Geochimica et Cosmochimica Acta*, **53**, 961-971.

Majecher E. M., Chorover J., Bollag J-. M., and Huang P. M. (2000) Evolution of CO_2 during the birnessite-induced oxidation of ^{14}C-labeled catechol. *Soil Science Society of America Journal*, **64**, 157-163.

Nagano T., Nakashima S., Nakayama S., Osada K. and Senoo M. (1992) Color variations associated with rapid formation of goethite from proto-ferrihydrite at pH 13 and 40°C. *Clays and Clay Minerals*, **40**, 600-607.

Pullin M. J. and Cabaniss S. E. (2003), The effect of pH, ionic strength, and iron-fulvic acid interactions on the kinetics of non photochemical iron transformations. II. The kinetics of thermal reduction. *Geochimica et*

Cosmochimica Acta, **67**, 4079-4089.

Ritchie J. D. and Perdue E. M. (2003), Proton-binding study of standard and reference fulvic acids, humic acids, and natural organic matter. *Geochimica et Cosmochimica Acta*, **67**, 85-96.

Schwertmann U. and Cornell R. M. (2000) *Iron oxides in the laboratory: preparation and characterization*, 2nd ed., pp. 188, New York: Wiley-VCH

Stumm W. and Morgan J. J. (1996) *Aquatic chemistry: chemical equilibria and rates in natural waters*, 3rd ed., pp. 1022, New York: Willey

Wang M. C. and Huang P. M. (2000) Ring cleavage and oxidative transformation of pyrogallol catalyzed by Mn, Fe, Al, and Si oxides, *Soil Science*, **165**, 934-942.

Zhou Q. Maurice P. A. and Cabaniss S. E. (2001) Size fractionation upon adsorption of fulvic acid on goethite: equilibrium and kinetic studies, *Geochimica et Cosmochimica Acta*, **65**, 803-812.

4.3. Interaction of fulvic acid and goethite under hydrothermal condition

4.3.1. INTRODUCTION

Geocatalysis is important for reactions with high activation energies such as redox reaction and transformation of humic substances and kerogen (Schoonen et al, 1998). Organic compounds are supposed to be decomposed and finally oxidized to CO_2 on some mineral oxide such as goethite (Otsuka and Nakashima, 2007). However mechanisms and rates of CO_2 formation on oxide minerals are not known.

Common dissolved organic compounds in the environment such as fulvic acids have been reported to be adsorbed on oxide minerals such as goethite (Gu et al, 1994; Filius et al, 2000; Zhou et al, 2001). Ferric iron in the iron hydroxides are often found to be reduced to ferrous iron in the presence of organic matter (LaKind and Stone, 1989; Chorover and Amistadi, 2001; Pullin and Cabaniss, 2003). Although the organic compounds are supposed to be oxidized in turn and have a possibility of forming CO_2, details of these redox reactions are not yet understood.

In order to investigate the formation processes of CO_2 from organic matter in the presence of iron hydroxides, interaction experiments between a representative dissolved organic compound, a fulvic acid, and a representative iron hydroxides, goethite, have been conducted. In addition to section 4.2., which analyzed gaseous compounds and adsorption behavior, ferrous ion, which is produced by the reductive dissolution of goethite, and ultraviolet-visible spectra of dissolved organic products are studied here. Two-step separation procedures were employed here to identify dissolved products. Based on the analytical results the reaction stoichiometry was estimated and kinetics of CO_2 formation in the presence of goethite has been investigated.

4.3.2. EXPERIMENTAL

4.3.2.1. Goethite and fulvic acid solution

Goethite samples were prepared after Schwertmann and Cornell (2000). Iron hydroxides were precipitated in a polyethylene vessel by adding 180 mL of 5 M potassium hydroxide to 100 mL of 0.1 M $Fe(NO_3)_3$ solution. The suspension was immediately diluted to 2 L with pure water (MilliQ-UV) and incubated at 70 °C for 60 hours. Yellowish brown precipitates were centrifuged and washed. These products were identified to be goethite by X-ray diffraction and FT-IR spectroscopy (Nagano et al., 1992).

One of standard fulvic acids, Nordic aquatic fulvic acid powder, was obtained

from the International Humic Substances Society (IHSS). Their elemental composition is C:52.3, H:4.0, O:45.1, N:0.7 weight percents. The functional group contents are: COOH 11.2 mmol gC^{-1} (13.4wt% of the carbon is in the form of COOH) and OH 3.2 mmol gC^{-1} (Ritchie and Perdue, 2003). The stock solutions of 200 and 500 mg L^{-1} Nordic fulvic acid were prepared with pure water. pHs of these solutions were adjusted to 4 using 0.01 M HCl and 0.01 M NaOH solutions.

4.3.2.2. Solution analysis of adsorption experiment

The interaction experiments between the fulvic acid solution and goethite were conducted together with the batch adsorption experiments in section 4.1. Adsorption experiments were conducted by adding 10 mL of 10 mg L^{-1} Nordic fulvic acid stock solution into the 10 g L^{-1} goethite suspension (the goethite: fulvic acid ratio were 10:1 and 100:1).

The product solutions were collected at 0, 15 and 30 minute, 2, 3, 6, 9 and 12 hours of the experiments at 25°C, and were immediately centrifuged for 15 min at 13500 rpm. Firstly, 15 ml of supernatant were extracted by using plastic syringe and filtered though 0.2 μm cellulose acetate membrane. This filtrate was named "bulk filtrate". Secondary, the residual solution was separated by filtration under reduced pressure though 0.45 and 0.2 μm cellulose acetate membranes. The second filtrate named "pore water filtrate". These two series of filtrates were analyzed by UV-VIS spectroscopy and pH.

UV-VIS analysis was conducted by ultraviolet-visible (UV-VIS) spectrometer (Jasco, V-530 and V-570). All spectra were obtained with a spectral range from 800 to 200 nm and with a scan speed of 100 nm $minute^{-1}$. A bandwidth of 2.0 nm was applied with a data acquisition of 1 nm step. Goethite suspension diluted with distilled water was also analyzed as a reference.

The pH measurement was conducted by pH meter (HM-30G, TOA). The sample pH were measured before the mixing (initial fulvic acid solution and goethite suspension), soon after the mixing, before the centrifugation with two sets of filtrate. The pH value were measured when they are stable for 5 seconds with drift of no more than ±0.01 pH units.

The FT-IR measurements were conducted by using micro FT-IR spectrometer equipped with a mercury cadmium telluride (MCT) detector (Jasco, FTIR-620 and IRT-30). The solution samples were dried on the CaF_2 crystal (thickness of CaF_2 is 1mm). The residue on the CaF_2 plate was measured with a 100 × 100 μm aperture. One hundred interferograms at 4 cm^{-1} resolution were co-added to produce a single spectrum from 700 to 4000 cm^{-1}.

The zeta potentials for Nordic fulvic acid solution and goethite suspension

were measured by zeta potential analyzer (Zetasizer Nano-ZS, MALVERN). The electrophoresis migration of particles was observed by direct light scattering method. The sample solutions were set into electrophoresis cell at 25°C.

4.3.2.3.Measurement of dissolved Fe^{2+} contents

Dissolved Fe^{2+} was measured by the ferrozine method (Stookey, 1970; Pehkonen, 1995; Viollier et al., 2000; Pullin and Cabaniss, 2001; Kononets et al., 2002). Ferrozine (a monosodium salt of 3-(2-pyridyl)-5,6-bis-(4-phenylsulfonate)-1,2,4-triazine) is widely used as a sensitive reagent for iron. The two major advantages of the use of ferrozine method are its sensitivity and selectivity. The absorbance maximum of the iron(II)-ferrozine complex (562 nm, molar absorptivity is 2.8×10^4 L mol^{-1} cm^{-1}; Fig.4.3.1) is larger than that of other iron-complex such as 1, 10-phenanthroline (1.1×10^4 L mol^{-1} cm^{-1}) (Stookey, 1970). Vilollier et al. (2000) showed that the presence of high concentration of dissolved organic matter do not create any significant artifacts, in the ferrozine method.

The ferrozine indicator was prepared by adding 49.3 mg of ferrozine monosodium salt to 10 mL of 1.0 M 2-(N-Morpholino) ethanesulfonic acid (MES) solution. 100 μL of sample solution was mixed with 100 μL of ferrozine indicator and analyzed by UV-VIS spectrometer (Jasco, V-570) in a spectral range from 800 to 220 nm and with a scan speed of 100 nm/minute. A bandwidth of 2.0 nm was applied with a data acquisition of 1 nm step.

The fulvic acid solution (15 mL of 200 mg/L) was added to the goethite suspension (15 mL of 20 g/L) in the hydrothermal vessel under nitrogen atmosphere. The product solutions were collected at 0, 15 and 30 minute, 1, 2, 4, 6, 9, 12, 18 and 24 hours, and filtered immediately by 0.45 μm MF-membrane™ filter. Because dissolved Fe^{2+} was immediately oxidized by atmospheric oxygen, the above sample mixing was conducted within 1 minute after the solution sampling.

4.3.2.4. Continuous analysis of volatile products from fulvic acid-goethite interaction by Gas cell FT-IR

A steel-lined PTFE (Teflon) reaction vessel was connected to a long path gas cell (10 m path length) placed in a Fourier transform infrared spectrometer (FT-IR)(Bomem MB154) (Fig.2.1.4). Reflecting IR mirrors are set at the both ends of the 25 cm long cell to obtain 40 times reflection, yielding totally 10 m optical path length. A 20 mL plastic syringe is used for introducing sample solutions and for sampling products (Fig.2.1.4). A vacuum pump and a N_2 gas bombe (99.9999%

purity) are connected to the lines to obtain non-oxidizing atmosphere throughout the whole system.

15 mL of 200 mg/L fulvic acid solution and 15 mL of 20 g/L goethite suspension were purged by ~99.9999% nitrogen gas in advance. The fulvic acid solution was added to the goethite suspension in the above hydrothermal reaction system under nitrogen atmosphere.

Hydrothermal experiments were conducted at 80 °C for 0 and 24 hours without goethite and for 0, 2, 4, 6, 9, 12, 18 and 24 hours with goethite. The product solutions were filtered by 0.45 μm MF-membrane™ filter. Ultraviolet – visible (UV-Vis) spectra of the filtered solutions were collected by a spectrophotometer (Jasco V-570) using 1.0 cm quartz cells.

Gaseous products during the hydrothermal reactions were introduced by the nitrogen gas to the long path gas cell FT-IR (Fig.2.1.4) to measure their IR spectra.

4.3.2.5. Kinetics analysis

The adsorption kinetics of adsorbates on minerals surfaces are very complicated and there are lots of models. Therefore I applied two kinetic analysis methods: the combination of two independent first order reactions and the first order reaction with the following diffusion limited process.

Two independent first order reactions are expressed by

$$[C = C_1 (1- \exp (k_1 t)) + (C_2)(1- \exp (k_2 t))]$$

where C_1 and C_2, are the initial concentrations of species and k_A and k_B are the first-order rate constants.

For the analysis of diffusion processes, Fick's law was introduced to rate determination.

where c is the concentration, x is the distance adsorbed and D is the diffusion

$$\frac{\partial c}{\partial t} = D(\frac{\partial^2 c}{\partial x^2})$$

coefficient. The total amount of diffusing substance entering or leaving the sphere is given by following eqation (Crank, 1975)

where a is the radius of a sphere. This equation can be simplified to

$$\frac{\Gamma_t}{\Gamma_\infty} = 1 - \frac{6}{\pi} \Sigma(\frac{1}{n^2}) \exp(\frac{Dn^2 \pi^2 t}{a^2})$$

$$\frac{\Gamma_t}{\Gamma_\infty} = \frac{6}{\pi} \sqrt{\frac{Dt}{a^2}}$$

Under appropriate boundary conditions, an expression for the time dependence of adsorption can be approximated to the above equation (Aharoni and Suzin, 1982).

Thus, the plots of square root of time versus natural logarithm of adsorption density would give diffusion-limited adsorption kinetics simulation.

4.3.3. RESULTS

4.3.3.1. Solution analysis of adsorption experiments of the fulvic acid on goethite

The UV-VIS spectra of the filtrates of pore water from the 15 min –12 hours adsorption experiments of the fulvic acid on the goethite were different from those of the bulk filtrate. The spectra of bulk filtrate showed featureless spectral shape similar to that of the initial fulvic acid solution (Fig.4.3.2.-1~7). On the other hand, the spectra of pore water filtrates showed four additional absorption bands: 1) a large band around 220 nm, 2) multiple bands around 260 nm, 3) a 290nm and 4) a 370 nm band (Fig.4.3.3).

The UV-VIS spectrum of goethite suspension (Fig. 4.3.4.) was in good agreement with Cornell and Schwertmann (1996). Absorption bands corresponding to various electronic transitions appeared as slope changes on the absorption curve. The second derivative maxima correspond to the two types of transitions: 1) as the ligand field transitions; $2(^6A_1) \rightarrow 2(^4T_1)$ transition (480 nm), $^6A_1 \rightarrow {}^4E{}^4A_1$ transition (434 nm), $^6A_1 \rightarrow {}^4E$ transition (367 nm) and $^6A_1 \rightarrow {}^4T_1$ transition (290 nm), and 2) the charge transfer transitions; $^6T_{1u} \rightarrow 2t_{2q}$ charge transfer (250 nm) and $1T_{2u} \rightarrow 2t_{2q}$ charge transfer (225 nm).

The pH values during the experiments are listed in Table 4.3.1. The value, initially 4.0, of initial pH slightly increased to 4.1. On the other hand, the pH of filtrates were increased with time from the initial pH of 4.1 to 7.1 for pore water filtrates and the initial pH of 4.1 to 4.3 for bulk filtrates (except for the experiment at 6 hour). The quantity of hydrogen ion and their difference are calculated by subtraction from initial pH by final pH values. The pH value changes (delta pH) correspond to decreased concentration of hydrogen ion $[H^+]$.

$$\Delta \text{ pH} = \text{Final pH} - \text{Initial pH}$$
$$[H^+] = 10^{-pH}$$

$$\Delta[H^+] = \text{quantity of hydrogen ion}$$
$$= [H^+](\text{mol/L}) \times \text{volume of solution (L)}$$
$$= \text{initial pH} \times 20 \times 10^{-3} - (\text{bulk filtrate pH} \times 15 \times 10^{-3} - \text{pore water filtrate pH} \times 5 \times 10^{-3})$$

The difference of the H+ concentration $\Delta[H^+]$ increased with time at 25°C as shown in Fig.4.3.5.

Table 4.3.1 The pH values during the fulvic acid – goethite interactions

Time	pH				Hydrogen ion
				pore water	
(hour)	Before	After	bulk filtrate	filtrate	(micromol)
0.17	4.08	4.07	4.09	5.72	0.44
0.5	4.12	4.14	4.17	5.34	0.48
2	4.07	4.1	4.14	7.02	0.62
3	4.06	4.09	4.22	6.89	0.84
6	4.05	-	5.78	7.10	1.76
9	4.02	4.1	4.25	7.02	1.07
12	4.01	4.11	4.20	7.04	1.01

The zeta potential at pH = 4 of synthesized goethite and Nordic fulvic acid are 30.9 mV and -44.9 mV, respectively and are in good agreement with the previous reports (Stumm, 1996; Section 3.1 of this thesis) as shown in Table 4.3.2. Goethite is positively charged by Fe(III) molecules and the fulvic acid is negatively charged due to carboxyl and hydroxyl functional groups. After the interaction experiment, the zeta potential of goethite decreased from 30.9 to 8.3 mV, while that of the fulvic acid increased from -44.9 to -25.1mV.

Table 4.3.2 The zeta potential before/after the fulvic acid – goethite interactions

	Zeta potential (mV)	
	goethite	fulvic acid
before	30.9	-44.9
after	8.3	-25.1

IR spectra of the Nordic fulvic acid, hydrothermally degraded fulvic acid and filtrate after the interaction between fulvic acid and goethite were shown in Fig. 4.3.6. Because Nordic fulvic acid has high carboxyl contents, the absorption peaks of carboxyl groups occurs at 1720, 1590, 1400 and 1260 cm^{-1}. These peaks are also overlapping with aromatic C=C stretching at 1600 cm^{-1}, aliphatic C-H bending at 1460 and 1370 cm^{-1}, C-O stretching of phenol-OH around at 1400 cm^{-1}, and C-O stretching of ether compounds around 1200 cm^{-1}.

The spectral shape of Nordic fulvic acid keeps its original one under hydrothermal conditions at 80°C after 30 hours heating (Fig. 4.3.6). However, that of Nordic fulvic acid interacted with goethite is greatly changed. Beside the peaks of carboxyl groups at 1720, 1590, 1400 and 1260 cm^{-1}, C=O stretching peaks derived from aldehyde and/or ketone at 1660 cm^{-1} are also observed. In addition, unknown peaks at 1360 cm^{-1} and 1160 cm^{-1} can be recognized.

4.3.3.2. Determination of dissolved Fe^{2+}

Dissolved Fe^{2+} concentrations of the filtrates were measured by ferrozine method forming iron(II)-ferrozine complex (562 nm absorbance). More Fe^{2+} are formed at higher temperatures at 50°C and 70°C. They increased with time during the adsorption experiments at 25 °C (Fig. 4.3.7). The experimental data in the initial stage from 10 minute to 4hours can be fitted by the first-order kinetics;

$$[Fe^{2+}] = [A]_0(1\text{-}\exp(-k_A t)) + X$$

, where $[A]_0$ are the initial concentrations of different Fe^{2+} species, X is the time-independent term and k_A are the first-order rate constants. Obtained k_A values are 1.6×10^{-4} s^{-1} at 25 °C, 2.4×10^{-4} s^{-1} at 50 °C, 4.1×10^{-4} s^{-1} at 70 °C.

4.3.3.3. The formation of CO_2 under the hydrothermal conditions

As shown in section 4-2, gaseous products during the batch hydrothermal experiments analyzed by gas cell FT-IR spectroscopy indicated only CO_2 as recognizable species. The cumulative amount of formed CO_2 at 25 °C, 50 °C, 60 °C and 70 °C with goethite showed a rapid increase at the initial stage, and then the CO_2 emission continued gradually with time (Fig. 4.3.8). Assuming that the CO_2 was formed by two independent first order reactions

$$[C = C_1 (1\text{- } \exp (k_1{}^{CO2} t)) + (C_0 - C_1)(1\text{- } \exp (k_2{}^{CO2} t))],$$

the first order CO_2 formation rates are obtained by fitting the data until 24 hours by the above equation as shown in Fig.4.3.8. This amount of CO_2 formed with goethite (C_1) is only about 6% of the initial carboxyl content (C_0) at 80°C.

4.3.4. DISCUSSION

4.3.4.1. Dissolved species

The UV-VIS spectra of the filtrates of pore water from the 15 min –12 hours adsorption experiments were similar to that of the initial goethite in the range of 280 – 600 nm. The ligand field transitions of Fe^3 in goethite; $2(^6A_1) \rightarrow 2(^4T_1)$ transition (480 nm), $^6A_1 \rightarrow {}^4E{}^4A_1$ transition (434 nm), $^6A_1 \rightarrow {}^4E$ transition (367 nm) and $^6A_1 \rightarrow {}^4T_1$ transition (290 nm) are observed. However, the band at 220 nm and multiple

bands around 261 nm are characteristic for the filtrates of pore water and different from the above goethite bands.

The $\pi \rightarrow \pi^*$ bands are sensitive to the geometry of the conjugated chromophore (Rao, 1967). The absorption band at 220 nm with ε of about 20000 is correlated to two chromophores conjugated each other such as diene (two coupled C=C double bonding) and/or α, β- unsaturated carbonyl compounds. This rule is well known as Woodward rules. Pestemer (1992) reviewed the effect of alkyl substitution on the main absorption band of buta-1,3-diene as shown in Fig.4.3.9. This 6-membered diene bands are similar to our results. It indicates that aromatic carbon structures are breaking into alkyl substituted diene.

The bands at 260 nm are usually identified as simple aldehyde and/or ketone with ε of about 20. It is due to $n \rightarrow \pi^*$ transition derived from C=O compounds. The multiple bands around 260 nm reflect that the carbonyl compounds vibrational fine structure may persist the $n \rightarrow \pi^*$ transition of C=O group (Timmons, 1992). If as simple aldehyde and/or ketone is conjugated such as α, β- unsaturated carbonyl compounds, multiple bands might flatten their curvature.

Based on the UV spectrum, some products from fulvic acid-goethite interaction can be expected. The absorption band positions and apparent absorptivities ε indicate that the chemical structures of the products might contain alkyl substituted diene and non-conjugated aldehyde. The estimated structures of the products are drawn in fig.4.3.10.

The production of aldehyde is also supported by FT-IR results. The peaks at 1660 cm^{-1}, usually identified as aldehyde or quinone, are only observed after interaction with goethite. In addition, the peaks of C-H stretching and bending vibrations at 2920, 1460 and 1370 cm^{-1} relatively increased against carboxyl groups. This also suggests that ring opening reactions may occur during the interaction between fulvic acid and goethite.

$$R\text{-}CH_2OH \rightarrow R\text{-}CHO + 2H^+ + 2e^- \quad (1)$$

$$R\text{-}CHO + H_2O \rightarrow R\text{-}COOH + 2H^+ + 2e^- \quad (2)$$

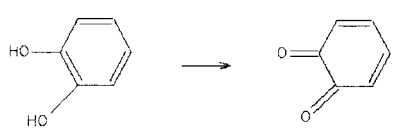

$+ 2H^+ + 2e^-$ (3)

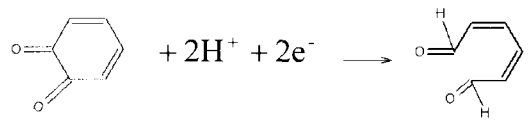

(4)

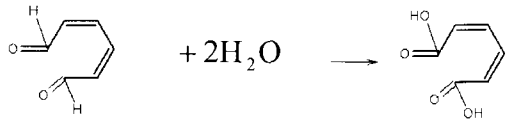

$$+ 2H_2O \longrightarrow + 4H^+ + 4e^- \quad (5)$$

4.3.4.2. Reaction stoichiometry

The fulvic acid – goethite interaction is discussed here with special attention to formation of CO_2. Two possibilities are considered. One is a reaction observed in the bulk solution. The other is a reaction occurred at the near field region of goethite particles. The reduction of ferric iron by the fulvic acid:

$$Fe^{3+} + e^- \rightarrow Fe^{2+} \quad (6)$$

The reductive iron dissolution from goethite are:

$$FeOOH + 3H^+ \rightarrow Fe^{3+} + 2H_2O \quad (7).$$

The sum of equations (6) and (7) are

$$FeOOH + 3H^+ + e^- \rightarrow Fe^{2+} + 2H_2O \quad (8).$$

On the other hand, under the presence of oxidizing agents, decarboxylation reaction of carboxylic acids (Britt et al. 1999) can be written as:

$$RCOO^- \rightarrow R\cdot + CO_2 + e^- \quad (9).$$

By the combination of half reactions ((8) and (9)), the fulvic acid – goethite interaction becomes:

$$FeOOH + RCOO^- + 3H^+ \rightarrow Fe^{2+} + R\cdot + 2H_2O + CO_2 \quad (10).$$

In addition, dissolved CO_2 is assumed to be in equilibrium with hydrogen carbonate ions (HCO_3^-).

$$CO_2 + OH^- \Leftrightarrow HCO_3^- \quad (11)$$

This equilibrium is greatly affected by the pH condition. The pH of near field region of goethite were neutral, especially 7 at >2 hour reaction time (at 25°C). The major proportion of carbon dioxide at near field region of goethite is in the form of hydrogen carbonate ions (HCO_3^-). Therefore, by using equation (10) and (11), the reaction can be rewritten as

$$FeOOH + RCOO^- + 2H^+ \rightarrow Fe^{2+} + R\cdot + H_2O + HCO_3^- \quad (12).$$

This reaction scheme is in good agreement with the observed ferrous ion and CO_2 formation at 25°C (Fig.4.3.11a). The ratio of observed ferrous ion and hydrogen

ion was 1:1-2 at 25°C (Fig.4.3.11b), close to the above stoichiometry.

4.3.4.3. Reaction kinetics between the fulvic acid and goethite

The cumulative amount of formed CO_2 at 25 °C, 50 °C, 60 °C and 70 °C with goethite showed a rapid increase at the initial stage, and then the CO_2 emission continued gradually with time (Fig. 4.3.8.). Kinetics of fulvic acid reaction on goethite surface show that adsorption reaction at the initial stage (< a few minutes) is very fast. On the other hand, the slow adsorption processes follows afterwards. These phenomena were reported in many researches on adsorption of cations and/or anions on oxides (Fuller et al., 1993, Axe and Anderson, 1997, Strawn et al., 1998). They concluded that diffusion process of solute into pore of metal oxides was the rate-determining step of adsorption kinetics (Fuller et al., 1993, Axe and Anderson, 1997, Strawn et al., 1998). Pores may be present in goethite as a original structural feature or as a result of aggregation of particles. In fact, our laser confocal microscope (LSCM) analysis showed that micrometer size pores were produced in the goethite precipitates. The particle distribution analysis also showed larger particles than primary particles are present in the goethite after the experiments, suggesting the aggregation of goethite particles. Naono et al.(1987) and Weidler et al. (1998) also reported goethite had some micro- or mesopores. Therefore, diffusion in microscopic pores in goethite might control the interaction kinetics of the fulvic acid and goethite.

In order to confirm contribution of diffusion processes to interaction kinetics of the fulvic acid and goethite, carboxyl contents adsorbed on the goethite by ATR-IR spectroscopy and CO_2 formation contents by the reaction gas cell FT-IR with goethite are plotted as a function of route t ($t^{1/2}$) as shown in Fig. 4.3.12. Since diffusion process is simplified to the equations in section 4.3.2.5, apparent diffusion coefficient can be given by following equation:

$$\frac{\Gamma_t}{\Gamma_\infty} = \sqrt{D_{app}}\sqrt{t}$$

Therefore, apparent diffusion coefficients can be calculated by the slopes in Fig. 4.3.12a.b. Fig. 4.3.13 shows apparent diffusion coefficients as a function of temperature (Arrhenius diagram) for the carboxyl contents adsorbed on the goethite and the CO_2 formation contents with goethite. The activation energies are 33 kJ mol^{-1} for the carboxyl contents adsorbed on the goethite and 37 kJ mol^{-1} for the CO_2 formation contents with goethite. Similar values of these activation energies indicate these processes have the same rate-limiting process.

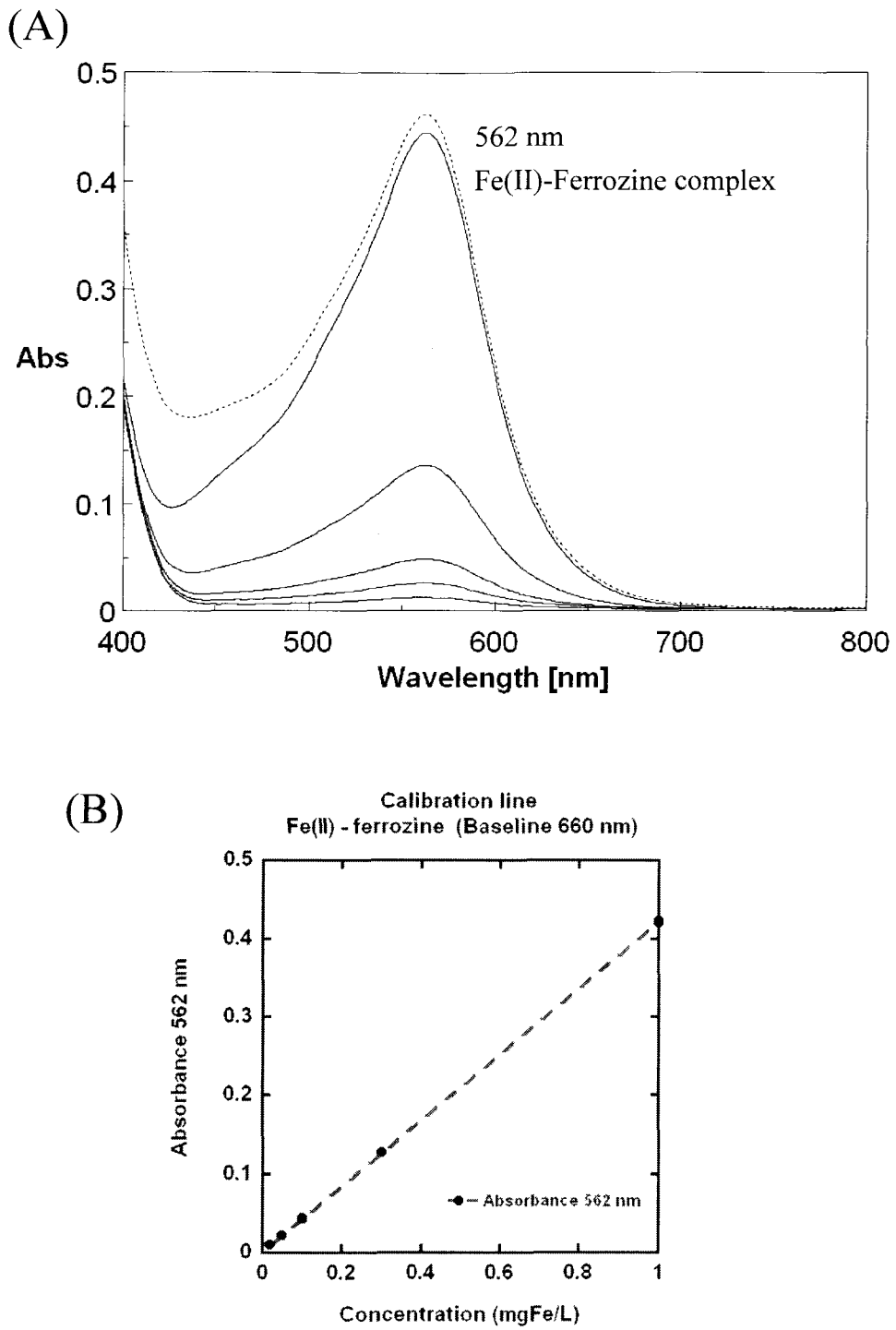

Fig. 4.3.1. (A) The absorbance maximum of the iron(II)-ferrozine complex (562 nm, molar absorptivity is 2.8 $\times$ 10^4 L mol^{-1} cm^{-1}) with 0.02, 0.05, 0.1, 0.3, 1.0 mgFe L^{-1} (straight line) and 1.0 mgFe L^{-1} with 50 mg L^{-1} of Nordic fulvic acid solution (dotted line); (B) Calibration lines for dissolved Fe^{2+} at absorbance 562 nm

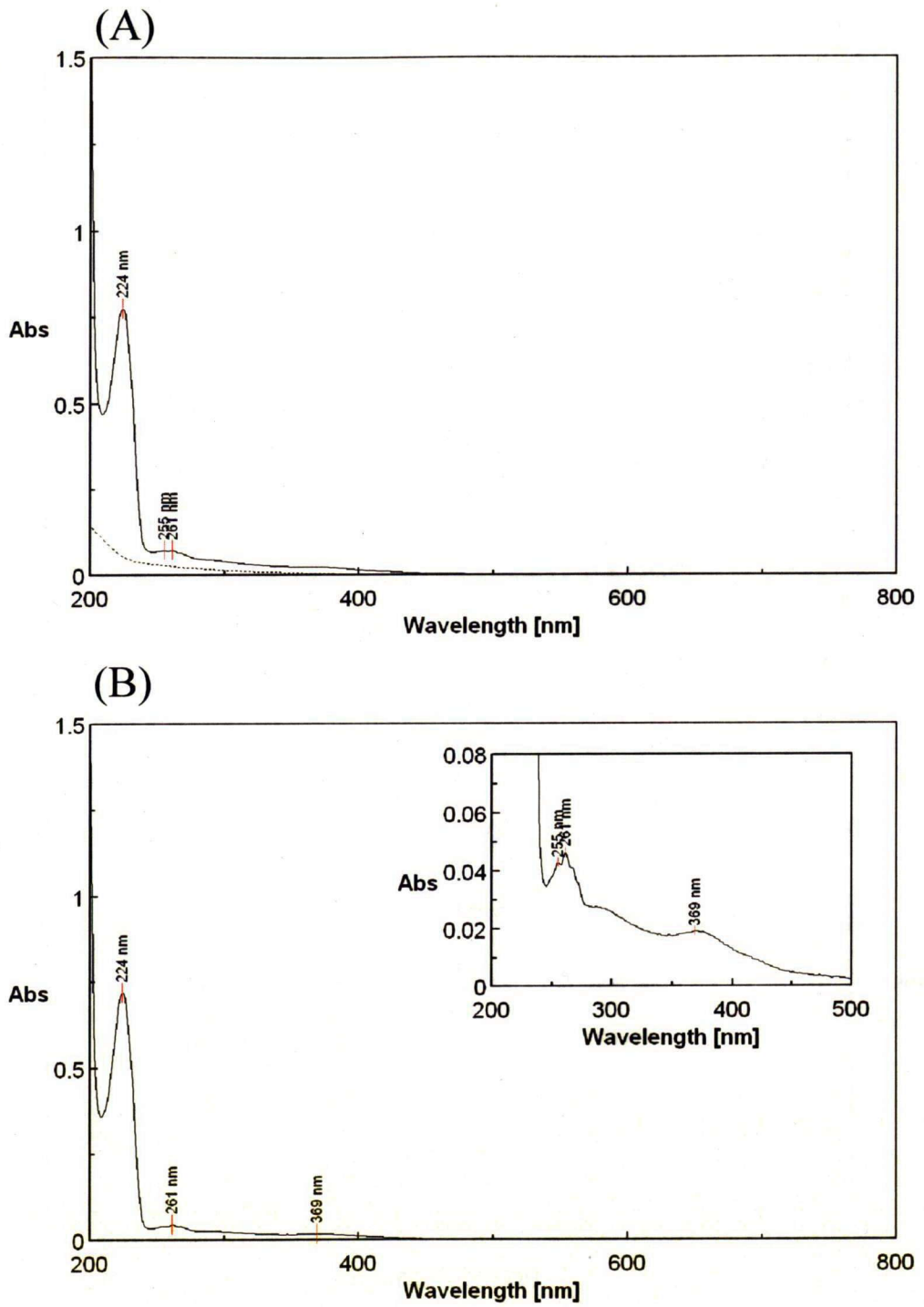

Fig.4.3.2.-1. The UV absorbance spectra of (A) bulk filtrate (dotted line) and filtrate of pore water (straight line) and (B) differential spectra between bulk and pore water filtrate at 25°C in 15 minutes adsorption experiment.

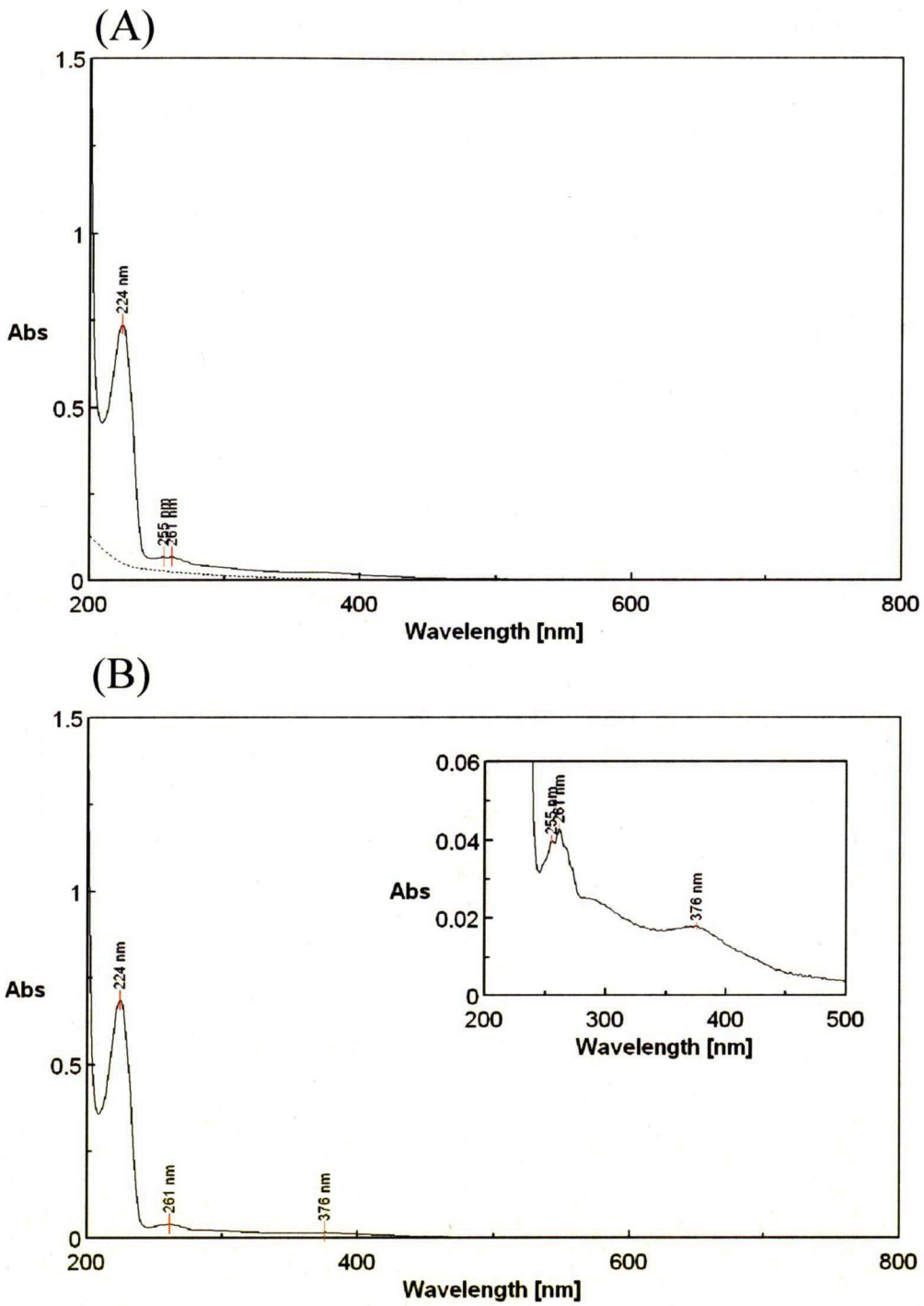

Fig.4.3.2.-2 The UV absorbance spectra of (A) bulk filtrate (dotted line) and filtrate of pore water (straight line) and (B) differential spectra between bulk and pore water filtrate at 25°C in 30 minutes adsorption experiment.

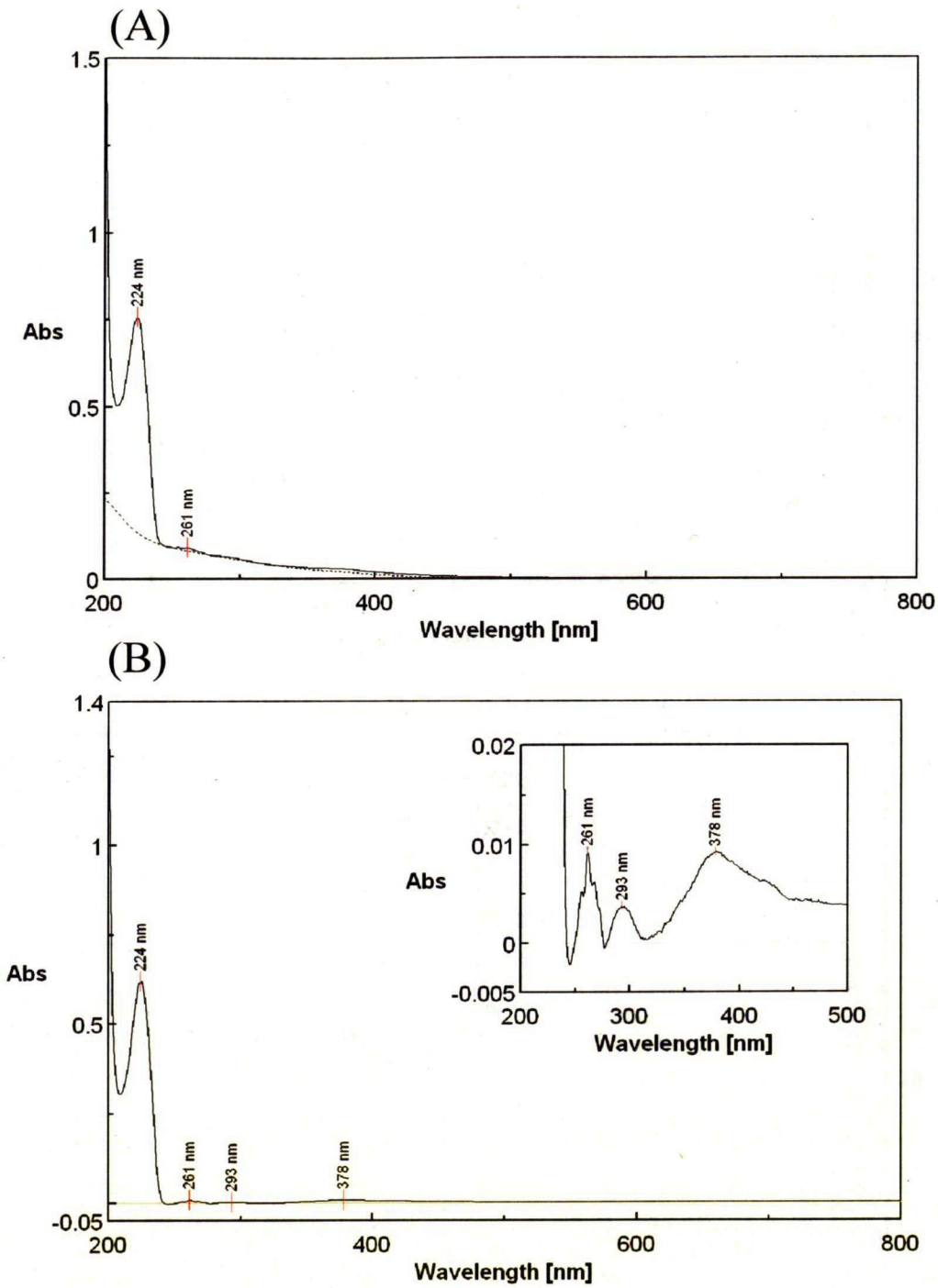

Fig.4.3.2.-3 The UV absorbance spectra of (A) bulk filtrate (dotted line) and filtrate of pore water (straight line) and (B) differential spectra between bulk and pore water filtrate at 25°C in 2 hour adsorption experiment.

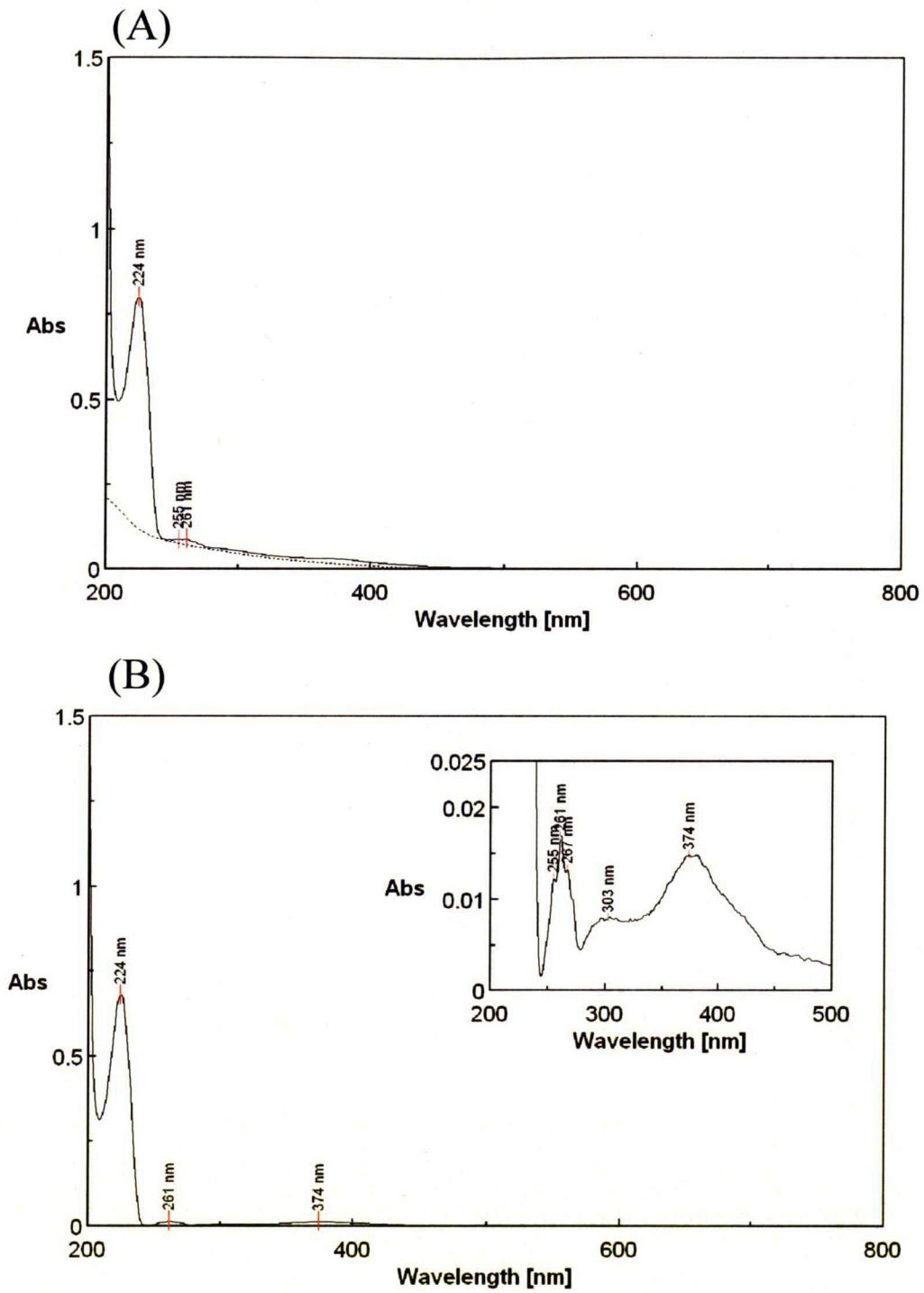

Fig.4.3.2.-4 The UV absorbance spectra of (A) bulk filtrate (dotted line) and filtrate of pore water (straight line) and (B) differential spectra between bulk and pore water filtrate at 25°C in 3 hour adsorption experiment.

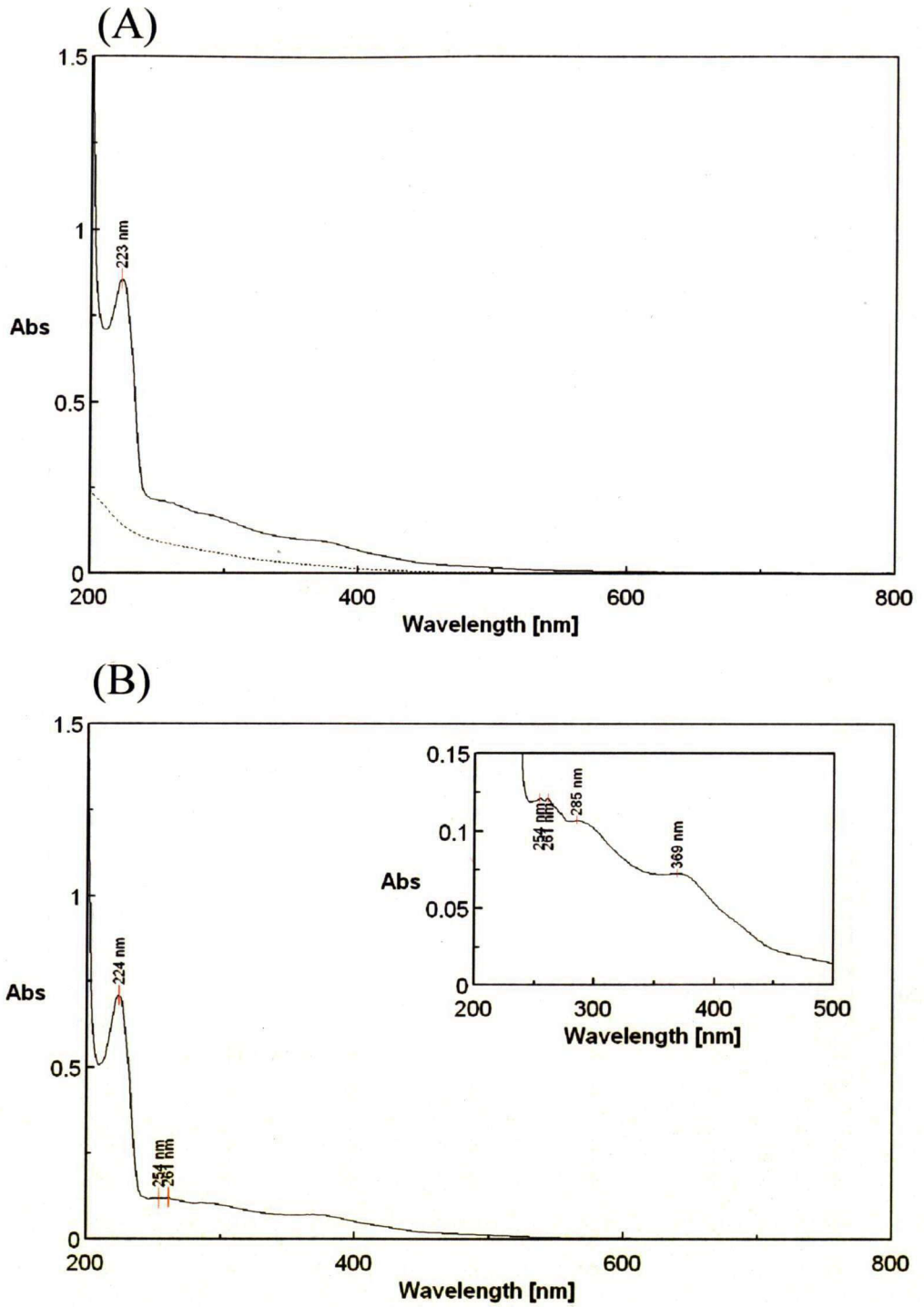

Fig.4.3.2.-5 The UV absorbance spectra of (A) bulk filtrate (dotted line) and filtrate of pore water (straight line) and (B) differential spectra between bulk and pore water filtrate at 25°C in 6 hour adsorption experiment.

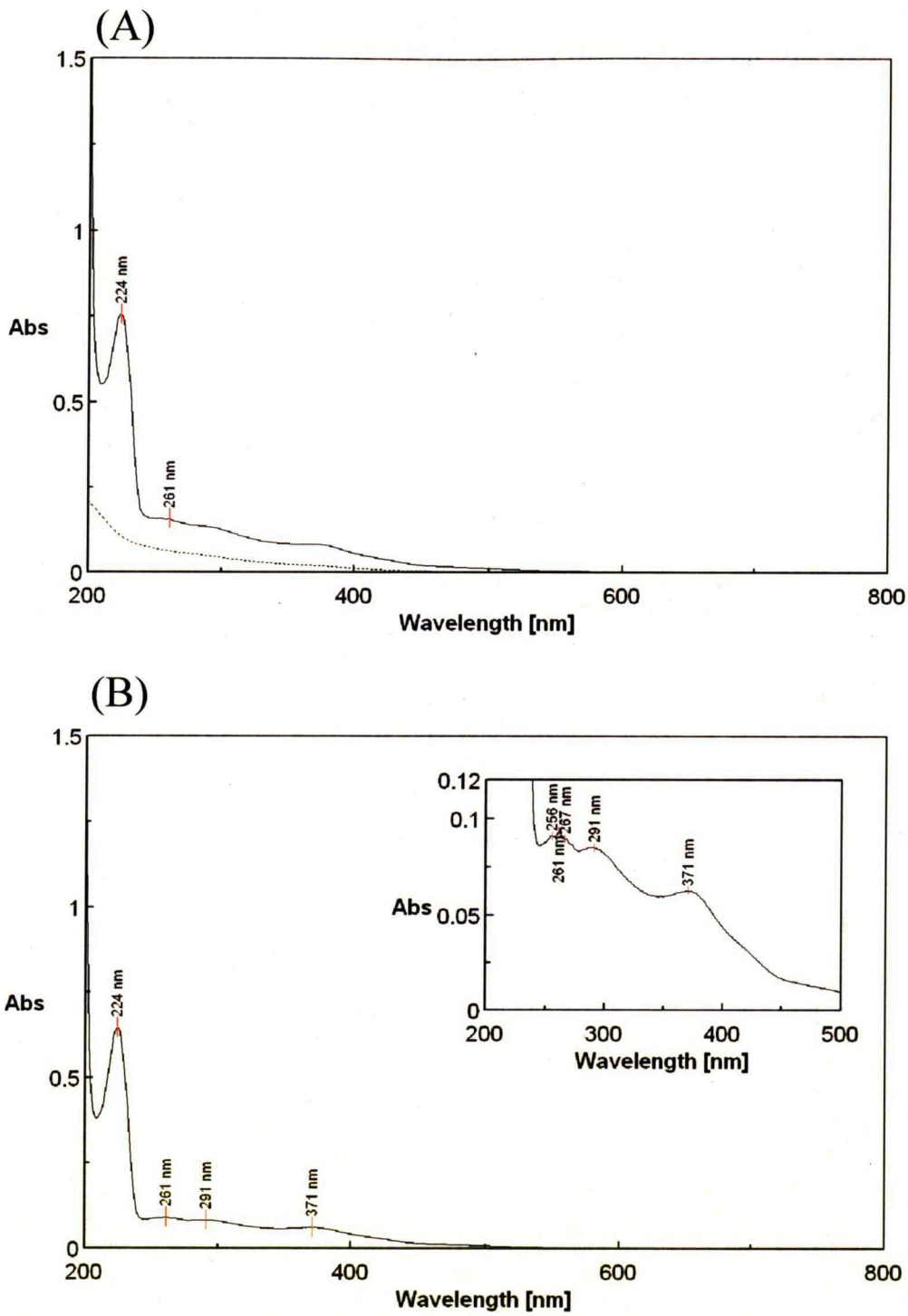

Fig.4.3.2.-6 The UV absorbance spectra of (A) bulk filtrate (dotted line) and filtrate of pore water (straight line) and (B) differential spectra between bulk and pore water filtrate at 25°C in 9 hour adsorption experiment.

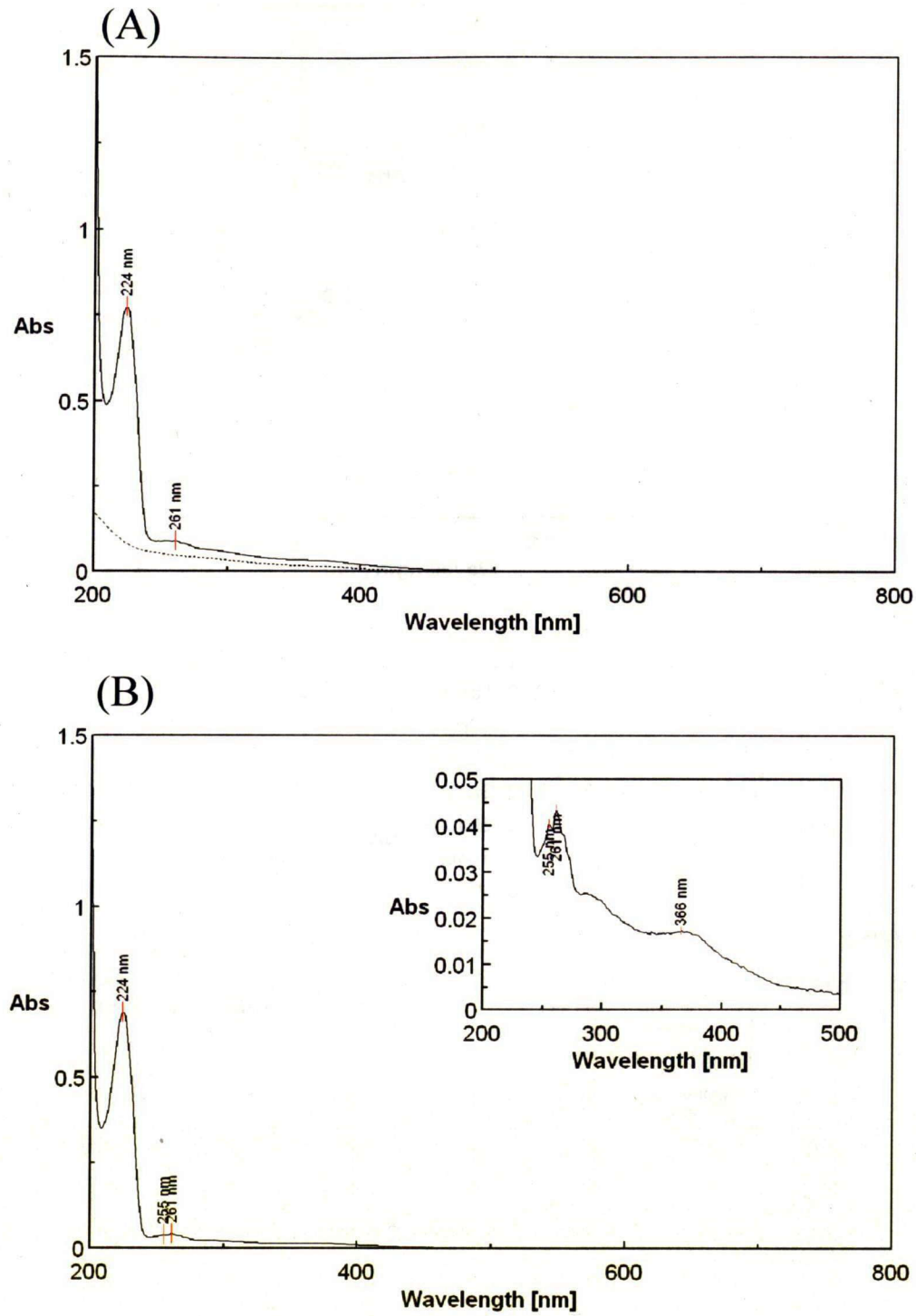

Fig.4.3.2.-7 The UV absorbance spectra of (A) bulk filtrate (dotted line) and filtrate of pore water (straight line) and (B) differential spectra between bulk and pore water filtrate at 25°C in 12 hour adsorption experiment.

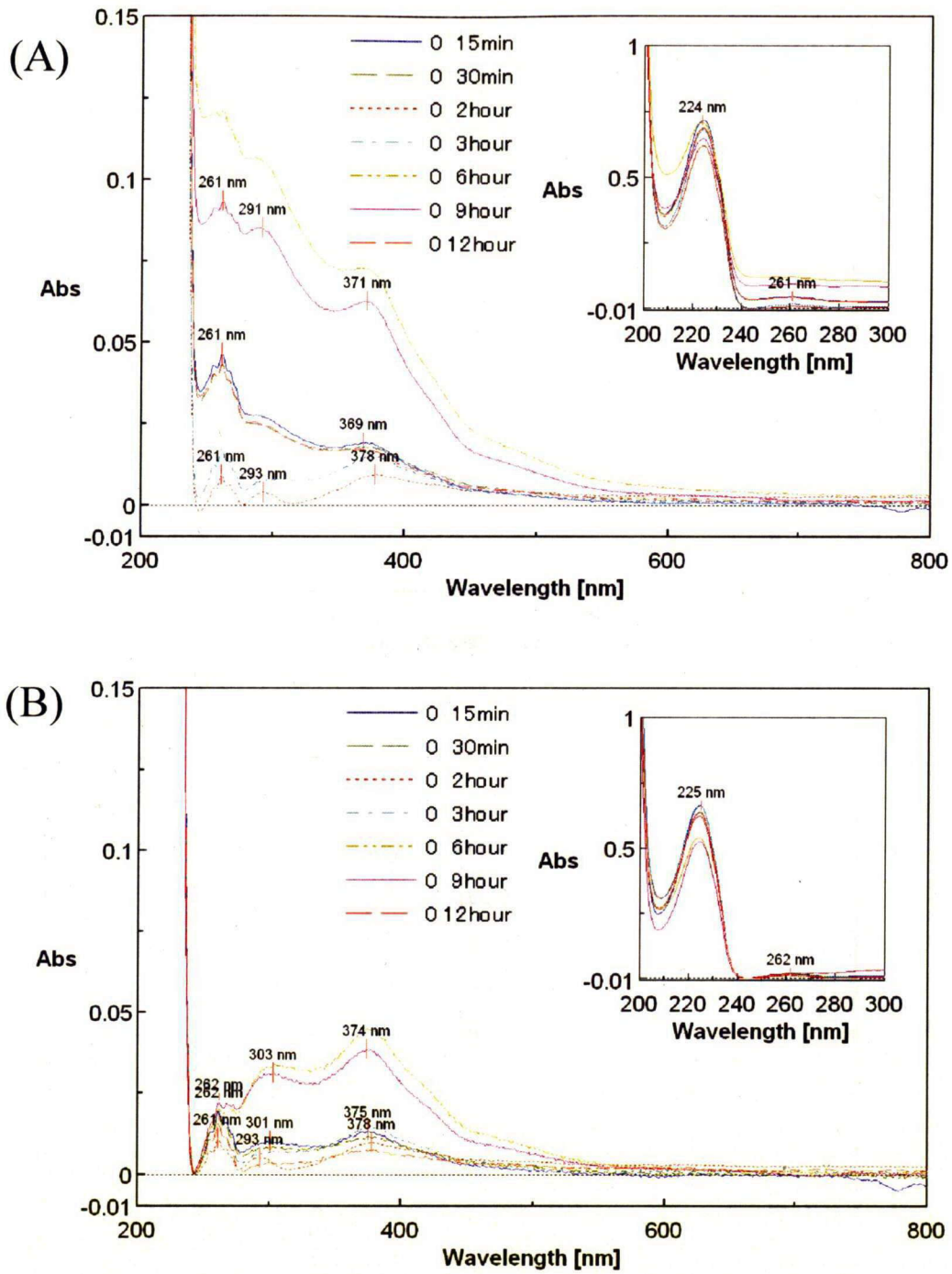

Fig.4.3.3.(A) The UV absorbance difference spectra between bulk filtrate (dotted line) and filtrate of pore water at 25°C in 15 min –12 hour adsorption experiment. (B) The difference spectra corrected to abs = 0 at 245 nm

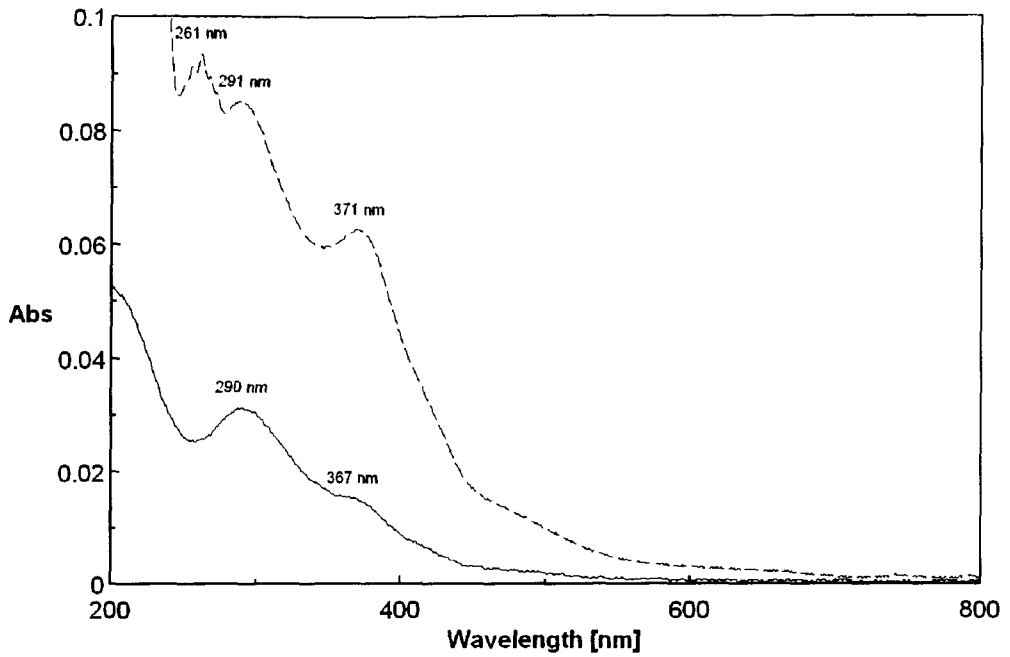

Fig.4.3.4. The UV absorbance spectra of goethite suspension (straight line) and filtrate of pore water (dotted line) at 25°C in 9h adsorption experiment (the same spectra with fig.4.3.2).

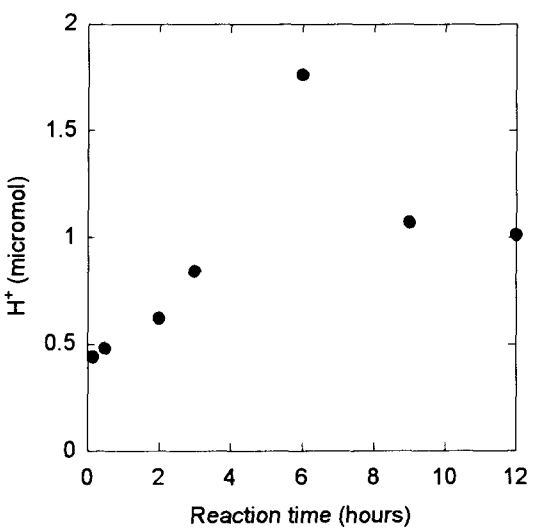

Fig. 4.3.5. The consumed H^+ during the fulvic acid – goethite interactions.

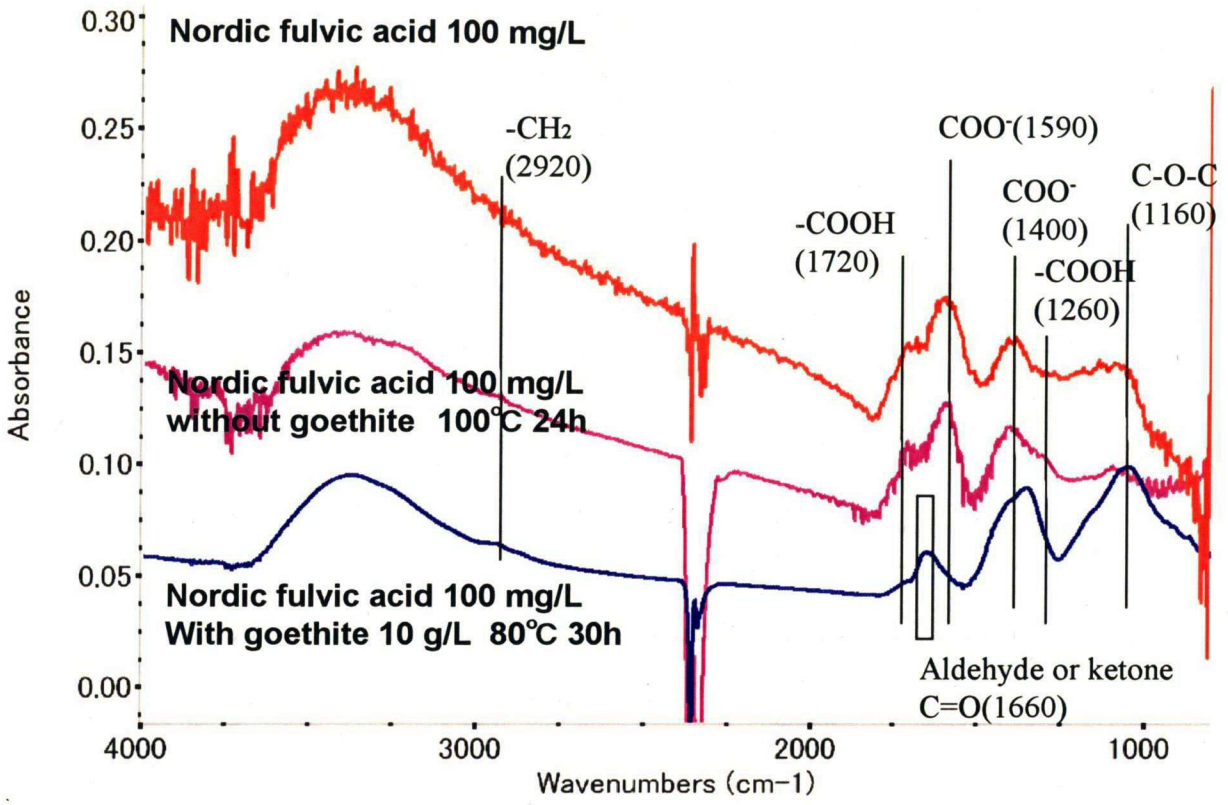

Fig. 4.3.6. FT-IR spectra obtained from the product precipitaions at 100 mg L^{-1} Nordic fulvic acid solution, that of 100 ° C for periods of 24 h in the absence of goethite, and that of at 80 ° C for periods of 30 h in the presence of goethite.

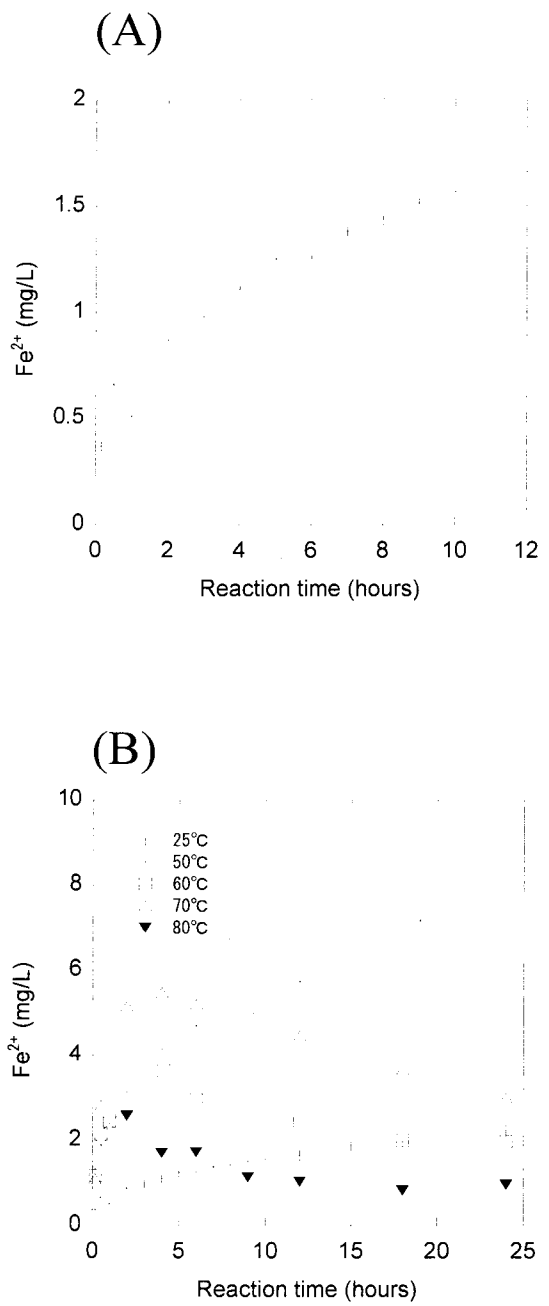

Figure 4.3.7. Changes in the dissolved Fe^{2+} with time (A) at 25°C and (B) at 25-80°C by the ferrozine method

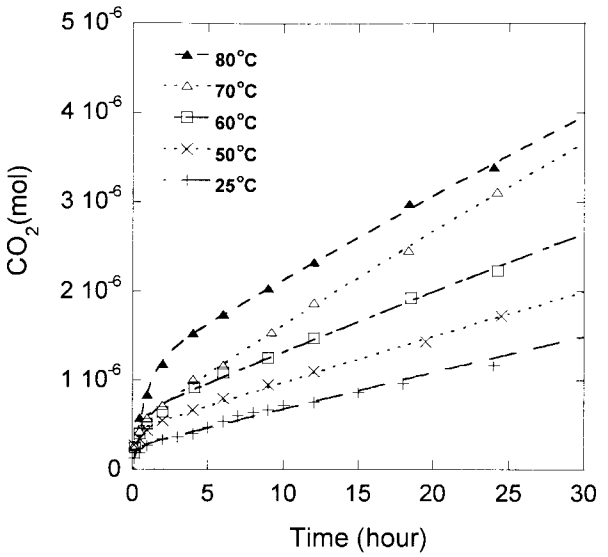

Fig. 4.3.8. Changes with time in CO_2 formation at 25-80°C with goethite by the reaction gas cell FT-IR.

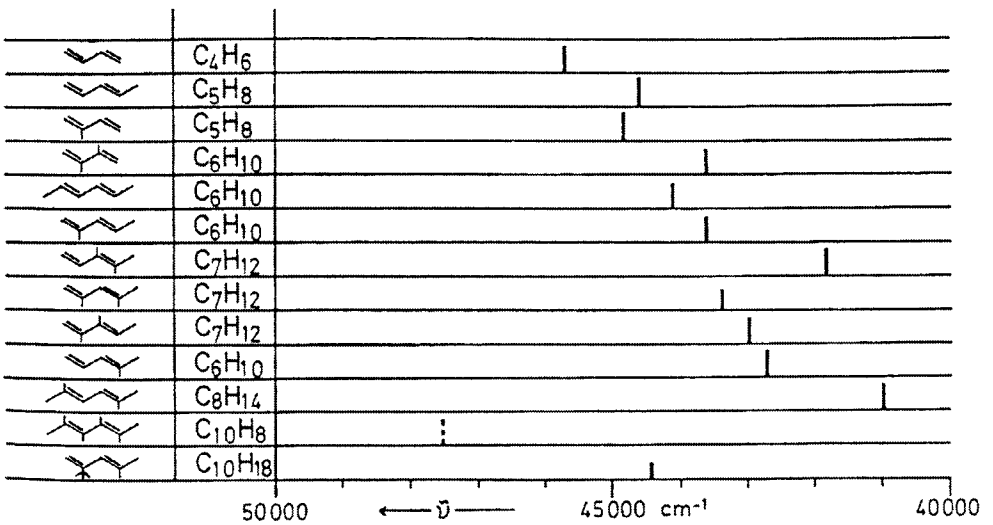

Fig.4.3.9. The effect of alkyl substitution on the main absorption band of buta-1,3-diene (Pestemer M. 1992, Reviews on the schedule groups *In UV-VIS atlas of organic compounds,* ed. Helmut H. figure.1)

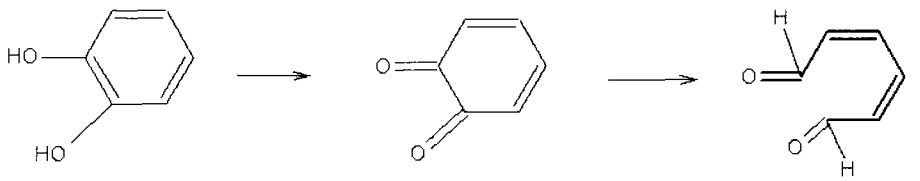

Fig.4.3.10. The estimated structures of the products products from fulvic acid-goethite interaction

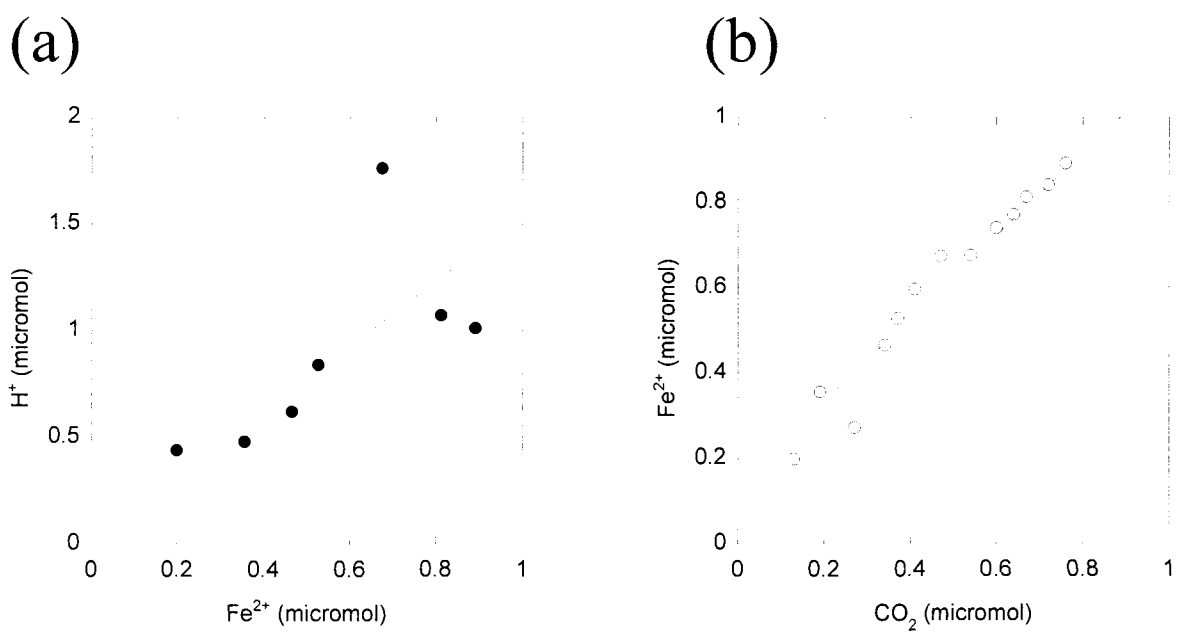

Fig. 4.3.11. The stoichiometric relations during the fulvic acid – goethite interactions.

(a) Relation between consumed H^+ and formed Fe^{2+} close to 2:1, (b) Relation between formed Fe^{2+} and formed CO_2 close to 1:1

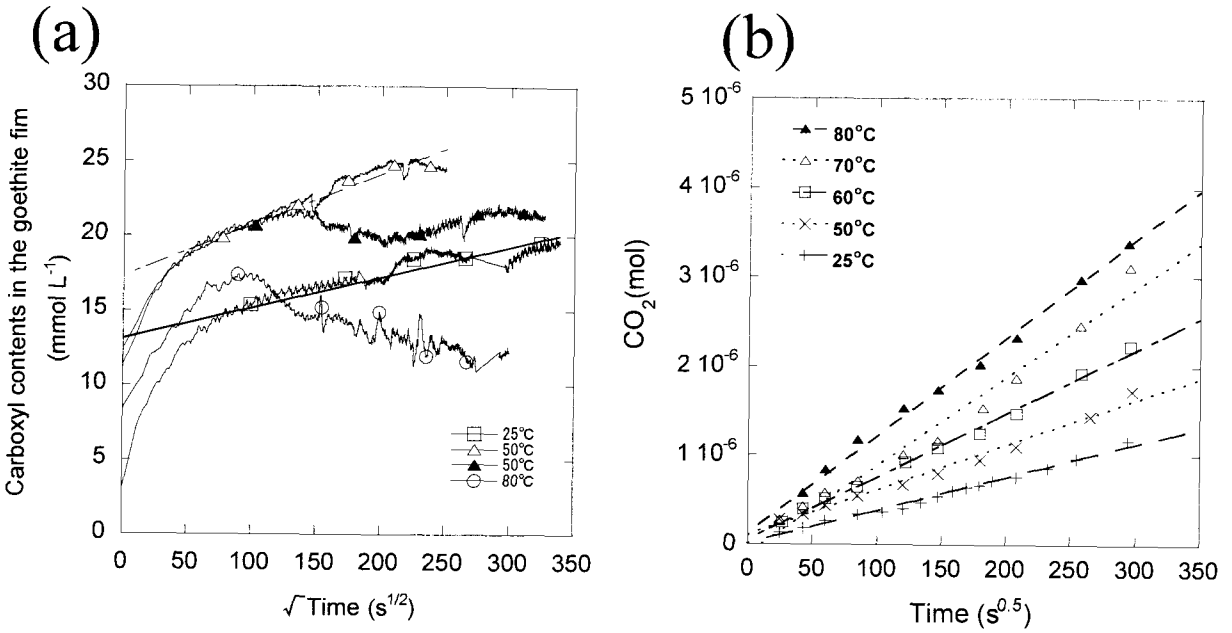

Fig. 4.3.12. Changes with time $t^{1/2}$ in (a) carboxyl contents absorbed on the goethite at 25°C, 50°C and 80°C for 10 min. to 25 hours and (b) CO_2 formation at 25-80°C with goethite by the reaction gas cell FT-IR.

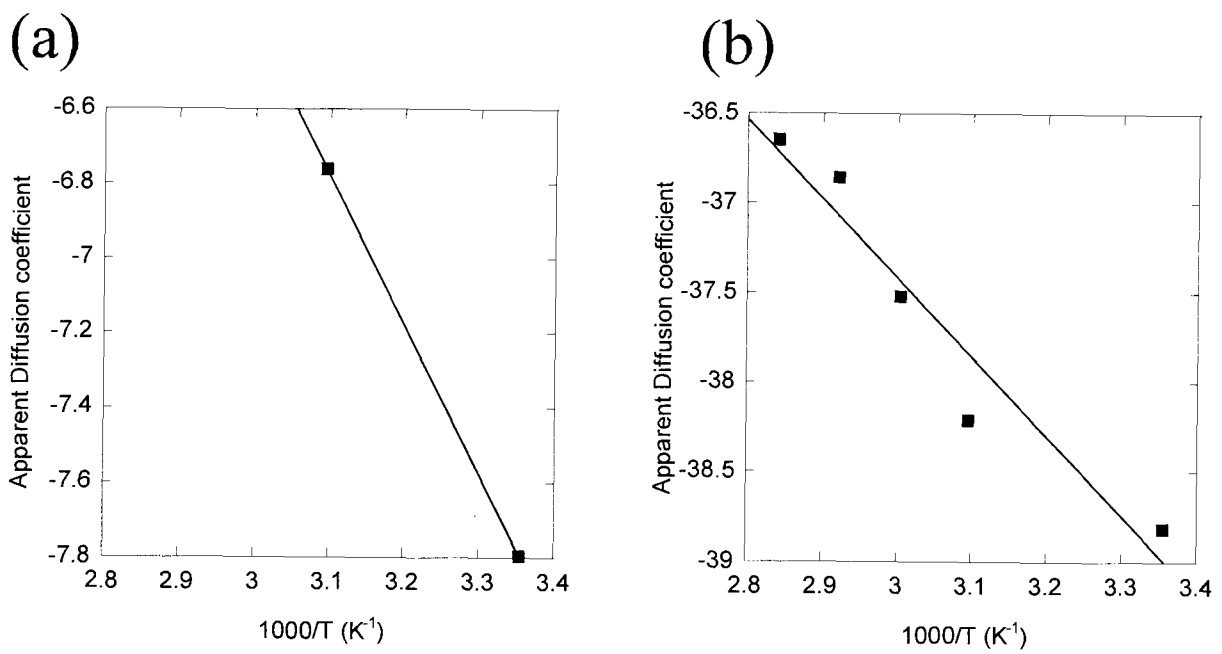

Fig. 4.3.13. The apparent diffusion coefficients as a function of temperature (Arrhenius diagram); (a) the adsorption of the fulvic acid on goethite by ATR-IR spectroscopy and (b) CO_2 formation with goethite by the reaction gas cell FT-IR.

REFERENCES

Artok L. and Schobert H. H. (2000) Reaction of carboxylic acid under coal liquefaction conditions 1. Under nitrogen atmosphere. *Journal of Analytical and Applied Pyrolysis,* **54**, 215-233

Axe L. and Anderson P. R. (1997) Experimental and theoretical diffusivities of Ca and Sr in hydrous ferric oxide, Journal of colloid and interface sciences, **185**, 436-448

Britt P. F., Buchanan III A. C., Eskay T. P. and Mungall W. S. (1999) Mechanistic investigation into the decarboxylation of aromatic carboxylic acids. *Invited Paper for presentation at the American Chemical society National Meeting, New Orleans, LA,*

Boles J. S., Crerar D. A., Grissom G. and Key T. C. (1988) Aqueous thermal degradation of galic acid, *Geochimica et Cosmochimca acta*, **52**, 341-344

Chateauneuf J., Lusztyk J. and Ingold K. U. (1988) Spectroscopic kinetic characteristics of aroyloxyl radicals. 1. The 4-methoxylbenzoyloxyl radical. *Journal of American Chemical Society*, **54**, 2877-2885

Filius J. D., Lumsdon D. G., Meeussen J. C. L., Hiemstra T. and van Riemsduk W. H. (2000). Adsorption of fulvic acid on goethite. *Geochimica et Cosmochimica Acta*, **64**, 51-60.

Gu B., Schmitt J., Chen Z., Liang L. and McCathy J. F. (1994) Adsorption and Desorption of natural organic matter on iron oxide: mechanisms and models. *Environmental Science and Technology*, 28, 38-46.

Hallem M. A., Farrouq K., Hakeem M. A. (1982) Kinetics of the decarboxylation of galic acid in pyrogallol, resorcinol and catechol, Chorover J. and Amistadi M. K. (2001) Reaction of forest floor organic matter at goethite, birnessite and smectite surfaces. *Geochimica et Cosmochimica Acta*, **65**, 95-109.

Kononets M. Yu., Pakhomova S. V., Rozanov A. G. and Proskurnin M. A. (2002) Determination of soluble iron species in seawater using ferrozine. *Journal of Analytical Chemistry*, **57**, 586-589

LaKind J. S. and Stone A. T. (1989) Reductive dissolution of goethite by phenolic reductants. *Geochimica et Cosmochimica Acta*, **53**, 961-971.

Li J. Brill T. B. (2003) Spectroscopy of hydrothermal reaction 23: the effect of OH

substituent on the rates and mechanism of decarboxylation of benzoic acid, *Journal of Physical Chemistry A*, **107**, 2667-2673

Otsuka T. and Nakashima S. (2007) The formation of CO2 by fulvic acid on the surface of goethite studied using ultraviolet and infrared spectroscopy, *Journal of Mineralogical and Petrological Sciences*, **102**, 302-305

Pehkonen S. (1995) Determination of the oxidation states of iron in natural waters. *Analyst*, **120**, 2655-2663

Pestemer M. (1992) Reviews on the schedule groups A. Compounds containing multiply bounded C atoms only, *In UV-VIS atlas of organic compounds,* (ed. Perkampus H-H.) pp.1525 Weinhelm, VCH

Pullin M. J. and Cabaniss S. E. (2001) Colorimetric flow-injection analysis of dissolved iron in high DOC waters. *Water Research*, **35**, 363-372

Pullin M. J. and Cabaniss S. E. (2003) The effect of pH, ionic strength, and iron-fulvic acid interactions on the kinetics of non photochemical iron transformations. II. The kinetics of thermal reduction, *Geochimica et Cosmochimica Acta*, **67**, 4079-4089.

Schoonen M. A. A., Xu Y. and Strongin D. R. (1998) An introduction to geocatalysis, *Journal of Geochemical Exploration, **62**,* 205-215

Stookey L. L. (1970) Ferrozine – A new spectrophotometric reagent for iron. *Analytical Chemistry*, **42**, 779-781

Stumm W. and Morgan J. J. (1996) Aquatic chemistry: chemical equilibria and rates in natural waters, 3rd ed., pp. 1022, New York: Willey

Strawn D. G. and Sceidegger A. M. and Sparks D. L. (1998) Kinetics and mechanisms of Pb(II) sorption and desorption at the aluminum oxide – water interface, Environ Science and Technology, **32**, 2596-2601

Timmons C. J., (1992) Reviews on the schedule groups B. Componds containing C=O and C=S, *In UV-VIS atlas of organic compounds,* (ed. Perkampus H-H.) pp.1525 Weinhelm, VCH

Venyaminov S. Y. and Prendergast F. G. (1997) Water (H2O and D2O) Molar absorptivity in the 1000-4000 cm-1 range and quantitative infrared spectroscopy of aqueous solution, analytical biochemistry, **248**, 234-245

Viollier E., Inglett P. W., Hunter K., Roychou dhury A. N., Van Cappellen P. (2000) The ferrozine method revisited: Fe(II)/Fe(III) determination in natural waters. *Applied Geochemistry*, **15**, 785-79

Zhou Q. Maurice P. A. and Cabaniss S. E. (2001) Size fractionation upon adsorption of fulvic acid on goethite: equilibrium and kinetic studies, *Geochimica et Cosmochimica Acta*, **65**, 803-812.

CHAPTER 5.

SUMMERY AND FUTURE PERSPECTIVES

CHAPTER 5

Dissolved organic carbon (DOC), defined as small organic compounds passing though 0.45μm filter, is widely distributed in natural aquatic environments. The major portion (around 80%) of DOC is dominated by dissolved humic substances, which are high molecular weight organic substances having brownish color with unknown variable chemical structures (Thurman, 1985). Humic substances (HS) have abundant hydrophilic functional groups such as –COOH and –OH that give their aqueous solubility, binding sites for metals, buffer capacities and other reactive characteristics (Stevenson, 1994). Because of their high abundance and reactivities, humic substances contribute primarily to the material cycling at the earth's surface. Therefore, long-term behaviors of HS in aquatic environments should be evaluated.

In this thesis, for studying reaction kinetics of organics by accelerating them at higher temperatures, several spectroscopic methods under hydrothermal conditions have been first developed (Chapter 2). By using these spectroscopic methods, hydrothermal transformations of humic substances (Nordic fulvic and humic acids) were studied (Chapter 3). Then interactions of these organics with an iron oxide (goethite) have been studied (Chapter 4). Finally, mechanisms and kinetics of these organic-inorganic interactions were discussed.

5.1. Developments of spectroscopic methods for monitoring hydrothermal aqueous organic reactions

In order to understand organic-inorganic interactions between dissolved organic substances and minerals in earth's aquatic environments, new spectroscopic monitoring methods were developed here for studying hydrothermal organic reactions. Recently, *in-situ* techniques for aqueous reactions have been developed enabling the kinetic tracing of reaction progress (Brill and Savage, 2004 Masuda, 2005). By applying these in-situ methods, numerous data can be acquired and detailed kinetic analyses became possible. In this chapter, three hydrothermal spectroscopic methods were developed: 1) Gas cell FT-IR for the analyses of emitted volatile compounds; 2) UV-VIS spectroscopy for the

determination of organic contents and aromatic natures; and 3) ATR-IR spectroscopy for the characterization of functional groups.

Gas cell FT-IR connected to a hydrothermal reaction vessel can be a new method for analyzing gaseous products formed during the hydrothermal transformation of dissolved organic substances, since FT-IR has been applied to trace gas analysis (Hanst et al. 1973). The reaction gas cell FT-IR system was constructed by combining a gas cell FT-IR (Bomem MB154) with a reaction vessel (Fig.5.1.1). A steel-lined PTFE (Teflon) reaction vessel was directly connected to a long path gas cell (10 m path length) placed in the FT-IR. A continuous measurement of volatile compounds formed in the hydrothermal reaction vessel was conducted by using this reaction gas cell FT-IR system equipped with nitrogen purge system and gas filter. The gas bubbling tube was inserted into the bottom of PTFE inner bottle in the vessel. Gaseous products during the hydrothermal reactions were introduced by bubbling of the nitrogen gas to the long path gas cell FT-IR to measure their IR spectra. For introducing sample solutions and for sampling products during the hydrothermal experiments, a plastic syringe is connected to this system (Fig. 5.1.1). The formation of CO_2 by the interactions of a fulvic acid and an iron oxide could be detected by this system.

In-situ UV-VIS spectroscopy was applied here to monitor contents and natures of dissolved organic compounds during hydrothermal reactions. Because of its high sensitivities to the trace concentrations of organic compounds mainly in the ultraviolet (UV) range, UV-VIS spectroscopy is an effective tool for monitoring aqueous organic reactions. In the present study, we have developped a real time UV-VIS spectroscopy system by using a static hydrothermal reaction cell up to 200 °C (Fig.5.1.2). The interactions between a fulvic acid and an iron oxide could be successfully monitored by this system.

Attenuated total reflection infrared (ATR-IR) spectroscopy is very useful in characterizing organic functional groups of dissolved organic compounds in solutions. This method use the penetration of evanescent waves less than about 1 micrometer at the total reflection of IR beam at the interface between a prism (ATR crystal) and liquid sample

(Harrick, 1966). In this study, for monitoring reactions on the surface of goethite, the goethite film is prepared on the flat ATR crystal by drying the goethite suspension. By using this ATR-IR cell with the hydrothermal flow-through system, hydrothermal transformation of organic compounds with time and temperature on the surface of goethite could be investigated (Fig.5.1.3).

5.2. Hydrothermal transformation of the fulvic acid

In this chapter, hydrothermal heating experiments of dissolved humic substances have been conducted with particular attentions to their functional groups. Volatile compounds formed during these processes have also been studied.

Firstly, before the transformation experiments, Nordic fulvic acid and humic acid as representative dissolved humic substances were characterized by various methods including UV-VIS and IR spectroscopy. The UV spectra of fulvic and humic acids show featherless absorptions toward UV region, while three dimensional fluorescence spectroscopy shows characteristic fluorescence peaks around 440 nm with excitation of 310 nm. ATR-IR spectra of the fulvic acid indicates abundant carboxyl groups in the functional groups.

Secondary, hydrothermal transformation experiments of the fulvic acid solution were conducted at 80-180 °C during 0-100 or 0-600 hours. The decreases in brownish color (monitored by UV absorbance at 254 nm: Abs_{254}, which is proportional to the concentration of humic substances) were observed in all the experiments (Fig 5.2.1). The decreases curves of Abs_{254} with time were simulated by the first order reactions giving their rate constants: $k^{UV} = 4.8 \times 10^{-8}$ s^{-1} at 80 °C, 1.1×10^{-7} s^{-1} at 100 °C, 1.2×10^{-6} s^{-1} at 120 °C, 3.2×10^{-6} s^{-1} at 140 °C, 1.0×10^{-5} s^{-1} at 160 °C and 2.1×10^{-5} s^{-1} at 180 °C. The apparent activation energy for this first order Abs_{254} decrease is 85 kJ mol^{-1} (Fig 5.2.2). Since this Abs_{254} generally reflects concentrations of substituted aromatic structure (benzene) with functional groups, the Abs_{254} decrease can be due to the decarboxylation from aromatic structures.

During the Abs_{254} decrease, pHs changed slightly to acidic conditions and, organic

carbon contents decreased. Fluorescence spectroscopy showed the decrease in aromaticity of organics at higher temperatures with the apparent activation energy of 76 kJ mol^{-1} (Fig 5.2.2). This aromaticity decrease can be explained by the aromatic ring opening and subsequent decarboxylation might have resulted in the Abs_{254} decrease.

The emission of carbon dioxide during the hydrothermal transformation of the fulvic acid were observed by the reaction gas cell FT-IR. However, the amounts of formed CO_2 were smaller than the contents of carboxyl groups in the humic substance, and the CO_2 emission rate is faster than the Abs_{254} decrease rates.

Thirdly, in order to understand initial stages of the above complex reactions, *in-situ* UV-VIS spectroscopy combined with the measurement of CO_2 emission monitored by gas cell FT-IR were conducted under hydrothermal conditions. In-situ UV monitoring shows dynamic decreases of Abs_{254} at initial stages with the first order rate constats: $k^{uv} = 1.6 \times 10^{-7}$ s^{-1} at 25 °C, 1.0×10^{-6} s^{-1} at 80 °C, 1.4×10^{-6} s^{-1} at 100 °C, 2.4×10^{-6} s^{-1} at 120 °C, 5.0×10^{-6} s^{-1} at 140 °C, 9.0×10^{-6} s^{-1} at 160 °C, 4.5×10^{-5} s^{-1} at 180 °C by fitting the data of first 10% decrease of Abs_{254} and/or until 10 hours with linear trends (Fig 5.2.3). The activation energy for this initial Abs_{254} decrease is determined to be 29 kJ mol^{-1} (Fig 5.2.5).

On the other hand, the CO_2 formation rate was determined to be $k_0^{CO2} = 3.2 \times 10^{-7}$ s^{-1} at 25 °C, 6.1×10^{-7} s^{-1} at 50 °C, 1.2×10^{-6} s^{-1} at 80 °C, 1.8×10^{-6} s^{-1} at 100 °C, 2.4×10^{-6} s^{-1} at 120 °C, 3.7×10^{-6} s^{-1} at 140 °C, by assuming that the maximum CO_2 formation is limited by the initial carboxylic content of the fulvic acid (Fig 5.2.4). The activation energy for the CO_2 formation is calculated to be 22 kJ mol^{-1} (Fig 5.2.5). The CO_2 formation rate from the fulvic acid is on the same order as the above initial rate of the Abs_{254} decrease. This indicates that CO_2 formation mechanism might be related to the decrease of 254 nm absorbance of the fulvic acid. The small values of activation energies for these two processes (29 and 22 kJ/mol) indicated that the rate-limiting step for these processes can be attributed to the decarboxylation reaction.

5.3. Hydrothermal reaction of fulvic acid and goethite

Common dissolved organic compounds in the environment such as fulvic acids generally co-exist with iron oxides in natural environments (Maranger and Pullin, 2003). Fulvic acids and iron oxides are known to interact each other. Fulvic acids are often adsorbed on oxide minerals such as goethite (Gu et al, 1994; Filius et al, 2000; Zhou et al, 2001) and ferric iron are reduced to ferrous iron (LaKind and Stone, 1989; Chorover and Amistadi, 2001; Pullin and Cabaniss, 2003). In other words, iron oxides can adsorb and oxidize fulvic acids in natural environments. These interactions, sometimes called as geocatalysis, are important for transformation of humic substances and kerogen by lowering high activation energies of redox reactions (Schoonen et al, 1998). In this chapter, adsorption and transformation of a fulvic acid on the surface of goethite were investigated.

Firstly, adsorption experiments of a fulvic acid on a representative iron hydroxides, goethite, have been conducted. The adsorption experiments were conducted in both batch and in-situ methods. The adsorbed fulvic acid on the surface of goethite were monitored by by 254 nm absorbance in UV-VIS spectroscopy. The batch experimental results showed that the adsorption process was very fast within several hours. In order to study the fast adsorption process, two types of in-situ observation methods were employed here by using UV-VIS spectroscopy (Fig. 5.3.1a) and ATR-IR spectroscopy (Fig. 5.3.2a). By using these in-situ spectroscopic methods, two adsorption processes were observed with their rates on the order of 10^{-3} and 10^{-4} s^{-1}, respectively.

Secondary, a hydrothermal reaction vessel was connected to a long-path gas cell FT-IR spectrometer to monitor volatile compounds formed on heating the fulvic acid at 80 °C. Carbon dioxide formed gradually with time from the fulvic acid solution in the absence of goethite ($k_0^{CO2} = 1.5 \times 10^{-6}$ s^{-1}) (Fig. 5.3.1b). On the other hand, the formation of CO_2 in the presence of goethite occurred via two first-order reactions. The initial first-order rate constant of CO_2 formation from fulvic acid in the presence of goethite ($k_1^{CO2} = 3.2 \times 10^{-4}$ s^{-1}) had the same magnitude as the decrease in absorbance at 254 nm (Fig. 5.3.1a). The second rate constant of CO_2 formation ($k_2^{CO2} = 1.8 \times 10^{-6}$ s^{-1}) had the same magnitude as CO_2 formation in the absence of goethite. These results suggest that the

formation of CO_2 from the fulvic acid is greatly accelerated by the presence of goethite, possibly through the adsorption of the fulvic acid on the goethite surface with subsequent redox reactions forming CO_2.

These experiments suggest that the fulvic acid is supposed to be decomposed and finally oxidized to CO_2 on the goethite surface (Otsuka and Nakashima, 2007). However mechanisms and rates of CO_2 formation on goethite were not clear. In order to investigate the formation process of CO_2 from the fulvic acid in the presence of goethite, detailed analyses of interaction experiments have been conducted. Two-step filtrate separations, from the bulk solution and pore water were employed here to identify dissolved products and to determine the reaction environment. In addition to above chapters, which analyzed gaseous compounds and adsorption behavior, dissolved ferrous ion, pH and UV absorption bands were investigated. The analysis of pore water filtrate showed higher pH (around 7) than the bulk solution (around pH 4). UV spectra of solution products showed absorption bands at 224 nm and 261 nm, which can be due to alkyl substituted diene and non-conjugated aldehyde, respectively. Based on the above results, the reaction scheme can be estimated as follows with the obtained stoichiometric relations (Fig.5.3.3):

$$FeOOH + RCOO^- + 2H^+ \rightarrow Fe^{2+} + R\cdot + H_2O + HCO_3^-$$

HCO_3^- is considered to be formed in micro pore environments in the near neutral medium (pH 7) on the goethite surface by the above reaction. The formed HCO_3^- can then diffuse into the bulk solution (pH 4), where the hydrogen carbonate anion becomes unstable to liberate CO_2:

$$HCO_3^- \Leftrightarrow CO_2 + OH^-$$

By using the above spectroscopic methods, the adsorption and transformation of the fulvic acid on the surface of goethite include two adsorption processes (very fast and fast; 26 and 32 kJ mol^{-1}) with their rates on the order of 10^{-3} and 10^{-4} s^{-1} and CO_2 formation process (30 kJ mol^{-1}) with the rate on order of 10^{-4} s^{-1} (Fig 5.3.4). The CO_2 formation may

be correlated with the second adsorption process possibly through the above diffusion process of hydrogen carbonate anion from the micropores in goethite to the bulk solution with subsequent CO_2 formation from the hydrogen carbonate.

5.4. Time scales of fulvic acid transformation in the aquatic environments

Humic substances in various environments (ex. soils, sediments and natural waters) have the following common characteristics; an extreme complexity of molecular structure, an abundance and wide array of acidic functional groups, an ability to form complexes with metal ions and to bind small organic compounds, an ability to fluoresce, and, a refractory nature to microbial decay (Malcolm, 1990).

The refractory nature of humic substances has been studied from the results of isotope chronology (^{14}C dating of soil) and various degradation experiments: ^{14}C-labeled study and gravimetric analysis in field experiments and microbial, photochemical and thermal degradation studies in laboratory experiments.

The ^{14}C dating methods are suitable for accurate age estimates from several hundred years to around 50,000 years. Of course, absolute ages for organic matter in soils cannot be determined by this method. The term "mean residence time" has been used to express the results of ^{14}C measurements for the average age of humic substance (Campbell, 1967; Hsieh, 1992). Stevenson (1994) summarized that the mean residence time of organic matter in typical soils have been reported as several hundred years with considerable variation (250 to 1900 years). These studies suggest that most fractions of humic substances do not decompose during several hundreds or thousands of years.

The ^{14}C dating has been also applied by using enriched ^{14}C, originated from bomb radiocarbon in 1950s - 60s, as a tracer for movement and turnover of organic C in soils (O'Brien and Stout, 1978). The ^{14}C enrichment layer in soil was located at dozen centimeters below the surface (Koarashi et al., 2004). This means that the enrichment layer has accumulated during 40 - 50 years. On the other hand, the distribution of carbon in soils shows that 60% of soil carbon exists within 4 cm below the surface, which was consisted of litter fraction (O horizon) and mineral upper soil (A horizon) (Koarashi et al., 2005).

These findings suggest that soil organic carbon (including humic substances) can decompose in a few decades.

Some researchers experimentally examined degradation of carbon in crop residues by using ^{14}C-labeled plants (Jenkinson, 1966; Shields and Paul, 1973) and in plant litter by gravimetric analysis (Berg et al., 1982; Berg and McClaugherty, 2003). These results showed that over half of carbon decomposed after the first year and one-half of the residual C was still present in the soil after a four-year period. These studies indicated that biomaterial easily degraded within a year and residual C becomes increasingly resistant to decomposition.

Comparing to these previous studies, I have investigated degradation rates of humic substances (fulvic acid) by means of kinetic experiments at higher temperatures under hydrothermal conditions for accelerating the reaction rates. Four types of reactions were observed under hydrothermal conditions with or without iron oxide; 1) aromaticity decrease (Chapter 3.2), 2) decarboxylation leading to CO_2 formation (chapter 3.3), 3) adsorption on iron oxide (Chapter 4.1) and 4) iron oxide induced CO_2 formation (Chapter 4.2 and 4.3). By using obtained rate constants plotted on the Arrhenius diagram, I will try to evaluate time scales of these reactions (Fig.5.4.1).

I introduce here the "half-life"of the above interactions as their typical time-scales. The half-life ($t_{1/2}$) is the time required to decrease the concentration of starting material A to the half of its initial value. Using the half-life, the rate equation can be written as:

$$\ln \frac{[A]}{[A]_0} = \ln \frac{1}{2} = -kt_{1/2}$$

Then,

$$t_{1/2} = \frac{0.693}{k}$$

The rate constants obtained under hydrothermal conditions in this study can be extrapolated to lower temperatures at the earth's surface by the Arrhenius equation:

$$k = \mathrm{A} \exp(\frac{E_a}{RT})$$

The rate constants k obtained by the extrapolation to ambient temperature (25°C) can be

converted to the half-life values ($t_{1/2}$) for evaluating the time scales of these processes.

Firstly, the long-term decrease of absorbance at 254 nm (Abs_{254}) of dissolved humic substances in the batch hydrothermal experiments (80% decrease of Abs_{254} during several hundreds of hours at 80-180 °C) corresponds mainly to the aromaticity decrease of humic structures with a relatively high activation energy of 85 kJ mol^{-1}(Fig.5.4.1). The extrapolation of this major humic decomposition to 25°C yields the half-life of about 100 years.

Secondly, the rapid initial Abs_{254} decrease of about 10% during 1-10 hours at 80-180 °C, observed by the in-situ UV spectroscopy with a low activation energy of 29 kJ mol^{-1}(Fig.5.4.1), corresponds to the decarboxylation reaction leading to the CO_2 formation detected by the reaction gas cell FT-IR. The half-life of this decarboxylation-CO_2 formation of humic substances at 25°C is estimated to be about several tens of days around 1 month.

Other two fast reactions occurred when a humic substance (fulvic acid) co-existed with goethite in aqueous environments. The first process is the very rapid adsorption of the fulvic acid on goethite within 10 minutes at 25-80 °C (activation energy: 26 kJ mol^{-1}) and the second one is its slower adsorption (activation energy: 30 kJ mol^{-1}). The second adsorption process has similar rates and activation energy to the enhanced CO_2 formation from the fulvic acid in the presence of goethite (activation energy: 32 kJ mol^{-1}). By extrapolating these rates to lower temperatures, the half-lives at 25°C of these interactions are around 10 minutes for the initial fast adsorption and around 10 hours for the CO2 formation induced by goethite.

The obtained half-lives at 25°C of transformation of the fulvic acid (enhanced CO_2 formation by goethite: 10 hours, decarboxylation leading to CO_2 formation: 1 month and major decomposition mainly by aromaticity decrease: 100 years) are much faster than the age estimates from the ^{14}C dating (several hundred years). Since the ^{14}C dating method can observe only residual carbon, these half-lives might be for the most refractory components persisting after the degrdation of labile components to low molecular weight components including CO_2, which are lost from the system.

The results of this thesis suggest that some parts of humic substances are easily decomposable, especially for their reactive functional groups such as carboxyls, with very short half-lives. Since these reactive groups are important binding sites for environmental pollutants such as heavy metals, their instability, especially in the presence of goethite, should be considered for re-evaluating fate and long-term behavior of environmental pollutants and CO_2 formation.

5.5. Future perspectives

The aromaticity decrease and decarboxylation from carboxyls of the fulvic acid studied here can be applied to most of humic substances in the environment which have aromatic structures and carboxyl groups. However, other types of transformations might exist for different functional groups. For example, the hydrolysis of methoxy group can occur for lignin-derived humic substances.

Moreover, the interaction of humic substances with minerals might not be limited to the adsorption of the fulvic acid to goethite and the enhanced CO_2 formation observed in this study. Other types of interactions can be present with other minerals, especially other redox processes than CO_2 formation. The mineral surfaces are considered to provide not only the adsorption and electron transfer sites but also the different pH media for organic-inorganic interactions.

Therefore, much more systematic studies are needed for different types of humic substances and various minerals. These abiotic interaction mechanisms and rates should also be compared with bacterial and photolytic degradation processes.

All these kinetic studies on the organic-inorganic interactions may lead to better understanding of the whole system of carbon cycle at the earth's surface environment.

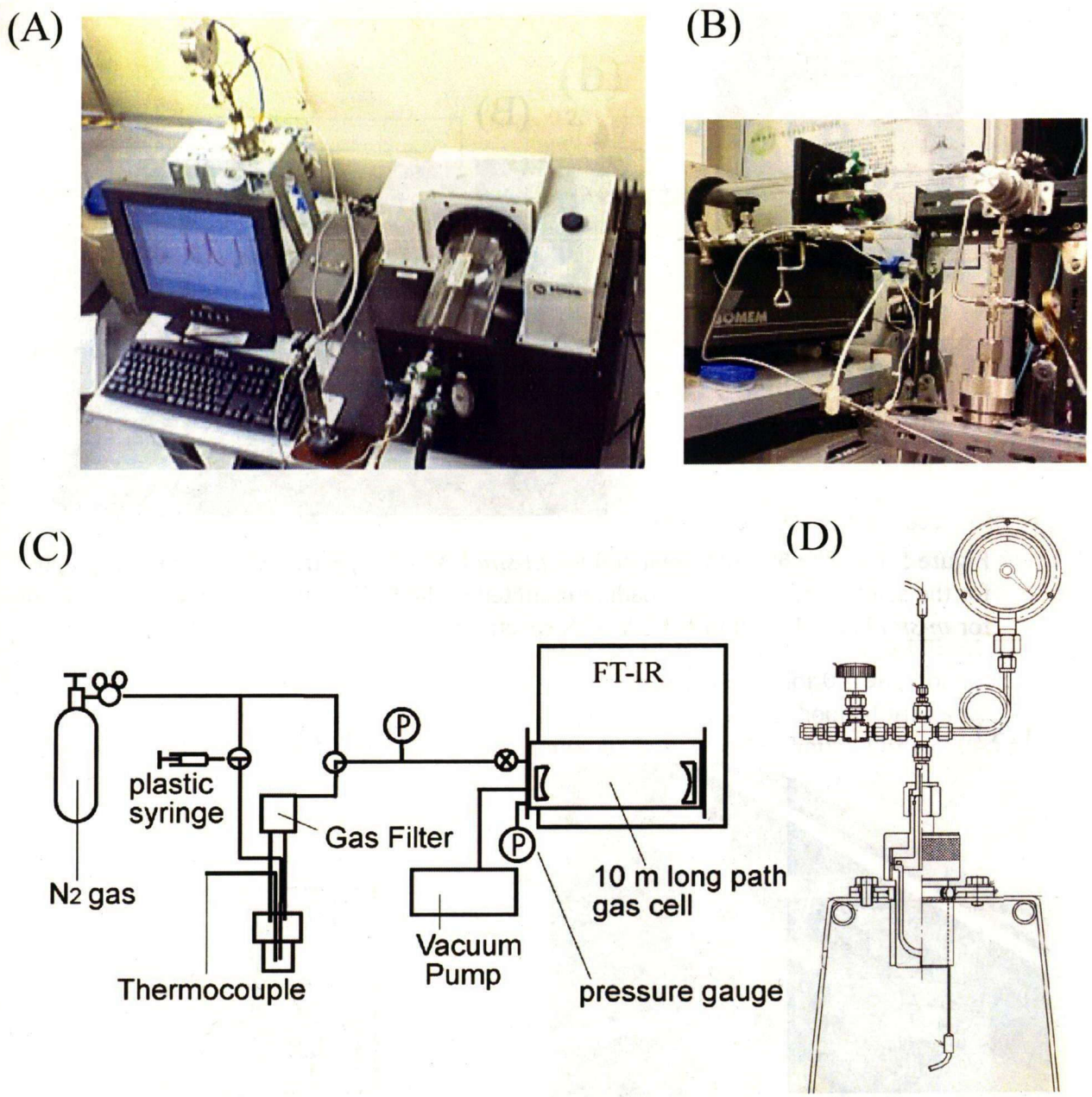

Figure 5.1.1. The reaction gas cell FT-IR system. (A) Photograph for the whole system, (B) Photograph for the connection parts between the hydrothermal reaction vessel and the 10 m long path gas cell FT-IR (Bomem MB154), (C) Schematic configuration of the whole system, and (D) Schematic configuration of the steel-lined PTFE (Teflon) hydrothermal reaction vessel.

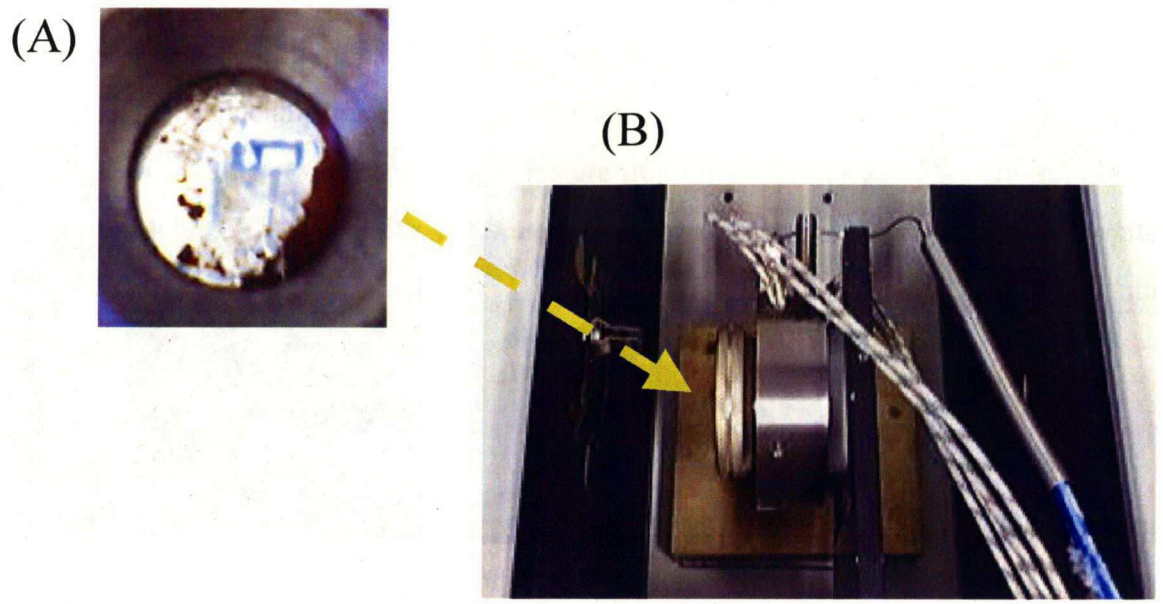

Figure 5.1.2. The hydrothermal cell for *in-situ* UV-VIS spectroscopy. (A) Photograph for the solution sample with goethite mounted in the CaF_2 windows and (**B**) Photograph for *in-situ* UV-VIS cell in the UV-VIS spectrometer

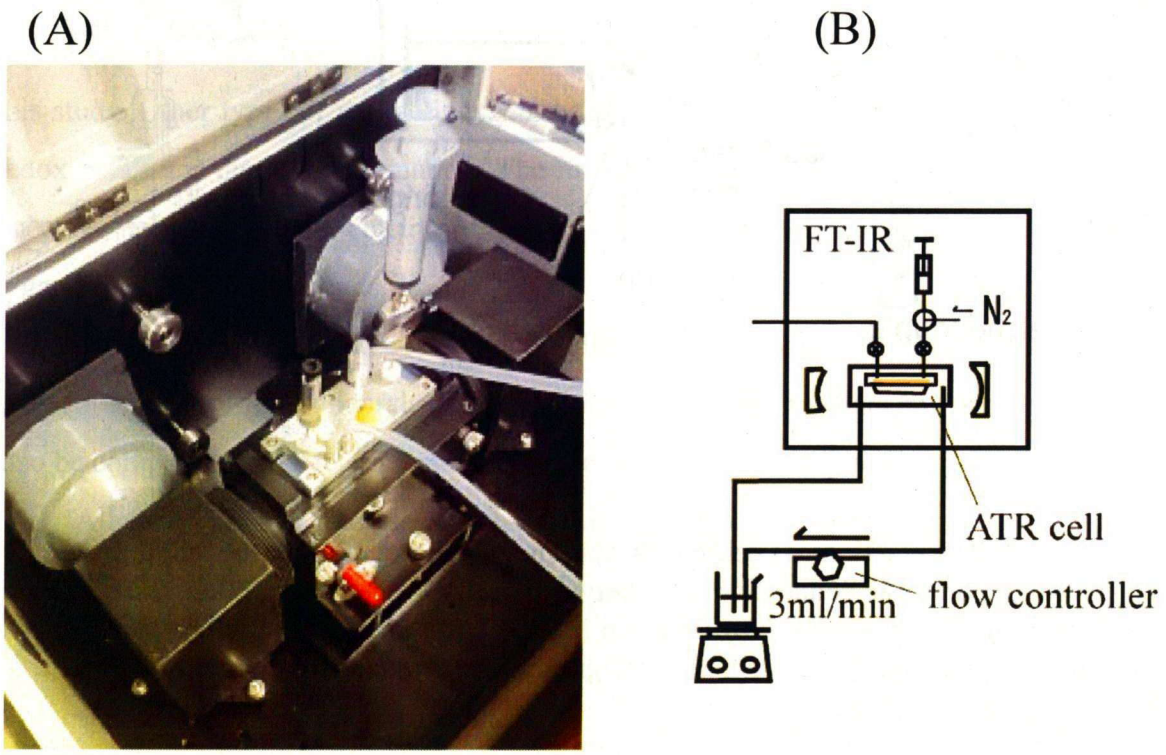

Figure 5.1.3. The hydrothermal ATR-IR spectroscopy system by using the ATR crystal (ZnSe) coated with goethite thin film and the flow-though system of heated solutions. (A) Photograph for the ATR cell and spectrometer and (B) Schematic configuration of the whole system

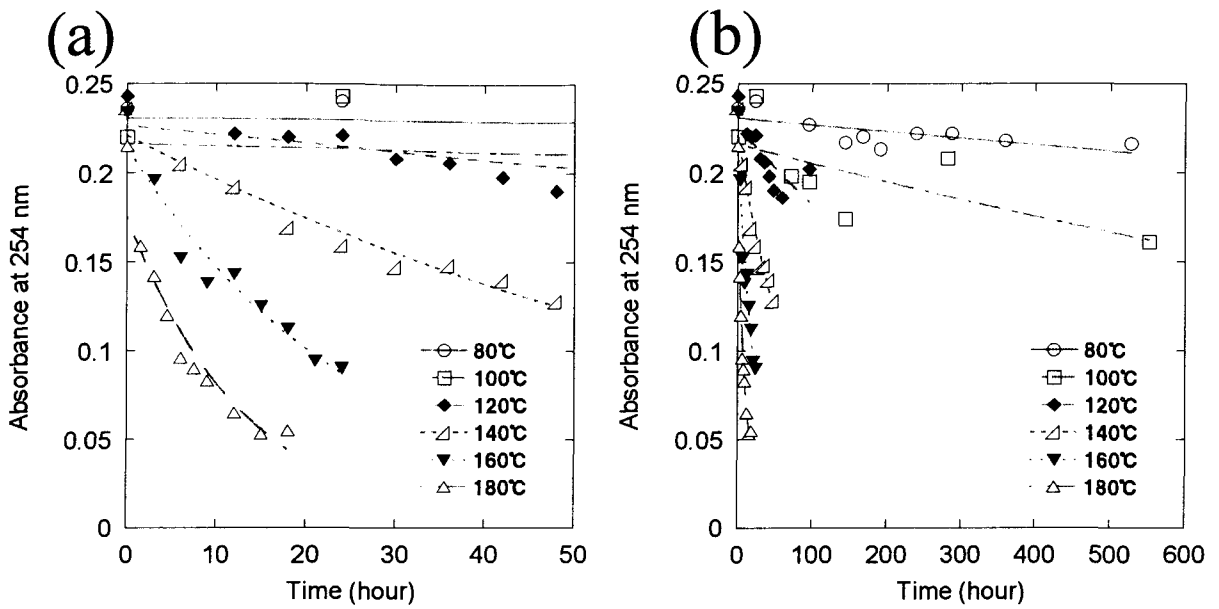

Fig. 5.2.1. Changes with time in 254 nm absorbances of Nordic fulvic acid solutions heated at 80 °C for 0 – 528 hours, 100°C for 0 – 552 hours, 120°C for 0 – 96h hours, 140°C for 0 - 48 hours, 160°C for 0 - 24 hours and 180°C for 0 - 18 hours during the batch heating experiments. a) from 0 to 50 hours; b) from 0 to 600 hours. Fitting curves by the first order kinetics are also shown.

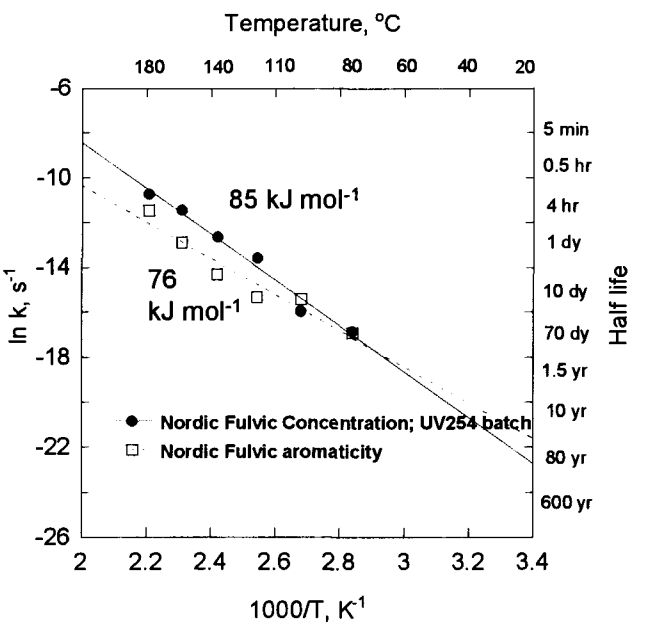

Fig. 5.2.2. The Arrhenius diagram for the first order decrease rates of the 254 nm absorbance and the aromaticity during the batch hydrothermal transformation of Nordic fulvic acid solutions.

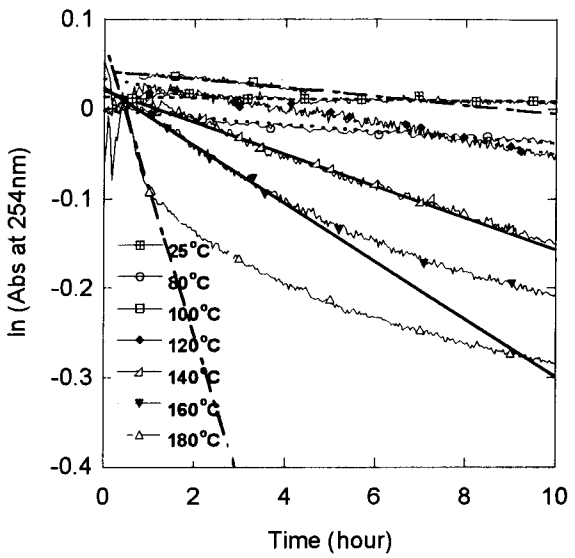

Fig. 5.2.3. Initial changes with time in 254 nm absorbances of Nordic fulvic acid solutions heated at 80-180°C in the in-situ UV cell.

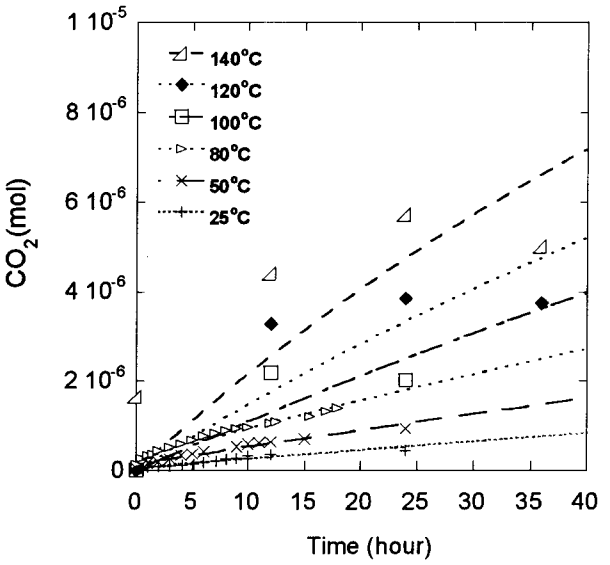

Fig. 5.2.4. Cumulative amounts of CO_2 formed from the hydrothermal reaction gas cell FT-IR system at 25-140°C.

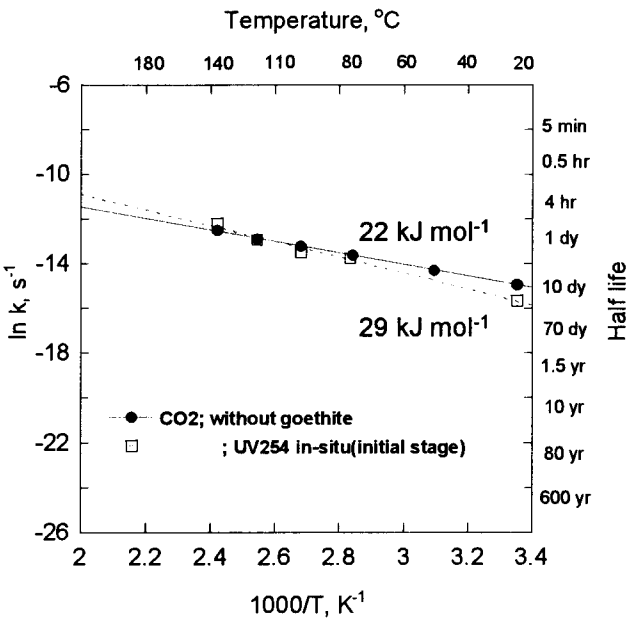

Fig. 5.2.5. The Arrhenius diagram for the initial decrease rates of 254 nm absorbance and CO_2 formation rates.

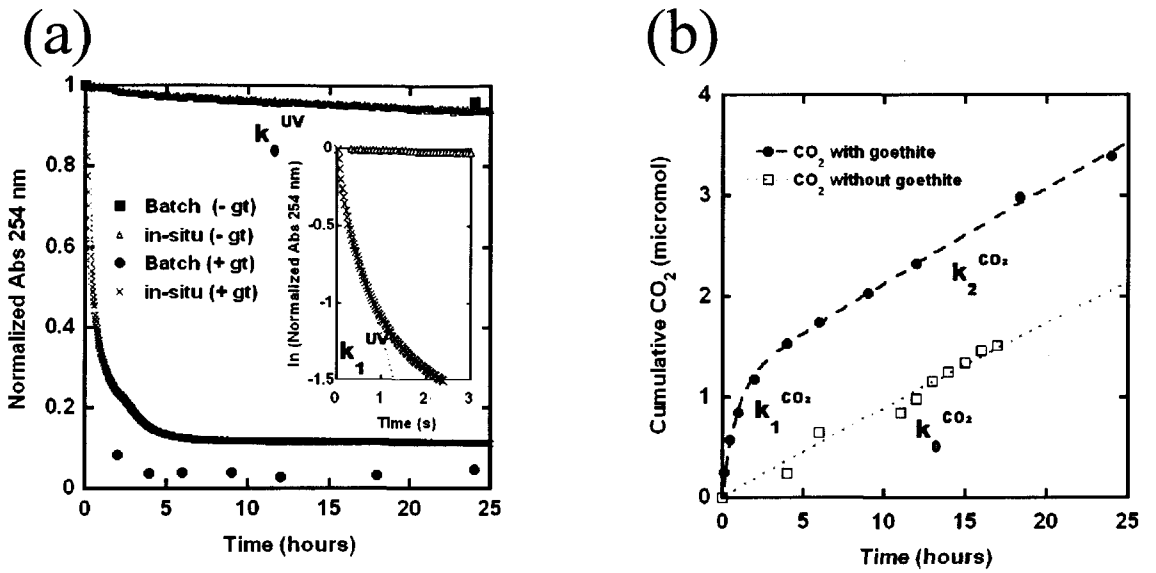

Fig. 5.3.1 Changes with time in (a) 254 nm absorbance (Abs_{254}) by in-situ UV-VIS spectroscopy and (b) cumulative amounts of formed CO_2 by the reaction gas cell FT-IR, with or without goethite during the hydrothermal heating experiments of the fulvic acid solution.

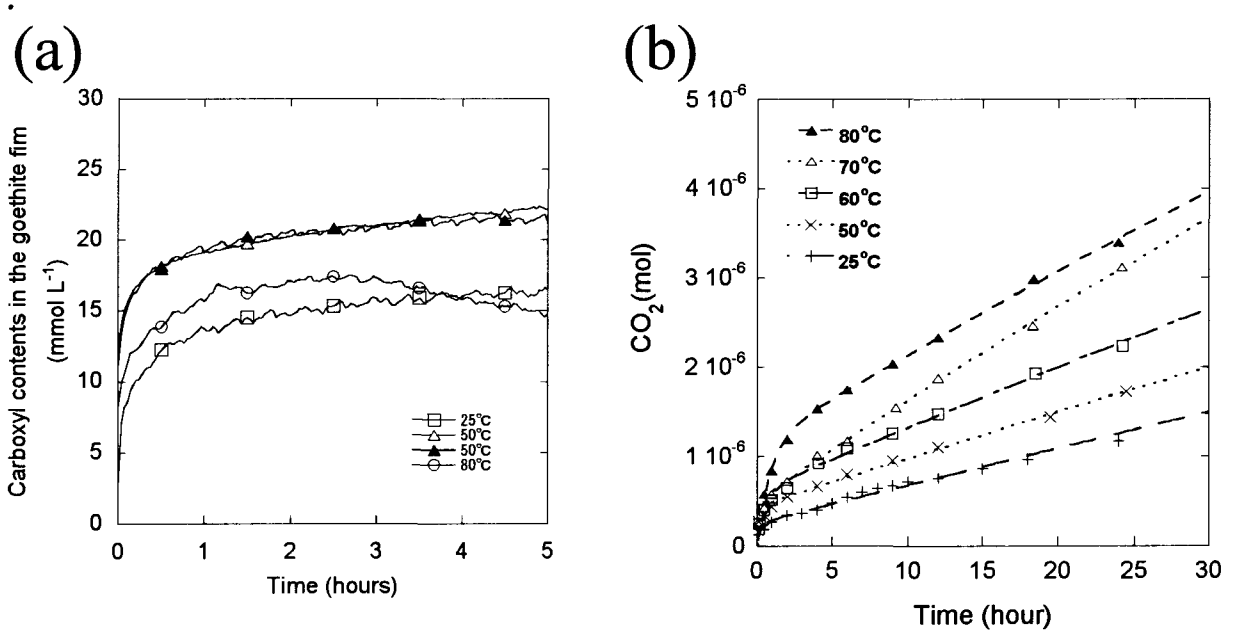

Fig. 5.3.2. Changes with time in (a) carboxyl contents adsorbed on the goethite surface by ATR-IR spectroscopy at 25-80°C during the initial stage and (b) CO_2 formation at 25-80°C with goethite by the reaction gas cell FT-IR.

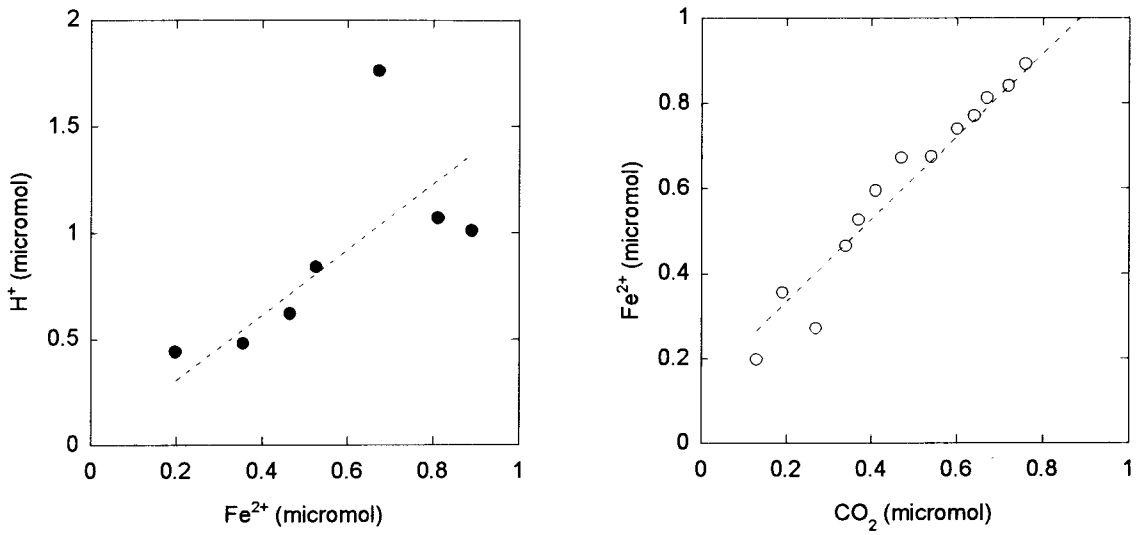

Fig. 5.3.3. The stoichiometric relations during the fulvic acid – goethite interactions.

(a) Relation between consumed H^+ and formed Fe^{2+} close to 2:1, (b) Relation between formed Fe^{2+} and formed CO_2 close to 1:1

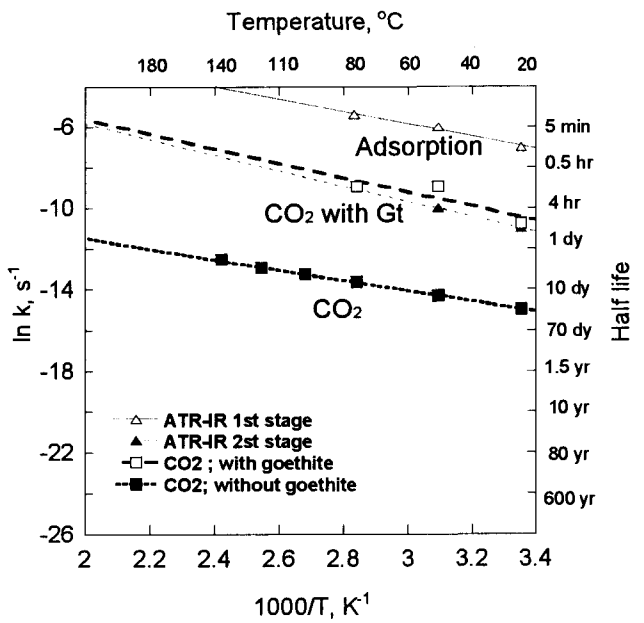

Fig. 5.3.4. The Arrhenius diagram for the adsorption rates of the fulvic acid on goethite by ATR-IR spectroscopy (first and second stages) and CO_2 formation rates with or without goethite.

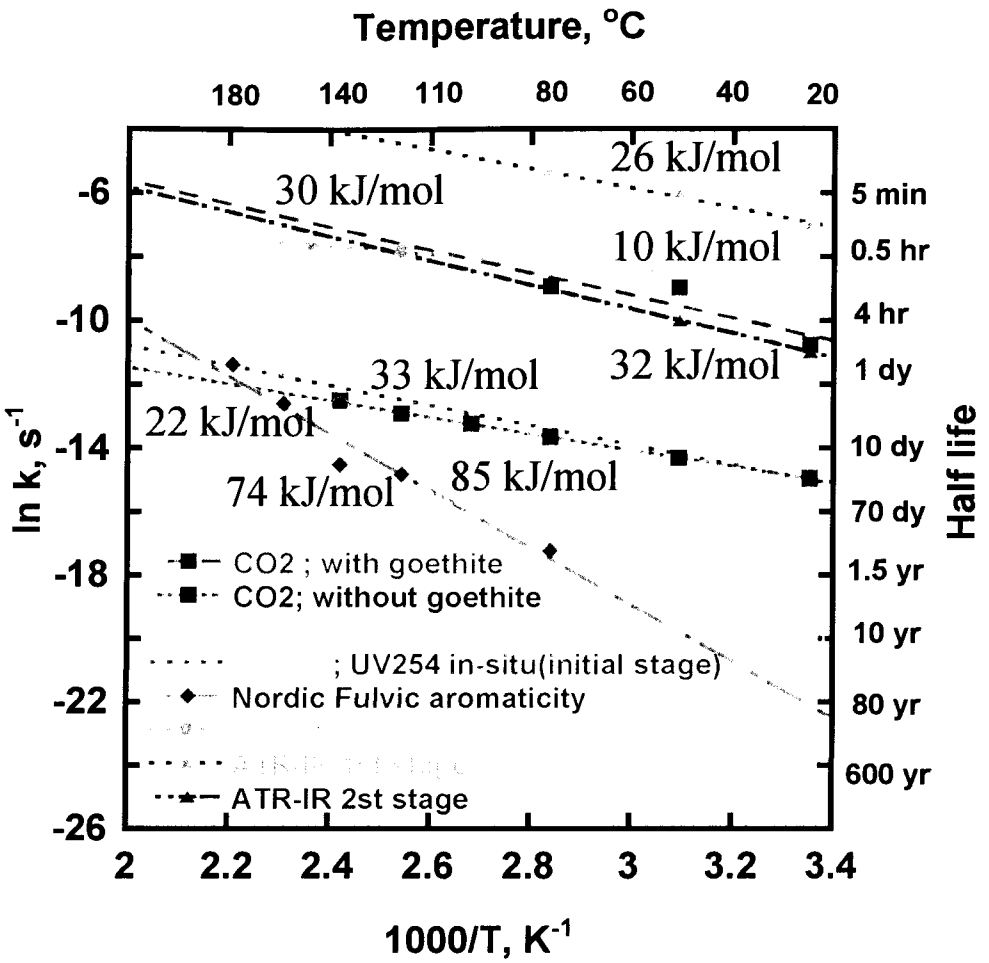

Fig. 5.4.1. The Arrhenius diagram for the decrease rates of 254 nm absorbance, the aromaticity decrease rates, the in-situ initial decrease rates of 254 nm absorbance, CO_2 formation rates with or without goethite and the adsorption rates of the fulvic acid on goethite by ATR-IR spectroscopy

REFERENCE

Berg B., Hannus K., Popoff T. and Theander O. (1982) Changes in organic-chemical components during decomposition. Long-term decomposition in a Scots pine forest I. *Canadian Journal of Botany*, **60**, 1310-1319

Berg B. and McClaugherty C. (2003) *Plant litter, decomposition, humus formation, carbon sequestration*, Berlin, Heidelberg: Springer-Verlag.

Brill. T.B., Savage, P. E. (2004), Aqueous systems at elevated temperatures and pressures, in *physical chemistry in water, steam, and hydrothermal solutions* (eds. Palmer, D. A., Fernandez-Prini, R., Harvey, A. H.), Amsterdam; Boston: Elsevier.

Campbell C. A., Paul E. A., Rennie D. A. and McCallum K. J. (1967) Applicability of the carbon-dating method of analysis to soil humus studies. *Soil Science*, **104**, 217-224

Coble P. G. (1996) Characterization of marine and terrestrial DOM in seawater using excitation-emission matrix spectroscopy, Marine chemistry, **51**, 325-346

Chorover J. and Amistadi M. K. (2001) Reaction of forest floor organic matter at goethite, birnessite and smectite surfaces. *Geochimica et Cosmochimica Acta*, **65**, 95-109.

Filius J. D., Lumsdon D. G., Meeussen J. C. L., Hiemstra T. and van Riemsduk W. H. (2000). Adsorption of fulvic acid on goethite. *Geochimica et Cosmochimica Acta*, **64**, 51-60.

Gu B., Schmitt J., Chen Z., Liang L. and McCathy J. F. (1994) Adsorption and Desorption of natural organic matter on iron oxide: mechanisms and models. *Environmental Science and Technology*, 28, 38-46.

Gu, B., Schmitt, J., Chen, Z., Liang, L., McCarthy, J. F., (1995) Adsorption and desorption of dirrenet organic-matter ractions on iron-oxide., *Geochimica et Cosmochimica Acta*, **59**, 219-229

Hanst P. L., Lefohn A. S. and Gay Jr B. W. (1973) Applied Spectroscopy, **27**, 188

Harrick, N. J.; du Pre, K. F. (1966) Effective thickness of bulk materials and of this films for internal reflection spectroscopy., *Applied Optics*. **5**, 1739-1966,

Hedges J. I. (2002) Why dissolved organic matter? In *Biogeochemistry of Marine Dissolved Organic Matter* (eds. Hansell D. A. and Carson C. A.) Amsterdam: Academic Press, pp.774

Hsieh Y. P. (1992) Pool size and mean age of stable organic carbon in cropland. *Soil Science Society of America Journal,* **56**, 460-464

Jenkinson D. S. (1966) Studies on the decomposition of plant material in soil II. Partial sterilization of soil and the soil biomass. *European Journal of Soil Science*, **17**, 280-302

Koarashi J., Iida T., Moriizumi J. and Asao T. (2004) Evaluation of 14C abundance in soil respiration using accelerator mass spectrometry, *Journal of Environment Radioactivity*, **75**, 117-132

Koarashi J., Iida T. and Asao T. (2005) Radiocarbon and stable carbon isotope compositions of chemically fractionated soil organic matter in a temperate-zone forest, *Journal of Environment Radioactivity*, **79**, 137-156

Korshin. G. V., Li, C. W., and Benjamin, M. M. (1997) Monitoring the properties of natural organic matter through UV spectroscopy: A consistent theory., *Water Research.* **31**, 1787-1795,

LaKind J. S. and Stone A. T. (1989) Reductive dissolution of goethite by phenolic reductants. *Geochimica et Cosmochimica Acta*, **53**, 961-971.

Landais P., Gize A. P. (1997) Organic matter in hydrothermal ore deposit, in Barnes H. L. ed., Geochemistry of hydrothermal ore deposits 3rd ed., New York, John Wiley & Sons, p613-656

Masuda, K. (2005) Development of in-situ heating spectroscopic methods for aqueous organic reactions, Doctral thesis, Department of Earth and Space Sciences, Tokyo

Institute of Technology

Malcolm R. L. (1990) Variations between humic substances isolated from soils, stream waters, and groundwaters as revealed by 13CNMR spectroscopy. In *Humic substances in soil and crop sciences; selected Readings*, (eds P. MacCarthy, C. E. Clapp, R. L. Malcolm, P. R. Bloom) pp. 13-35. Madison, Wisconsin: American Society of Agronomy and Soil Science Society of America,

O'Brien and Stout (1978) Movement and turnover of **soil** organic matter as indicated by carbon isotope measurements. *Soil Biology and Biochemistry*, **10**, 309-317

Otsuka T. and Nakashima S. (2007) The formation of CO2 by fulvic acid on the surface of goethite studied using ultraviolet and infrared spectroscopy, *Journal of Mineralogical and Petrological Sciences*, **102**, 302-305

Pullin M. J. and Cabaniss S. E. (2003), The effect of pH, ionic strength, and iron-fulvic acid interactions on the kinetics of non photochemical iron transformations. II. The kinetics of thermal reduction. *Geochimica et Cosmochimica Acta*, **67**, 4079-4089.

Maranger R. and Pullin M. J. (2003) Elemental complexation by dissolved organic matter in lakes: Implications for Fe speciation and the bioavailability of Fe and P, In *Aquatic ecosystems interactivity of dissolved organic matter*, (eds. Findlay S. E. G. and Sinsabaugh R. L.) pp.186-214, Sun Diego, London: Academic press

Shields J. A. and Paul E. A. (1973) Decomposition C^{14}-labelled plant material under field conditions. *Canadian Journal of Soil Science*, **58**, 297

Stevenson F. J., Humus chemistry: genesis, composition, reactions 2nd ed., New York: Wiley, 1994

Schoonen M. A. A., Xu Y. and Strongin D. R. (1998) An introduction to geocatalysis, *Journal of Geochemical Exploration, **62**,* 205-215

Thurman. E. M. (1985) *Organic geochemistry of Natural waters*, Dordrecht, M. Nijhoff, 1-4

Zhou Q. Maurice P. A. and Cabaniss S. E. (2001) Size fractionation upon adsorption of fulvic acid on goethite: equilibrium and kinetic studies, *Geochimica et Cosmochimica Acta*, **65**, 803-812.

LIST OF PUBLICATION

Peer reviewed paper

1. **Takahiro OTSUKA**, Satoru NAKASHIMA (2007) The formation of CO_2 by fulvic acid on the surface of goethite studied using ultraviolet and infrared spectroscopy, *Journal of Mineralogical and Petrological Sciences*, **102**, 302-305

2. Kenji ISHIKAWA, Atsushi TANI, **Takahiro OTSUKA**, Satoru NAKASHIMA (2007) Transformation of γ–ray-formed methyl radicals in methane hydrate at 10MPa. *Japanese Journal of Applied Physics*, **46**, 455-460.

Proceedings, Reports, Books, Abstruct

3. **Takahiro OTSUKA**, Satoru NAKASHIMA, Satoshi MIWA and Masanori SUNOSE (2003) *Geochimica et Cosmochimica Acta*, Vol.67, No.18 (S1), A367

4. Kaori MASUDA, Yuki ITO, **Takahiro OTSUKA**, Satoru NAKASHIMA (2003) Thermal stability of dissolved humic acid as revealed by in-situ UV spectroscopy, *Geochimica et Cosmochimica Acta*, Vol.67, No.18 (S1), A276

5. **Takahiro OTSUKA**, Kaori MASUDA, Mihoko MORIIZUMI and Satoru NAKASHIMA (2004) Thermal transformation for functional groups of dissolved humic substances, *Monthly Earth*, Kaiyou Shuppan, 26(8), 535-537, 2004

Presentations in international conferences

6. **Takahiro OTSUKA**, Satoru NAKASHIMA and Kaori MASUDA "Long-path gas cell FT-IR spectroscopy for volatile organics from thermal decomposition of dissolved organic matter",The 227th ACS National Meeting, CA, USA, 2004, Poster Presentation

7. **Takahiro OTSUKA**, Satoru NAKASHIMA, Satoshi MIWA and Masanori SUNOSE "Long-path gas cell infrared spectroscopy of volatile organic pollutants", The 13th Annual V. M. Goldschmidt Conference, A367, Japan, 2003, Poster Presentation

8. Atsushi TANI, Kenji ISHIKAWA, Kei TAKEYA, **Takahiro OTSUKA** and Satoru NAKASHIMA "ESR study on methane hydrate", 19th General Meeting of the International Mineralogical Association, Kobe, Japan, 2006, Poster Presentation

9. **Takahiro OTSUKA**, Kaori MASUDA and Satoru NAKASHIMA "In-situ UV spectroscopic studies of thermal decomposition reactions of aquatic dissolved humic substances", The 230th ACS National Meeting, GEOC115, Washington,D.C USA,

2005, Oral presentation

10. Kaori MASUDA, **Takahiro OTSUKA** and Satoru NAKASHIMA "In-situ kinetic spectroscopic monitoring for hydrothermal transformation of humic substances", Earth System Processes 2, 14-4, Calgary, Canada, August 8-11, 2005, Oral presentation

11. Kaori MASUDA, Taishiro HARAMAKI, **Takahiro OTSUKA** and Satoru NAKASHIMA "In-situ heating UV and ATR-IR spectroscopy for kinetic behaviors of dissolved organic matter", The 227th ACS National Meeting, GEOC182, Anaheim, CA, March 28-April 1,2004, Oral presentation